Development of Integrated and Flexible Ultrasonic Transducers for Aerospace Applications

Kuo-Ting Wu

Department of Electrical and Computer Engineering
McGill University
Montreal, Quebec, Canada
November 2010

A thesis submitted to McGill University in partial fulfillment of the requirements of the degree of Doctor of Philosophy

Abstract

High temperature (HT) integrated (IUTs) and flexible ultrasonic transducers (FUTs) for potential aerospace applications in the area of nondestructive testing (NDT) and structural health monitoring (SHM) are developed. The main merits are that IUTs can be fabricated on-site and FUTs are feasible and attractive for on-site installation. The piezoelectric composite films of these HT ultrasonic transducers (HTUTs) are made by sol-gel spray fabrication. Lead-zirconate titanate composite (PZT-c), bismuth titanate composite (BIT-c), or lithium niobate composite ($LiNbO_3$-c) films were coated onto metallic substrates with planar and curved surfaces and investigated as IUTs. Their maximum operating temperatures were demonstrated at up to 150°C, 400°C, and 800°C, respectively. PZT-c or BIT-c films were coated onto 75 μm or 38 μm thick metallic membranes and were investigated as FUTs. They can be bonded onto flat or curved surfaces for NDT and SHM. An FUT made of BIT-c film coated onto a stainless steel membrane glued onto a steel plate was performed at up to 300°C. Besides being coated onto metallic materials, sol-gel sprayed composite films were also coated onto graphite/epoxy (Gr/Ep) plates as IUTs and 50 μm thick polyimide films as FUTs for the thickness and delamination evaluation.

Using acoustic mode conversion techniques, HTUTs for shear (S) wave, surface acoustic wave (SAW), and plate acoustic wave (PAW), have been developed. HT ultrasonic probes simultaneously producing one longitudinal (L) and two orthogonally polarized S waves were demonstrated in metallic and Plexiglas probes. The potential applications of these probes were discussed. Also applying mode conversion approaches, HT symmetrical, anti-symmetrical, and shear horizontal (SH) PAWs UTs for NDT and SHM were developed. The results showed that the SH PAWs may be the best candidate for NDT and SHM purposes for plate structures. Generation and detection of guided acoustic waves for NDT were demonstrated by using IUTs or FUTs with metallic wedges, mechanical gratings or interdigital transducers as well. The experiments with these three approaches were performed at up to 300°C.

Furthermore, two non-contact ultrasonic measurement techniques by sol-gel sprayed composite films were presented in this thesis. One is using lasers to generate ultrasound and IUTs as receivers, and the other is using induction-based non-contact ultrasonic measurement technique with IUTs. NDT of bonded composite patches on aluminum plates was performed using laser generated ultrasound and IUT receivers. The induction-based ultrasonic measurement of a Gr/Ep composite plate rotated at 1000 rpm was demonstrated.

The IUTs and FUTs developed in this thesis are able to provide signals with good signal-to-noise ratios at elevated temperature on structures and parts having a curved surface. They are light weight and miniature in size. They may be used for real-time, *in situ*, nondestructive local and global (large area) damage detection and assessment in aerospace NDT and SHM applications.

Résumé

Des capteurs intégrés (CIU) et flexibles (CFU) ultrasonores à haute température (HT) on été développés pour des applications potentielles en aérospatiale dans le domaine des évaluations non destructives (END) et la surveillance de la santé structurelle (SSS). Le principal avantage des CIUs et des CFUs est leur capacité à être fabriqués sur site. Ces capteurs ultrasoniques à haute température (CUHT) sont fabriqués à partir de la technique sol-gel qui consiste à déposer une mince couche d'un composé piézo-électrique. Ces couches peuvent être constituées de zirconate titanate de plomb (PZT-c), ou de titanate de bismuth (BIT-c), ou encore, de niobate de lithium (LiNbO3-c), déposées sur des substrats métalliques plats ou courbes et évaluées comme CFUs. Les températures maximales d'opérations de ces capteurs furent évaluées et sont respectivement de 150°C, 400°C et 800°C. Les couches de PZT-c ou de BIT-c furent déposées sur des membranes métalliques d'épaisseurs de 75 μm ou de 38 μm et furent évaluées comme CFUs. Ils peuvent être collés sur des surfaces plates ou courbes pour de l'END et de la SSS. Un CFU fait à partir de BIT-c déposé sur des membranes d'acier inoxydable et collé sur une plaque d'acier fut démontré jusqu'à une température de 300°C. De plus, ces composés piézo-électriques peuvent être déposés sur des plaques de graphite/époxy (Gr/Ep) et être traités comme des CIUs, ou encore, sur des films de polyimide comme CFUs pour mesurer des épaisseurs et évaluer le délaminage.

En utilisant la technique de conversion de mode acoustique les ondes de cisaillement (C) des CUHTs, les ondes acoustiques de surface (OAS) et les ondes acoustiques de plans (OAP) ont été développées. Les capteurs ultrasonores à HT produisent une onde longitudinale (L) et deux ondes perpendiculaires polarisées (S). Ces deux types d'ondes furent démontrés pour des palpeurs métalliques et en « Plexiglass ». De plus, en utilisant cette technique acoustique pour des CUHTs des OAS symétrique, antisymétrique et cisaillement horizontal (CH) pour l'END et la SSS furent développés. Les résultats démontrent que les CH d'OAS sont probablement les meilleurs candidats pour l'END et la SSS de structures plates. La génération et la détection d'ondes acoustiques guidées pour l'END furent démontrées en utilisant des CUIs et des CFUs

avec des coins métalliques, des grilles mécaniques ou bien des capteurs interdigitaux. Les expériences avec ces trois approches furent faites jusqu'à une température de 300°C.

En plus, deux méthodes de mesures ultrasoniques sans contact pour des capteurs ultrasoniques faits à partir de la méthode sol-gel sont présentées dans cette thèse. L'une est l'utilisation de LASER pour la génération d'ultrasons et des CIU comme receveurs. L'autre est l'utilisation sans contact d'une technique de mesure ultrasonore basée sur l'induction qui utilise des CIUs comme receveurs. L'END de plaques de composites déposées sur des plaques d'aluminium fut effectué en utilisant le LASER comme générateur et des CFUs comme receveurs. La mesure ultrasonique basée sur l'induction d'une plaque composite de Gr/Ep tournant à 1000 RPM fut démontrée.

Les CFU et les CIU développés dans cette thèse ont de très bons ratios signal sur bruit à température élevée sur des structures et des surfaces courbes. Ils sont légés et miniatures. Ils peuvent être utilisés en temps réels, *in situ* et pour la détection de dommages sur de petite ou large surfaces en END pour les domaines de l'aérospatial et pour des applications en SSS.

Acknowledgements

First of all, I would like to gratefully and sincerely thank my supervisor Dr. Cheng-Kuei Jen for his guidance, support and encouragement throughout this study. I appreciate what I have learned through him not only concerning research, but also concerning the testimony of a spirit of power and of love and of sobermindedness.

I would also like to thank the National Research Council's Industrial Materials Institute, where this thesis research was performed, and especially the members of Diagnostics of Materials and Processes Group, Dr. Makiko Kobayashi, Dr. Yuu Ono, Dr. Zhigang Sun, Dr. Jacques Tatibouet, Mr. Harold Hebert, Mr. Jean-Francois Moisan, Mr. Qingli Li, Ms. Li Song, Ms. Lijuan Zhao, Mr. Wei-Lin Liu and Ms. Jeanne Shih, for their precious inputs, valuable discussions and helpful assistance, which made the completion of this study possible. The financial support from Natural Sciences and Engineering Research Council of Canada and National Research Council Graduate Student Scholarship Supplement Program is gratefully acknowledged.

Special thanks go to Dr. Rob Hui and Mr. Sing Yick (IFCI-CNRC) for the collaboration on the screen printing and tape casting films in Section 2.3.4; Professor Jose E. B. Oliveira (CTA-ITA-IEEC) for the collaboration on the SH wedge design in Section 4.2.2; Dr. Alain Blouin, Mr. Martin Lord and Mr. Christian Neron (IMI-CNRC) for the collaboration on the laser generated ultrasound in Section 5.1; Dr. Nezih Mrad (Defence R&D Canada) for the collaboration on the structural health monitoring of composites in Section 5.2; Professor Riichi Murayama (Fukuoka Institute of Technology) for the collaboration on the induction-based ultrasonic measurement in Section 5.3; Dr. Antipas R. Desai for English corrections. I also thank Prof. Ishiang Shih for his kind guidance and encouragement during the entire process.

Finally, and most importantly, I would like to thank my dear wife, my parents, my brother and my sister for their love, encouragement, support and quiet patience for the duration of my research and writing.

Table of Contents

List of Figures

List of Tables

List of Symbols

AC	alternating current
Al	aluminum
A_{SV}	anti-symmetrical plate acoustic wave
B	fractional bandwidth of the signal
BAW	bulk acoustic wave
BIT	bismuth titanate
BIT-c	bismuth titanate composite
CMUT	capacitive micromachined ultrasonic transducer
D	electric displacement
d	piezoelectric constant
DC	direct current
Δt	time delay
ε	dielectric constant
E	Young's modulus
E_c	coercive field
EDM	electrical discharge machining
EMAT	electromagnetic acoustic transducer
ESAT	electrostatic acoustic transducer
ET	electromagnetic testing
ε_r	relative dielectric constant
ε_0	dielectric constant for free space
f_0	center frequency
FFT	fast Fourier transform
FUT	flexible ultrasonic transducer
Gr/Ep	graphite epoxy
HDPE	high-density polyethylene
HT	high temperature
HTUT	high temperature ultrasonic transducer
IUT	integrated ultrasonic transducer

k_t	thickness mode electromechanical coupling factor
λ	wave length
L	longitudinal
L_i	incident longitudinal wave
L^n	longitudinal nth trip echo
L_r	reflected longitudinal wave
LDPE	low-density polyethylene
LN	lithium niobate
LU	laser ultrasonics
MEMS	micro electromechanical system
MSAT	magnetostrictive acoustic transducer
MT	magnetic particle testing
NDT	nondestructive testing
NDT&C	nondestructive testing and characterization
PAW	plate acoustic wave
Pb	lead
PE	polyethylene
PT	penetrant testing
PZT	lead zirconate titanate
PZT-c	lead zirconate titanate composite
PVDF	polyvinylidene fluoride
θ	angle
ρ	density
r	radius
RAW	Rayleigh acoustic wave
R_{sl}	energy reflection coefficient
RT	radiographic testing
S	shear
SAW	surface acoustic wave
SEM	scanning electron microscope
S_H	shear horizontal wave

SHM	structural health monitoring
S_L	symmetrical plate acoustic wave
S^n	shear nth trip echo
SNR	signal-to-noise ratio
S_r	reflect shear wave
SS	stainless steel
S_V	shear vertical wave
S_Y	shear wave polarized in Y direction
S_X	shear wave polarized in X direction
σ	tensile strength
T	time window length
τ	temperature
t	thickness
T_c	Curie temperature
Ti	titanium
μ	shear modulus
UT	ultrasonic transducer
V	voltage
V_L	longitudinal wave velocity
V_S	shear wave velocity
VT	visual and optical testing
v	Poisson's ratio
ω	angler frequency
ξ	particle displacement
XRD	X-ray diffraction
Z	impedance
Zr	zirconium

CHAPTER 1

INTRODUCTION

At present many commercial and military airplanes have exceeded or reached their designed life time, and it is crucial to extend their usage life span. In 2000, the service life span of 75% of US Air force aircrafts was 25 years beyond their initial design [1][2]. Also, emerging airplanes are subject to stringent requirements of increased intelligence in flight control and light weight for fuel consumption minimization which reduces the global green house effect. Therefore there is an urgent need for light weight and miniature integrated sensors for real-time, *in-situ*, non-intrusive, nondestructive local and global (long distance) damage detection and assessment in aerospace applications.

Ultrasonic techniques are often used to perform nondestructive testing (NDT) and characterization of aerospace structures and materials because of the simplicity, speed, economy and capability to probe the interior of opaque metallic and graphite/epoxy (Gr/Ep) composite materials such as airplane structures and components. They are one of the promising candidates for structural diagnostic and health monitoring. Also, ultrasonic techniques employing piezoelectric ultrasonic transducers (UTs) have been widely used to carry out NDT and structural health monitoring (SHM) on metallic structures such as airframes, engines, pipes, nuclear power plant structural parts, etc, because of the above mentioned subsurface inspection capability, simplicity and cost-effectiveness [3][4][5].

Many ultrasonic technique applications such as corrosion, erosion, defect detection, etc, are required at high temperatures (HT) [6][7]. Therefore HT ultrasonic transducers (HTUTs) [8][9] are needed. The limitations of the current HTUTs are that they are (1) complicated to be used for curved surfaces, (2) difficult to be applied in pulse-echo mode due to noises caused by imperfect damping in backing materials at HT and (3) not efficient at temperatures higher than 400°C. Such demands initiated this study to develop HTUTs which are able to perform NDT and SHM for aerospace parts and structures having curved surfaces and at HT.

Most existing HTUTs can generate and receive longitudinal (L) waves. However, shear (S) waves may be in certain situations superior to L waves for NDT and characterization of materials because liquid and gas medium do not support S waves. In addition, for the evaluation of material properties, sometimes it is necessary to measure shear modulus and viscoelastic properties in which S wave properties are a requisite. For example, the combination of L and S waves can measure the Youngs' [10] and shear modulus [11], axial load of screws [12][13][14] having isotropic properties. Furthermore, L and two S waves of orthogonal particle displacement may provide the residual stress or texture in the textured steel [15][16] or aluminum (Al) plates. Therefore, there is a need to develop HT ultrasonic probes simultaneously producing L and S waves.

Recently, guided acoustic waves have drawn much attention for NDT and SHM applications because they may inspect parts or structures of a large area within a short time period using a few UTs [5][17][18]. For aerospace industry such NDT and SHM may require that the UTs operate from -80°C to 100°C. In other areas such as power plants, oil and gas industries, the operation temperatures may be required to be higher. Guided waves may be surface (SAW) or plate acoustic waves (PAWs). Thus there is considerable interest to develop HT guided acoustic wave UTs.

To achieve fast NDT and SHM of rotation components, non-contact ultrasonic measurement approaches are desired as well. Using pulsed lasers to generate ultrasound is an attractive and effective non-contact method in which the pulsed laser and the object may be meters away [19][20][21][22]. Other non-contact detection techniques such as

electromagnetic acoustic transducers [23], micro-machined capacitive [24], piezoelectric air-coupled UTs [25], and inductively coupled transducers [26], have been also demonstrated. The merits of most of these non-contact methods include the ability to perform NDT or characterization of materials having curved surfaces and at HT, but may not be suitable for SHM due to being bulky in size or expensive in cost. It may be useful to develop miniature, light weight and inexpensive non-contact ultrasonic measurement techniques for SHM of aerospace industry.

Sol-gel sprayed piezoelectric films have been demonstrated to be able to be coated onto planar and curved surfaces such as UTs [27][28][29][30][31]. The objective of this study is to explore the merits of combing the sol-gel sprayed piezoelectric composite films, mode conversion and non-contact techniques, and to develop HT integrated UTs (IUTs) with on-site fabrication capability and flexible UTs (FUTs) with on-site installation capability in the areas of NDT and SHM for aerospace applications.

1.1 NDT and SHM in Aerospace Industry

NDT and SHM are major concerns of the aerospace community when considering aging aircrafts whose growing maintenance costs can reduce their life extension and safety [2][32]. Also, emerging new airplanes are increasingly required to be equipped with intelligence for improved diagnostics of their structural health condition and safety of the critical parts and structures [1][33]. Therefore, there are demands for miniaturized, lightweight, integrated, and *in situ* sensors for local and global damage diagnostics.

The common inspection methods used in aerospace industry are visual and optical testing (VT), penetrant testing (PT), radiographic testing (RT), magnetic particle testing (MT), electromagnetic testing (ET), and ultrasonic testing. They are briefly described below.

(1) VT [34][35] may be carried out by an inspector's eyes or by computer controlled camera systems. The main advantage of VT is that it is fast when

surface imperfections are visible, but VT may not be used for subsurface inspection.

(2) PT [36][37] is to coat the test object with a visible or fluorescent dye solution, then remove the excess solution from the surface of the object but leave the solution in the surface-breaking defects, and finally to apply developer to draw the trapped penetrant out of imperfections open to the surface. PT is a low-cost inspection method to locate surface-breaking defects in all non-porous materials.

(3) RT [38][39] uses short wavelength electromagnetic radiation to penetrate various materials and to examine materials' and products' defects. An X-ray machine or a radioactive source is used as a source of radiation, and radiation is directed through a specimen and onto film or a radiation detector. The resulting shadowgraph may show the internal features of the specimens. Sensitivity decreases with increasing thickness of specimens, and radiation hazards need to be considered.

(4) MT [40][41] uses the tendency of magnetic lines of flux of an applied field to pass through the metal rather than through the air. A defect at or near the metal surface distorts the distribution of the magnetic flux and some of the flux is forced to pass out through the surface, so the field strength is increased in the area of the defect, which will attract the applied fine magnetic particles and form a pattern around the defect. The pattern of particles provides a visual indication of a defect. MT may inspect ferromagnetic materials only and detect surface or slightly subsurface flaws.

(5) ET [42][43][44] uses electromagnetic induction to detect flaws in conductive materials. Electrical currents (eddy currents) are generated in a conductive material by a changing magnetic field, and variations in the electrical conductivity or magnetic permeability of the test object, or the presence of flaws, will cause a change in eddy current flow. By measuring the change in

the phase and amplitude of current, flaws in the materials may be detected. ET can detect small cracks in or near the surface of material.

(6) In ultrasonic testing [3][4][5], ultrasonic (or acoustic) waves with a frequency greater than the upper limit of human hearing (20 kHz) and normally between 1 MHz and 20 MHz are transmitted into a material to detect imperfections or to locate changes in material properties, due to the different velocities, attenuations and scattering of acoustic waves in different materials. With high penetrating power and high sensitivity, ultrasonic testing may allow the detection of flaws deep in the specimens and permits the detection of small flaws compared with the other NDT methods.

In general, ultrasonic methods have been widely used for real-time, *in situ* or off-line NDT and evaluation of large metallic and polymeric composite structures and parts including those of airplanes and automobiles, because of their subsurface inspection capability, elastic property characterization ability, fast inspection speed, simplicity and cost-effectiveness.

1.2 Ultrasonic Testing for NDT and SHM

A typical ultrasonic testing system consists of a pulser/receiver, UTs, and display devices. The pulser generates high voltage electrical pulses onto UTs. The receiver amplifies the received electrical pulses from UTs and shows the signal on the display devices. The UT converts these electrical pulses into ultrasonic pulses (vibrations) propagating to the material and also converts them, e.g. mechanical or elastic waves, transmitted through or reflected from the defects or any boundaries in or of the material, into electrical pulses.

Electromagnetism, thermoelasticity, magnetostriction, electrostatics, and piezoelectricity, etc are common physical mechanisms to generate ultrasonic pulses for NDT. Some mechanisms generate ultrasonic pulses in the inspected parts directly, and

some generate ultrasonic pulses in standalone transducers and then coupled to inspected parts.

(1) An electromagnetic acoustic transducer (EMAT) [45][46][47] generates ultrasonic pulses in the inspected parts directly with two interacting magnetic fields. A relatively high frequency magnetic field, generated by electrical coils, interacts with a low frequency or static field generated by magnets to create ultrasonic pulses in the surface of the test material. EMATs are also used to detect reflected or transmitted ultrasonic pulses. EMAT is one of the non-contact ultrasonic testing where the transducers may be several millimeters (mms) away from the object to be inspected. However, EMAT is only applicable for inspection of conductive materials, and with its electronic system may be bulky.

(2) Thermoelasticity and ablation are the two mechanisms for generating ultrasound by lasers, and both of them are using laser beams to impact test materials directly. In the thermoelastic regime, ultrasound is generated by the sudden thermal expansion due to the absorption of the heating of a tiny surface of the test material by laser pulse. If the energy density of the laser pulses reaches the threshold where the surface starts to melt and then to be vaporized, ultrasound is then generated by the recoil effect produced by the vaporized material, and this is called ablation. To detect ultrasound, the surface of the test material can be illuminated by a laser beam, and then an optical receiver is used to collect the scattered or reflected light. In laser ultrasonics (LU) [19][20][21][22], transduction is made by light, and the test material is actually the emitting transducer of ultrasound. Laser ultrasonics is a non-contact ultrasonic testing and has been noted for the complexity of the technique, which makes it generally a high cost solution, but in spite of that, it turned out to be cost effective for several applications [48].

(3) Magnetostriction is the changing of a material's physical dimensions in response to changing its magnetization [49]. Magnetostrictive acoustic

transducers (MSATs) utilize the magnetostrictive property of a material to convert the energy in a magnetic field into mechanical energy. The magnetic field is provided by a coil of wire which is wrapped around the magnetostrictive material. When a flow of electrical current is supplied through the coil of wire, a magnetic field is created, and the magnetic field causes the magnetostrictive material to contract or elongate and ultrasonic pulses are generated. When test material is magnetostrictive, the test material may be used as part of the MSAT, and non-contact ultrasonic testing can be carried out [50][51][52].

(4) The fundamental mechanism of electrostatic transduction is the vibration of a thin plate under electrostatic forces. It can be used for generating and receiving ultrasonic waves [53][54]. The simplest form of an electrostatic acoustic transducer (ESAT) is a thin metal membrane stretched above a back electrode forming a small gap, and it constitutes a capacitor, which is charged by a DC voltage. If the biased membrane is driven by an AC voltage, ultrasonic pulses are generated, and vice versa. Recent advances in the silicon micromachining techniques enabled the fabrication of microelectro-mechanical systems (MEMS) based electrostatic transducer, and it is called capacitive micromachined UT (CMUT) [55][56]. As ESAT has a better inherent impedance match between the transducer and air, it is usually used for non-contact ultrasonic testing.

(5) Piezoelectricity is the physical mechanism of a material to generate an electric potential with a applied mechanical stress, and piezoelectric materials also have the opposite effect called reverse piezoelectric effect, where the application of an electrical field creates mechanical deformation of piezoelectric materials. The transduction from electrical field to the dimension change of piezoelectric materials is used to generate ultrasound, and that from the dimension change of piezoelectric materials to electrical pulses is used to detect ultrasound.

Historically, piezoelectric materials, e.g. piezoelectric crystals, ceramics, polymers, and composite materials [57][58][59][60][61][62][63][64][65], have been used to generate and detect ultrasound due to its high electromechanical factor and low cost. Quartz crystals were the first commercially exploited piezoelectric material [57]. However, when piezoelectric ceramics were introduced, they soon became the dominant materials for UTs because of their good piezoelectric properties and ease of manufacture into a variety of shapes and size [58]. Both piezoelectric crystals and ceramics are nonconformable. Piezoelectric polymer, such as [65][66][67], polyvinylidene fluoride (PVDF) UTs have become popular in recent years because of their flexibility and better acoustic impedance match with liquids, polymers, composites, biomaterials and tissues, but PVDF UTs may not work at HT since PVDF has a Curie temperature (T_C) of only around 100°C. Many different types of piezoelectric composite materials [59][60][63] [64][67][68] have been investigated for UT applications because of the need for a combination of desirable material properties that cannot be obtained in signal-phase materials. Piezoelectric ceramic-polymer composites, combining piezoelectric ceramic and non-piezoelectric polymer, have been developed for the past three decades, and have promising ultrasonic performance but may still not be suitable for HT operation due to the nature of the polymer involved.

Recently piezoelectric sol-gel composites including piezoelectric ceramic powder and piezoelectric sol-gel solution, instead of non-piezoelectric polymer, have been reported [27][28][62][63][69]. As the piezoelectric sol-gel composites have good ultrasonic performance at elevated temperatures, and the capability to be fabricated by sol-gel spray technique at a curved surface, this type of piezoelectric composite has been chosen to fabricate HT IUTs and FUTs in this thesis.

1.3 Sol-gel Sprayed Piezoelectric Composite UTs

Sol-gel techniques [70][71][72][73][74] are commonly used for the fabrication of thin films because of its low capital equipment costs and processing temperatures. A sol is a solution with materials dissolved into an appropriate solvent, and a gel is formed

when the dissolved materials in the sol form long polymers and span the entire sol. In the sol-gel process, the sol-gel solution may be coated onto the substrate by dip [73], spin [70], or spray coating [74]. The solvent in the coated film is removed by a drying process. A further thermal treatment, firing process [70], is used to transform the gel to an amorphous ceramic film. An annealing process, an additional thermal treatment with a higher temperature, is applied to enhance mechanical properties and structural stability. Coating and thermal treatments are multiplied till the film achieves the desired thickness which relates to operating frequencies of the UTs [75]. As UTs operate in the thickness mode, at least a 14 μm thick film is required for NDT applications, and it is difficult to achieve by the sol-gel technique because of added internal stress caused by increased film thickness.

D.A. Barrow, *et al*. invented the sol-gel composite technique to fabricate thick films up to 200 μm [27][76]. In the sol-gel composite fabrication, selected ceramic powders are added to the sol-gel solution and coated onto the substrate, and then thermal treatments follow as the same as those used in the traditional sol-gel techniques. The adding of ceramic powders in the sol-gel solution introduces pores into the composite film. The porosity of the composite film reduces the ultrasound velocity in the film, and thus the required film thickness for a desired UT operation frequency. The porosity of the film also increases the UT frequency bandwidth due to increased ultrasonic loss (damping) in the film, but deteriorates the piezoelectricity. Kobayashi and Jen further developed this technology by using spray coating instead of spin coating, and used corona discharge poling instead of traditional contact poling, and different piezoelectric materials [28][77]. These improvements enhanced the piezoelectricity of films and enabled the on-site UT fabrication. The spray coating method may increase the porosity but also increase the flexibility of the piezoelectric films, and thermal durability.

In sol-gel spray composite film, the sol-gel solution serves as adhesive material not only among adjacent powders, but also among powders and substrate. Therefore the sol-gel sprayed composite UTs can be integrated onto substrates and no couplant is required even at elevated temperatures. Compared with conventional piezoelectric UTs, which require bulky backing materials to damp the ultrasound and increase the frequency

bandwidth, sol-gel sprayed composite UTs do not need such backing material because of the porosity of the films. Ultrasonic signals with a broad frequency bandwidth can achieve improved ultrasonic transit time resolution which is closely related to measured range, distance or thickness. The lack of the requirements of backing material and couplants makes sol-gel sprayed composite UTs feasible for the NDT and SHM applications at elevated temperatures. The sol-gel sprayed composite UTs are also feasible for the measurements at low temperatures [30]. *In situ* ice and structure thickness monitoring using integrated and flexible UT has been carried out and repored in [82], and will not be included in this thesis. Such sol-gel sprayed composite UTs are further studied and improved in this thesis. The intended center operation frequency for NDT and SHM purposes ranges from several hundred kHz to 40 MHz.

1.4 Mode Conversions of Acoustic Waves

Ultrasonic waves used in NDT and SHM of materials are mechanical (or elastic) waves, composed of oscillations of discrete particles of material. According to the relations between the directions of particle movement and wave propagation, and material geometry, ultrasonic waves are defined as various modes. L waves, in which the particle movement direction is aligned with the wave propagation direction, are the most widely used wave mode in ultrasonic NDT because L waves could be generated and received efficiently by piezoelectric UTs, which have a high electromechanical factor and are low cost.

S waves, in which the particle movement direction is perpendicular to the wave propagation direction, is also important in ultrasonic NDT because S wave can not propagate in liquid or gas, and this feature can be used, for instance, to detect the liquid-filled or gas-filled small cracks in solid materials with high reflection or scattering coefficients. S waves are often directly generated by a piezoelectric plate vibrating in a direction perpendicular to the plate thickness. It is rather difficult to fabricate broadband MHz S wave UTs for HT operations. Since the mode conversion from L to S wave due to reflection at a solid-air interface has been reported [78][79], the L wave HT UTs together

with L-S mode conversion techniques will be developed as HT broadband S wave probes in this thesis.

1.5 Guided Acoustic Waves

It is known that SAWs and PAWs can be used for NDT and SHM of metals such as steel and Al alloys in the range of hundreds of mms depending on the attenuation characteristics of the materials tested. In common practice the L or S UTs and wedges are used to generate and receive the desired SAW and PAW with the proper mode conversion inside and through the wedge. There is a requirement of an ultrasonic couplant between the wedge and the object under test. It is difficult to apply these UTs and wedges on curved surfaces and, in particular, at HT. Therefore additional purposes of this study are to develop (a) HT wedges together with HT couplants and (b) integrated transducers directly coated onto desired parts having planar or curved surfaces without the need of couplant to generate and receive SAW and PAW for NDT and/or SHM applications at HT and room temperature.

1.6 Overview of Thesis

Since conventional planar UTs show poor inspection performance on curved surfaces and at HT, the design, fabrication, evaluation, and application of IUTs directly coated onto desired metallic structures for NDT and SHM applications at HT and room temperature environments are one major study of this thesis. IUTs have the merit to be possibly fabricated on-site. In addition, the design, fabrication, evaluation and application of FUTs, which may be bonded onto structures of complex shapes, are another major investigation direction. FUTs may be fabricated in mass volume in the lab or factory, and have the very attractive on-site installation capability by using permanent or temporary gluing and bonding techniques.

This study will use the IUTs and FUTs fabricated by the sol-gel spray techniques, mode conversion methods, HT L wave, S wave, SAW, and PAW UTs to demonstrate

potential local and global NDT and SHM applications for aerospace industry. Two non-contact techniques, one using laser generation of ultrasound and IUTs as receivers of ultrasound, and other using induction-based ultrasonic measurements, will be explored for such demonstration as well.

In Chapter 2, sol-gel sprayed piezoelectric composite films as HTUTs are presented. Three different types of piezoelectric powders will used, and the maximum working temperature can be up to 800°C. The fabrication processes and ultrasonic performances of two types of HT UTs, e.g. IUTs and FUTs, will be also described. Metal membranes and polyimide membranes of thickness 38 μm, 50 μm, or 78 μm, will be used as the substrates of FUTs. Besides metallic materials, light weight Gr/Ep composite laminates, which are recently becoming the materials of choice for aerospace structures to reduce the fuel consumption, will be examined by IUTs and FUTs.

In Chapter 3, using acoustic mode conversion and L wave IUTs and FUTs, ultrasonic S wave probes, L and S wave probes and L and two orthogonally polarized S wave probes which are able to operate at temperatures up to around 350 °C, will be presented. The energy mode conversion efficiencies for all bulk wave mode conversion experiments will be evaluated. The measurements of temperature, Young's modulus, shear modulus, Poisson's ratio, material anisotropy and thickness of materials or manufactured parts at elevated temperatures will be demonstrated or discussed.

Chapter 4 demonstrates HT piezoelectric SAW and PAW UTs using acoustic mode conversion and IUTs and FUTs. A preliminary comparison between symmetrical, anti-symmetrical and shear horizontal (SH) PAWs for NDT and SHM of metal plates will be made from study. Each guided acoustic wave mode in plates used for the experiments will be identified by using the theoretically calculated dispersion curves comparing with the experimentally measured group velocities. The generation and detection of guided acoustic waves for NDT using HT wedges will be also presented. In this Chapter analytical analysis of the coupling coefficient from the S waves in the wedge to the SH PAWs in the plate will be presented. Additional types of guided acoustic wave transducers using mechanical gratings together with mode conversion will be also given

in this chapter. HT interdigital transducers (IDTs) fabricated by sol-gel spray technique will be also introduced in this chapter to generate and detect SAW and PAW. Several experimental results to verify the guided acoustic wave NDT capability will be compared with the numerical simulation results carried out by commercially available software based on a finite difference method.

In Chapter 5, two types of non-contact ultrasonic measurement techniques will be introduced. One is using laser to generate ultrasound and using IUTs as ultrasonic receivers. Using this technique the demonstration will be carried out at room temperature and 400°C. NDT of bonded composite patches on Al beams will be also presented as one potential application. The other type of non-contact ultrasonic measurement technique using the induction-based method will be also introduced. The measurement setup and ultrasonic performance of IUT on a rotated part will be shown.

Finally, the conclusions and claims of originality of this study, and future works, will be presented in Chapter 6.

CHAPTER 2

SOL-GEL SPRAYED COMPOSITE FILMS AS HTUTS

Two types of HTUTs made of sol-gel sprayed thick (> 14 μm) piezoelectric composite films [27][28] are presented. Piezoelectric powders to be used are PZT, BIT and $LiNbO_3$ which have T_C of 350°C, 675°C and 1210°C, respectively. One type is that these films are directly deposited onto the parts to be tested, and called IUTs [28]. Such IUTs do not require an ultrasonic couplant. In certain situations parts or structures to be tested cannot be exposed to HT generally used during certain fabrication procedures of the IUT. In such cases another type of HTUTs, named FUTs, can be fabricated off-line and applied with a HT ultrasonic couplant between the FUT and the object to be tested. FUTs are that piezoelectric films are coated onto thin substrates such as 75 μm thick stainless steel (SS) or titanium (Ti) membranes or 50 μm thick polyimide membranes.

Corrosion and erosion are general safety concerns for metallic parts and structures. In particular, stress corrosion cracking, corrosion pitting and exfoliation corrosion are commonly found in aircraft structures [80][81]. There is a critical need to perform *in situ* quantitative thickness measurements to determine the degree of corrosion and erosion and provide correlation to component's remaining useful life time. One of the objectives in this chapter is to develop HT IUTs and FUTs having good ultrasonic performance in pulse-echo mode which only requires one side access, so that corrosion or erosion can be detected clearly and high thickness measurement accuracy can be obtained at HT [82]. Since composite materials such as Gr/Ep laminates are becoming the materials of choice

for aerospace and other transportation structure because of the high strength to weight ratio, NDT and SHM of these materials will also be performed.

Another objective of this chapter is to fabricate HT IUT onto one end of an ultrasonic delay line (or buffer rod) [83][84][85], and use the probing end (opposite to the IUT end) to perform at temperatures which can be higher than the maximum temperature of the HT IUT. The evaluation of the ultrasonic strength of all IUTs and FUTs in this chapter will be based on commercially available pulser-receiver devices EPOCH LT which is nearly daily used in the NDT industry, or Panametrics 5072PR which is commonly used in NDT lab. In all experiments performed in this thesis the excitation pulses generated by EPOCH are negative 100 V(olts) spike pulses with a pulse width of 34 ns, and negative 120 V spike pulses with a pulse width of 37 ns for Panametrics 5072PR. The bandwidth of the receiver of EPOCH LT and 5072PR are 20 MHz and 35 MHz, respectively. Besides these two pulser-receiver devices, Panametrics 5073PR will be used for the 40 MHz IUT evaluation only in this chapter because a short pulse width (6.2 ns for 5073PR) and a broad bandwidth receiver (75 MHz for 5073PR) are required for IUTs of high operation frequency. For convenience in the measurements at HT, the electrical contacts during the majority of the measurements will be obtained using a spring-loaded two-pin probe. However, reliable connections will be carried out and presented for certain samples.

2.1 Sol-Gel Spray Fabrication Process

The sol-gel based UT fabrication process consists of six main steps [27][28][29]: (1) powders and solution preparation, (2) mixing and ball milling, (3) spray coating, (4) heat treatment, (5) electrical poling, and (6) top electrodes fabrication. Steps (3) and (4) are used multiple times to produce optimal film thickness for specified ultrasonic operating frequencies. The flow chart of the general fabrication process is shown in Figure 2-1. The fabrication process was firstly reported by Barrow, *et al* [27], and further developed by Kobayashi and Jen [28][77], but in this thesis induction heating is

introduced during the heat treatment process (4) to improve ultrasonic performance and reduce fabrication time of the sol-gel sprayed composite films.

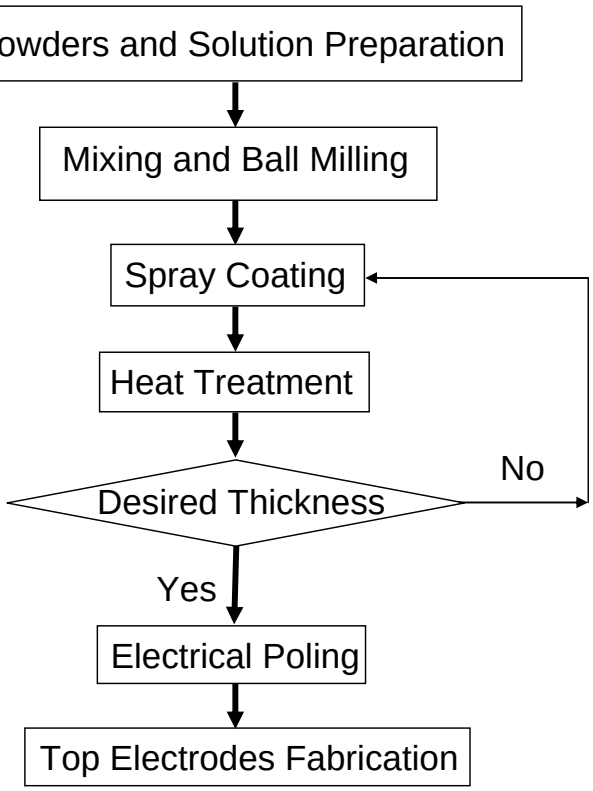

Figure 2-1 Flow chart of sol-gel based UT fabrication process

2.1.1 Step 1: Powders and solution preparation

Three piezoelectric powders, PZT, BIT and $LiNbO_3$, which have T_C of 350°C, 675°C and 1210°C, respectively, and high dielectric constant PZT solution are selected in this thesis to fabricate HTUTs. High dielectric constant PZT solution acts as bonding material among piezoelectric powders, and between powders and substrates. As the PZT solution has high dielectric constant, most of the voltage applied across the piezoelectric films of the IUTs or FUTs will fall onto the piezoelectric powders and enable efficient ultrasonic performance. Most piezoelectric materials operate up to one half of their T_C but some can function up to a higher degree due to their specific phase diagram. At temperatures above the T_C of PZT solution the piezoelectric strength of the composite film entirely depends on the powders of the film. Therefore piezoelectric powders BIT

and $LiNbO_3$ which have high T_C are chosen in this thesis for NDT or SHM at temperatures higher than 150°C when PZT starts to lose or reduce its piezoelectricity. Figure 2-2 shows the purchased piezoelectric powders and the sol-gel made in the lab.

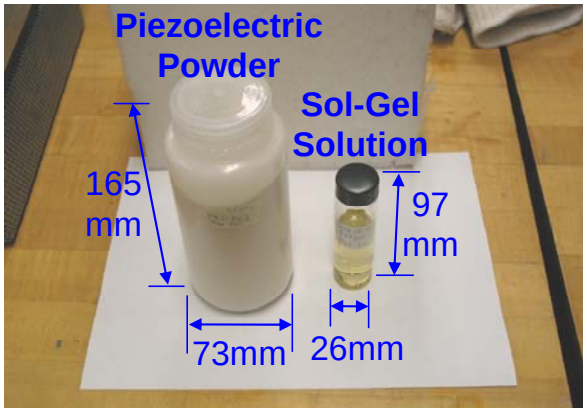

Figure 2-2 Piezoelectric powder and prepared sol-gel solution before mixing. The first step of sol-gel based UT fabrication process shown in Figure 2-1.

2.1.2 Step 2: Mixing and ball milling

To ensure a homogeneous composite film, piezoelectric powders need to be of small sizes and dispersed uniformly in sol-gel solutions. Small particle size and appropriate powder concentration should be used to obtain a good quality composite film. The powders and solution have a selective amount ratio for mixture depending on the desired properties such as piezoelectricity, flexibility, the thickness of the film, and the bandwidth of the UT. Based on the concept of composite materials, the composite material is called as powder composite (POWDER-c) in this thesis. For instance, PZT composite (PZT-c) represents PZT powders with PZT solution, and BIT-c and $LiNbO_3$-c represent BIT powders with PZT solution and $LiNbO_3$ powders with PZT solution, respectively. Ball milling is a grinding and mixing method to realize fine powders of diameters of less than 1 μm, and to enhance the uniformity of powder dispersion in the sol-gel solution. The length of time required for ball milling depends on the purchased particle size and the desired particle size of the piezoelectric powders.The larger the purchased particle size, the longer the ball milling time required. A picture of one homemade ball milling machine is shown in Figure 2-3.

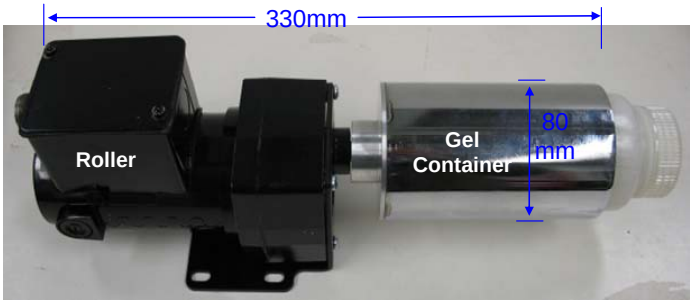

Figure 2-3 Ball milling of the mixture of powder and sol-gel solution in Figure 2-2. The second step of sol-gel based UT fabrication process shown in Figure 2-1.

2.1.3 Step 3: Spray coating

Slurries well mixed from Steps 1 and 2 are coated onto the substrate by a spray coating method to produce a layer of wet slurry film with a thickness between 5 and 20 μm. Compared with other coating methods, spray coating has capability to coat composite films onto substrates in various size, shape, and weight, and onto narrow or small size locations such as edges of thin metallic plates. In this study, well-mixed composite slurries are sprayed onto the substrate surface using a small and light weight air brush, as shown in Figure 2-4. As the spray coating is performed at room temperature, paper, plastic tape or metal foil can be used as masks to fabricate films in the desired areas and shapes. Several parameters of the spray coating, including air pressure, distance between the air brush nozzle and substrate surface, moving speed of the air brush, coating angle, and coating times, will affect characteristics such as porosity and piezoelectricity of the sprayed film and need to be controlled and optimized. With multiple coatings, film thicknesses range from 14 to 125 μm in this investigation, and up to 200 μm in refs. [26], [27] and [28]. Films of thickness less than 14 μm or larger than 200 μm may be also achieved by the spray technique. It is noted that all film thicknesses are measured by micrometers in this thesis. Spray coating used in this thesis produces porous film, which results in, for example, broadband UTs but also reduces piezoelectric strength of UTs. Such phenomenon will be further explained later in the thesis.

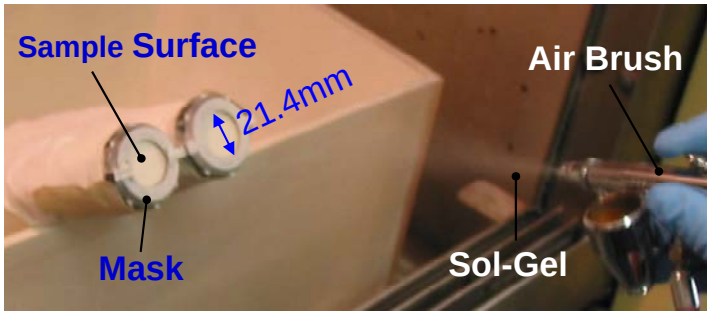

Figure 2-4 Spray coating operation by hand using an air brush. The third step of sol-gel based UT fabrication process shown in Figure 2-1.

2.1.4 Step 4: Heat treatment

Heat treatment is a crucial step for the slurry to become a solid composite film in which PZT films transformed from the gel portion realize their high dielectric constants. It affects the piezoelectricity of the PZT-c film because PZT powder and PZT films solidified by the gel can both function as piezoelectric films under 150°C. In this thesis, heat treatment is divided into two steps: drying and annealing. Drying is carried out at around 120°C to evaporate water and solvent inside the composite slurry. Annealing is normally done at around 650°C for the film to crystallize. However, sometimes a temperature of 650°C can harm or oxidize the substrate, so a lower temperature was applied in certain cases to be specified later. Heat treatment of lower annealing temperature will produce composite films with lower dielectricity, and normally with lower piezoelectricity. Besides the annealing temperature, the annealing speed will also affect the ultrasonic performance of the composite film. Rapid annealing can produce denser films with higher ultrasonic frequencies and higher ultrasonic signal strengths. However, it will reduce the flexibility of the composite film. Induction heating, as shown in Figure 2-5, is the rapid annealing apparatus used in this thesis. This may be the first time in the literature to use induction heating for the heat treatment of sol-gel spray fabrication process of composite films. The other apparatuses for heat treatments applied in this thesis are hot plates, furnaces, propane torches, and heat guns. The induction heatings used in this study focus on localized heating and only near the substrate surface. It takes a short time to reach the desired temperature of the substrate to be coated with piezoelectric composite film. A temperature controller is used to maintain the temperature

in a certain period of time; then the heating is turned off. Due to localized heating, the require time to cool the sample for the next spray is greatly reduced.

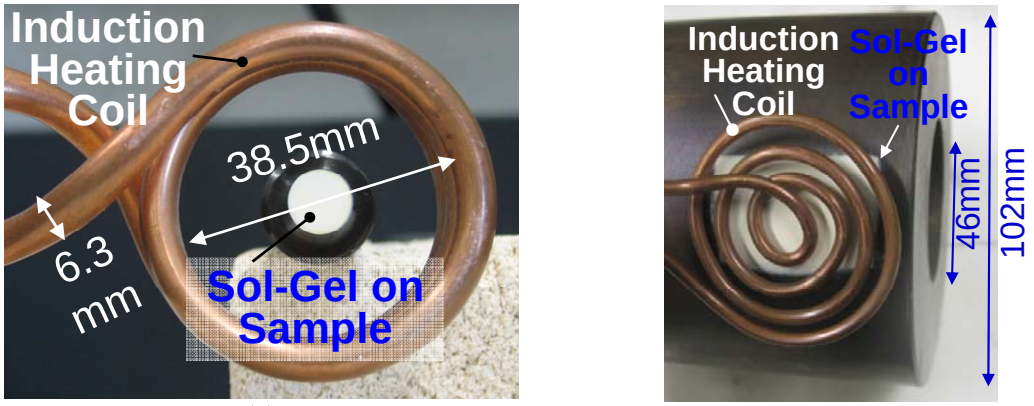

(a) (b)

Figure 2-5 Heat treatment by induction heating. The forth step of sol-gel based UT fabrication process shown in Figure 2-1.

2.1.5 Step 5: Electrical poling

Electrical poling is a step to induce piezoelectricity for polycrystalline piezoelectric film by applying high electric field at a temperature near but lower than the T_C of the powder material. A corona poling technique is used in this thesis; however, a few composite films were poled by traditional poling for comparison purposes. Corona poling, as shown in Figure 2-6, applies a high DC positive voltage to a sharp needle, and then corona discharge is generated by strong electric fields associated with the needle. During corona poling, positive ions produced by electron impacts are transported to the grounded metal plate, so that the corona discharge from the sharp needle is sprayed onto the top surface of the film and creates a strong electric field on it. Corona poling can be applied to large and curved areas, and the composite film IUTs or FUTs can be figured flexibly by fabricating top electrodes after the poling. As no electrode on the surface of the film is required during corona poling, there will be no electric shorting at weak spots, such as locations of composite films having too thin thickness or too high porosity or both, compared with traditional poling. In traditional poling, a high electric field is applied across the top and bottom electrodes sandwiching the piezoelectric film, and dielectric breakdown occurs sometimes at weak spots of the film. A few samples poled by

traditional poling will be described in the later part of this chapter, and all other samples in this thesis without special notes were poled by corona poling. The important parameters for corona poling are the shape of the needle, poling temperature, poling time, electric field, and the distance between the needle and composite film. No top electrode required during corona poling offers a unique advantage providing convenience and flexibility to fabricate top electrode with specific patterns, in particular, for array configuration.

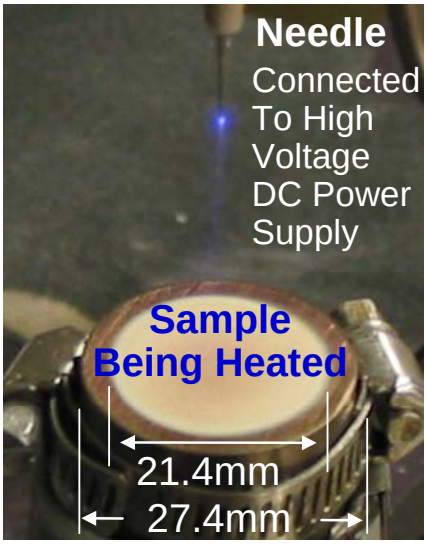

Figure 2-6 Corona poling using a sharp needle with a high DC voltage. The fifth step of sol-gel based UT fabrication process shown in Figure 2-1.

2.1.6 Step 6: Top electrodes fabrication

For IUTs or FUTs, ultrasound waves are generated by applying electric voltage across the top and bottom electrodes which sandwich the piezoelectric composite film. When the piezoelectric composite films are fabricated on metal substrates, which comprise most of the cases in this thesis study, the metal substrates can serve as bottom electrodes, and only top electrodes are needed to be fabricated. Colloidal silver, silver pastes, platinum pastes, and aluminum, are used to fabricate top electrodes in this study by spraying, painting, pasting, or vacuum deposition. The silver top electrode can work well at temperatures up to 300°C and platinum one up to 800°C. As the active areas of IUTs or FUTs are defined by electrodes, a transducer array or an IDT, as shown in Figure

2-7, can be conveniently achieved by suitable top electrode configuration with appropriate masks made of paper, plastic or metallic foils.

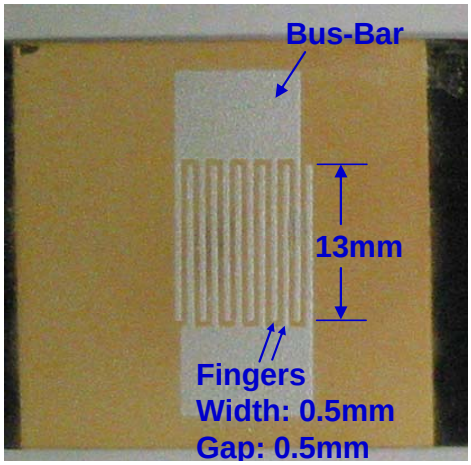

Figure 2-7 Top electrode of IDT configuration made by colloidal silver spray. The sixth step of sol-gel based UT fabrication process shown in Figure 2-1.

2.2 Fabrication and Ultrasonic Performance of IUTs on Metal Substrates

In this section piezoelectric PZT-c, BIT-c and $LiNbO_3$-c films which will operate at temperatures up to 150°C, 400°C and 800°C will be presented.

2.2.1 IUTs made of PZT-c films for applications at temperatures up to 150°C

Figure 2-8 shows an IUT made of a 62 µm thick PZT-c film deposited onto a 12.7 mm thick steel plate and measured by a handheld EPOCH model LT pulser-receiver (from Olympus-Panametrics, USA) at room temperature. The highest heat treatment of the sample in a furnace was 650°C. This particular type of handheld device is used daily for NDT in industrial environments and has dimensions of 238 cm by 138 cm by 38 mm and a weight of 1 Kg. EPOCH LT are mainly used by NDT industrial engineers. It does not have the functionality of signal averaging and filtering and only displays raw ultrasonic measurement data. Performance levels which will be demonstrated on this

handheld device with the fabricated IUTs on flat and curved surfaces help to demonstrate the applicability of such IUTs under current industrial NDT and SHM settings. It is noted that in this thesis all the ultrasonic measurements performed by this EPOCH LT will use the excitation pulses of negative 100 V spike pulses with a pulse width of 34 ns even though larger voltage spike pulses can be generated by this device. A typical value of d_{33} measured for the PZT-c film on steel substrates is 30 x 10^{-12} m/V, the K_t 0.2, the relative dielectric constant 320, the density 4400 kg/m^3 and the L wave velocity 2200 m/s [77]. The porosity of the piezoelectric films, which are controlled during film fabrication mentioned in Section 2.1., achieves the frequency bandwidth of the IUTs to be presented. It means that IUTs presented here do not need backing which may be bulky and not convenient for curved surfaces, in particular, at HT, to broaden the frequency bandwidth. Figure 2-9 shows a typical scanning electron microscope picture of a PZT-c film. This picture demonstrates that the average sizes of the PZT powders are sub-micron. Certain porosity exists in the composite film which is desired in NDT applications.

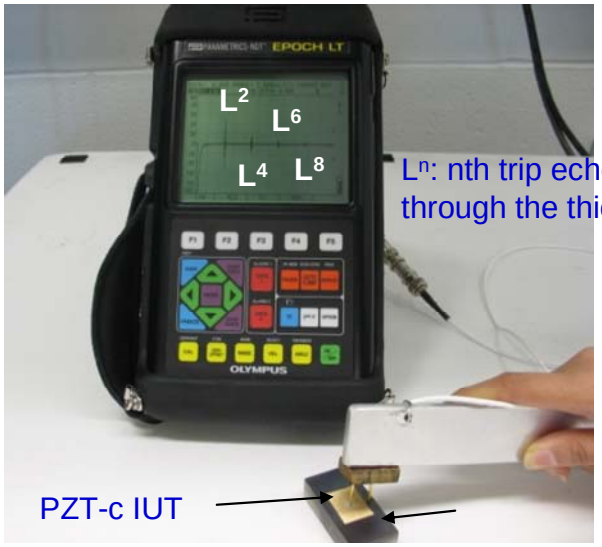

Figure 2-8 Measurement setup for an IUT made of PZT-c film using an EPOCH LT in pulse-echo mode.

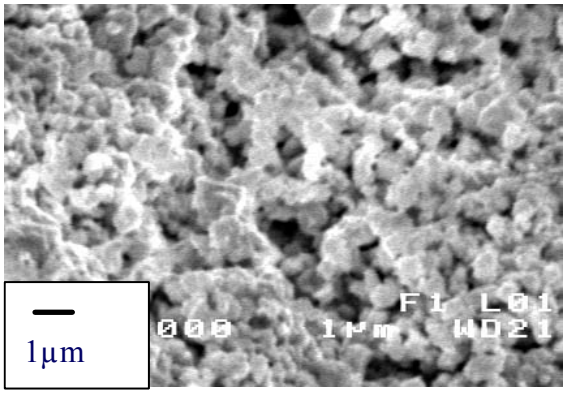

Figure 2-9 SEM image of PZT-c film made by sol-gel spray

The diameter of the silver paste top electrode of this IUT was 5 mm which achieved the maximum signal strength in pulse-echo mode for this PZT-c film at room temperature. It is noted that the diameters of the top electrodes of IUTs throughout the studies were chosen so that the electrical impedance of the IUT can suitably match to that of the pulser/receiver used. The measured ultrasonic data in pulse-echo mode is also presented in Figure 2-10, where L^n is the nth trip L echo through the plate thickness. The center frequency and the 6 dB bandwidth of L^2 echo are 14.6 MHz and 14.0 MHz respectively. In Figure 2-8 the pulse energy used (100 V negative pulses with a pulse width of 34 ns) was the lowest available from the EPOCH LT and 0 dB gain (i.e. no amplification) out of the available 100 dB receiver gain was used. The signal-to-noise ratio (SNR) of the L^2 echo is 46 dB. The SNR is defined as the ratio of the amplitude of the first echo (here L^2) over that of the surrounding noises.

2.2.1.1 Performance comparison between PZT-c film IUTs and commercial UTs at room temperature

When commercial broad bandwidth UTs with a center frequency at 5 MHz and 10 MHz are used at the other side of the steel plate shown in Figure 2-8 together with the necessary commercially available ultrasonic couplant, as shown in Figure 2-11, the measured results are shown in Figure 2-12(a) and Figure 2-12 (b), respectively, where L^n is the nth trip L echo through the plate thickness. The receiver gains used by the EPOCH pulser/receiver were 2 dB and 4.5 dB, respectively. These show that while using the EPOCH LT, the signal strength of the IUT shown in Figure 2-10 was at least as good as

those of the two commercially purchased broadband UTs. The center frequency and the 6 dB bandwidth of L^2 echo in Figure 2-12 (a) are 5.5 MHz and 5.3 MHz and those in Figure 2-12 (b) are 8.7 MHz and 8.1 MHz, respectively. Figure 2-12 indicates that the bandwidth of the commercial broadband width UTs is higher than that of the IUT shown in Figure 2-8. Further comments on the sufficiency of the bandwidth of IUTs for certain NDT and SHM applications will be given in the next sections.

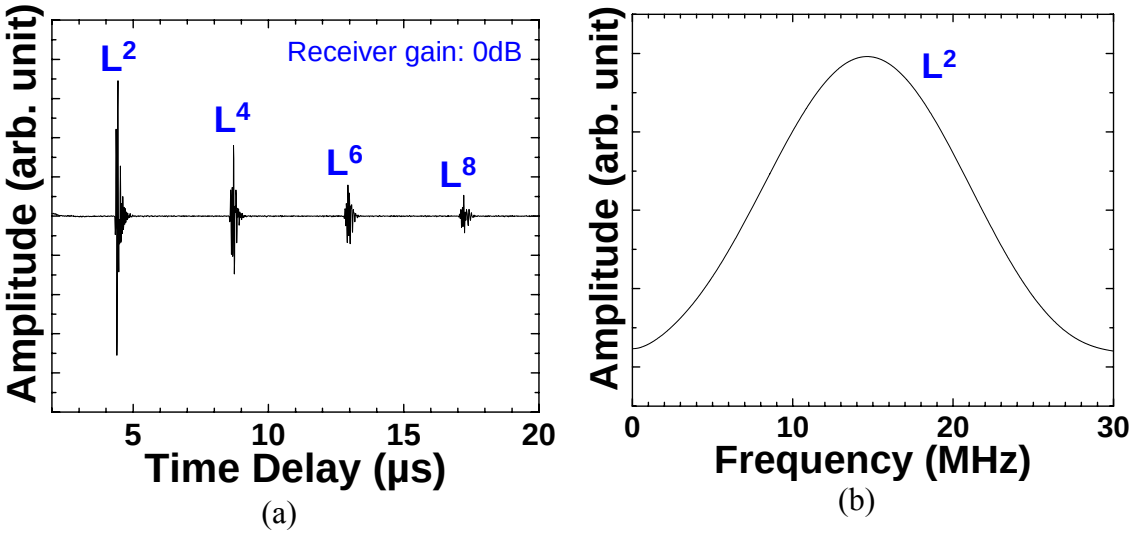

Figure 2-10 Measured ultrasonic data for the setup in Figure 2-8 in (a) time and (b) frequency domain.

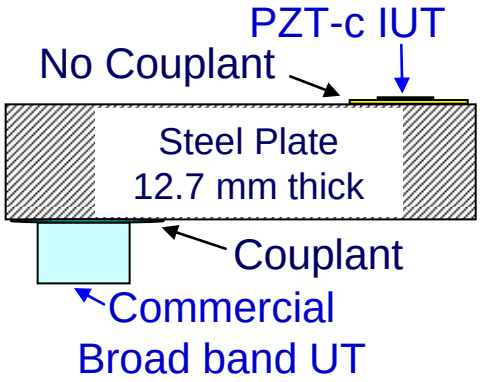

Figure 2-11 Measurement setup of commercial UTs in pulse/echo mode at the opposite surface of the steel plate coated with IUT shown in Figure 2-8

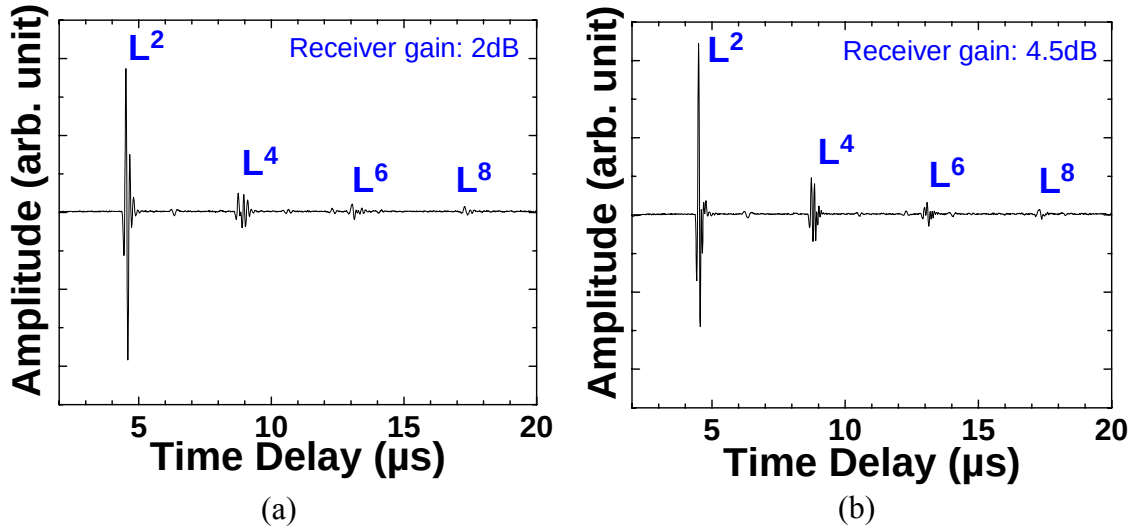

Figure 2-12 Measured ultrasonic signals of commercial UTs with a center frequency of (a) 5 MHz and (b) 10 MHz operated in pulse/echo mode at the opposite surface of the steel plate coated with IUT shown in Figure 2-8.

2.2.1.2 IUT array configuration

As mentioned in Section 2.1.6 that the active areas of IUTs are defined by the top electrodes, IUT array can be configured flexibly by fabricating top electrodes after the corona poling. Figure 2-13 shows an IUT array made of a 71 μm thick PZT-c film deposited onto a 12.7 mm thick steel plate. The array was configured by five silver top electrodes with the diameters of 0.31 mm, 0.65 mm, 0.85 mm, 1.21 mm and 5.5 mm. The measured signals in the time domain of this UT array are shown in Figure 2-14, where L^n is the nth trip L echo through the steel plate thickness.

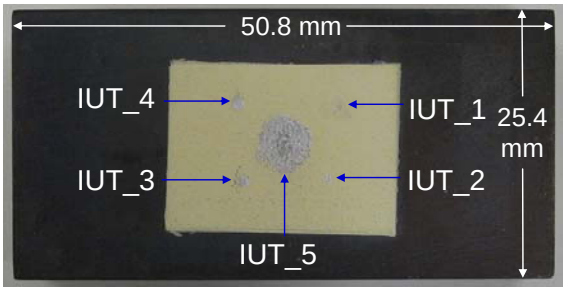

Figure 2-13 PZT-c IUT with array configuration. The top electrode of IUT_1, IUT_2, IUT_3, IUT_4 and IUT_5, are 0.31 mm, 0.65 mm, 0.85 mm, 1.21 mm and 5.5 mm in diameter, respectively.

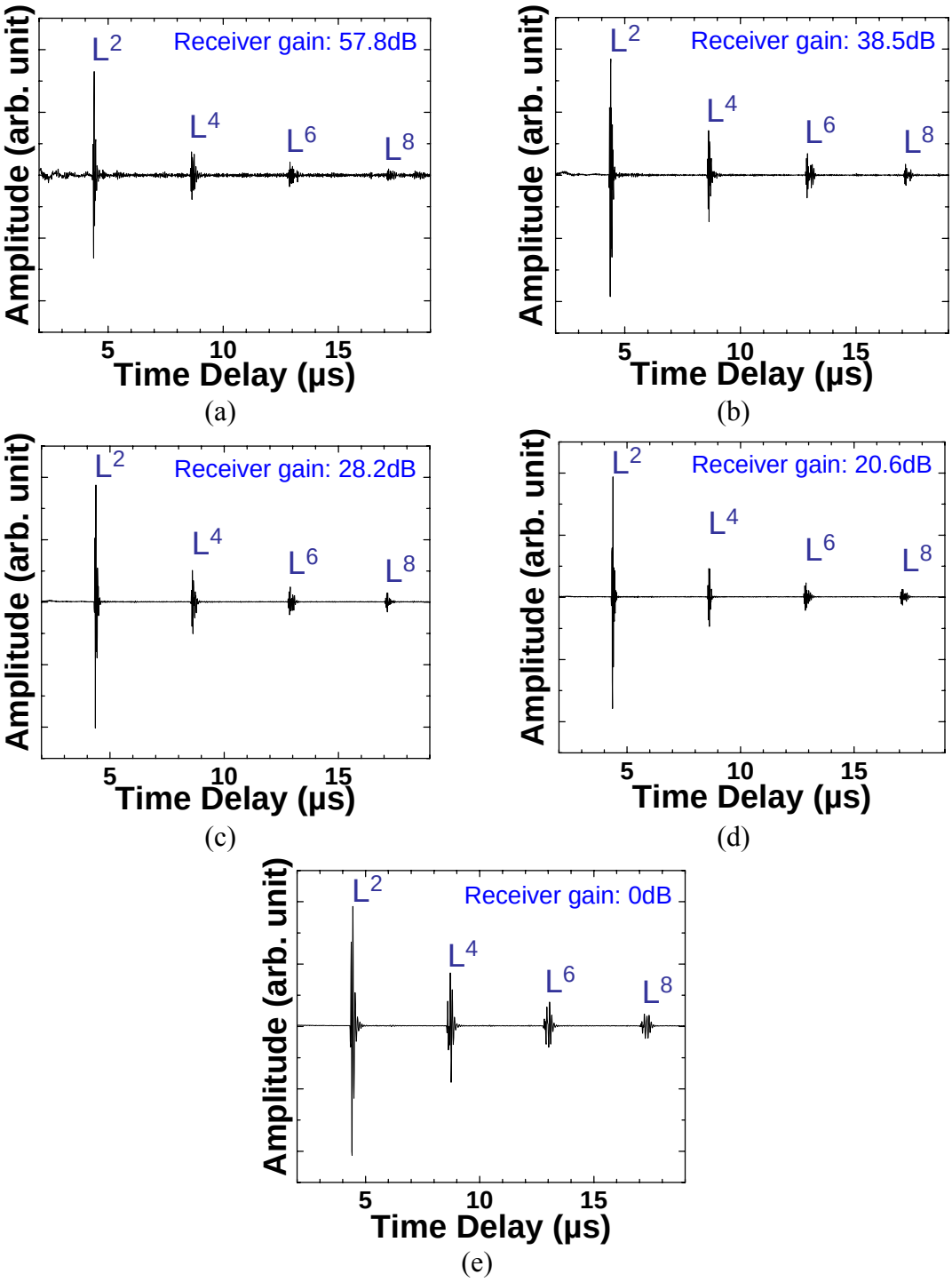

Figure 2-14 Measured ultrasonic signals of the array configuration PZT-c IUT shown in Figure 2-13. (a) is the signals in time domain from IUT_1, (b) IUT_2, (c) IUT_3, (d) IUT_4 and (e) IUT_5.

Because the design operation frequency of this IUT array was around 11 MHz, IUT_5 with the top electrode of 5.5 mm diameter shown in Figure 2-13, achieved the

maximum signal strength in pulse-echo mode at room temperature with the SNR of 45 dB. The signal strengths of the other IUTs having a smaller size of top electrodes than 5.5 mm diameter were weaker than IUT_5, but they still had good SNRs. The SNRs of IUT_4, IUT_3, IUT_2 and IUT_1, are 43 dB, 42 dB, 31 dB and 27 dB, respectively. The signal strength of UT4, UT3, UT2 and UT1, are 20.6 dB, 28.2 dB, 38.5 dB, 57.8 dB, respectively, smaller than the one of IUT_5. More discussion about the optimum size of the top electrode was reported in [28], but basically the IUTs having higher operation frequency have smaller optimum size of top electrodes.

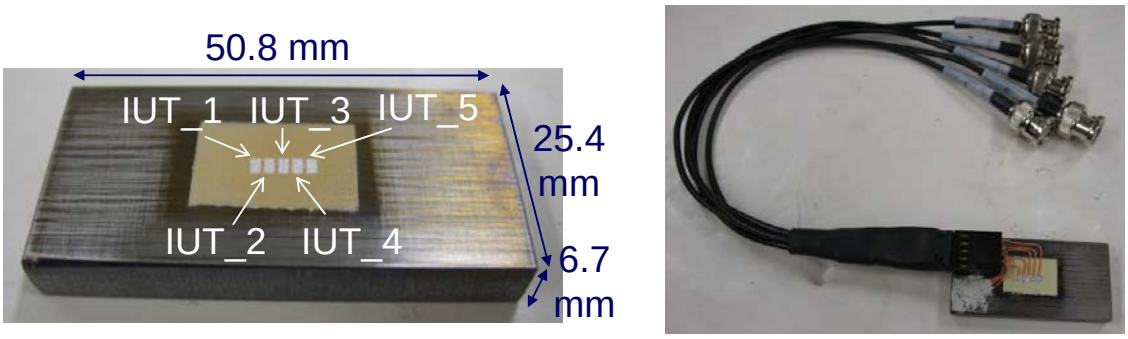

(a) (b)

Figure 2-15 (a) IUT array having the center frequency of 40 MHz. (b) IUT array with connection.

Figure 2-15 (a) shows an IUT array with a small optimum size of top electrodes, because its high operation frequency of 40 MHz. Five 1 mm by 2 mm top electrodes were fabricated on a 14 μm thick PZT-c film. Five insulated wires with 0.5 mm diameter were connected from the five top electrodes to a ten-pin connector glued on the edge of the Ti plate, and the other five insulated wires were connected from the ten-pin connector to the Ti plate which works as IUT bottom electrode. Then five BNC connectors were connected from the other side of the ten-pin connector through five coxial cables. The IUT array with connections was shown in Figure 2-15 (b). Ti plate, instead of steel, with the thickness of 6.7 mm was chosen because some aerospace materials are made of Ti. In order to generate and receive high frequency ultrasound, Panametrics 5073PR which can generate negative 85 V excitation pulses with a pulse width of 6.2 ns and have 75 MHz receiving bandwidth was used. The measured signals in pulse-echo mode of IUT_1 in time and frequency domains were shown in Figure 2-16 where L^n is the nth trip L echo

through the Ti plate thickness. The SNR of the L^2 was 30.7 dB. The measured signals of the other IUTs were similar with IUT_1 and were not shown here.

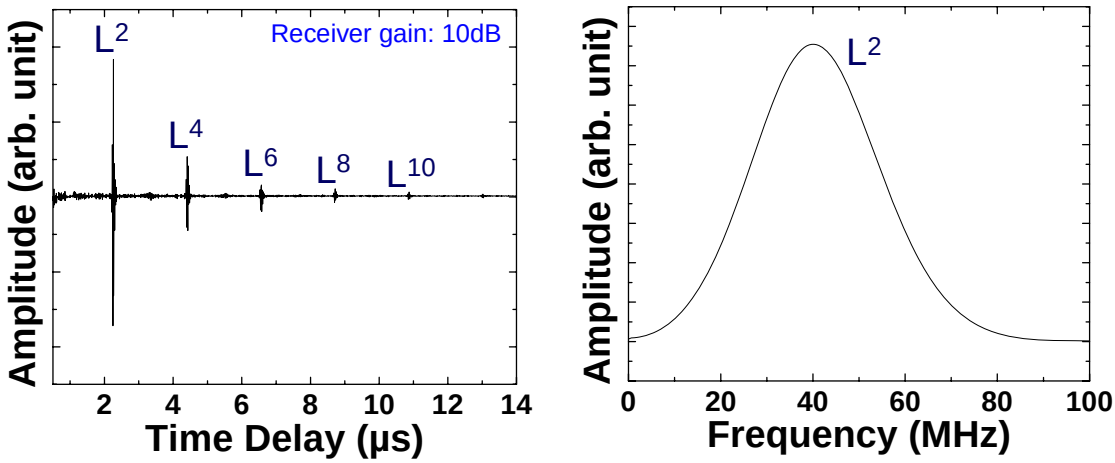

Figure 2-16 Measured ultrasonic signals in pulse-echo mode in (a) time and (b) frequency domain.

The results here show IUT array may be easily achieved by making an array configuration in the sol-gel spray fabrication process. Top electrode size will affect the IUT performance. The ultrasonic signal strength variation due to the top electrode size changing from 5.5 mm into 0.31 mm diameter reaches 57.8 dB. Therefore the top electrode size should be optimized according to the IUT operation frequency. An array IUT with ~40 MHz center operation frequency was demonstrated by five small top electrodes (1 mm by 2 mm) on a sol-gel sprayed PZT-c film (14 μm thick). It is noted that in Section 2.3.3, a FUT array with a 2.6 MHz center operation frequency will be demonstrated by five top electrodes of average 11 mm diameter on a sol-gel sprayed 120 μm thick PZT-c film. Therefore these PZT-c film IUTs or FUTs fabricated by the sol-gel spray technique can operate from a center frequency of 2.6 MHz up to 40 MHz.

2.2.1.3 Performance of PZT-c IUTs at 150°C

An IUT made of a 90 μm thick PZT-c film and deposited onto a 12.7 mm thick steel plate and measured by a handheld EPOCH LT pulser-receiver at 156°C is shown in Figure 2-17. The highest heat treatment temperature for this sample in the furnace was

650°C. The diameter of the silver paste top electrode of this IUT was 6.0 mm, which was optimized for room temperature applications. In Figure 2-18 L^n is the nth trip L echo through the steel plate thickness. The SNR of the L^2 echo at 156°C is 28 dB. In this measurement at 156°C 9.9 dB gains out of the available 100 dB receiver gain was used. This result indicates that this L wave IUT is efficient. At 156°C the center frequency and the 6 dB bandwidth are 8.0 MHz and 7.8 MHz respectively.

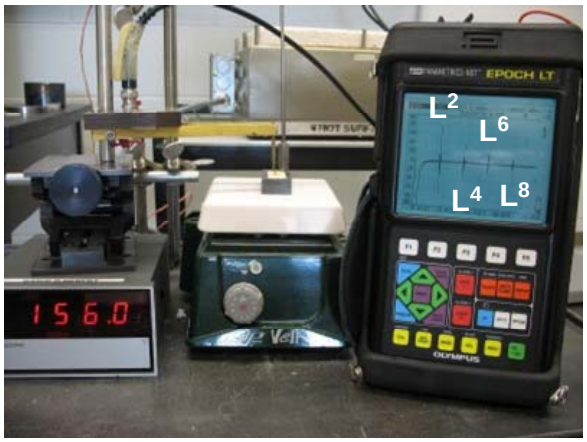

Figure 2-17 Measurement setup for an IUT made of PZT-c film at 156°C using an EPOCH LT.

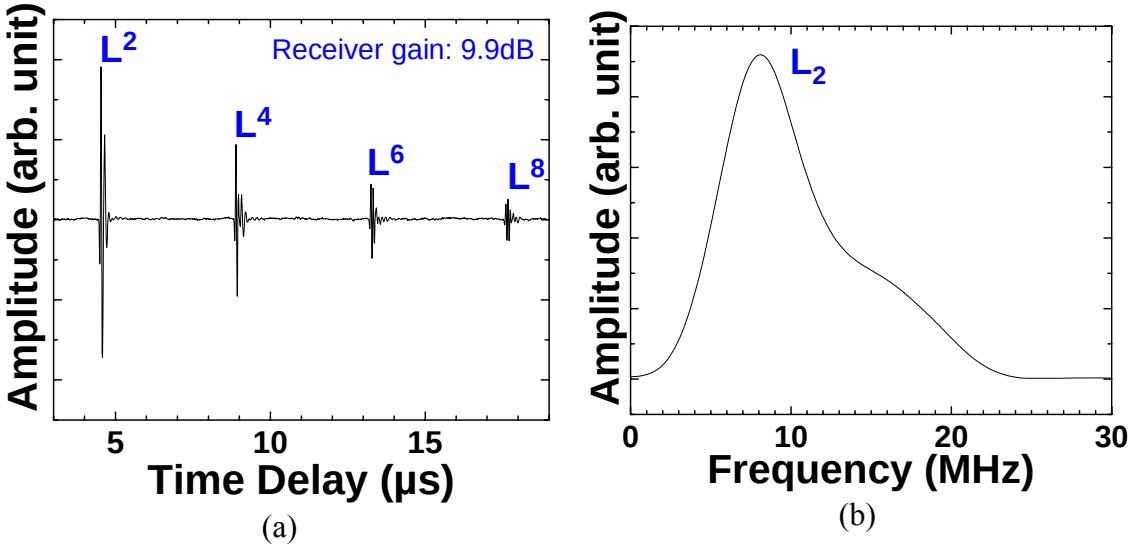

Figure 2-18 Measured ultrasonic data in pulse-echo mode at 156°C in (a) time and (b) frequency domain.

It is noted that PZT-c IUT can function up to at least 150°C. #375 thermal cycles of such IUTs have been carried out. Each thermal cycle consisted of 5-10 minutes heating from room temperature to 150°C, 30 minutes remaining at 150°C and 10 to 30 minutes cooling from 150°C to room temperature. There was no deterioration of the ultrasonic performance after these cycles. It means that the adhesion between the PZT-c film and the steel substrate is strong even though their thermal expansion coefficients have a large difference. #200 hours of electrical fatigue testing with 1 kHz pulse repetition frequency (PRF) of 125 V p-p excitation pulses on a PZT-c film IUT was performed, and there was also no deterioration of the ultrasonic performance.

2.2.2 IUTs made of BIT-c film for applications at temperatures up to 400°C

An IUT made of a 79 μm thick BIT-c film and deposited onto a 12.7 mm thick steel plate which is the same as the one used in Section 2.2.1 and measured by the EPOCH LT at 400°C as shown in Figure 2-19. The BIT-c film was made by sol-gel spray fabrication process as described in Section 2.1. The highest heat treatment temperature for this sample in a furnace was also 650°C. The dimension of the top rectangular silver paste electrode of this IUT is 8.0 mm by 8.0 mm. At 400°C 47.4 dB out of the available 100 dB receiver gain of EPOCH LT was used for producing the L^2 echo reflected form the end of the substrate. The measured ultrasonic data at 400°C in pulse-echo mode after passing through a high pass filter is presented in Figure 2-20 (a) for time domain and in Figure 2-20 (b) for frequency domain, where L^n is the nth trip L echo through the steel plate thickness. At 400°C the center frequency and the 6 dB bandwidth of L^2 echo are 5.5 MHz and 4.6 MHz respectively, and its SNR is 23 dB. It is noted that BIT-c IUT can function up to at least 500°C [28]. However, when above 200°C the contribution of the piezoelectricity mainly comes from BIT powders and not from PZT film solified from the PZT sol-gel. #375 thermal cycles of such IUTs have been carried out. Each thermal cycle consisted of 15 minutes heating from room temperature to 400°C, 30 minutes remaining at 400°C and 20 to 45 minutes cooling from 400°C to room temperature. There was no deterioration of the ultrasonic performance. It also means that the adhesion between the BIT-c film and the steel substrate is strong even though their thermal expansion

coefficients have a big difference. #1500 hours of electrical fatigue testing with 1 kHz PRF of 125 V p-p excitation pulses on a BIT-c film IUT was performed, and there was also no deterioration of the ultrasonic performance. The measured relative dielectric constant of the BIT-c film was about 80. The d_{33} measured by an optical interferometer was 10×10^{-12} m/V [77].

Figure 2-19 Measurement setup for an IUT made of BIT-c film at 400°C using an EPOCH LT.

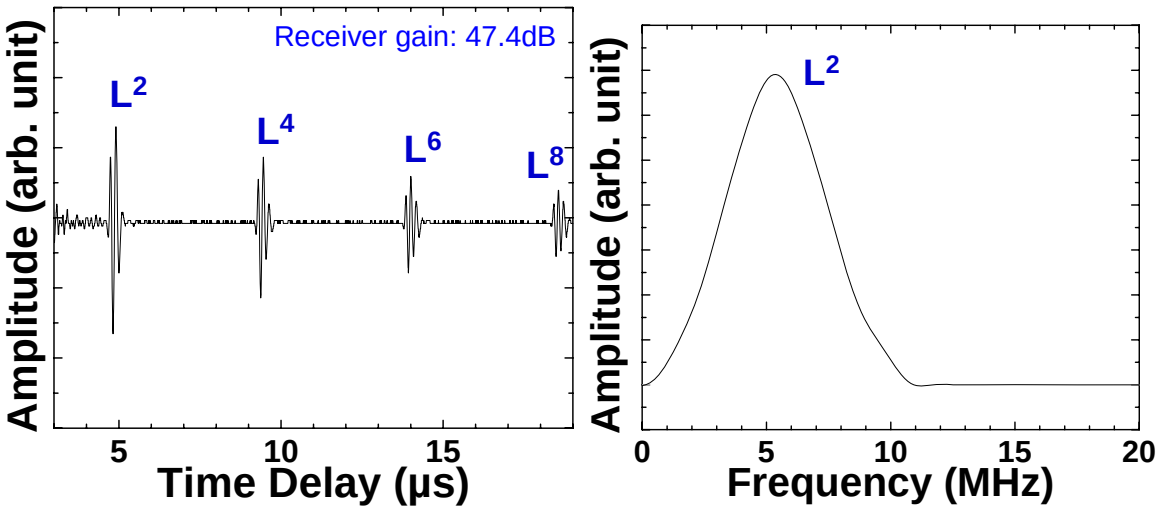

Figure 2-20 Measured ultrasonic data in pulse-echo mode at 400°C in (a) time domain and (b) frequency domain.

2.2.3 IUTs made of $LiNbO_3$-c film for applications at temperatures up to 800°C

Figure 2-21 shows an IUT made of a 125 μm thick $LiNbO_3$-c film and deposited onto a 25.4 mm diameter 26.3 mm long Ti rod and measured by the EPOCH LT at room temperature, and the measured ultrasonic data in pulse-echo mode is shown in Figure 2-22. The Ti rod is chosen because of less oxidation at temperatures higher than 500°C. The heat treatment procedures used here are different from the one used in Sections 2.2.1 and 2.2.2. A specially designed induction heating device, as shown in Figure 2-5, was developed to perform the local heat treatment. The maximum temperature is higher than 700°C. The dimensions of the square top platinum paste electrode of this IUT are 10 mm by 10 mm. The heating setup of an IUT made of $LiNbO_3$-c film using a propane gas torch is shown in Figure 2-23, and the measured ultrasonic data at 800°C in pulse-echo mode after passing through a high pass filter is shown in Figure 2-24 where L^n is the nth trip L echo through the Ti rod length. The center frequency and the 6 dB bandwidth of the L^2 were 4.4 MHz and 3.2 MHz, respectively. At 800°C 90.0 dB out of the available 100 dB receiver gain of EPOCH LT was used for producing the L^2 echo reflected from the end of the rod. The SNR of the L^2 echo at 800°C is 20.3 dB. It is noted that $LiNbO_3$-c IUT can function at even more than 800°C and its relative dielectric constant is ~2. Ten thermal cycles of such IUTs from room temperature to 800°C were performed using a gas torch heating method. Each thermal cycle had a total duration of 40 minutes. There was no deterioration of the ultrasonic performance after ten cycles. It also means that the adhesion between the $LiNbO_3$-c film and the Ti substrate is strong even though their thermal expansion coefficients have a large difference. #1000 hours of electrical fatigue testing with 1 kHz PRF of 125 V p-p excitation pulses on a $LiNbO_3$-c film IUT was performed, and there was also no deterioration of the ultrasonic performance.

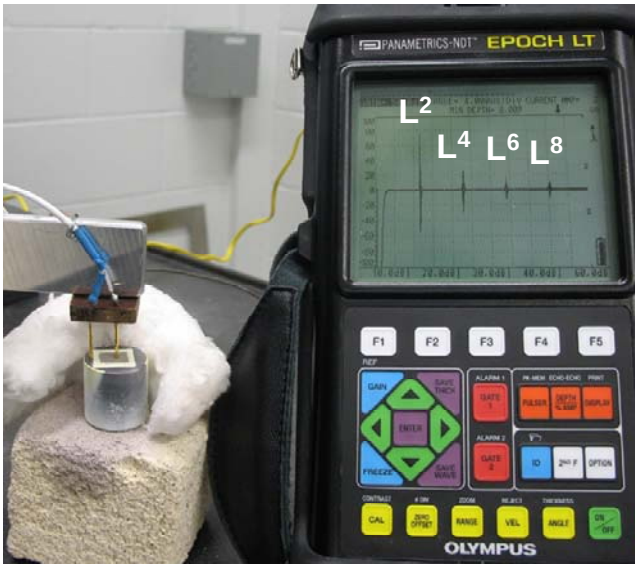

Figure 2-21 Measurement setup for an IUT made of $LiNbO_3$-c film at room temperature using an EPOCH LT.

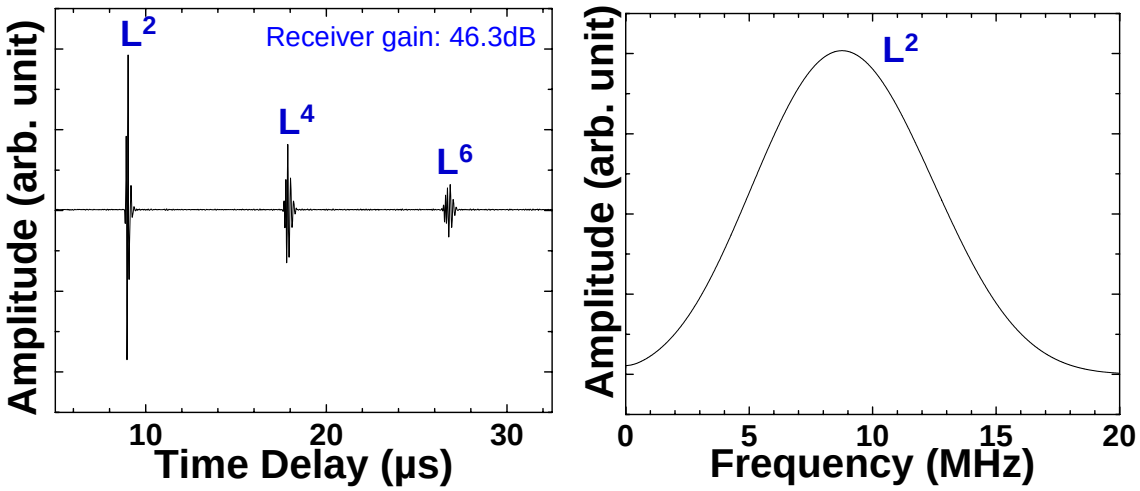

Figure 2-22 Measured ultrasonic data at room temperature in (a) time domain and (b) frequency domain.

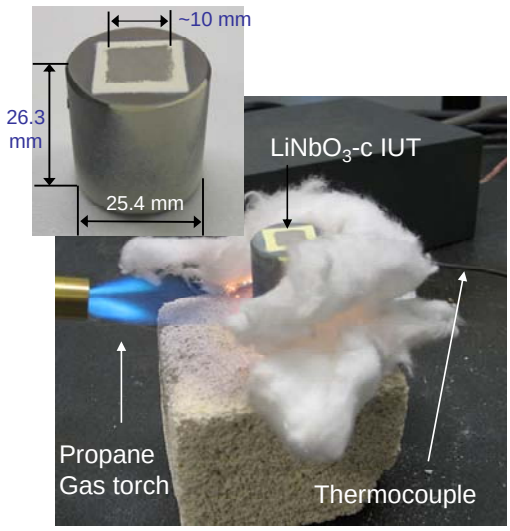

Figure 2-23 Heating of a $LiNbO_3$-c IUT at temperatures up to 800°C.

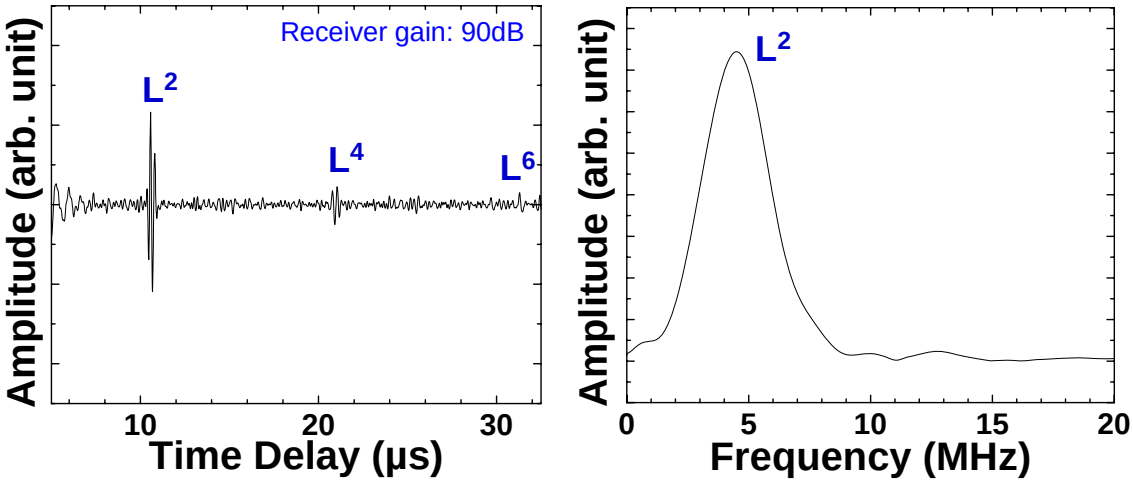

Figure 2-24 Measurement data of an IUT made of $LiNbO_3$-c film in pulse-echo mode at 800°C in (a) time domain and (b) frequency domain.

2.2.4 Performance comparison of IUTs made of PZT-c, BIT-c and $LiNbO_3$-c films

Figure 2-25 (a) and Figure 2-25 (b) show the signal strength variation and SNRs, respectively, of one PZT-c film IUT on a steel plate, one BIT-c film IUT on a steel plate and one $LiNbO_3$-c film IUT on a Ti rod in pulse-echo mode at different temperatures using an EPOCH LT. Figure 2-25 (b) indicates that IUTs made of PZT-c, BIT-c and $LiNbO_3$-c films mentioned above have SNR more than 45 dB, 23 dB and 20 dB,

respectively at all temperatures displayed. Their signal strengths and SNRs may be sufficiently strong for many NDT and SHM applications.

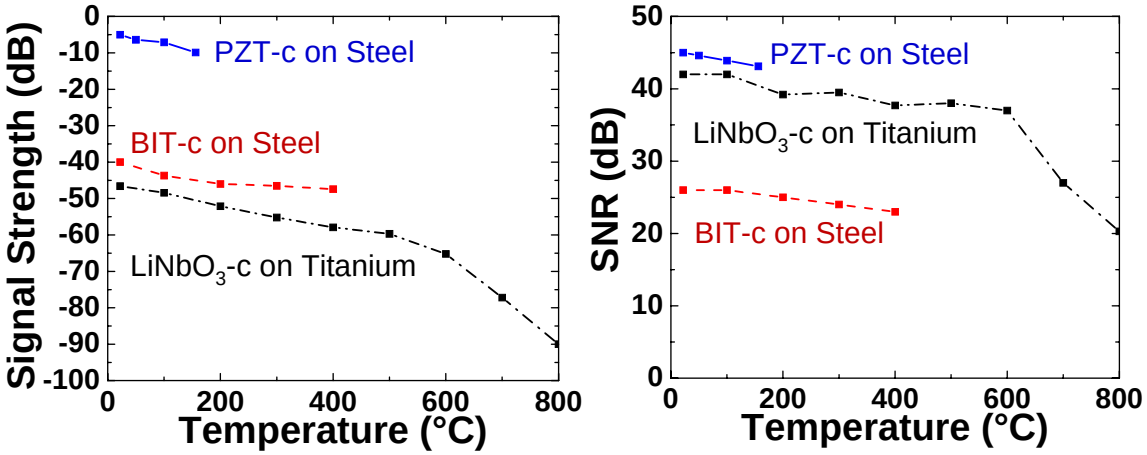

Figure 2-25 (a) Signal strength variation and (b) SNR of PZT-c film on steel, BIT-c film on steel and $LiNbO_3$-c film on Ti in pulse-echo mode at different temperatures using an EPOCH LT.

2.2.5 IUTs deposited onto clad buffer rods

As mentioned in the beginning of this chapter, another objective of this study was to deposit HT IUT onto one end of a long ultrasonic delay line (or buffer rod) [83][84][85], the probing end (opposite to the IUT end) can perform NDT at temperatures even higher than the maximum temperature of the HT IUT (e.g. 800°C). Figure 2-26 (a) presents IUTs made of ~106 μm thick PZT-c film and deposited onto two clad steel buffer rods [84][85] measured by an EPOCH LT system. The temperature at the IUT end is 151°C and that at the other rod end (probing end) is 182°C. The heat treatment procedures used here are also different from the one used in Section 2.2.1 and Section 2.2.2. A specially designed induction heating device, as shown in Figure 2-5, was developed to perform the local heat treatment and the maximum temperature was higher than 700°C.

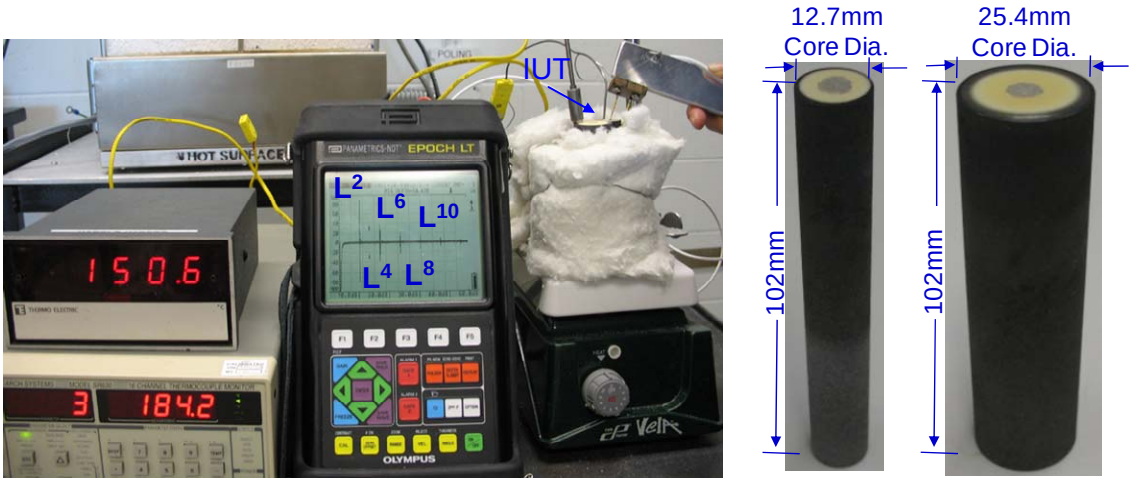

Figure 2-26 Measurement setup for an IUT made of PZT-c film at 150°C using an EPOCH LT.

The clad steel buffer rod [84][85] consists of a steel core and a stainless steel (SS) cladding made by a thermal arc spray process. As shown in Figure 2-26 (b) the clad steel rod shown on the left has a core diameter of 12.7 mm and another shown on the right has a core diameter of 25.4 mm. Both rods have ~1 mm thick SS cladding and a length of 102 mm. The clad steel rod is chosen because of its high SNR, in particular, in pulse-echo mode which provides advantages for in-line ultrasonic monitoring of industrial material manufacturing such as polymer extrusion [86] and molten metal processes [85]. The diameter of the silver paste top electrode of the IUT is 6.5 mm and 7.0 mm, respectively, on the small and large diameter. When the IUT was at room temperature, 50°C, 100°C and 150°C, only 5.0 dB, 5.5 dB, 7.1 dB and 10.1 dB gain, respectively, out of the available 100 dB receiver gain were used for the small diameter clad steel rods for producing the same signal strength of the L^2 echo reflected from the end of the rod. L^n is the nth trip L echo through the rod length. At the probing end (the rod end opposite to the IUT) the measured temperature was 182°C which is 31°C higher than 151°C. It is noted that the length of the probe can be made much longer because of the high signal strength of the IUT and SNR, the temperature at the probing end can be much higher than 151°C. For the large diameter clad buffer rod IUT at room temperature, 50°C, 100°C and 150°C 18.0 dB, 18.1 dB, 18.3 dB and 20.0 dB gains, respectively, were used. The relative dielectric constants of the IUT for small and large diameter clad rods are 290 and 190,

respectively. The difference between the relative dielectric constants of the PZT-c deposited on the clad rods shown in Figure 2-26 (b) and that of the steel plate shown in Figure 2-17 comes from the different heat treatment procedures. The measured ultrasonic data at 150°C in pulse-echo mode for the small and large diameter rods shown in Figure 2-26 (b) are shown in Figure 2-27 (a) and Figure 2-27 (b), respectively. At 150°C the center frequency and the 6 dB bandwidth of the L^2 echo were 7.0 MHz and 5.9 MHz, respectively for the small diameter rod and 6.8 MHz and 3.7 MHz, respectively for the large diameter rod. The SNRs of the L^2 echoes for IUTs at 150°C are 26 dB and 30 dB, respectively, for the small and large diameter clad rods. In Figure 2-27 (b) the reason of the amplitude of L^6 echo is larger than that of L^4 echo is due to the diffraction effect. Figure 2-27 (a) and Figure 2-27 (b) confirm that PZT-c IUTs have attractive performance at 150°C. It is expected that these IUTs deposited onto these clad steel rods will perform the same during thermal cycles as the PZT-c film coated onto steel substrate as mentioned in Section 2.2.1.

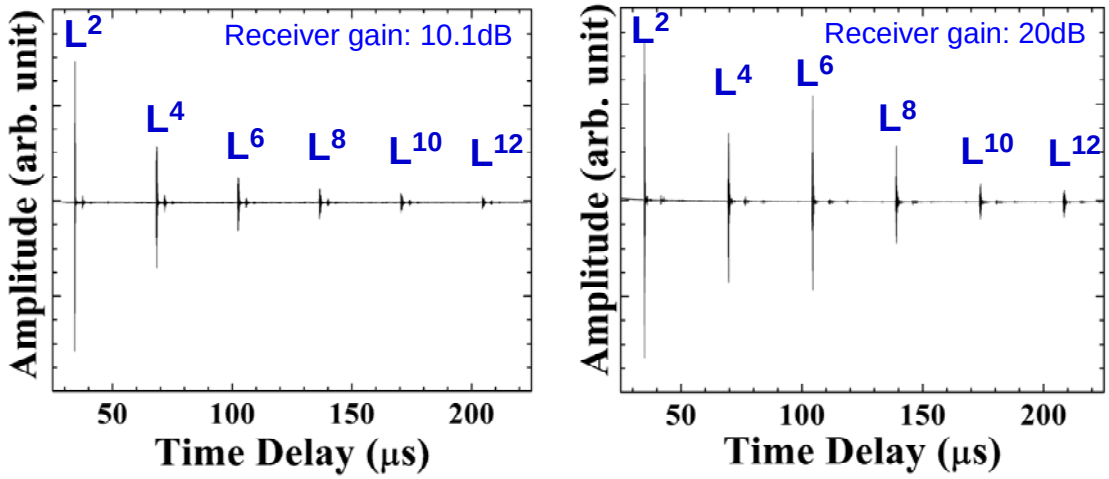

Figure 2-27 Measured ultrasonic data of IUT at 150°C in pulse-echo mode for (a) small and (b) large diameter clad steel rod shown in Figure 2-26 (b).

2.2.6 Thickness measurement accuracy estimation

As mentioned at the beginning of this chapter, corrosion monitoring is an important NDT application. Therefore an example of the thickness measurement accuracy at high temperatures is presented here using the two clad steel rods shown in Figure 2-26 (b). The clad steel rod may represent thick steel samples. The temperature at the IUT side is 151°C and that at the other end of the rod is 182°C. Assuming these two clad rods are under a constant temperature of 150°C, Eq. 2-1 (Eq. 19 in reference [87]) is used here for the estimation of the measurement accuracy for the time delay and then length of the clad steel rod using IUTs, where f_0 is the center frequency, T the time window length for the selected echoes, e.g. L^2 and L^4, for the cross correlation, B the fractional bandwidth of the signal (the ratio of the signal bandwidth over f_0), ρ the correlation coefficient used in cross correlation, SNR_1 and SNR_2 the SNR of the 1st echo (e.g. L^2 in Figure 2-27 (a) and Figure 2-27 (b) for small and large clad rod) and 2nd echo (e.g. L^4 in Figure 2-27 (a) and Figure 2-27 (b) for small and large clad rod), respectively, $\sigma(\Delta t - \Delta t')$ the standard deviation of the measured time delay (Δt the true time delay; $\Delta t'$ the estimated time delay), and V_L (5884 m/s) the measured L wave velocity in the steel core. Since a sampling rate of 100 MHz is used in the experiment, with the use of cross correlation method including interpolation [11] the time measurement error which may be additionally introduced is estimated to be around 2 ns. The best estimated rod length measurement accuracies (assuming under the constant temperature of 150°C) for small and large clad steel rods with a length of 102 mm using the above parameters given in Table 2-1 are 32 μm and 40 μm, respectively. This evaluation demonstrates that IUTs having broad bandwidth and high SNR can be used for accurate corrosion or erosion evaluation which may be in certain aspects considered as a thickness reduction.

$$\sigma(\Delta t - \Delta t') \geq \sqrt{\frac{3}{2 f_0^3 \pi^2 T (B^3 + 12B)} \left(\frac{1}{\rho^2} \left(1 + \frac{1}{SNR_1^2} \right) \left(1 + \frac{1}{SNR_2^2} \right) - 1 \right)} \qquad (2\text{-}1)$$

Table 2-1: Parameters for Eq. 2-1 and digitization resolution.

Parameters	Small dia. Buffer Rod @ 150°C	Large dia. Buffer Rod @ 150°C
f_0	7 MHz	6.8 MHz
T	0.6 μs	0.6 μs
B	5.9/7	3.7/6.8
ρ	0.68	0.7
SNR_1	26 dB	30 dB
SNR_2	19 dB	25 dB
$\sigma(\Delta t - \Delta t')$	9.0 ns	11.7 ns
Digitization resolution (100 MHz) together with interpolation	2 ns	2 ns
Total time delay Uncertainty	11 ns	13.7 ns
V_L	5884 m/s	5884 m/s
Thickness measurement accuracy	32 μm	40 μm

2.3 Fabrication and Ultrasonic Performance of FUTs on Metal Membranes

The other type of sol-gel sprayed HTUTs used in this thesis is FUTs, which can be made off-line and then installed on-site. Since in certain situations parts or structures for NDT cannot be exposed to high fabrication temperatures required for IUTs, then such HT FUTs may be alternatively used for HT NDT or SHM. For HT NDT applications HT ultrasonic couplant must be used between the FUT and sample to be tested, and for HT SHM applications HT FUT may be bonded onto the samples using HT glues.

It is noted that FUTs can be made of piezoelectric polymers such as PVDF [66] and piezoelectric ceramic/polymer composites [67][65][88][89]. However, both materials include polymer which prevents the use of such FUTs at an elevated temperature. For instance, PVDF shows significant piezoelectric deterioration above 65°C. Several copolymers have superior temperature stability compared to PVDF, however, operational temperature is limited to around 90 - 100°C. In addition, piezoelectric polymers have low electromechanical coupling coefficients. Recently piezoelectric PZT paint [90] has been

also reported. At present, such flexible paint transducers only operated up to several hundreds of kHz which is low for certain NDT applications and also suffer low electromechanical coupling coefficient. The operation temperature limit of such piezoelectric paint has not been reported.

The HT FUTs [63] made of sol-gel sprayed piezoelectric films are able to work at HT and are used in this thesis. The sol-gel sprayed film FUTs, called FUTs in this thesis, consist of a metal membrane, a piezoelectric composite film and a top electrode, as shown in Figure 2-28. The flexibility of the FUTs is achieved because of the thinness of metal membrane and the porosity in the composite film. Metal membranes are used as the substrates because they could sustain the heat treatment in the sol-gel srpayed fabrication process described in 2.1 and HT applications. In order to ensure flexibility of FUTs, the thickness of the metal membrane should be small. SS membranes with thickness of 38 μm and 75 μm, and 75 μm thick Ti membranes were used for FUTs in this thesis. Compared to SS membranes, Ti ones have better flexibility and less oxidation after the heat treatment in the sol-gel spray fabrication process. The reduced oxidation between the piezoelectric composite film and Ti membranes seems to improve the FUT ultrasonic performance according to the experimental results, but SS membranes are still worthy of testing due to their ability to be brazed onto steel for aerospace applications [91]. Theoretical calculations showed even thinner membranes can be used [63]. However, the robust properties would be of concern when thinner membranes were used. The other contribution to the FUT flexibility was the porous piezoelectric film made by the sol-gel spray process. The porosity of the sol-gel sprayed PZT-c film mentioned in Secion 2.1 was estimated at more than 20 volume percent [77]. In this section, the PZT-c and BIT-c films with thickness from 50 μm to 120 μm were presented. As the bonding of FUTs at temperatures above 500°C is not easy to be achieved, no FUTs made of $LiNbO_3$-c films for application at temperatures up to 800°C is presented in this thesis.

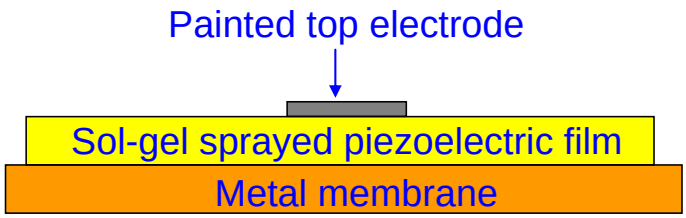

Figure 2-28 Schematic diagram of an FUT made of a sol-gel sprayed piezoelectric film.

2.3.1 FUTs made of PZT-c films for applications at temperatures up to 150°C

An FUT made of a 74 μm thick PZT-c film deposited onto a 75 μm thick Ti membrane was shown in Figure 2-29. The diameter of the silver paste top electrode of this FUT was 5 mm which could achieve the maximum signal strength in pulse-echo mode at room temperature. The FUT was pressed onto a 12.7 mm thick steel plate with a commercially available ultrasonic couplant between them as shown in Figure 2-30, and then measured by a handheld EPOCH LT at room temperature for the performance comparison between the FUT and commercial UTs. The measurement setup is the same with the one performed in 2.2.1.1, except there was no couplant between IUT and steel plate. The measured ultrasonic data in pulse-echo mode is presented in Figure 2-31, where L_n is the nth trip L echo through the steel plate thickness. The center frequency and the 6 dB bandwidth of L_2 echo are 9.8 MHz and 9.3 MHz respectively. 2 dB gain out of the available 100 dB receiver gain of the EPOCH LT were used. The SNR of the L_2 echo is 36.6 dB. The SNR is defined as the ratio of the amplitude of the 1^{st} echo (here L_2) over that of the surrounding noises.

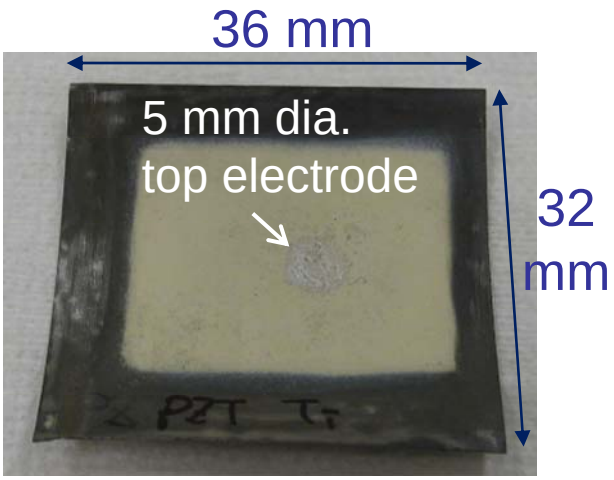

Figure 2-29 FUT made of 5 mm diameter top electrode, 74 μm thick PZT-c film, and 75 μm thick Ti membrane.

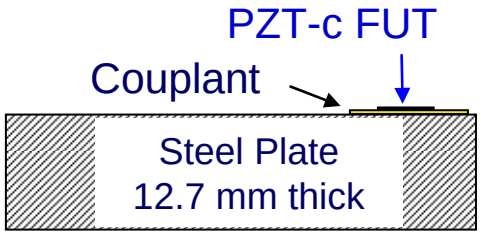

Figure 2-30 Measurement setup of the FUT shown in Figure 2-29 and commercial UTs in pulse/echo mode at a steel plate for ultrasonic performance comparison.

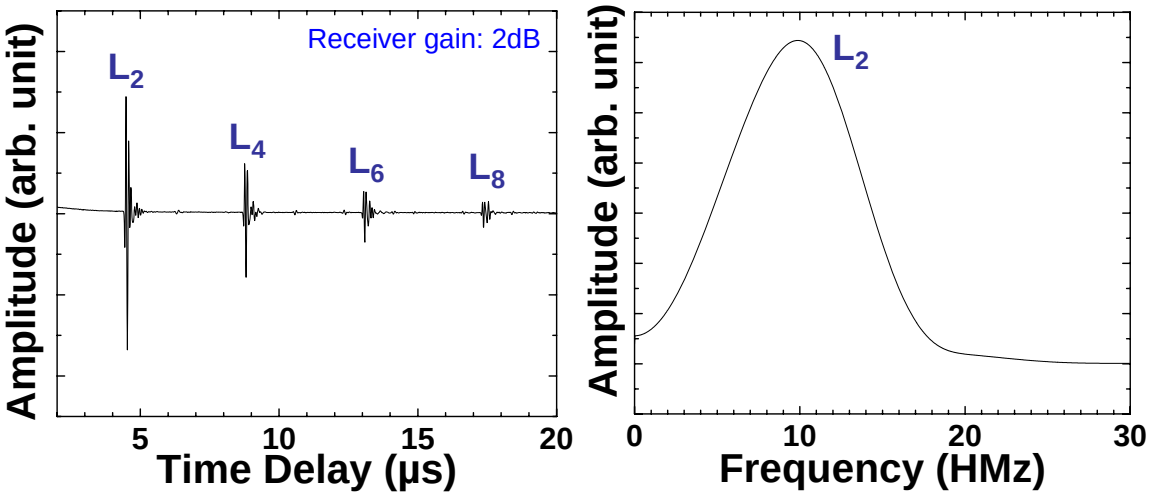

Figure 2-31 Measured ultrasonic data of the FUT in Figure 2-29 in pulse/echo mode in (a) time and (b) frequency domain for a 12.7 mm thick steel plate.

2.3.1.1 Performance comparison between PZT-c film FUTs and commercial UTs at room temperature

The performance comparison between PZT-c film FUTs and commercial UTs was carried out by pressing the commercial broad bandwidth UTs with a center frequency at 5 MHz and 10 MHz at the same steel plate together with the necessary ultrasonic couplant, as shown in Figure 2-32. The measured data of the commercial UTs has been shown in Section 2.2.1.1 for the performance comparison between IUTs and commercial UTs, but was described here again for the performance comparison between FUTs and commercial UTs. The receiver gains used by the EPOCH LT were 2 dB and 4.5 dB, respectively. The center frequency and the 6 dB bandwidth of L^2 echo in Figure 2-11 (a) are 5.5 MHz and 5.3 MHz and those in Figure 2-11 (b) are 8.7 MHz and 8.1 MHz, respectively. These results show that while using the EPOCH LT, the signal strength of the FUT shown in Figure 2-31 was at least as good as those of the two commercially purchased broadband UTs. Moreover, the NDT or SHM applications of FUTs on a curved surface and at HT will be demonstrated in later chapters of this thesis, which may not be achieved easily by commercial broadband UTs.

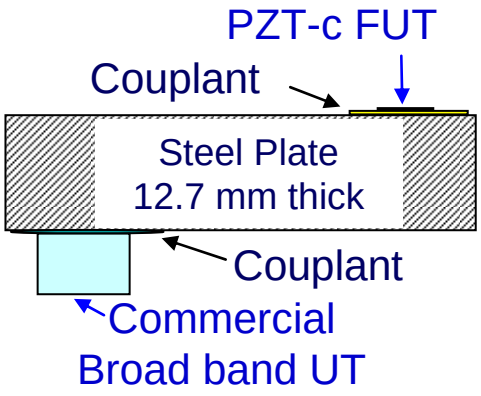

Figure 2-32 Measurement setup of commercial UTs in pulse/echo mode at the same steel plate for ultrasonic performance evaluation of the FUT shown in Figure 2-29.

2.3.1.2 FUT array configuration

Since we have mentioned in Section 2.1.6 that the active areas of IUTs are defined by the top electrodes, an IUT array has been presented in Section 2.2.1.2. Figure 2-33

shows an FUT array made of an 82 μm thick PZT-c film deposited onto a 75 μm thick SS membrane. The array was configured by eight silver top electrodes with the diameter of 4 mm. In order to keep the flexibility of the FUT array, the connections from the top electrodes to the edge of SS membrane were made by sprayed colloidal silver layer, and then connected to coxial cables and BNC connectors. To prevent the short circuit between the colloidal silver connection and the SS membrane, and to prevent the colloidal silver connection directly contacting the PZT-c film and changing the active areas of the FUT, an electrical insulation layer was first deposited onto the SS membrane and PZT-c film except the top electrode areas. This insulation layer was painted by using a small brush and was cured at room temperature for about two hours. Then the colloidal silver was sprayed onto this insulation layer as an electrical connection. Finally, the same insulation material was again painted onto the the whole surface and cured as a protection layer. The schematic drawing of the FUT array was shown in Figure 2-34. Although the connections for eight FUTs were available at the edge of the SS membrane Figure 2-33 (a), only FUT_2 and FUT_7 were connected to BNC connectors for the demonstration purpose as shown in Figure 2-33 (b).

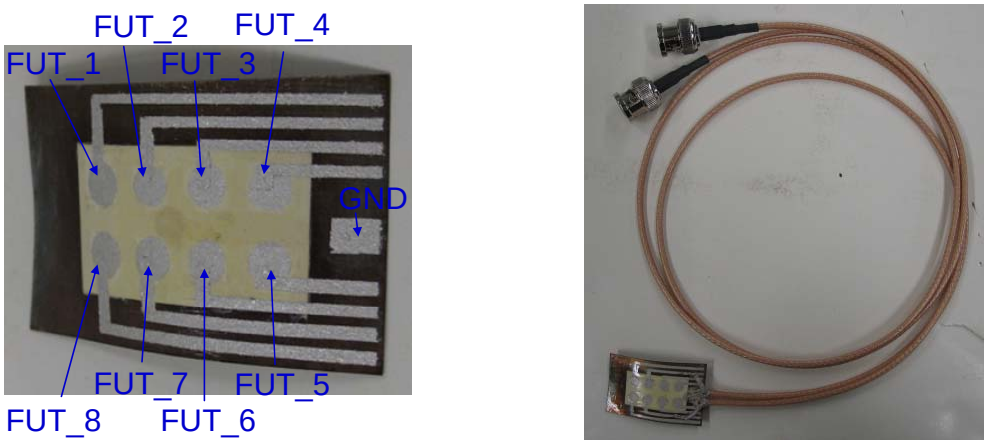

Figure 2-33 (a) PZT-c FUT with array configuration. (b) FUT array with connections for FUT_2 and FUT_7. A 40 mm x 25 mm x 75 μm SS membrane was used as substrates. The eight top electrodes are all 4 mm in diameter.

The measured signals in pulse-echo mode of FUT_2 and FUT_7 on a 13.1 mm thick Al plate were shown in Figure 2-35 where L_n is the nth trip L echo through the Al

plate thickness. The center fequency and the 6 dB bandwidth of FUT_2 and FUT_7 are 8.7 MHz and 8 MHz, 9.6 MHz and 8.7 MHz, respectively. The results here show FUT array can be easily achieved by making array configuration in the sol-gel spray fabrication process.

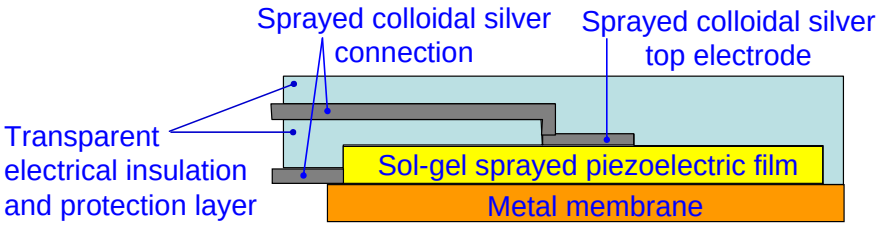

Figure 2-34 Schematic drawing of the FUT array shown in Figure 2-33 (a).

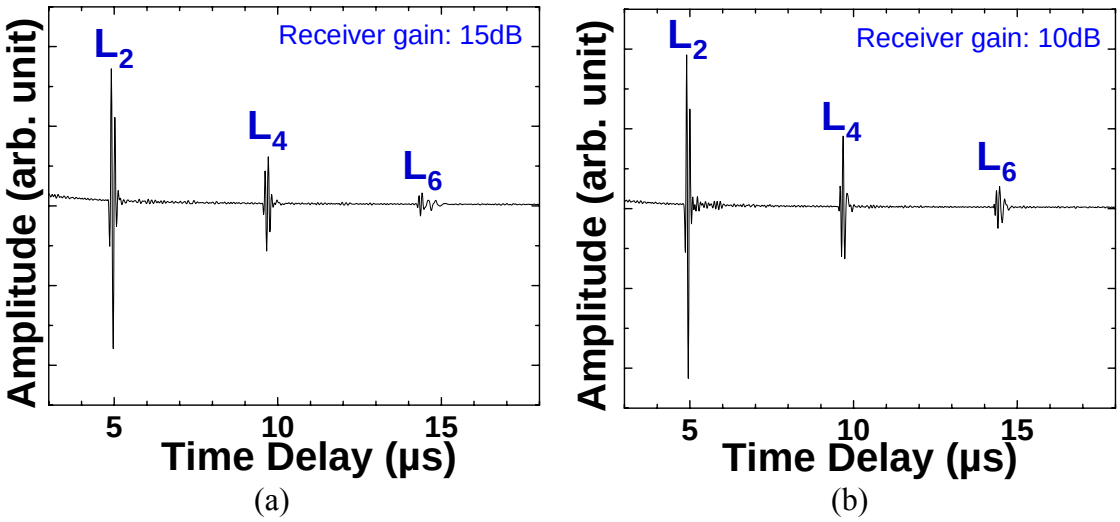

Figure 2-35 Measured ultrasonic signals of the array configuration PZT-c FUT shown in Figure 2-33 on a 13.1 mm thick Al plate. (a) is the signals in the time domain from FUT_2 and (b) FUT_7.

2.3.1.3 Performance of PZT-c FUTs at 150°C

Figure 2-36 shows the measurement setup of an FUT on a 13.8 mm thick SS plate at 150°C. This FUT was made of a PZT-c film deposited onto a 75 μm thick SS membrane. The entire FUT was sandwiched by polyimide film excluding the probing side of the membrane (the side opposite to the PZT-c film), and copper strips were used for electrical connections. HT oil couplants were placed between the probing side of the SS membrane and the SS plate during the measurement.

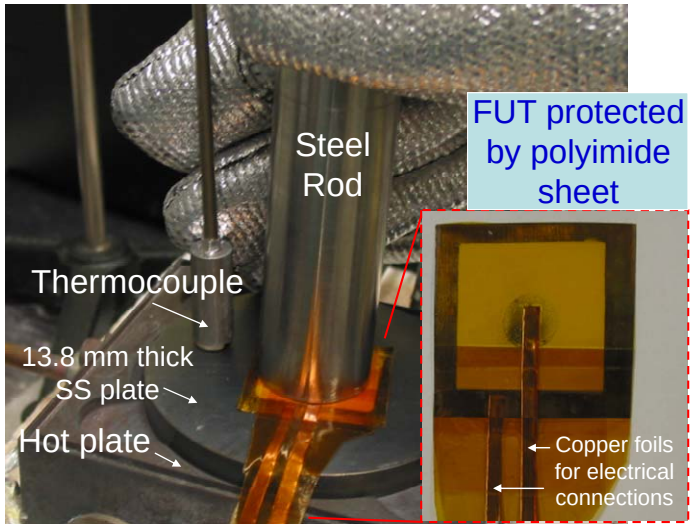

Figure 2-36 Measurement setup for an FUT made of PZT-c film on a 13.8 mm thick SS plate at 150°C. A steel rod was used to make the FUT a good contact with the SS plate for ultrasound propogation. HT oil couplants were placed between the probing side of the FUT and the SS plate during the measurement.

Figure 2-37 and Figure 2-38 show the measured ultrasonic data in pulse-echo at room temperature and at 150°C, respectively. L_2, L_4 and L_6, are the 1st, 2nd and 3rd round trip echoes through the thickness of the SS plate. The center fequency and the 6 dB bandwidth of the L_2 are 3.3 MHz and 3.1 MHz, respectively.

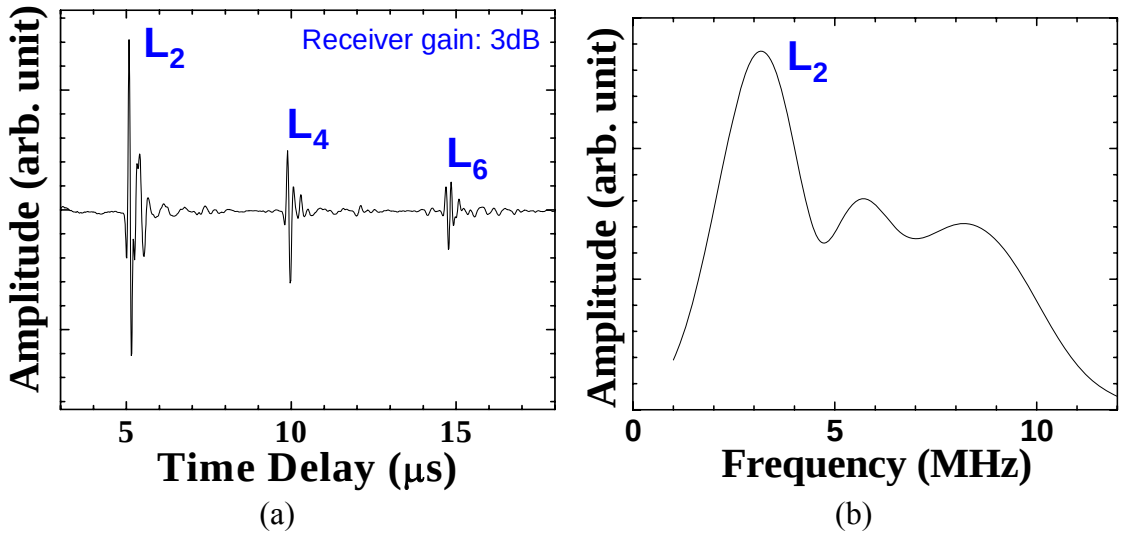

Figure 2-37 Ultrasonic signals of the measurement setup in Figure 2-36 at room temperature in (a) time and (b) frequency domain for a 13.8 mm thick SS plate.

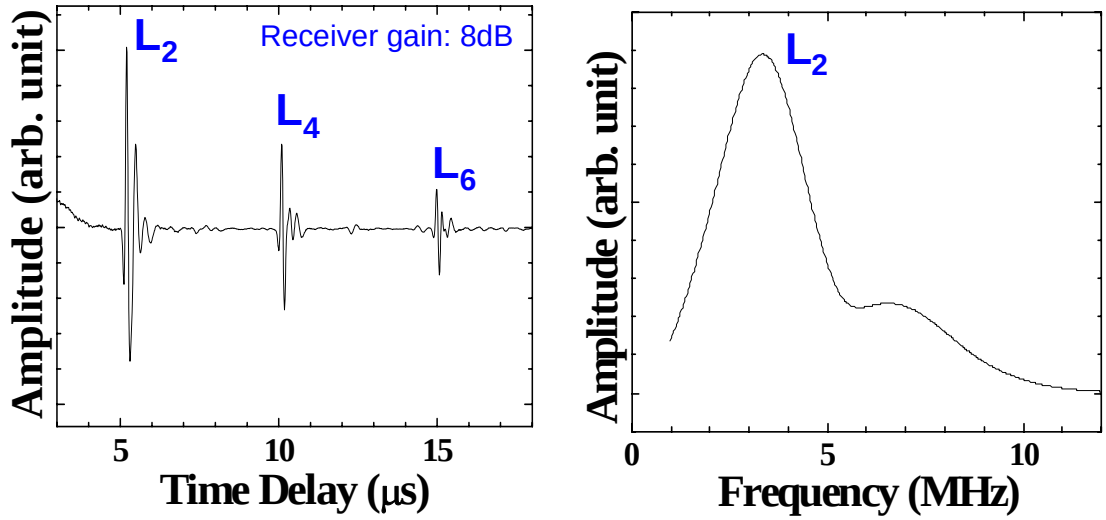

Figure 2-38 Ultrasonic signals of the measurement setup in Figure 2-36 at 150°C in (a) time and (b) frequency domain for a 13.8 mm thick SS plate.

2.3.2 FUTs made of BIT-c film for applications at temperatures up to 400°C

As BIT has Curie temterature of 675°C, FUTs made of BIT-c films on thin metal membranes are used for applications at temperatures of more than 150°C. In this study, a BIT-c film was deposited onto a 38 μm thick SS membrane as an FUT. The BIT-c film was made by the sol-gel spray fabrication process. The sol-gel spray fabrication process was described Section 2.1. The BIT-c FUTs have been examined after a one thousand times bending test with a curvature of 25 mm diameter. There is no observable damage both in visual appearance and ultrasonic performance. Such FUT was bonded onto a 12.7 mm thick steel substrate using a metallic adhesive (from Cotronics Corp., Brooklyn, NY.) cured at 300°C for two hours. Figure 2-39 (a) shows the measurement setup at 303°C for the BIT-c FUT bonded onto a 12.7 mm thick steel substrate, and the measured ultrasonic data after passing through a high pass filter is presented in Figure 2-39 (b) where L_n is the nth trip L echo through the steel plate thickness. The center frequency and the 6 dB bandwidth of the L_2 echo at 303°C were 10.7 MHz and 8.2 MHz, respectively. The SNR of the L_2 echo is 22 dB. The 303°C test temperature is limited due to the HT bonding material used. When the FUT was operated at 303°C, 69 dB gain ±1 dB out of the available 100 dB receiver gain were used. Since the bonding material is used as the HT

ultrasonic couplant, one desires such bonding material which not only provides good ultrasonic coupling between the FUT and the surface of the sample to be tested at HT, but also such that does not induce high noises.

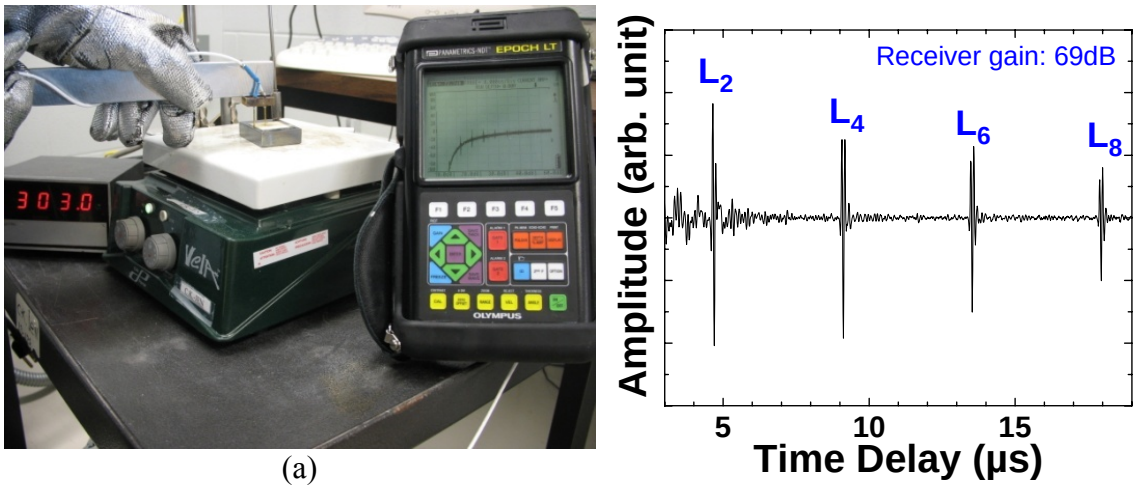

(a) (b)

Figure 2-39 (a) Measurement setup using an EPOCH LT for an FUT made of BIT-c film deposited onto a 38 μm thick SS membrane and bonded onto a 12.7 mm thick steel substrate; (b) Measurement data of the FUT in pulse-echo mode at 303°C.

It is noted that such an FUT or FUT array itself can function at least up to 400°C. It is expected that these FUTs made of BIT-c film and deposited onto SS membrane will perform the same during thermal cycles as the BIT-c film coated onto steel substrate mentioned in Section 2.2.2.

2.3.3 Using PZT-c FUT Array as immersion UT probe

Figure 2-40 illustrates two views of a 120 μm thick PZT-c film with five FUTs array directly fabricated onto a 75 μm thick SS membrane. The five top electrodes have an average diameter of 10 mm and are made by silver paste of about 20 μm thick. Like the FUT presented in Section 2.3.1.3, here the entire transducer array structure was sandwiched by polyimide films excluding the probing side of the membrane, so that it may be protected from the moisture in the environment and could be used as an immersion UT probe. Ultrasonic performance of the array configuration FUT (FUT_3) in

time and frequency domains for NDT of a 13.8 mm thick steel plate at 150°C was shown in Figure 2-41 where L_n is the nth trip L echo through the steel plate thickness. The center frequency, 6 dB bandwidth and SNR of the L_2 echo are determined to be 2.6 MHz, 2.6 MHz and 22 dB, respectively.

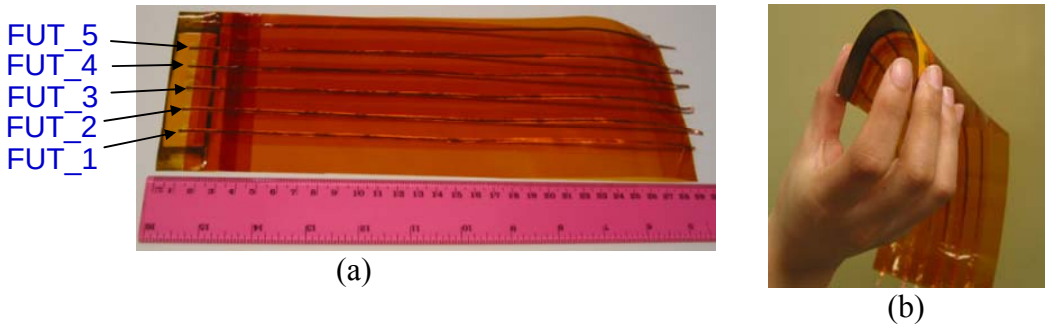

(a) (b)

Figure 2-40 A five UT array FUT with 120 μm thick PZT-c film using a 75 μm thick SS membrane as substrate.

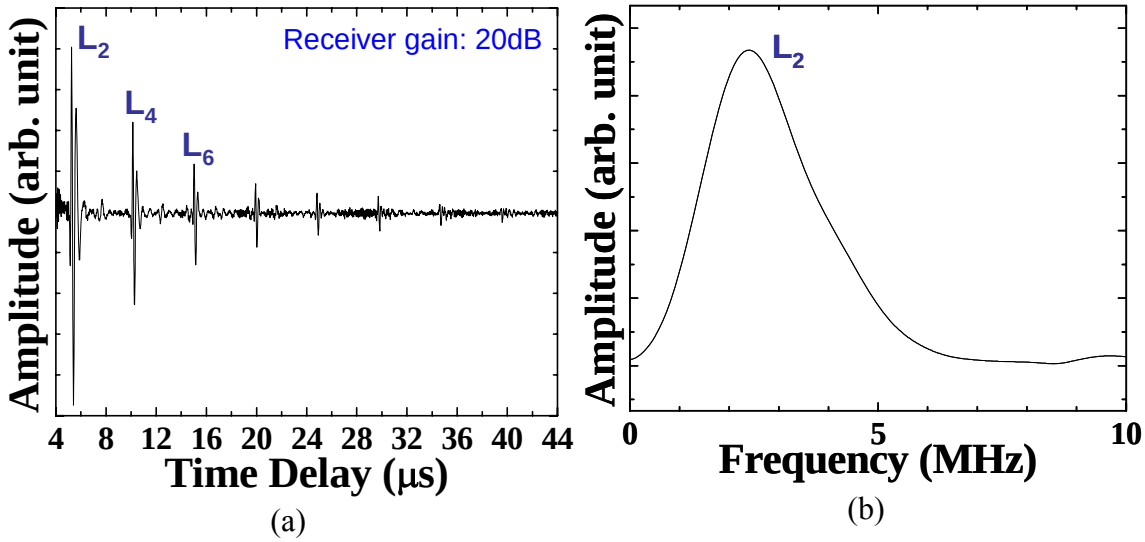

(a) (b)

Figure 2-41 Ultrasonic performance of the array configuration FUT (FUT_3) in (a) time and (b) frequency domains for NDT of a 13.8 mm thick steel plate at 150°C.

To demonstrate that this FUT array could be used as an immersion UT probe, the FUT array shown in Figure 2-40 (a) was completely immersed in water for three days and operated as immersion ultrasonic probes for NDT of Al plate. The measurement setup is shown in Figure 2-42. Figure 2-43 shows the ultrasonic performance of the FUT_3 as shown in Figure 2-40 (a) when placed 46 mm away from a 25.5 mm thick Al plate in a

water tank, where L_n is the nth trip L echo reflected from the front side of the Al plate and $L_{2'}$ is the one reflected from the back side of the Al plate through the plate thickness. The center frequency, 6 dB bandwidth and SNR of the L_2 echo, are determined to be 2.4 MHz, 2.1 MHz and 10 dB, respectively.

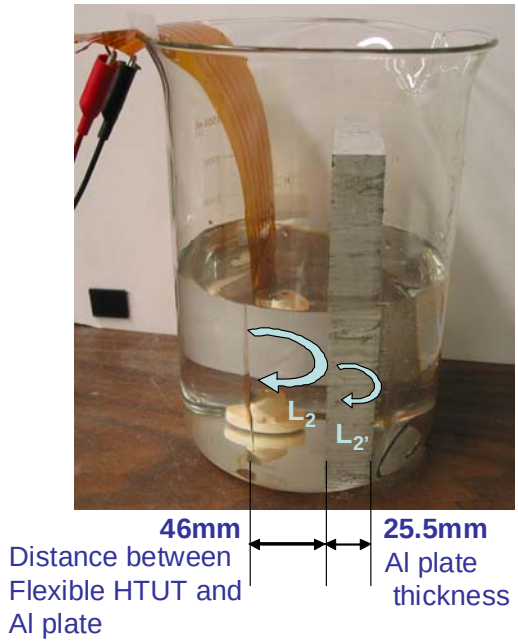

Figure 2-42 Measurement setup for an FUT array operated as an immersion probe for NDT of Al plate.

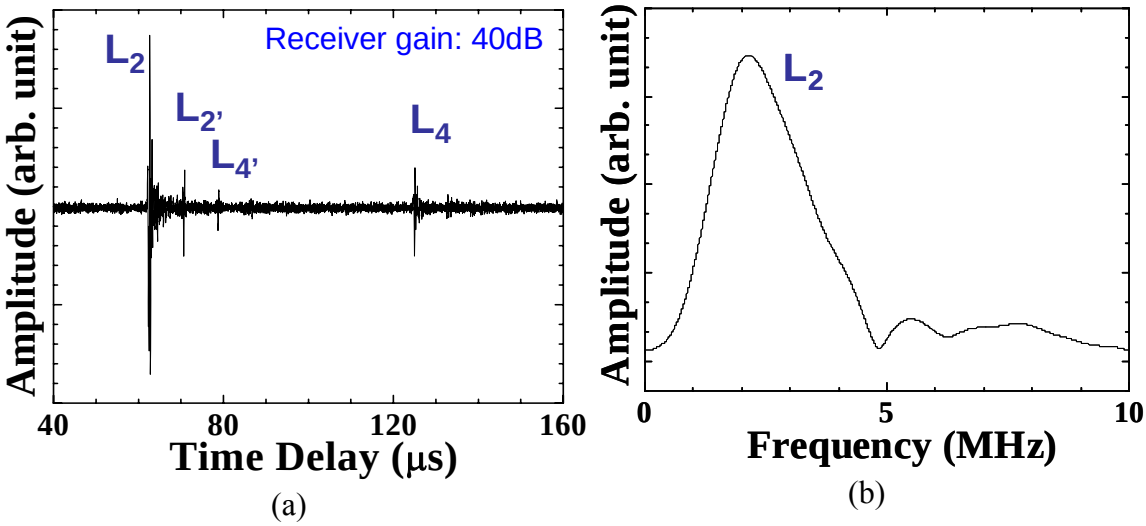

Figure 2-43 Ultrasonic performance of the FUT_3 in (a) time and (b) frequency domains at 22°C immersed in water for NDT of a 25.5mm thick Al plate.

Due to the flexibility of these flexible probes it is our expectation that the inspection of curved objects may be easier than those planar commercially available UTs. The proper curvature of the SS membrane may lead the FUT to become a cylindrically or spherically focused ultrasonic probe as well. In addition, polymer based coating as a water protective layer is also being further developed for immersion FUT applications.

2.3.4 Comparison of FUTs fabricated by sol-gel spray, tape casting and screen printing

Although the sol-gel techninque was used to fabricate the piezoelectric composite films for FUTs and IUTs in the thesis, FUTs made of films fabricated by tape casting [92][93] and screen printing [94][95] were explored and compared with the FUTs made of sol-gel sprayed films. The fabrication process of tape casting and screen printing used in this investigation are briefly described in this section and a comparison of the ultrasonic performances of the FUTs made by these three techniques at room temperature and 150°C is also presented. The objective is to evaluate the alternative methods for FUT fabrication.

2.3.4.1 PZT films made by tape casting and screen printing

Alcohol based solvent and organic binder was first added to the purchased PZT powders. Then the ball milling was operated to achieve the appropriate viscosity as PZT slurry for tape casting and/or screen printing. SS membranes of 75 μm thick, 25 mm wide and 52 mm long were used as substrates for tape casting. Rectangular masks of 23 mm×45 mm square patterns were cut from 120 μm thick masking tapes and placed onto the above mentioned SS membranes. PZT slurry was then applied to the exposed SS surfaces. A straight edge was held at around a 20° angle and manually dragged along the long side of the mask. The PZT slurry was also screen printed in a mesh screen onto the same substrate with the same mask as tape casting. The masked metal strips were fixed slightly below a screen. The PZT slurry was applied on top of the screen. A blunt plastic knife was pressed on the screen and then dragged manually. The fabrication of PZT films

by tape casting and screen printing were carried out at the Institute for Fuel Cell Innovation, NRC.

After tape casting or screen printing, heat treatments of up to 650°C were performed at IMI, NRC. It is noted that the films without further sintering at temperatures higher than 1000°C were used as piezoelectric films in order to assure the flexibility and to avoid microstructure change of SS membranes. Such an approach is the main difference between the reported tape casting and screen printing techniques and our approach presented here. Figure 2-44 and Figure 2-45 show the PZT films onto 75 µm SS membranes fabricated by tape casting and screen printing, respectively. By the tape casting and screen printing, 50 µm thick piezoelectric films were fabricated only by one coating. It was found that these PZT films, especially made by screen printing, had poor mechanical strength and chemical resistance. Chemical treatments will be added for the tape casting and the screen printing process to improve the mechanical strength and chemical resistance but without increasing process temperature.

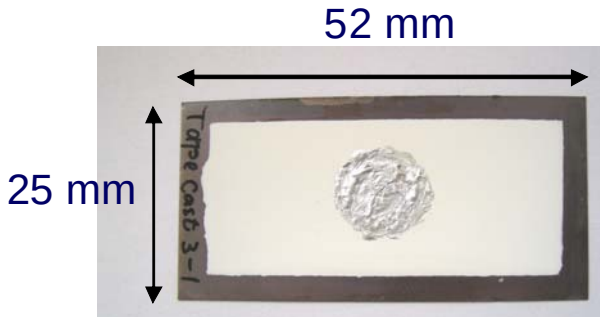

Figure 2-44 Photograph of a a 50 µm thick PZT film coated onto a 75 µm thick SS membrane by tape casting.

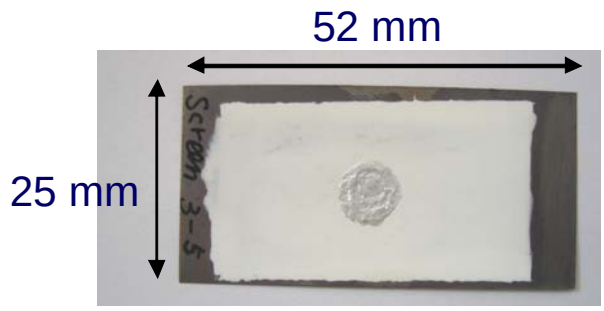

Figure 2-45 Photograph of a a 50 µm thick PZT film coated onto a 75 µm thick SS membrane by screen printing.

2.3.4.2 Corona poling and traditional poling

Films of 50 μm thickness were then electrically poled using a corona discharging technique [96]. The corona poling method was chosen here again because it could pole the piezoelectric powder mixed with low dielectric constant material efficiently over a large area with low risk of short-circuits during poling. It should be mentioned that the traditional poling using two (top and bottom) electrodes were also attempted. But all samples made by tape casting and screen printing were electrically short circuited after such traditional poling. Empirically it was found that during the traditional poling of piezoelectric composite consisting of PZT powders and low dielectric constant material, the leakage current was relatively high, and dielectric breakdown often occurs in a short period. In this study sol-gel sprayed PZT-c films were poled both by corona and traditional poling methods. The sample poled by corona poling had about 15 dB higher signal strength than that poled by traditional poling and the reason could be the limitations of the equipments used in the lab or others.

2.3.4.3 Characterization and ultrasonic performance comparison of the FUTs

The capacitances of every film were measured by a Hewlett Packard 4192A LF Impedance Analyzer at 1 kHz in order to calculate the relative dielectric constant. The diameter of the top electrode was 9 mm for each sample. The relative dielectric constants of 50 μm thick FUTs made by tape casting, screen printing, and sol-gel spray technique were about 55, 20, and 130, respectively. The dielectric constants of PZT bulk powder and sol-gel are 1800 and 300, respectively. The lower dielectric constants of PZT FUTs made by sol-gel spray, tape casting and screen printing compared with that of bulk PZT may reflect higher porosity and existence of bonding material. It is noted that the bonding material of the sol-gel spray technique is PZT sol-gel and it may result in higher dielectric constant than tape casting and screen printing because the dielectric constants of organic residue used in tape casting and screen printing are much lower than that of PZT sol-gel.

The SEM images of the PZT film made by sol-gel spray, tape casting, and screen printing show that the grain size is less than 1 μm and the film was not dense. Due to the

porosity in the piezoelectric film, thin metallic membrane substrate and thin top electrodes, all FUTs made by tape casting, screen printing, and the sol-gel spray technique achieved certain flexibility. This porosity also shows the good agreement with the low dielectric constant results.

In order to compare the ultrasonic performance of the FUTs using the sol-gel spray technique, tape casting and screen printing, the FUTs were pressed onto a 13.8 mm thick SS plate at room temperature. The ultrasonic couplant was placed between the probing side of the SS membrane and SS plate. Figure 2-37 (a) and Figure 2-37 (b) show the transducer response made by the sol-gel spray technique in time and frequency domains, respectively. The center frequency, the 6 dB bandwidth and SNR of the L_2 echo are determined to be 3.3 MHz, about 3.1 MHz and 25 dB, respectively. Figure 2-46 (a) and Figure 2-46 (b) show the transducer response made by tape casting in time and frequency domains respectively, in pulse-echo mode at room temperature. L_2, L_4 and L_6 are the 1st, 2nd, and 3rd round trip echoes through the thickness of the SS plate. The center frequency, the 6 dB bandwidth and SNR of the L_2 echo are determined to be 3.7 MHz, 3.3 MHz and 20 dB, respectively.

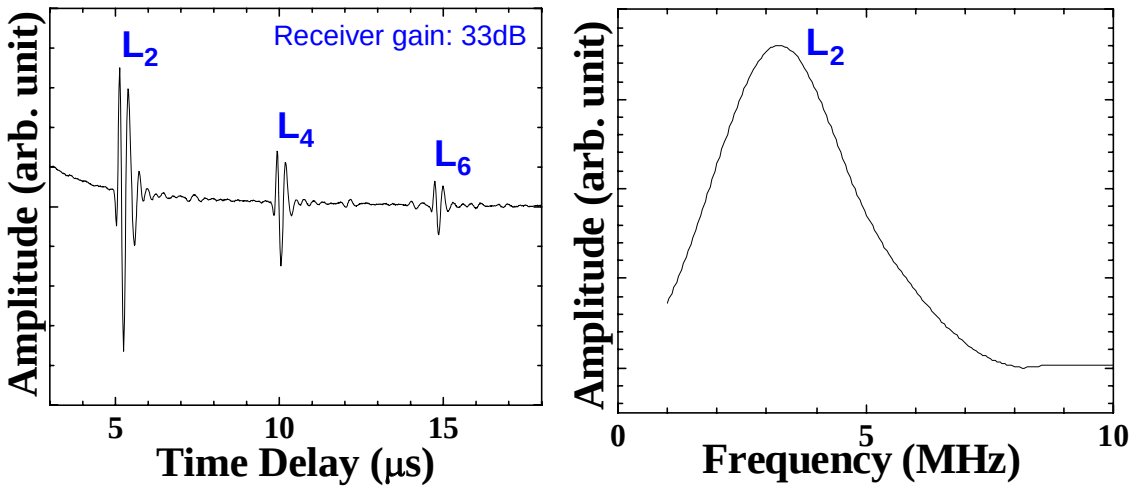

Figure 2-46 Ultrasonic performance of the FUT made by tape casting at room temperature in (a) time and (b) frequency domain for a 13.8 mm thick SS plate.

Figure 2-47 (a) and Figure 2-47 (b) show the transducer response made by screen printing in time and frequency domains respectively, in pulse-echo mode at room temperature. The center frequency, the 6 dB bandwidth and SNR of the L_2 echo are determined to be 3.4 MHz, 3.2 MHz and 20 dB, respectively. It was found out that the signal strengths of the FUTs made by sol-gel spray was 31 dB higher than that of the FUT made by tape casting, and was 50 dB higher than that of the FUT made by screen printing. The low capability of the tape casting and screen printed FUT may be related to the high existence of organic residue and the high porosity. In the observation, the low signal strength and the broadband characteristic indicate that the film will suffer high ultrasonic loss. As it has been mentioned before, further research of chemical treatment of the film may be required to improve the performance.

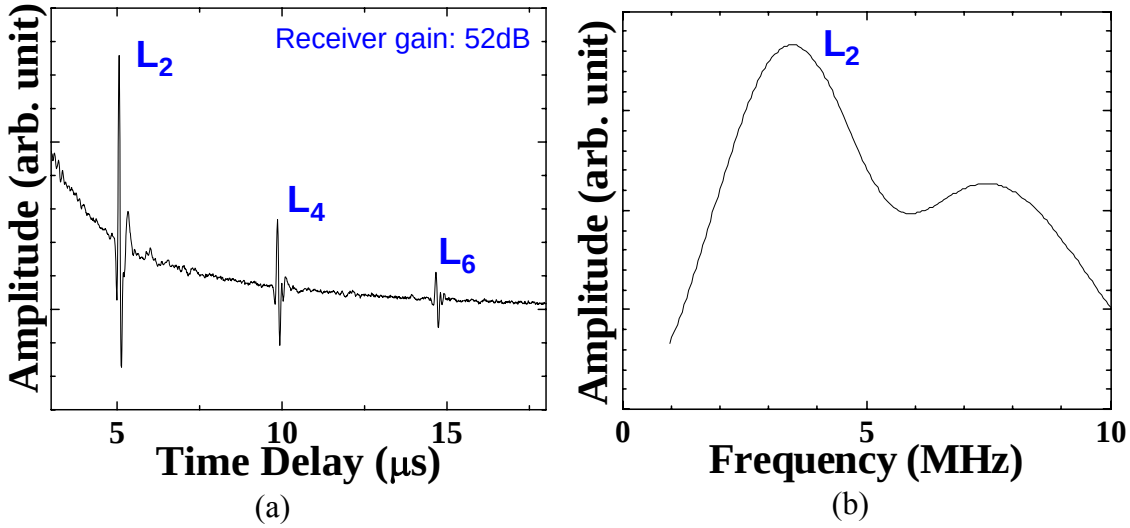

Figure 2-47 Ultrasonic performance of the FUT made by screen printing at room temperature in (a) time and (b) frequency domain for a 13.8 mm thick SS plate.

In order to demonstrate the performance of the FUT made by the sol-gel spray technique and tape casting at an elevated temperature, the FUTs were pressed onto the same SS plate, which was used in the previous experiment but heated up to 150°C here. HT oil couplant was placed between the probing side of the SS membrane and SS plate. Figure 2-38 (a) and Figure 2-38 (b) show the transducer response made by the sol-gel spray technique, in time and frequency domains respectively, in pulse-echo mode at

150°C. The center frequency, the 6 dB bandwidth and SNR of the L_2 echo are determined to be 3.3 MHz, 3.1 MHz and 25 dB, respectively. Figure 2-48 (a) and Figure 2-48 (b) show the transducer response made by tape casting, in time and frequency domains respectively, in pulse-echo mode at 150°C. The center frequency, the 6 dB bandwidth and SNR of the L_2 echo are determined to be 3.7 MHz, 3.5 MHz and 20 dB, respectively. Both FUTs were about 5 dB weaker than the measurement results at room temperature. It means that at 150°C the signal strength of the FUT made by the sol-gel spray method is still 31 dB stronger than that made by the tape casting method. The sol-gel spray process has therefore been chosen for the remaining part of this thesis.

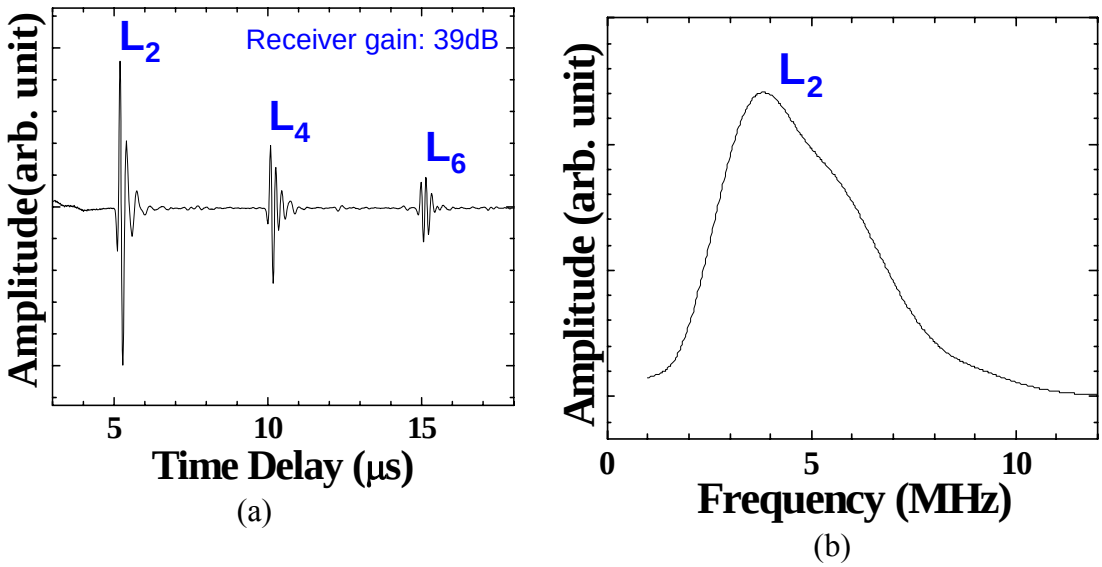

Figure 2-48 Ultrasonic performance of the FUT made by tape casting at 150°C in (a) time and (b) frequency domain for a 13.8 mm thick SS plate.

2.4 Fabrication and Ultrasonic Performance of FUTs on Polyimide Membranes

Instead of using metal membranes as FUT substrates presented in Section 2.3, a 50 μm thick polyimide membrane was chosen due to its promising flexibility, better acoustic impedance match with composite material than with a metal membrane, and the capability to sustain heating at up to 350°C. The HT capability of polyimide is important at the fourth step (heat treatment) of the sol-gel spray fabrication process. The flow chart

of the sol-gel based UT fabrication process for non-conductive substrates is shown in Figure 2-49, which consists of the same six main steps: (1) powders and solution preparation, (2) mixing and ball milling, (3) spray coating, (4) heat treatment, (5) electrical poling, and (6) top electrodes fabrication, described in Section 2.1.1, but an additional step is required when the substrates are non-conductive. Because the polyimide membrane is non-conductive, it is required to fabricate the bottom electrode layer before spray coating of piezoelectric composite film.

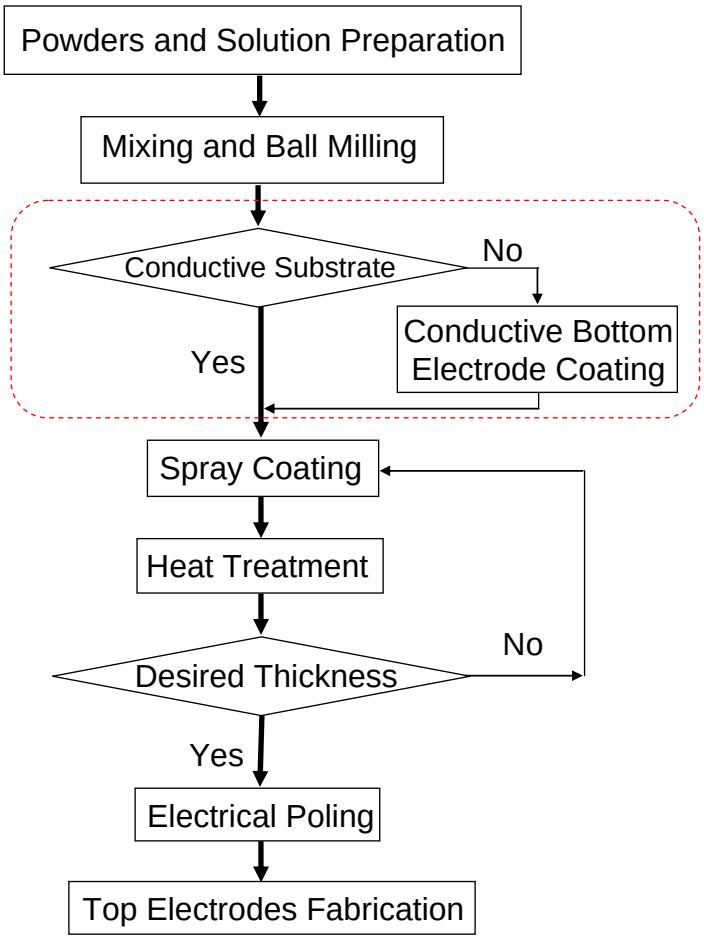

Figure 2-49 Flow chart of sol-gel based UT fabrication process for non-conductive substrates. The steps enclosed by the red dashed line are added for non-conductive substrates and are different from the process described in Figure 2-1.

In this thesis, two methods, spray coating and electroless plating, were chosen to build up bottom electrode layer. For spray coating, silver colloid was sprayed directly

onto polyimide membrane by using an airbrush and cured around 120°C. The thickness of the sprayed silver layer was ~2 µm. Colloidal silver spray is a direct coating approach. For electroless plating, nickel plating is chosen because of simplicity. First, polyimide membranes were immersed in electroless nickel bath containing nickel salt, reducing agent, and complexing agent for nickel. Then the electroless bath was heated at 90°C and the immersion time was about 10 minutes. The thickness of electroless plated nickel alloy layer was less than 1 µm. After the conductive layer was coated onto the polyimide as the bottom electrode, the following steps were similar to the ones to fabricate sol-gel sprayed film onto metal substrates presented in Section 2.3.

2.4.1 Ultrasonic performance of FUTs onto metal materials

Figure 2-50 shows an FUT array using polyimide membrane coated with colloidal silver. First an approximately 2 µm thick colloidal silver layer is sprayed onto the polyimide membrane as the bottom electrode. Then a 60 µm thick PZT-c film was fabricated onto the bottom electrode. The schematic diagram and an actual four-transducer FUT array used for this study are shown in Figure 2-50 (a) and Figure 2-50 (b), respectively. The top four electrodes have an average diameter of 8.5 mm and they are made by silver paste of about 20 µm thick. The flexibility of such FUTs is achieved due to the thin polyimide, porous PZT-c ceramics (~20% porosity) and thin electrodes [28][63].

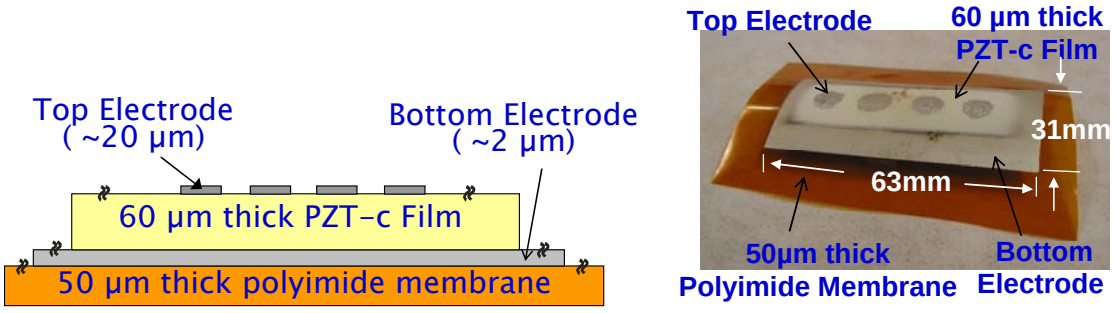

(a) (b)

Figure 2-50 (a) Schematic diagram and (b) an actual FUT using 50 µm thick polyimide membrane as the substrate. A ~2 µm thick colloidal silver layer was sprayed onto the polyimide membrane as the bottom electrode.

The FUT array shown in Figure 2-50 (b) was then pressed onto a 13.8 mm thick SS plate at room temperature and 150°C. HT oil couplant was placed between the probing side of the polyimide membrane and the SS plate. Figure 2-51 shows the measured signals in time and frequency domains, in pulse-echo mode at room temperature. L_2, L_4 and L_6 are the 1st, 2nd and 3rd round trip echo through the thickness of the SS plate. The center frequency, 6 dB bandwidth and SNR of the L_2 echo were 11.3 MHz, 5.1 MHz and 24 dB, respectively. The measured signals at 150°C are shown in Figure 2-52. It is observed that the signal strength of the L_2 echo at room temperature was decreased by about 5 dB as the FUT operated at 150°C.

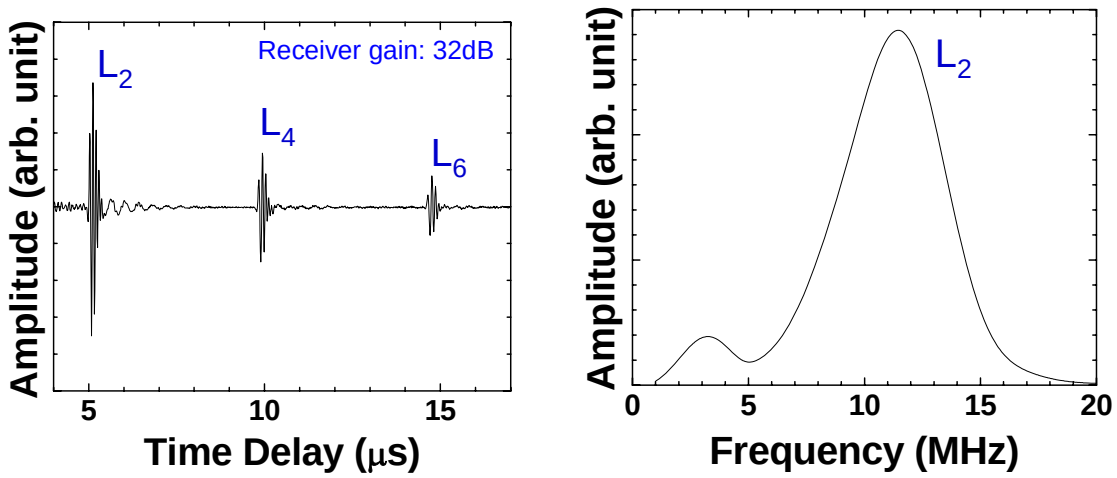

Figure 2-51 Ultrasonic performance of the FUT shown in Figure 2-50 pressed onto a 13.8 mm thick SS plate in (a) time and (b) frequency domain at room temperature. Pulse-echo mode was used.

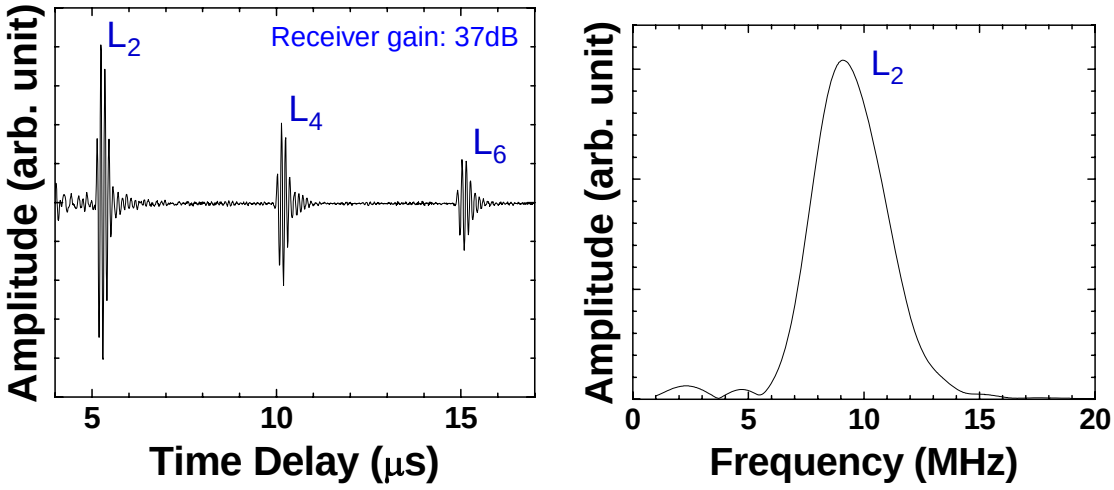

Figure 2-52 Ultrasonic performance of the FUT shown in Figure 2-50 pressed onto a 13.8 mm thick SS plate in (a) time and (b) frequency domain at 150°C. Pulse-echo mode was used.

Figure 2-53 shows an FUT using polyimide membrane with electroless nickel alloy layer as bottom electrode. The thickness of electroless nickel alloy layer was less than 1 μm, and the PZT-c film was about 61 μm thick. Then this FUT was also pressed onto a 13.8 mm thick SS plate for ultrasonic performance evaluation at room temperature and 150°C. The measured signals in pulse-echo mode at room temperature in time and frequency domains were shown in Figure 2-54, where L_n is the nth trip echo through the thickness of the SS plate. The center frequency, 6 dB bandwidth and SNR of the L_2 echo is 13.8 MHz, 5.5 MHz and 17 dB, respectively. The measured signals at 150°C were shown in Figure 2-55. It is observed that the signal strength of the L_2 echo at room temperature was decreased by about 6 dB as the FUT operated at 150°C.

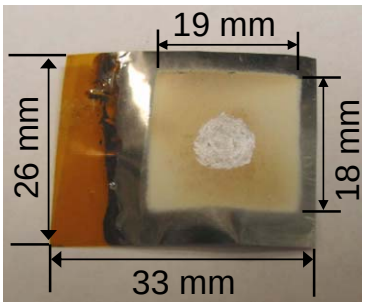

Figure 2-53 An FUT using polyimide membrane as the substrate with electroless coated nickel alloy layer as bottom electrode.

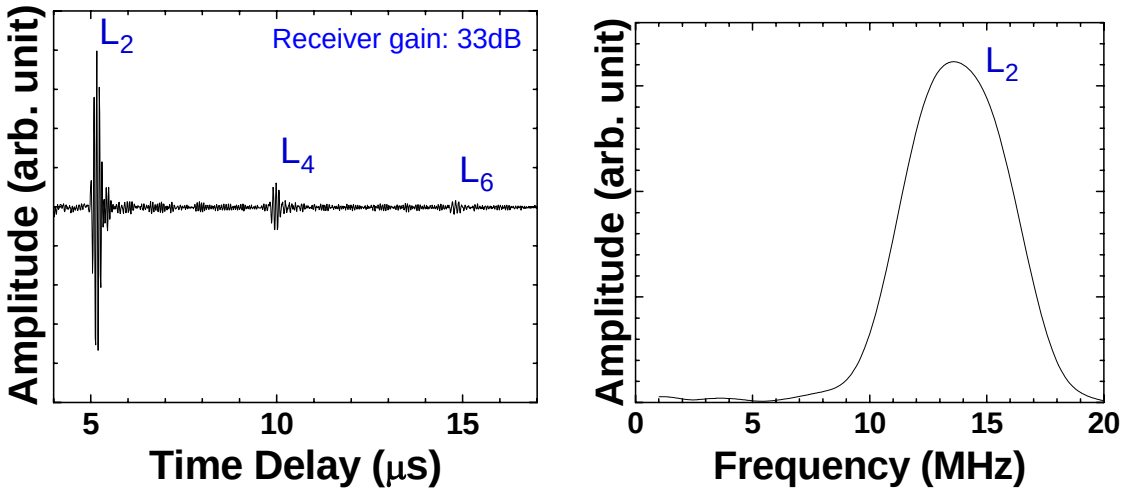

Figure 2-54 Ultrasonic performance of the FUT shown in Figure 2-53 pressed onto a 13.8 mm thick SS plate in (a) time and (b) frequency domain at room temperature.

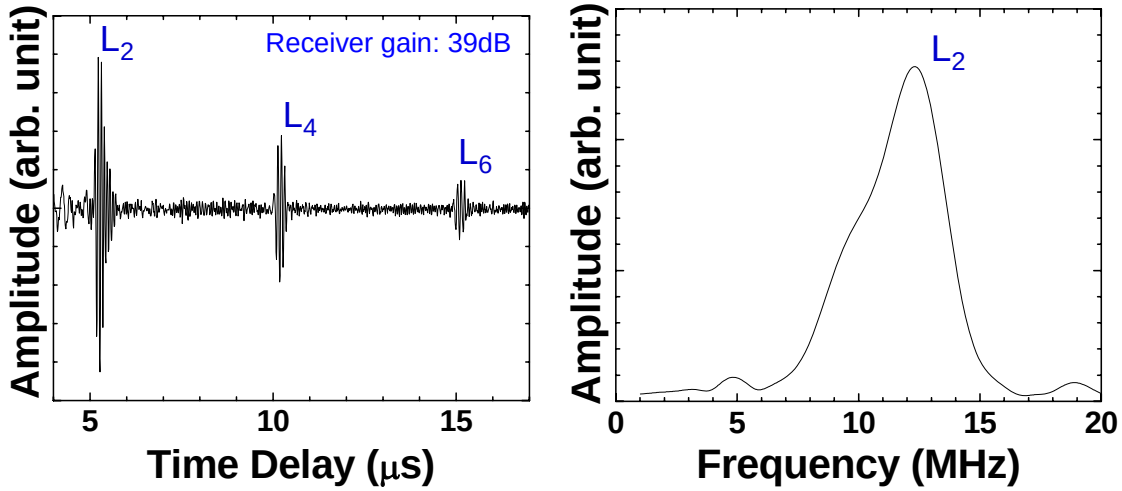

Figure 2-55 Ultrasonic performance of the FUT shown in Figure 2-53 pressed onto a 13.8 mm thick SS plate in (a) time and (b) frequency domain at 150°C.

According to the data observed in this section, the FUTs using polyimide membranes coated by colloidal silver spray or electroless nickel plating have similar ultrasonic performance. Compared to the FUTs using metal as substrates presented in Section 2.3.1, the FUTs using polyimide as substrates are about 30 dB weaker in ultrasonic signal strength for NDT of metal materials, due to the lower fabrication temperature of the FUTs on polyimide membranes. However, the FUTs on polyimide

membranes have promising flexibility, and acoustic impedance match with composite materials. The ultrasonic performance of FUTs onto Gr/Ep composites will be presented in the following section.

2.4.2 Ultrasonic performance of FUTs onto Gr/Ep composites

Due to its promising flexibility, the FUT can be wrapped around a human thumb. Here the FUT shown in Figure 2-50 (b) is attached to the cylindrical tube made of braid Gr/Ep composite of 3.3 mm thickness with a commercially available ultrasonic couplant as shown in Figure 2-56. The inner diameter of the cylinder is 76 mm. Figure 2-57 shows the measured ultrasonic signals using one of the four FUTs in Figure 2-50 (b). The gain was 51 dB out of the available 100 dB receiver gain when the EPOCH LT was used. The center frequency and 6 dB bandwidth of the L_2 echo are 1.9 MHz and 3.0 MHz, respectively.

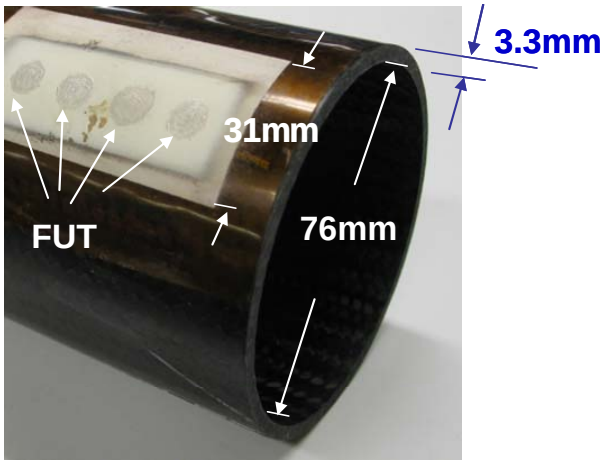

Figure 2-56 An FUT shown in Figure 2-50 (b) was attached onto the external surface of a cylindrical braid Gr/Ep composite of 3.3 mm thickness.

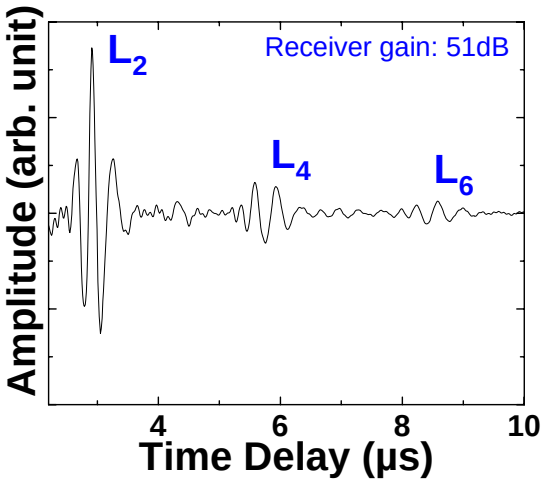

Figure 2-57 Measured ultrasonic signals in time domain at room temperature using the measurement setup shown in Figure 2-56.

FUT can be also used to evaluate thick Gr/Ep composite. Figure 2-58 shows that the same FUT shown in Figure 2-50 (b) is attached to a 27.9 mm thick 0° and 90° cross plies Gr/Ep composite with a normal ultrasonic couplant. The measured ultrasonic signals using one of the four FUTs in the FUT array are given in Figure 2-59. The center frequency and 6 db bandwidth of the L_2 echo are 2.2 MHz and 1.6 MHz, respecrively.

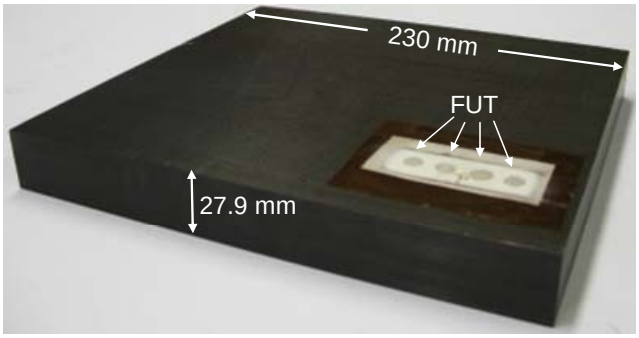

Figure 2-58 An FUT shown in Figure 2-50 (b) was attached onto the top surface of a 27.9 mm thick 0° and 90° cross plies Gr/Ep composite plate.

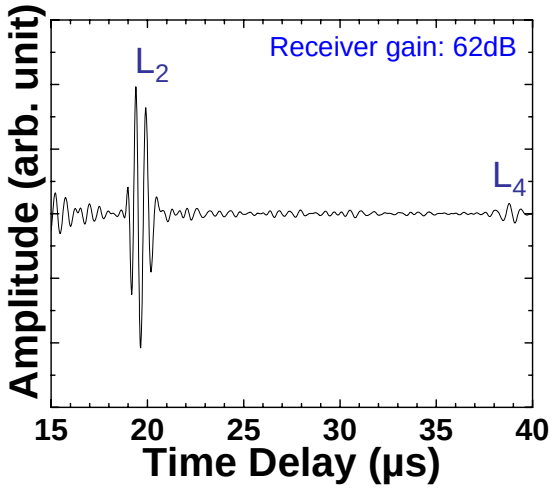

Figure 2-59 Measured ultrasonic signals in time domain at room temperature using the measurement setup shown in Figure 2-58.

A 6.9 mm thick Gr/Ep sample with delaminations caused by impact damage is used for the demonstration of the defect detection capability of FUT as shown in Figure 2-60. This sample was firstly inspected by an ultrasonic C-scan and the locations of the good and delaminated regions were identified. Then the same FUT shown in Figure 2-50 (b) is attached to the Gr/Ep composite plate with a normal ultrasonic couplant. The measured ultrasonic signals gone through a 1 MHz high pass filter using one of the four FUTs at the region without and with delaminations are given in Figure 2-61 (a) and Figure 2-61 (b), respectively. The center frequency and 6 dB bandwidth of the L_2 echo, the first echo through the plate, are 6.8 MHz and 6.6 MHz, respectively. The center frequency and 6 dB bandwidth of the $L_{D,2}$ echo, the first echo reflected from the delamination, are 9.9 MHz & 7.8 MHz, respectively. The gain was 55 dB out of the available 100 dB receiver gain when the EPOCH LT was used. It is clearly demonstrated that FUTs may be used for NDT and SHM of Gr/Ep composites.

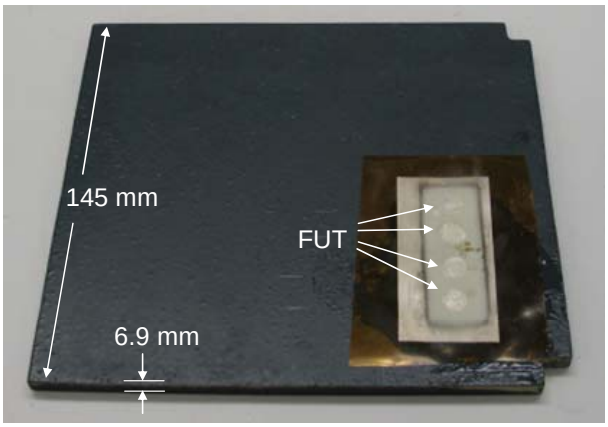

Figure 2-60 An FUT shown in Figure 2-50 (b) was attached onto the top surface of a 6.9 mm thick Gr/Ep composite plate having impact damages.

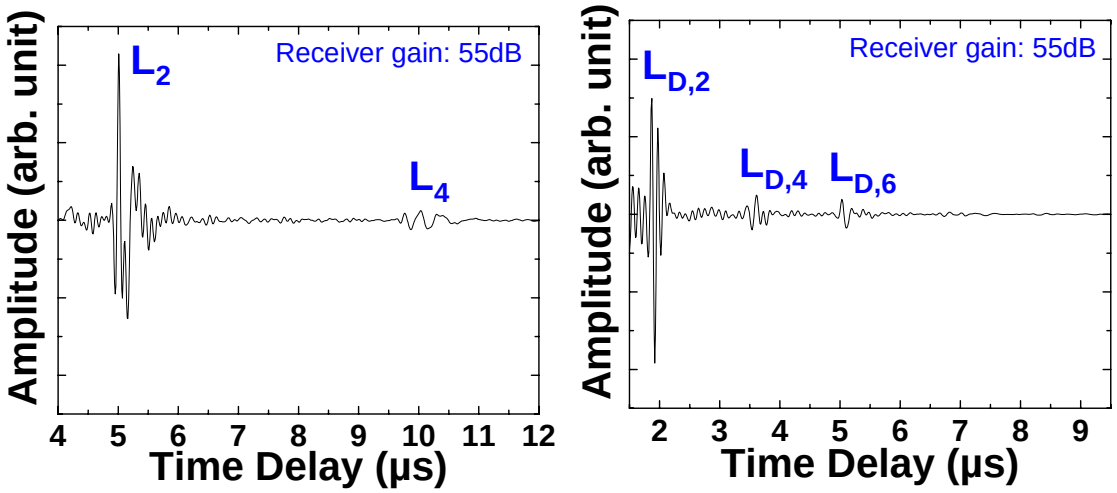

Figure 2-61 Measured ultrasonic signals in time domain at room temperature at a region (a) without and (b) with delaminations using the measurement setup in Figure 2-60. L_2 is the first round trip echo through the plate, and $L_{D,2}$ is the first round trip echo reflected from the delamination.

The FUT using a metal membrane as substrate and presented in Section 2.3.1.1 was also pressed onto the Gr/Ep cylindrical tube shown in Figure 2-56 and the Gr/Ep plate shown in Figure 2-58. The wave forms of the signals measured by that FUT are similar, (and about 20 dB strong in signal strength, but about 2 dB weaker in SNRs), to the ones shown in Figure 2-57 and Figure 2-59 measured by the FUT using a polyimide membrane as substrate. However, the FUT on polyimide membrane is easily conformed to curved surfaces due to its promising flexibility.

2.5 Fabrication and Ultrasonic Performance of IUTs on Composite Substrates

Composite materials such as Gr/Ep laminates are becoming the materials of choice for aerospace structures because of the high strength to weight ratio. NDT and SHM technologies are increasingly being investigated by the aerospace industry to enable condition-based maintenance for cost-effective increased safety and eco-efficient designs [3][5][17][97]. Ultrasonic techniques are frequently used for NDT and SHM purposes because of their subsurface inspection capabilities, fast inspection speed, simplicity and ease of operation. In this thesis FUTs used for NDT of Gr/Ep composites have been presented in Section 2.4.2. Here IUTs will be presented for NDT and SHM of Gr/Ep composite of the thickness ranging from 1 mm to 12.7 mm with planar or curved surface. All measurements will be carried out in pulse/echo mode.

IUTs as piezoelectric PZT-c films of thickness greater than 30 μm will be deposited directly onto planar and curved Gr/Ep composite surfaces. These composite substrates may have high or low electrical conductivity and their resistivity will be measured using a standard four-point-probe. For high electrical conductivity material, the Gr/Ep will be used as the bottom electrode of the IUT. For low electrical conductivity material, a thin conductive layer will be coated onto the Gr/Ep as the bottom electrode. The sol-gel based UT fabrication process for low electrical conductivity Gr/Ep is the same process for the polyimide membrane as described in Section 2.4. In this study, electroless plating of nickel layer is used for one poor conductive Gr/Ep composite and colloidal silver spray for two poor conductive Gr/Ep composites. The thickness of electroless plated nickel alloy layer was about 1 μm. For spray coating, silver colloid was sprayed directly onto poor conductive Gr/Ep composites and cured around 120°C. The thickness of the sprayed silver layer was about 2 μm. Another airbrush was then used to spray the PZT-c sol-gel directly onto bottom electrodes of the Gr/Ep composites. The detailed fabrication process of the sol-gel spray technique has been described in Section 2.1. PZT-c IUTs can operate in the temperature range between -100°C and 150°C and can be made on site. In this study L wave UTs are used.

2.5.1 Ultrasonic performance of IUTs on Gr/Ep Composites

Figure 2-62 illustrates two PZT-c film IUTs that are directly deposited onto planar and curved surfaces of a Gr/Ep composite with a thickness of 12.7 mm and a radius of 50.8 mm. The composite shown in Figure 2-62 was made of 0° and 90° cross plies. The measured resistivity of this composite on the top surface was 0.72 Ω-m which is low enough to serve as the bottom electrode of IUT. For the IUT coated onto the planar surface (IUT_P) the thickness of the PZT-c film was 96 μm and the top circular electrode has a diameter of 8 mm, defining the IUT_P active area. The thickness of the PZT-c film for the IUT sprayed onto the curved surface (IUT_C) was 99 μm and the top rectangular electrode had an area of 6 mm by 7 mm. The choices of circular and rectangular electrodes were carried out arbitrarily. It is noted that since the PZT-c film has a large area, several IUTs with diameters of 7.5 mm may be made within the same film area. The advantages of such IUTs are that they can be directly deposited or coated onto curved surfaces without the need of a couplant.

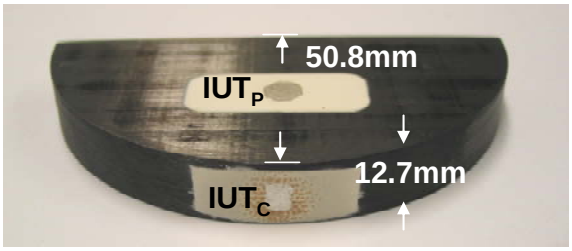

Figure 2-62 IUTs deposited onto the planar and curved surfaces of a 12.7 mm thick and a radius of 50.8 mm Gr/Ep composite plate.

The maximum fabrication temperature of the IUTs shown in Figure 2-62 was 175°C, which was the maximum fabrication temperature of the Gr/Ep composites used in this study. Such low temperature fabrication is to avoid material damages during the heat treatment process during IUT fabrication. However, the lower the fabrication temperature, the weaker the ultrasonic signal strength of IUTs. These IUTs can be employed in operational temperatures, ranging from -80°C to 150°C, commonly experienced in aircraft environments.

Figure 2-63 shows the IUT_P deposited onto a 12.7 mm thick Gr/Ep composite plate and measured by the commercial handheld pulser-receiver EPOCH LT. L^n is the nth trip L echo through the plate thickness. In this measurement 70 dB out of the available 100 dB receiver gain and no averaging was used. It indicates that this L wave IUT_P is efficient even though the IUTs have been fabricated below the temperature of 175°C.

Figure 2-63 Measurement setup for the IUT_P shown in Figure 2-62 at room teamperature using an EPOCH LT.

Figure 2-64 (a) and Figure 2-64 (b) show the measurement results of IUT_P and IUT_C, respectively. In Figure 2-64 (a) L^2, L^4 and L^6 traveled a distance of 25.4 mm, 50.8 mm and 76.2 mm, respectively in the thickness direction of the composite. The ultrasonic velocity and attenuation in the thickness direction are 2883 m/s and 6.3 dB/cm, respectively. However, the L^2, $L^4$and L^6 shown in Figure 2-64 (b) traveled a distance of 101.6 mm, 203.2 mm and 304.8 mm, respectively in the radial direction of the composite. The ultrasonic velocity and attenuation in the radial direction are 6350 m/s and 0.8 dB/cm, respectively. It means that the anisotropy introduced by the 0° and 90° cross plies can be evaluated. The low ultrasonic attenuation observed in these ultrasonic signals indicates that this Gr/Ep composite has good quality (high density). The center frequencies and 6 dB bandwidth of the L^2 signal in Figure 2-64 (a) and Figure 2-64 (b) are 1.8 MHz & 2.1 MHz and 1.3 MHz & 1.2 MHz, respectively.

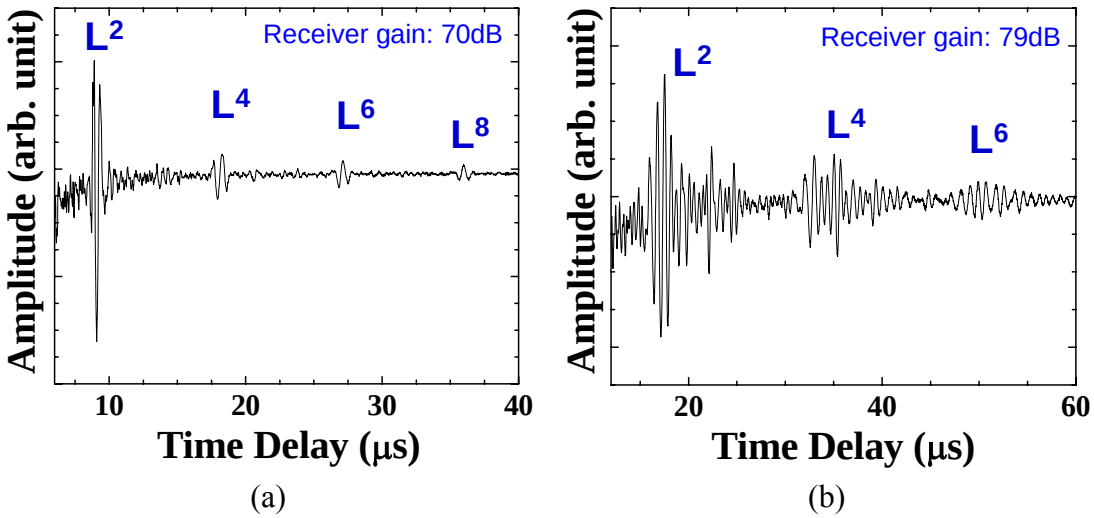

Figure 2-64 Measured ultrasonic signals in time domain at room temperature using the (a) IUT_P and (b) IUT_C shown in Figure 2-62.

For the experiments a 1 mm thick uni-directional Gr/Ep composite as shown in Figure 2-65 was also used. This composite has dramatic different resistivity ranging from 0.2 Ω-m to 22,000 Ω-m at different locations, and in general, its resistivity is higher than several hundreds Ω-m. Therefore it was decided that an electroless plating of 1 μm thickness of nickel was carried out to serve as the bottom electrode of the IUT. The area of nickel plated layer is shown in Figure 2-65 with graded shade. A layer of 95 μm thick PZT-c film was then deposited on top of this nickel layer and poled. A top electrode of 7 mm diameter was made using silver paste. The measured ultrasonic signals gone through a 1 MHz high pass filter are given in Figure 2-66 and the gain was 31 dB out of the available 100 dB when the EPOCH LT was used. The center frequency and 6 dB bandwidth of the L^2 echo, the first round trip echo through the 1 mm thick composite plate, are 10.5 MHz and 13.6 MHz, respectively. In Chapter 5 this sample will be also used for non-contact measurements. Figure 2-66 indicates that the signal strength, center frequency and bandwidth were sufficient for certain NDT or SHM of this 1 mm thick Gr/Ep composite plate.

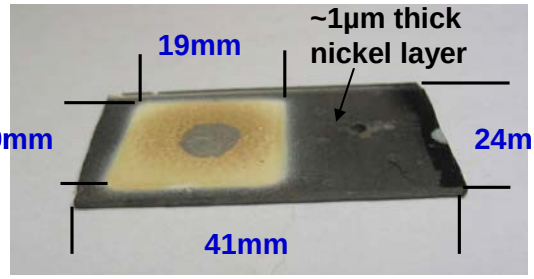

Figure 2-65 An IUT deposited onto a 1 mm thick Gr/Ep composite plate.

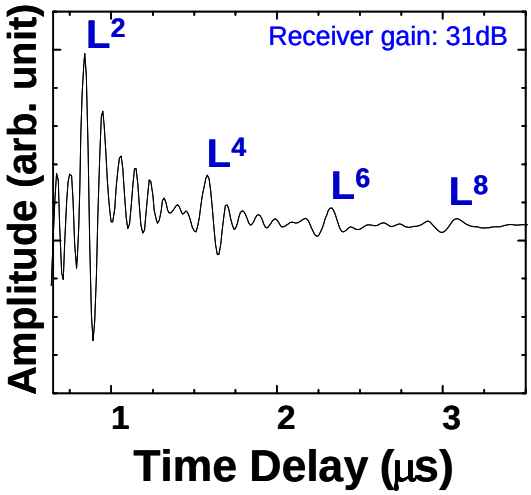

Figure 2-66 Measured ultrasonic signals in time domain at room temperature using the IUT shown in Figure 2-65.

In order to show that PZT-c film IUT can be deposited onto braid structure composites a Gr/Ep cylindrical tube sample shown in Figure 2-67 is selected, and it is the same tube measured by FUT in Section 2.4.2. The resistivity measured for this sample was about 1.5 Ω-m. An approximately 2 μm thick colloidal silver layer as the bottom electrode of the IUT was coated and cured as shown in Figure 2-67. In our experience the colloidal silver spray coating of bottom electrode is much simpler than electroless nickel plating. However, they both work as well as the bottom electrode of IUT. A layer of 58 μm thick PZT-c film was then deposited and poled. Silver paste was used to form the top electrode of IUT. Here the measured ultrasonic signals gone through a 1 MHz high pass filter using the IUT indicated in Figure 2-67 are shown in Figure 2-68. The thickness of the Gr/Ep sample at the IUT location is 3.3 mm. The center frequency and 6 dB bandwidth of the L^2 echo, the first round trip echo through the tube wall, are 2.7 MHz and

3.7 MHz, respectively. For this composite sample the gain was 60 dB out of the available 100 dB receiver gain when the EPOCH LT was used. Figure 2-68 clearly shows that IUT can be deposited and operated on such braid structure composite for certain NDT or SHM applications.

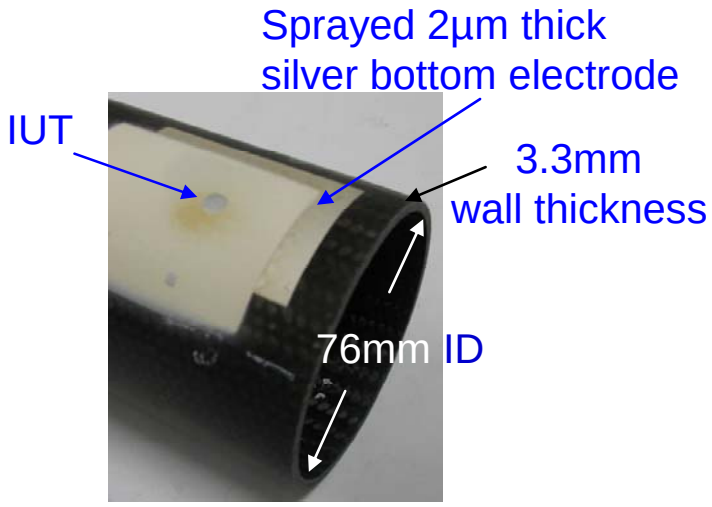

Figure 2-67 An IUT deposited onto a cylindrical braid 3.3 mm thick Gr/Ep composite tube.

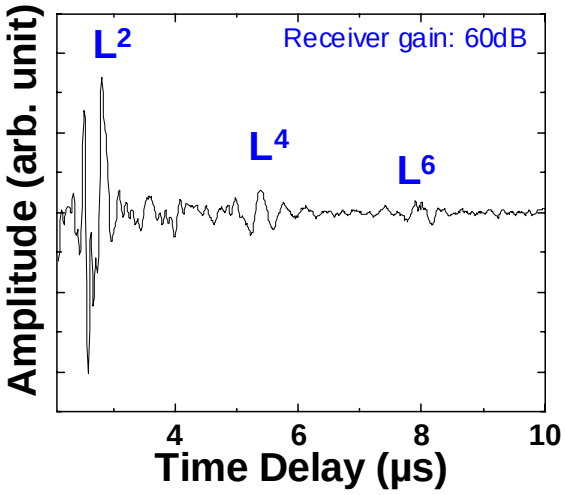

Figure 2-68 Measured ultrasonic signals in time domain at room temperature using the IUT shown in Figure 2-67.

A 6.9 mm thick Gr/Ep sample with delaminations caused by an impact damage shown in Figure 2-69 is also used for the demonstration of the defect detection capability of IUT. This sample was firstly inspected by an ultrasonic C-scan and the locations of the good and delaminated regions were identified. Then the detection of delamination by

FUTs was demonstrated in Section 2.4.2. Finally, IUTs of 30 μm thick were deposited directly onto one location with no delamination and another with delamination.

Figure 2-69 IUTs deposited onto a 6.9 mm thick Gr/Ep composite plate having impact damages.

Figure 2-70 (a) and Figure 2-70 (b) show the measured ultrasonic signals in time domain gone through a 1 MHz high pass filter at room temperature at locations without and with delamination, respectively. The center frequency and 6 dB bandwidth of the L^2 echo, the first round trip echo through the plate, in Figure 2-70 (a) are 11.6 MHz and 11.5 MHz, respectively. The center frequency and 6 dB bandwidth of the L_D^2 echo, the first round trip echo reflected from the delamination which arrives earlier than L^2 echo because of shorter path length, in Figure 2-70 (b) are 14.5 MHz and 14.3 MHz, respectively.The gain was 52 dB out of the available 100 dB receiver gain when the EPOCH LT was used.

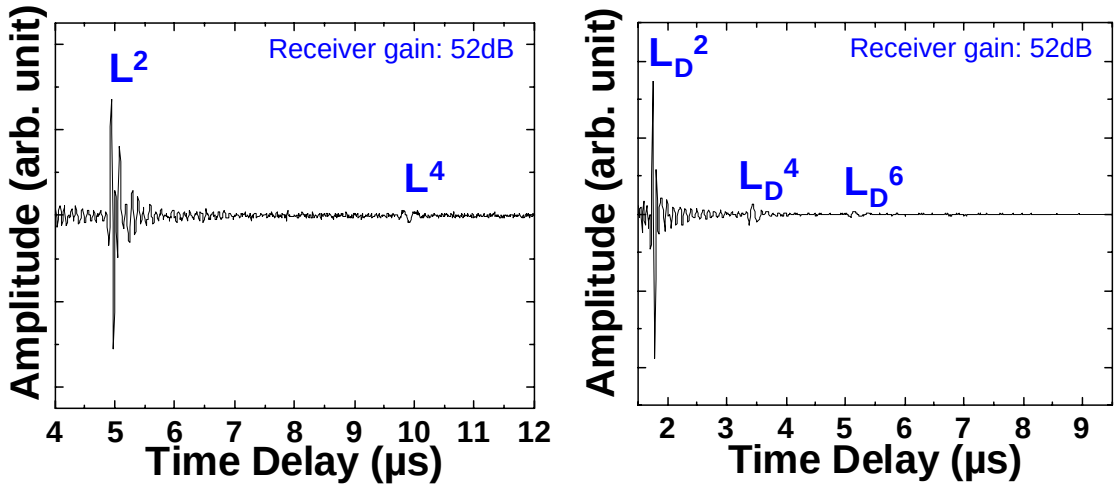

Figure 2-70 Measured ultrasonic signals in time domain at room temperature using an IUT at a location (a) without delamination, and (b) with delamination using the IUT shown in Figure 2-69. L^2 is the first round trip echo through the plate, and L_D^2 is the first round trip echo reflected from the delamination.

2.6 Summary

Piezoelectric thick (thickness range from 14 μm to 125 μm) composite films have been coated onto metallic and Gr/Ep composite substrates as HTUTs using a sol-gel spray technique. The sol-gel spray fabrication process was briefly described in Section 2.1, which consists of six main steps: (1) powders and solution preparation, (2) mixing and ball milling, (3) spray coating, (4) heat treatment, (5) electrical poling, and (6) top electrodes fabrications. The fabrication process was first reported by Barrow, *et al* [57], and further developed by Kobayashi and Jen [28][69], but in this thesis induction heating is introduced for the heat treatment process (4) to improve ultrasonic performance and reduce fabrication time of the sol-gel sprayed composite films. Two types of sol-gel sprayed HTUTs, e.g. IUTs and FUTs, and their ultrasonic performance were presented in this chapter.

In Section 2.2, the fabrication and ultrasonic performance of sol-gel sprayed HT IUTs made of PZT-c, BIT-c and $LiNbO_3$-c films on metal substrates are presented for thickness measurement at temperatures up to 150°C, 400°C and 800°C respectively. No

couplant is required for IUTs to carry out NDT and SHM. This IUT approach has the on-site fabrication capability. IUTs made of PZT-c films on a steel plate, BIT-c films on a steel plate, and $LiNbO_3$-c films on a Ti rod have SNRs more than 45 dB, 23 dB and 20 dB, respectively at temperatures up to 150°C, 400°C and 800°C. The center frequencies of these IUTs ranged from 4.4 MHz to 8.0 MHz. Their signal strengths were evaluated by a hand held EPOCH LT pulser/receiver which is used on a daily basis for NDT in industrial environments. 0 dB gain (i.e. no amplication) out of the available 100 dB receiver gain was used for PZT-c IUTs on a 12.7 mm thick steel plate. The results showed that the signal strength of the PZT-c IUTs was as good as commercially available broadband UTs, and these IUTs may have sufficiently strong signal strength for many NDT and SHM applications. Moreover, the IUTs are able to be coated onto a curved surface and operated at HT. A five IUT array and its electrical connections were also demonstrated. The center frequency, 6 dB bandwidth and SNR, were 40 MHz, 38 MHz, and 30.7 dB, respectively.

PZT-c films were also deposited onto the end of one 12.7 mm diameter and 102 mm long and that of one 25.4 mm diameter and 102 mm long clad steel rod ultrasonic delay lines to perform ultrasonic measurement at 150°C. At 150°C the center frequencies and the 6 dB bandwidths of the first round-trip echoes reflected from these two rod ends were 7.0MHz and 5.9MHz, respectively for the small diameter rod and 6.8 MHz and 3.7 MHz, respectively for the large diameter rod. The signal strengths and SNRs of these echoes at 150°C were 10 dB and 20 dB, and 26 dB and 30 dB, respectively, for the small and large diameter clad rods. At 150°C only 10 dB of the available 100 dB receiver gain was used. Because of such strong signal strength and high SNR of the first reflected echo from the rod end, if the length of the clad steel rod is made much longer, the temperature at the probing end can be much higher than 150°C. The experimental results also show the best rod length measurement accuracies at 150°C for small (12.7 mm diameter) and large (25.4 mm diameter) clad steel rods with a length of 102 mm are 32 μm and 40 μm, respectively. This evaluation demonstrates that the presented IUTs having broad bandwidth and high SNR may be used for accurate erosion and corrosion evaluation.

In Section 2.3, the fabrication and ultrasonic performance of sol-gel sprayed HT FUTs on metal substrates were presented. In certain situations, parts or structures for NDT and SHM cannot be exposed to HT fabricate procedures of the IUT, in which case HT FUT may be fabricated off-line in mass production and then be used for HT NDT and SHM. Unlike the IUT case, HT ultrasonic couplant must be used between the FUT and the sample to be tested. However, FUT attached or glued onto samples may be an attractive and promising on-site installation approach.

First, an FUT made of a 74 μm thick PZT-c film and a 75 μm thick Ti membrane was demonstrated to have signal strength as good as commercial broad UTs, and could be applied onto curved surfaces and at an elevated temperature [91]. It would be commonly difficult to use commercial broad band UTs to perform NDT of parts with a curved surface and at HT. The center frequency, 6 dB bandwidth, and SNR of the FUT were 9.8 MHz, 9.3 MHz and 36.6 dB, respectively. Then an FUT array, in which a PZT-c film was coated on a 75 μm thick SS membrane, operating as an immersion probe was also presented, and its center frequency, 6 dB bandwidth and SNR were 2.4 MHz, 2.1 MHz, and 10 dB, respectively. Subsequently, an FUT made of BIT-c film coated onto a 38 μm thick SS membrane was bonded to a steel plate using a HT metallic adhesive, and ultrasonic measurement was performed up to 303°C. The center frequency and the 6 dB bandwidth of the first round-trip echo reflected from the back of the steel plate at 303°C were 10.7 MHz and 8.2 MHz, respectively and its SNR was 22 dB.

In order to see whether a good alternative FUT fabrication method other than sol-gel spray technique can be found, the FUTs made of piezoelectric films fabricated by tape casting and screen printing were also explored in Section 2.3, and compared with the FUTs made of sol-gel sprayed films. 50~120 μm thick film FUTs were fabricated by sol-gel spray, tape casting or screen printing techniques. The substrates used were 75 μm thick SS membranes. The sol-gel spray technique included multiple coatings and each coating involved spray and heat treatment. It required commonly 4 or 5 layers to reach 50 μm thicknesses. For tape casting and screen printing, only one layer of 50 μm was directly casted and printed onto the membrane substrate and then treated by the heat. All heat treatments were carried out in the furnace up to 650°C for 5 to 30 minutes. The

relative dielectric constant of the sprayed thick film was around 130 and those of the tape casting and screen printing ones were lower than 100. The reason for the lower dielectric constants of the UTs may be porosity and the existence of other phases such as PZT sol-gel or organic residue. Porosity was also confirmed by SEM pictures. In ultrasonic measurements it was found out that the signal strength of the FUTs made by sol-gel spray was 31 dB higher than that of the FUT made by tape casting, and was 50 dB stronger than that fabricated by the screen printing. At 150°C, the FUT made by the sol-gel spray method was still 31 dB higher than that made by the tape casting method. The piezoelectric films made by the sol-gel spray technique had superior mechanical strength and were more robust than the ones made by tape casting and screen printing. Therefore the sol-gel spray technique was continuously developed and used in this thesis.

In Section 2.4, FUTs using 50 μm thick polyimide membranes as substrates were demonstrated. Polyimide membranes were chosen due to their promising flexibility, a better acoustic impedance match with composite material than with a metal membrane, and capability to sustain heating at up to 350°C. A thin electrical conductive layer was made, either by electroless nickel plating or by a colloidal silver spray technique, onto the non-conductive polyimide membrane to serve as the bottom electrodes of the FUTs. The flexibility of such FUTs was achieved due to the thin polyimide, porous PZT-c films and electrodes. Such FUTs could be attached to or bonded onto a host composite structure with planar or curved surfaces on-site. The measured ultrasonic signals showed that FUTs could generate and receive L waves propagating in composite, and were able to detect the delaminations in the composite. Compared with PZT-c film FUTs on metal membranes, PZT-c film FUTs on polyimide have about 30 dB weaker ultrasonic signal strength due to the lower fabrication temperature, but are more flexible and have a better acoustic impedance match for ultrasound testing on Gr/Ep composites or low impedance materials such as plastics.

In Section 2.5, PZT-c film IUTs were deposited onto planar and curved surfaces of Gr/Ep composites of thickness ranging from 1 mm to 12.7 mm. PZT-c films were coated directly onto Gr/Ep composites with high electrical conductivity, but for the ones with low electrical conductivity, PZT-c films were coated after thin conductive layers were

deposited as bottom electrodes. The thin conductive layers were made either by electroless nickel plating or by a colloidal silver spray technique. The latter is found to be simpler that the former approach. These piezoelectric PZT-c film based FUTs with a film thickness ≥ 30 μm were fabricated using a sol-gel spray technique. The top electrodes can be made using silver paste or colloidal silver spray to form desired array configuration with ease. In this study the center operation frequency of these transducers ranged from 1.3 MHz to 14.5 MHz. All measurements were carried out in pulse/echo mode. PZT-c film IUTs can operate in the temperature range between -100°C to 150°C where the operation temperature of the Gr/Ep composites in aerospace industry normally ranges from -60°C to 100°C. The obtained ultrasonic signals showed that IUTs could generate and receive L waves propagating in Gr/Ep composites for more than 300 mm. Also delaminations in the composite were detected and the ultrasonic anisotropy of 0° and 90° cross ply composite was measured. When accessibility to desired locations of Gr/Ep components of, for example, an aircraft, is prohibited for the fabrication of the IUTs, FUT may be used. The ultrasonic performance of the IUTs directly deposited onto the Gr/Ep composites was nearly the same as the FUTs on 50 μm thick polyimide membranes presented in Section 2.4.

CHAPTER 3

BULK ACOUSTIC WAVE MODE CONVERSION

For NDT and SHM in the aerospace industry it is crucial to know the elastic properties such as Young's modulus [10], shear modulus [11], Poisson's ratio anisotropy [98], texture [15][99] or stress[15][16][100][101]. Ultrasonic techniques are often used to evaluate or characterize such properties nondestructively [3][4][102]. Since many parts or structures are performed at HT, it is of interest and sometimes even mandatory to characterize the above mentioned properties at HT. Thus HTUTs are in demand [7][9][28][69][103][104][105][106]. The Young's modulus E, shear modulus μ and Poisson's ratio v of an isotropic material can be obtained with the L wave velocity V_L and S wave velocity V_S, and their relations are given in Eqn. (3-1), (3-2) and (3-3), respectively [4][78][10].

$$E = \frac{\rho V_S^2 \left(3V_L^2 - 4V_S^2\right)}{V_L^2 - V_S^2} \tag{3-1}$$

where E, Young's modulus, is the ratio of the applied longitudinal stress to the longitudinal strain when a rod is subjected to a uniform stress over its end planes and its lateral surface is free to expand.

$$\mu = \rho V_S^2 \tag{3-2}$$

where μ, shear modulus, is the ratio of transverse stress to transverse strain.

$$\nu = \frac{1 - 2\left(V_S / V_L\right)^2}{2\left[1 - \left(V_S / V_L\right)^2\right]} \tag{3-3}$$

where ν, Poisson's ratio, is the ratio of the lateral contraction (expansion) to the longitudinal extension (contraction) of the rod.

In references [15][16][11][98], anisotropy or texture of materials with hexagonal symmetry such as unidirectional Gr/Ep composite and orthorhombic symmetry such as rolled Al and steel plates can be also found to have relations with ultrasonic L wave and S wave velocities. Furthermore, S waves may be advantageous over L waves for NDT and SHM because liquid and gas medium do not support S waves. For example, S waves will have a much larger reflection coefficient than L waves if they meet the boundaries between solids and gases or liquids. In order to evaluate and characterize metallic and Gr/Ep composite material properties, it is a necessity to develop HTUTs not only for L waves but also for S waves. Various efforts have been devoted to develop HT L wave UTs [9][28][69][103][104][106]. However, it seems that commercially there are neither HT S wave probes nor HT L-S probes available which are able to operate at HT, e.g. up to around 350 °C. L-S probe means that a probe can generate and/or detect both L and S waves simultaneously at the same center operation frequency and near the same probing location. The purpose of this chapter is to demonstrate the fabrication and performance of integrated HT S probes and L-S probes. Potential NDT and SHM applications using these probes will be demonstrated as well.

3.1 HT S and L-S Wave Probes

In this study all thick piezoelectric composite films IUTs will serve as L wave UTs as mentioned in Chapter 2. PZT-c and BIT-c films IUTs will be used for demonstration in this chapter.

3.1.1 S and L-S probes using mode conversion

The mode conversion from L to S wave due to reflection at a solid-air interface was reported in refs. [78] and [79]. This means that the L wave UT together with L-S mode conversion can be effectively used as a S wave probe as shown in Figure 3-1. In Figure 3-1, L_i waves generated by an L wave UT reach a solid-air interface and are reflected as L_r and S_r waves. The equations governing the reflection and mode conversion with respect to the L wave incident angle θ can be given in Eqs. (3-4), (3-5), and (3-6) [107], where φ is a reflection angle of the S waves, V_L and V_S are L and S wave velocities in the solid, respectively, and R_{ll} and R_{sl} are energy reflection coefficients of the L and S waves, respectively.

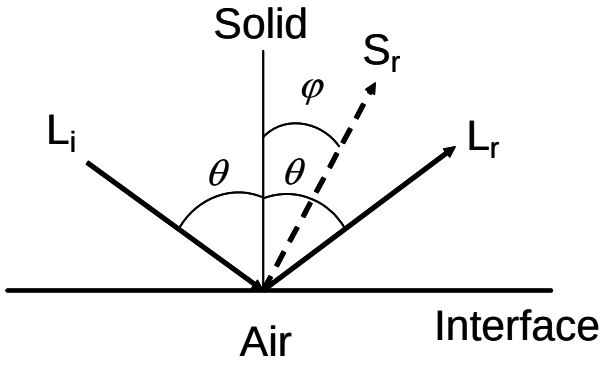

Figure 3-1 Reflection and mode conversion with an L wave incidence at a solid-air interface.

$$\frac{V_L}{\sin\theta} = \frac{V_S}{\sin\varphi} \tag{3-4}$$

$$R_{ll} = \left[\frac{\cos^2 2\varphi - \left(V_S / V_L\right)^2 \cdot \sin 2\theta \cdot \sin 2\varphi}{\cos^2 2\varphi + \left(V_S / V_L\right)^2 \cdot \sin 2\varphi \cdot \sin 2\theta}\right]^2 \tag{3-5}$$

$$R_{sl} = \frac{4 \cdot \left(V_S / V_L\right)^2 \cdot \cos^2 2\varphi \cdot \sin 2\theta \cdot \sin 2\varphi}{\left[\cos^2 2\varphi + \left(V_S / V_L\right)^2 \cdot \sin 2\varphi \cdot \sin 2\theta\right]} \tag{3-6}$$

In this study, a mild steel with V_L = 5900 m/s and V_S = 3200 m/s at room temperature was used as the substrate. Figure 3-2 shows the calculated energy reflection coefficients of R_{ll} (dotted line) and R_{sl} (solid line) based on Eqs. (3-2) and (3-3), respectively, at the mild steel-air interface. It indicates that the maximum energy conversion rate from the L_i wave to the S_r wave is 97.5% at θ = 67.2°, and the reduction of the energy conversion rate is within 1% in the θ range between 60.8° and 72.9°.

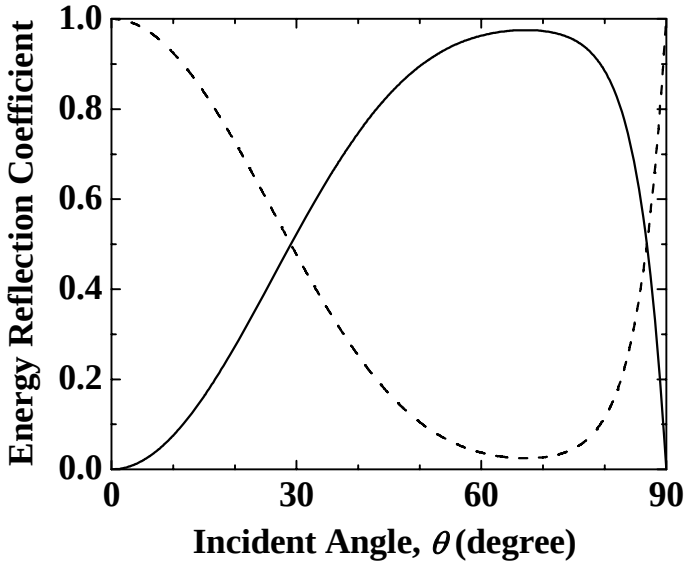

Figure 3-2 Energy reflection coefficients of R_{ll} (dotted line) and R_{sl} (solid line) vs. L wave incident angle θ at solid (mild steel)-air interface

In order to achieve S wave HTUTs, an L wave IUT of a 100 μm-thick BIT-c film onto a mild steel substrate is made using the sol-gel spray technique described in Chapter 2. BIT-c film is chosen here to demonstrate the measurement temperature up to 350°C which is arbitrarily selected. Let this L IUT be in a plane parallel to the mode converted S wave direction as shown in Figure 3-3. This approach could reduce machining time of the substrate and the sol-gel sprayed thick film fabrication difficulty. An actual S wave probe is shown in Figure 3-4. The top electrode was made by a platinum paste which can sustain the temperature at up to more than 450°C. By considering this criterion, $\theta + \varphi$ is required to be 90°. From Eq. (3-1), which is the Snell's law, one can obtain θ = 61.5°. At this angle, the L-S conversion rate is 96.7% that is only 0.8% smaller than the maximum conversion rate (97.5%) at 67.2°, based on the result in Figure 3-2.

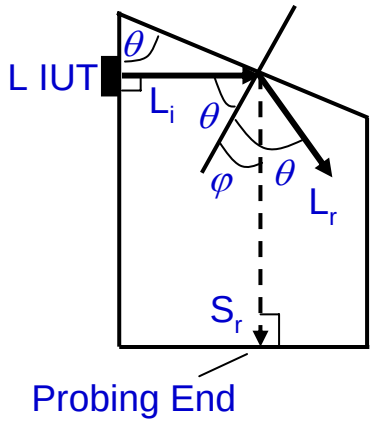

Figure 3-3 Schematic diagram of an integrated S wave UT probe with the L wave UT located in a plane parallel to the direction of mode converted S wave at θ = 61.5°.

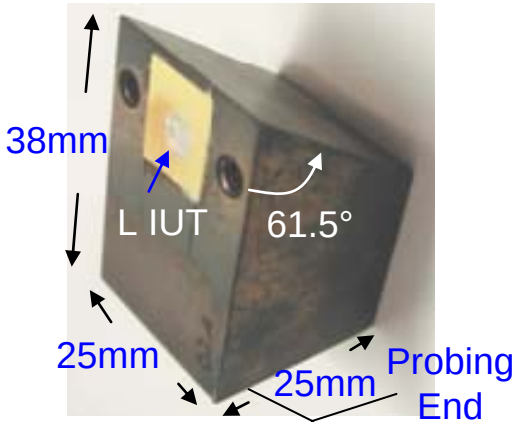

Figure 3-4 An actual integrated S wave UT probe with the L wave IUT located in a plane parallel to the direction of mode converted S wave at θ = 61.5°.

Figure 3-5 (a) and Figure 3-5 (b) show the ultrasonic signals in time and frequency domain, respectively, of the received S_r wave in a pulse-echo mode at 350 °C. The S^n represents nth trip of the S_r wave echoes traversing back and forth between the L IUT and the probing end in Figure 3-3. The center frequency of the S^2 echo was 6.7 MHz and the 6 dB bandwidth was 3.8 MHz. The SNR of the S^2 echo was about 30 dB. The SNR is defined as the ratio of the amplitude of the S^2 echo over that of the undesired signals among the S^n echoes in Figure 3-5 (a). The signal strength of the S^2 echo at 350°C was 5 dB smaller than that at room temperature. This additional loss of signal strength may be caused by the additional propagation loss in the steel and reduction of piezoelectric

strength of BIT-c film at 350°C. It can be seen that the L_r wave was not observed due to the fact that the dimension of the substrate has been chosen so that the reflected L_r wave does not enter into the aperture of the L IUT.

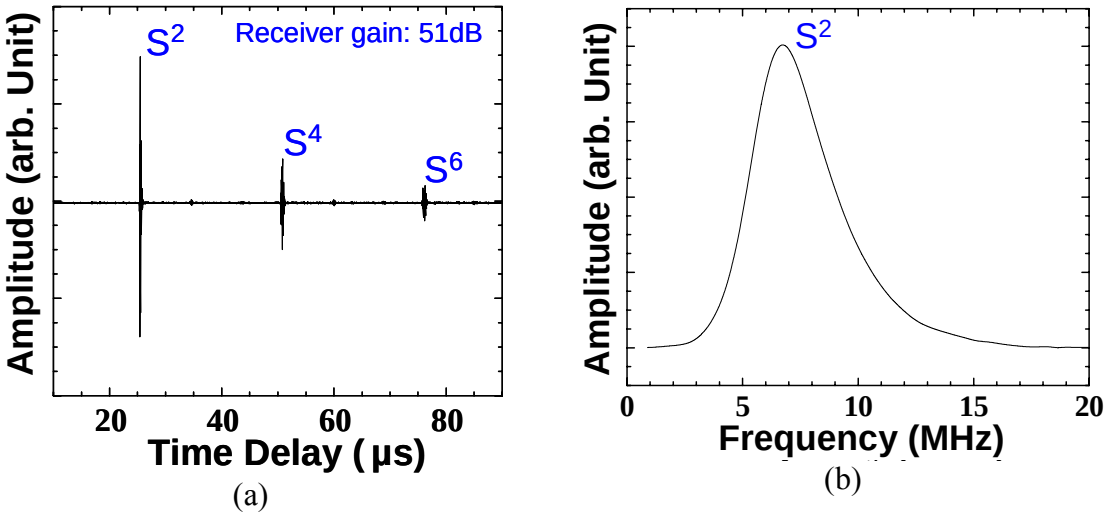

Figure 3-5 Ultrasonic signals in (a) time and (b) frequency domain of the S wave UT probe shown in Figure 3-4 at 350 °C.

3.1.2 L-S probes using one L wave IUT

If one would like to generate and receive both L and S waves at the same time, then the S wave probe shown in Figure 3-3 can be modified to achieve such a purpose. In fact, it simply makes a slanted surface with an angle of 45° from the intersection of the slanted plane and the line from the center of the L IUT as shown in Figure 3-6. An actual L-S probe is presented in Figure 3-7. The 45° angle plane will reflect the energy of the L_i wave into the $L_{r,45°}$ wave normal to the probing end as shown in Figure 3-6. Therefore, in principle, the upper part of the L_i wave, generated from L IUT, can be used to produce the S_r wave and the lower part to produce the $L_{r,45°}$ wave. Figure 3-8 shows ultrasonic signals in time domain in the pulse-echo mode at 350 °C, in which the S_r (S^2) and $L_{r,45°}$ (L^2) waves are observed simultaneously. Since BIT-c film can work up to 400°C, here 350C° was arbitrarily chosen because of the convenience in measurements using a hot plate. The L^2 represents the first round trip $L_{r,45°}$ wave echo traversing between the L IUT and the probing end. The center frequencies of the S^2 and L^2 echoes were 7.0 MHz and 7.0 MHz

and the 6 dB bandwidths were 3.0 MHz and 3.8 MHz, respectively. During the top electrode fabrication, the area and position of the top electrode were adjusted so that the amplitude of the reflected S^2 and L^2 waves was nearly the same. The SNRs of the L^2 and S^2 were about 20 dB. Weak signals appearing between the L^2 and S^2 and after the S^2 in Figure 3-8 were spurious echoes due to reflections and mode conversions at many faces of the probe.

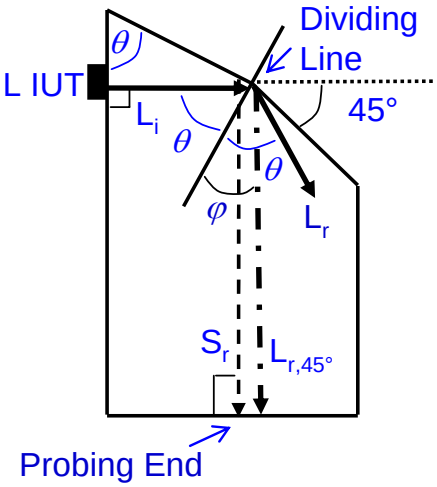

Figure 3-6 Schematic diagram of an integrated L-S wave probe with the L wave UT located in a plane parallel to the direction of S_r wave.

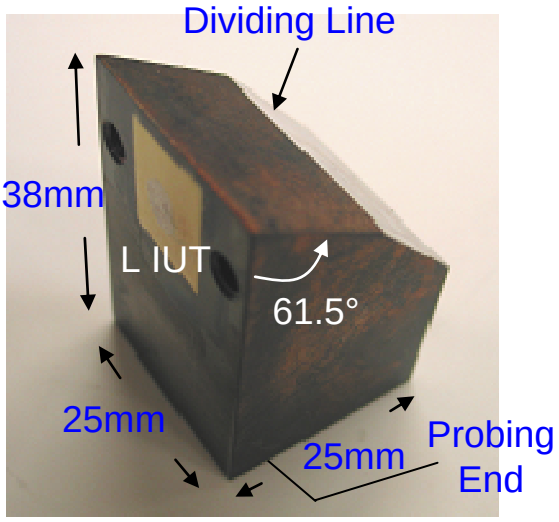

Figure 3-7 An actual integrated L-S wave UT steel probe with the L wave IUT located in a plane parallel to the direction of mode converted S wave at $\theta = 61.5°$.

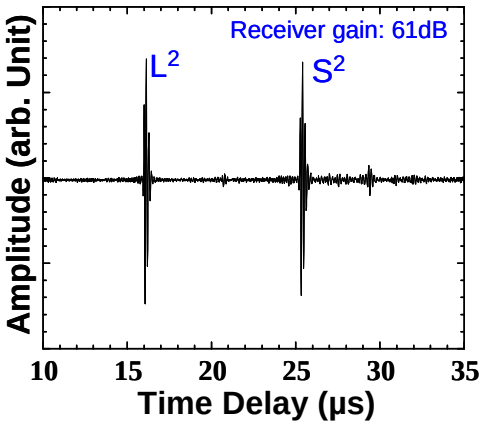

Figure 3-8 Ultrasonic signals in time domain of the L-S wave UT probe shown in Figure 3-7 at 350°C.

3.1.3 L-S probes using two L wave IUTs

In Figure 3-2 the calculated energy reflection coefficients of R_{ll} (dotted line) for the 45° reflection plane between the mild steel and air is only 16.8%. In order to improve the L wave efficiency, an alternative approach using two IUTs, one for L wave and one for L wave mode converted to S wave, is presented as shown in Figure 3-9 with Cartesian coordinates X, Y and Z. An actual L-S probe following this approach is shown in Figure 3-10. In fact, this probe can generate and receive two orthogonally polarized S waves S_X and S_Y which will be further discussed in the later sections of this chapter. The particle displacements of S_X and S_Y waves are parallel to X and Y axies, respectively. In Figure 3-10 the piezoelectric composite film is PZT-c and the thickness of the top IUT is 79 μm and that of the side IUT is 85 μm.

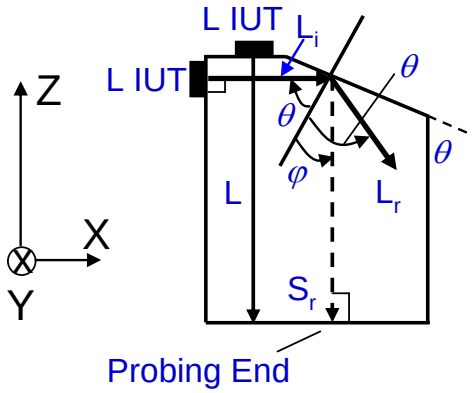

Figure 3-9 Schematic diagram of an integrated L-S wave probe with two L wave IUTs.

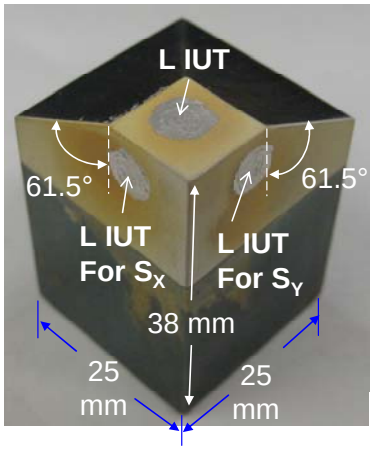

Figure 3-10 An actual integrated L-S wave UT steel probe with one L wave IUT located on the top plane perpendicular to and one in a plane parallel to the direction of mode converted S wave at θ = 61.5°.

Figure 3-11 shows ultrasonic signal in time domain in the pulse-echo mode at 150 °C, in which the S_r (S^2) and L^2 waves are observed simultaneously with an electrical wire connecting between the top electrodes of the two L IUTs. Since PZT-c film can work up to 200°C, 150°C was arbitrarily chosen here. The L^2 represents the first round trip L wave echo traversing between the L IUT on the top surface of Figure 3-8 and the probing end. The top surface is perpendicular to the probe, Z axis. The center frequencies of the S^2 and L^2 echoes were 13.2 MHz and 14.8 MHz and the 6 dB bandwidths were 13 MHz and 10.7 MHz, respectively. The SNRs of the L^2 and S^2 were 50 dB and 40 dB, respectively. When a 2.28 mm thick flat glass plate is used as the sample for the measurement of its V_L and V_S, a thin ultrasonic liquid gel is added between the probing end of the probe shown in Figure 3-10. The ultrasonic measurement of both the L and S wave echoes in the glass plate is shown in Figure 3-12. L_n and S_n are the nth trip echo travelling through the thickness of the glass plate. The obtained V_L and V_S of this glass are 5876 m/s and 3495 m/s, respectively. Then a 0.83 mm thick Plexiglas plate is used to replace the glass. The measured ultrasonic signals are shown in Figure 3-13. Both L and S waves transferring back and forth within the Plexiglas plate have been observed. The measured V_L and V_S of this Plexiglas are 2032 m/s and 989 m/s, respectively. Therefore Figure 3-12 and Figure 3-13 indicate that the probe shown in Figure 3-10 can be used for the measurements of both Young's modulus [10] and shear modulus [11] of isotropic materials.

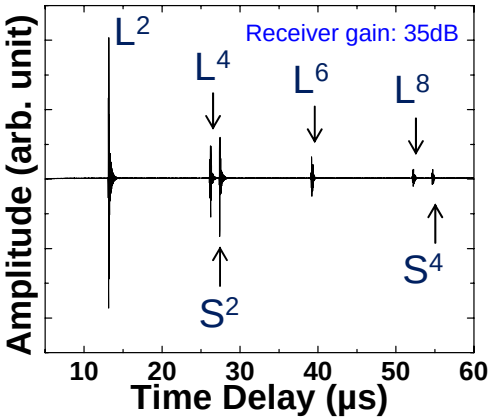

Figure 3-11 Ultrasonic signals in time domain of the L-S wave IUT probe shown in Figure 3-10 at 150°C.

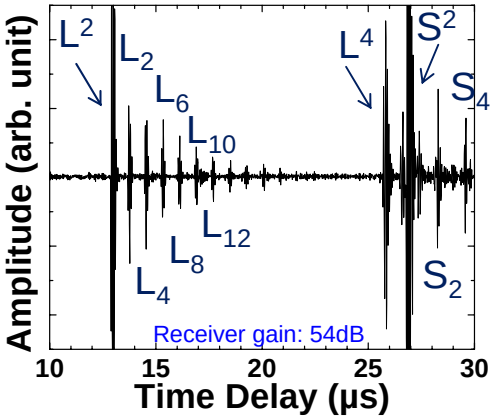

Figure 3-12 Ultrasonic signals in time domain of the L-S wave IUT probe shown in Figure 3-10 together with one 2.28 mm thick glass plate at room temperature.

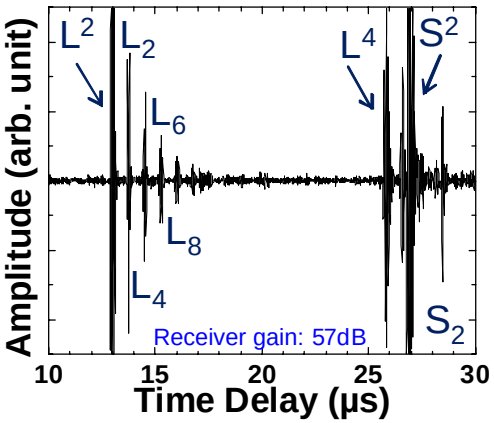

Figure 3-13 Ultrasonic signals in time domain of the L-S wave IUT probe shown in Figure 3-10 together with one 0.83 mm thick Plexiglas plate at room temperature.

3.1.4 L-S probes using two L wave FUTs

Ultrasonic characterization of low acoustic impedance materials such as Gr/Ep composites and plastics are also of importance. It is also of interest to use a probe shown in Figure 3-9 using Plexiglas which has improved acoustic impedance match over the metallic probe for Gr/Ep composites or plastic materials. For this reason a probe made of Plexiglas is fabricated as shown in Figure 3-14. Still it is the intention to have the mode converted S wave be parallel to the probing axis. From Eq. (3-1) one can obtain $\theta = 63.2°$. At this angle, the L-S conversion rate is 86.6%, which is 0.2% smaller than the maximum conversion rate (86.8%) at 65°. Since Plexiglas cannot sustain high heat treatment temperature, an alternative way using FUTs (mentioned in Chapter 2) glued to the top and side surfaces of the probe to replace IUTs is used and shown in Figure 3-15. Again using an electrical wire to connect the L wave FUT on the top surface and the one at the side surface of the probe as indicated in Figure 3-15, the ultrasonic measurement result is shown in Figure 3-16. The center frequencies of the S^2 and L^2 echoes were 3.7 MHz and 7.5 MHz and the 6 dB bandwidths were 4.4 MHz and 2.9 MHz, respectively. The SNRs of the L^2 and S^2 were about 26 dB. When a 2.28 mm thick flat glass plate and a 0.83 mm thick Plexiglas plate are used as the samples separately, the ultrasonic signals are shown in Figure 3-17 and Figure 3-18, respectively. The measured V_L and V_S are 5868 m/s and 3501 m/s, and 2026 m/s and 953 m/s respectively and they agree with the measurement data obtained by the steel probe shown in Figure 3-10. It is noted that the improved acoustic impedance matching between the probe and the sample at the probe-sample interface will induce small reflected echo at interface and increase the transmitted acoustic energy into the sample, and thus enable to measure the material properties such as Young's and shear modulus of a relatively thin sample. One can clearly see that L_2/L^2 in Figure 3-18 is larger than that Figure 3-17 because of improved acoustic impedance matching between Plexiglas probe and another Plexiglas sample over that between Plexiglas probe and glass plate sample. It is observed that the Plexiglas probe and Plexiglas sample have a little different material property.

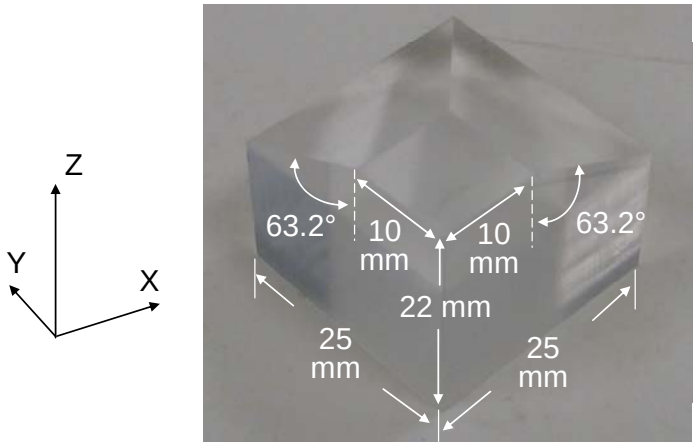

Figure 3-14 An actual L-S wave probe made of Plexiglas without FUTs.

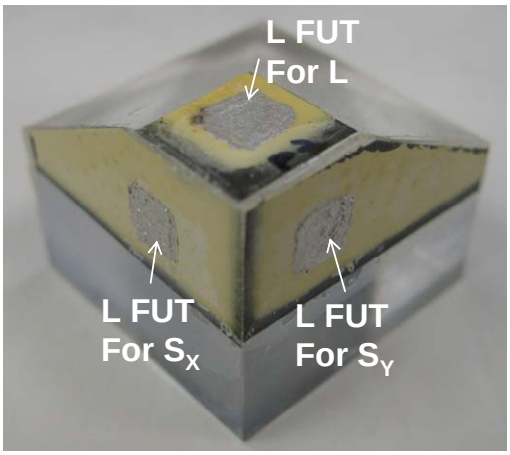

Figure 3-15 An actual integrated L-S wave FUT probe with one L wave FUT located on the top plane perpendicular to and one in a plane parallel to the direction of mode converted S wave at θ = 63.2°.

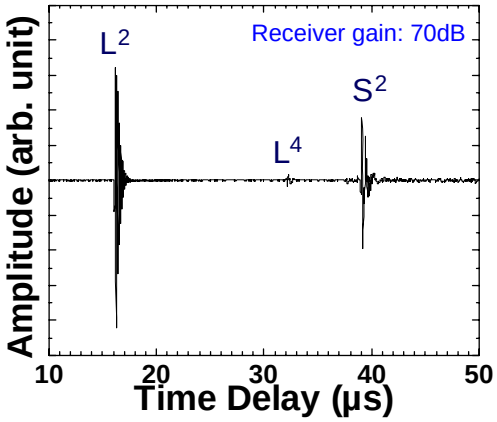

Figure 3-16 Ultrasonic signals in time domain of the L-S wave FUT probe shown in Figure 3-15 at room temperature.

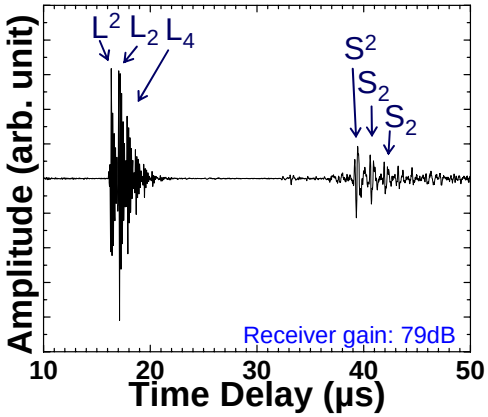

Figure 3-17 Ultrasonic signals in time domain of the L-S wave FUT probe shown in Figure 3-15 together with one 2.28 mm thick glass plate at room temperature.

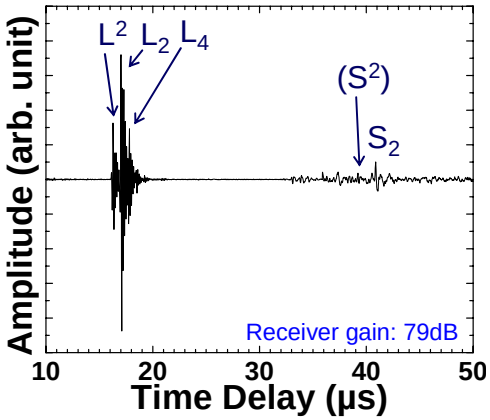

Figure 3-18 Ultrasonic signals in time domain of the L-S wave FUT probe shown in Figure 3-15 together with one 0.83 mm thick Plexiglas plate at room temperature.

3.2 Screws for Axial Load and Temperature Measurements Using Ultrasound

Structural parts which are held together by screws (bolts, rivets or fasteners) under tensile stress must be designed and assembled so that these screws are sufficiently loaded to prevent the parts from separating while the structure is in service. Therefore a reliable measurement of the axial load or preload in such screws is essential to secure structural safety, and a precise control of the fastening force is required. Several ultrasonic methods have been studied for axial load measurement. The most promising ones are measuring the time delays of both L and S wave along the screw direction [12][13][14]. In the most

recent report [14] the use of L and S waves allowed the elimination of time-of-flight measurement of both waves in the unstressed state. Thus the tightening tension can be evaluated without loosening the assemblies bolted. All the previous works use conventional UTs which need ultrasonic couplants and cannot be easily operated at elevated temperatures.

Temperature measurements are also of importance to structures such as engines or hypersonic airplane parts. The thermocouple may not be rugged enough when HT flames are present. It has been reported that ultrasonic waveguide with discontinuities can be used as temperature sensor [108][109][110][111]. In this study, one approach is that the screws used for engines or airframes may be used for temperature measurements. Thus near the end of the screw whose diameter is more than several wavelengths, one discontinuity in the screw outer diameter will be created. Then the ultrasonic time delay or velocity measurement in the region between the discontinuity and the screw end may be used for the average temperature evaluation within the discontinuity section. Furthermore, the ability to measure the Young's and shear modulus of isotropic materials at HT is of interest for the aerospace material evaluation as well.

Therefore here IUTs will be coated onto screws which can provide simultaneous measurements of both L and S wave velocity at elevated temperatures. Discussions on how these screws may be used for axial load, temperature measurement and material properties will be presented. The future goal is that every screw like the ones to be presented may be used as integrated structural sensors for aerospace applications.

3.2.1 UT fabrication

A screw or probe made of mild steel which is the same as that used in Section 3.1.1 shown in Figure 3-19 (a) is chosen for the investigation. This mild steel for screw fabrication is the same as the probe shown in Figure 3-7. This screw has a length of 76.2 mm and its diameter including the thread is 15.9 mm. A miniaturized PZT-c film IUT was directly fabricated onto the head of the screw by the sol-gel spray technique described in Chapter 2 as shown in Figure 3-19 (b). The PZT-c film thickness is 75 μm.

Silver paste was used to fabricate the top electrode which defines the IUT active region. This IUT shown in Figure 3-19 (b) has a width of 7 mm and a height of 4 mm.

As shown in Figure 3-19 a mode conversion angle $\theta = 61.5°$ ($\neq \theta_{max}$) is chosen so that the mode converted S wave will propagate back and forth along the axial direction. Similar to the explanations given in Section 3.1.1 because $\theta = 61.5°$, the energy conversion rate is 96.7% at room temperature.

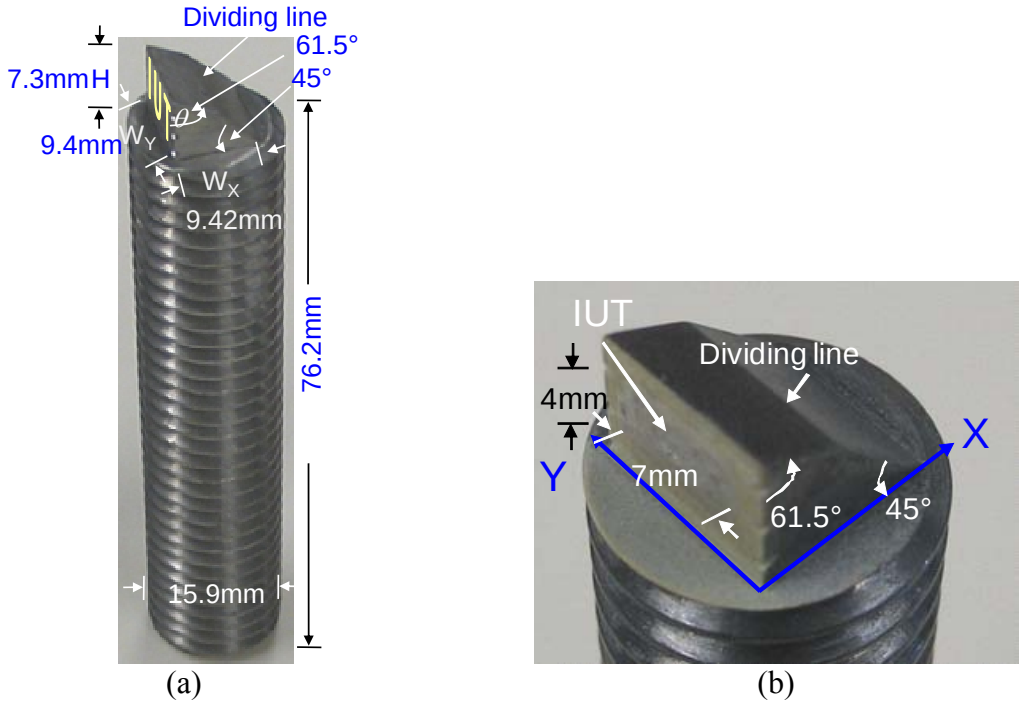

Figure 3-19 (a) A screw made of mild steel for the propagation of both L and S waves. (b) Zoomed picture of the head of the screw shown in (a).

Figure 3-20 (a) shows the measured ultrasonic signals of the screw shown in Figure 3-19 at room temperature in time domain. The center frequencies and 6 dB bandwidths of the L and S waves are 17.0 MHz and 13.8 MHz, and 16.6 MHz and 20.6 MHz, respectively. L^n and S^n are the nth trip L and S echoes, respectively, from IUT to the end of the screw. The SNRs of the L^2 and S^2 waves are above 20 dB. The signal which appeared at time delay near 41 μs is a noise which is speculated to be caused by an ultrasonic signal traveling one screw length in S wave and another screw length in L wave because of the imperfect mode conversion angle θ machined for the experiment,

and limited numerical resolution for this θ used in the calculation. The numerically simulated result in time domain using commercial available software package (Wave3000, CyberLogic Inc., New York, NY) based on a finite difference method which solves the 3D visco-elastic wave equations is given in Figure 3-20 (b). Comparing Figure 3-20 (a) and Figure 3-20 (b) a good agreement between the experimental obtained and numerically calculated signals in signal bandwidth and time delay has been achieved. A slight difference in amplitude and time delays between the experimental obtained and numerically calculated results may come from the texture of the actual screw which is not considered in the theoretical simulation. The texture of the steel may increase or decrease the ultrasonic velocity depending on the orientation of the grains in the screw. For example, if the grain orients along the axial direction of the screw, then the ultrasonic velocity will be faster than that in a screw having isotropic structure. It is noted that the position and size of the IUT shown in Figure 3-19 (b) can be adjusted so that the amplitude ratio between L^2 and S^2 may be varied.

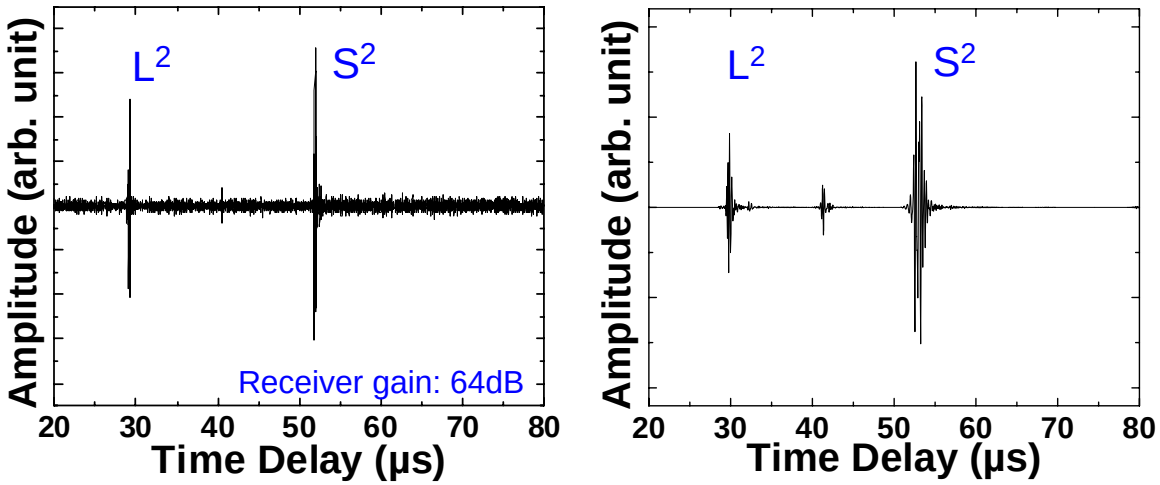

Figure 3-20 (a) Measured and (b) numerically calculated ultrasonic signals in time domain at 22°C in the probe as shown in Figure 3-19.

The measured ultrasonic signals of the screw shown in Figure 3-19 (a) at 150°C are presented in Figure 3-21. The center frequencies and 6 dB bandwidths of the L and S waves are 15.0 MHz and 14.2 MHz and 13.8 MHz and 8.5 MHz, respectively. The SNRs of the L^2 and S^2 waves are above 12 dB. The variation of the amplitudes of L^2 and S^2

from room temperature to 150 °C is due to the different ultrasonic attenuation in the screw, and reflection and mode conversion at the steel/air interface. Comparing the arrival time of L^2 and S^2 shown in Figure 3-20 (a) with those shown in Figure 3-21 one can see that the arrival time has been increased due to the increased temperature as expected.

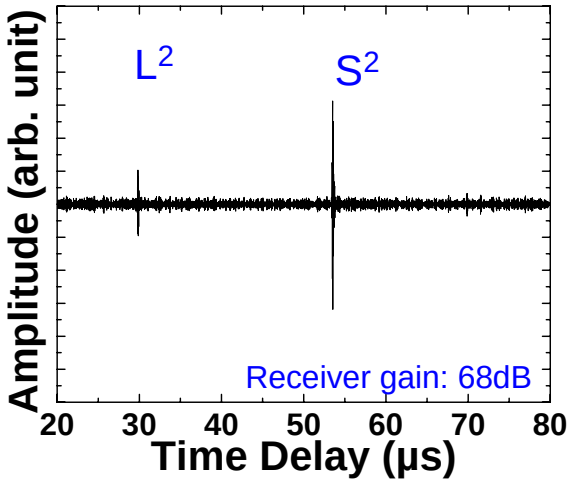

Figure 3-21 Measured ultrasonic signals in time domain at 150°C in the probe as shown in Figure 3-19.

3.2.2 Screws for temperature measurements using ultrasound

In order to demonstrate that the screw shown in Figure 3-19 can be used for the temperature measurements, the reduction of the screw diameter in a 1.72 mm length has been made near its end. The discontinuity is designated as D1 as shown in Figure 3-22 (a) so that the reflected echoes from this discontinuity and the screw end can be well separated in time domain. Such a reduced diameter screw section called "step" also permits the determination of V_L and V_S of the screw which can be used for the measurement of Young's and shear modulus at even HT. The diameter (5 mm) of the screw in this step is also designed so that not only the echoes, L_{D1}, and/or S_{D1} reflected from the step D1 is strong enough but also the echoes L^2 and S^2 reflected from the reduced screw end of 5 mm diameter can be still strong enough for the measurement of V_L and V_S of the screw. An experiment for temperature measurement using this one-step screw was performed. During this measurement the screw was placed vertically on a hot plate, and the surface of the 5 mm diameter step was contacted with and heated by the hot

plate. A commercial thermocouple was also placed on the hot plate to measure the temperature. Figure 3-22 (b) shows that measured signal of the screw with a step at the screw end at 150°C. One can see that the echoes, L_{D1} and L^2, S_{D1} and S^2 are clearly observed and separated. Since the ultrasonic velocity (time delay) in the screw section between D1 and the screw end is a function of temperature which can be measured in an off-line calibration setup, the average temperature of the screw in this section can be obtained on-line and real-time using the time delay difference between the echoes L^2 and L_{D1} or between S^2 and S_{D1} [110]. The thermal expansion coefficients of the screw material must be included for the temperature measurements. Using the machined step size, 1.72 mm, between D1 and the screw end and the time delay differences between L_{D1} and L^2 and S_{D1} and S^2, the L and S velocities of the screw in this step region at room temperature and 150°C are 5911 m/s and 3201 m/s, 5858 m/s and 3140 m/s, respectively.

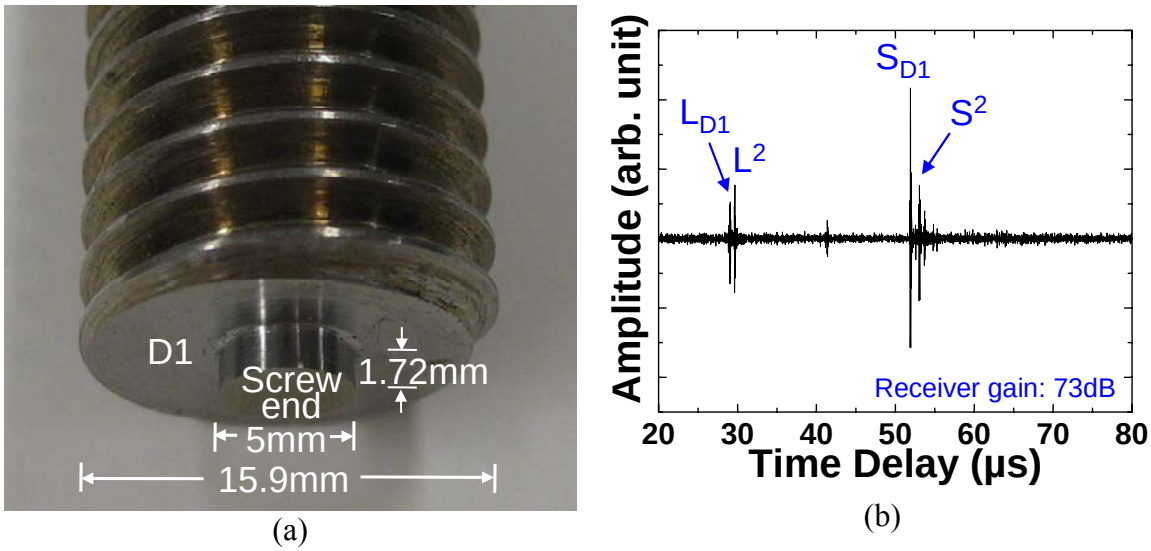

Figure 3-22 (a) One step, D1, made near the end of the screw shown in Figure 3-19 for temperature measurement. (b) Measured ultrasonic signals in time domain at 150°C in the probe having a step. L_{D1} and L^2, and S_{D1} and S^2 are the reflected L and S wave echoes, respectively, from the discontinuity D1 and screw end.

Both of the L and S waves could be used for temperature measurement. However, as the discussion in Section 3.1 that the energy reflection coefficient (96.7%) of the converted S wave from L wave is higher than the one (16.8%) of reflected L wave by the

45° reflection plane between the mild steel and air, and also the well separated S wave echoes due to its slower velocity, S waves were used to demonstrate the temperature measurement here. Please note the length of the screw is 76.2 mm and the IUT is coated at the screw head, as shown in Figure 3-19 (b), which is opposite to the screw end with one step designed for average temperature measurement within the discontinuity (1.72 mm), as shown in Figure 3-22 (a), so the screw is able to measure the temperature above the IUT operation temperature. Figure 3-23 shows the calculated S velocities from room temperature up to 400°C using the signals S_{D1} and S^2 in Figure 3-22 (b) reflected from the 1.72 mm step and screw end, respectively. The thermal expansion coefficients of the screw material should be, but are not included here. Improved results are expected when the thermal expansion of the screw is considered.

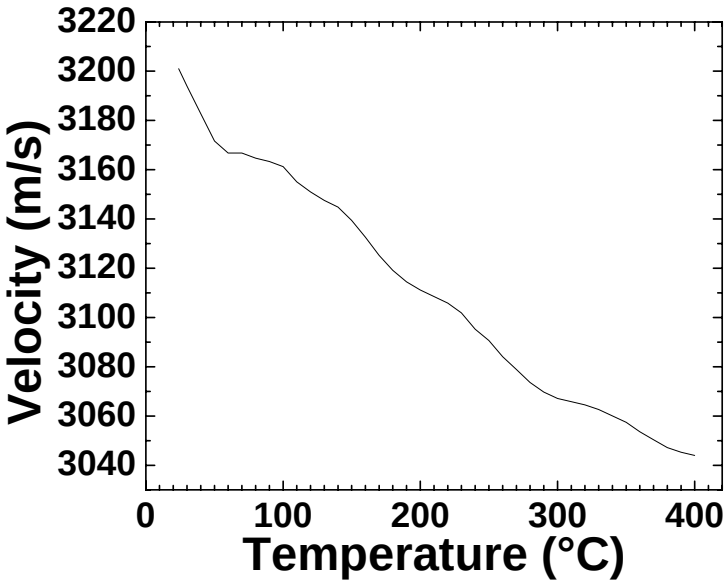

Figure 3-23 Relation between temperature and measured S wave velocity.

3.2.3 Screws for axial load measurement using ultrasound

When the screw is inserted into two hex caps shown in Figure 3-24, the value of axial load, *F*, exerted between the two caps can be calculated from the following first order approximated relationship [14]

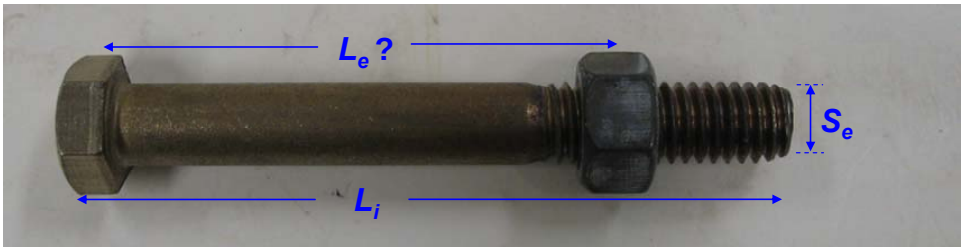

Figure 3-24 Schematic diagram for the axial load measurement.

$$\frac{t_{d,S}{}^{\sigma}}{t_{d,L}{}^{\sigma}} \cong \frac{V_L^0}{V_S^0}\left[1-\frac{L_e}{L_i}\left(A_S - A_L\right)\frac{F}{S_e}\right] \tag{3-4}$$

where $t_{d,L}{}^{\sigma}$ and $t_{d,S}{}^{\sigma}$ are the time of flight of the L and S wave, respectively, in the screw in the stressed state; $V_L{}^0$ and $V_S{}^0$ L and S wave velocities, respectively of the screw in the unstressed state; $L_i = L_0 + L_e$ and L_e the effective length and L_0 the unstressed portion of the screw; A_L and A_S the longitudinal and transverse acoustoelastic coefficients, respectively; and S_e the effective cross-sectional area of the screw. The capability to measure both the time delay of L and S waves in the screw allows the elimination of time-of-flight measurement of both waves in the unstressed state [14]. Reference [14] has also demonstrated that $V_L{}^0$, $V_S{}^0$, L_e, L_i and S_e can be obtained for screws. If $t_{d,L}{}^{\sigma}$ and $t_{d,S}{}^{\sigma}$ can be obtained, then the value of axial load F can be derived.

Figure 3-21 and Figure 3-22 (b) clearly indicate that the IUTs on the screw heads shown in Figure 3-19 can measure $t_{d,L}{}^{\sigma}$ and $t_{d,S}{}^{\sigma}$ even at 150°C. The high center frequency, large bandwidth and high SNR of IUT integrated onto the screw will enable the high precision time delay measurement of $t_{d,L}{}^{\sigma}$ and $t_{d,S}{}^{\sigma}$ as illustrated by Eq. (2-1) and Table 2-1. It is expected that the tightening tension force F may be evaluated without loosening the assemblies bolted with this screw and the measurement of the axial load F [14]. It is also an expectation that when a stress is exerted onto the screw (bolts, rivets or fasteners) bolting two plates due to a misalignment of the two plates or the sliding of one plate over the other because of the uneven load, the screw decribed here and equipped with the IUT sensor may be able to use the measured irregular or excessive F to detect such misalignment or uneven load situation for NDT and SHM applications.

3.2.4 Probes for curing monitoring

The curing process of Gr/Ep composites of large and complex shapes during fabrication is crucial for the determination of their integrity such as Young's modulus and shear modulus. Because of different thicknesses at different locations the reliable cure of Gr/Ep composites may be assured if proper monitoring and evaluation can be performed. *In situ* monitoring is preferred due to the cost effectiveness. For most Gr/Ep composite manufacturings using autoclave the maximum temperature is around 176°C [112]. Ultrasonic monitoring has been carried out using air cooled or water cooled UTs bonded or attached to the steel molds. Since L wave and mode-converted IUTs can operate above 176°C, they are chosen here for the demonstration of cure monitoring at an elevated temperature. Due to the limitation of the equipment available the cure monitoring of a polymer melt in a polymer injection molding (IM) machine is used here for illustration purposes. In this study, the probes which may provide simultaneous measurements of L and S at HT will be developed for the specific polymer IM machine. Information such as Young's and shear modulus of the polymer from melt solidified to solid will be studied.

Figure 3-25 (a) shows the developed L-S probe of mold insert, and the probe head has been designed as shown in Figure 3-19 (a) but with smaller dimensions for real-time non-invasive cure monitoring during the polymer IM process at HT. The IUT has a dimension of 6 mm by 5 mm and its thickness is about 81 μm. In Figure 3-25 (b) such a transducer probe is fitted into a medium steel mold insert with electrical connections. Then this medium mold insert is integrated into the mold of a 150 tons Engel IM machine as shown in Figure 3-26 for *in situ* monitoring. Ultrasonic signals in time domain of the L and S wave of the L-S probe reflected from the end of the probe at room temperature are presented in Figure 3-27. L^2 and S^2 are the first round-trip echoes reflected from the bottom of the probe. The center frequencies and 6 dB frequency bandwidths of the L^2 and S^2 waves are 12.5 MHz and 12 MHz, and 13.8 MHz and 12.8 MHz, respectively. The SNRs of the L^2 and S^2 wave are above 14 dB without any signal processing.

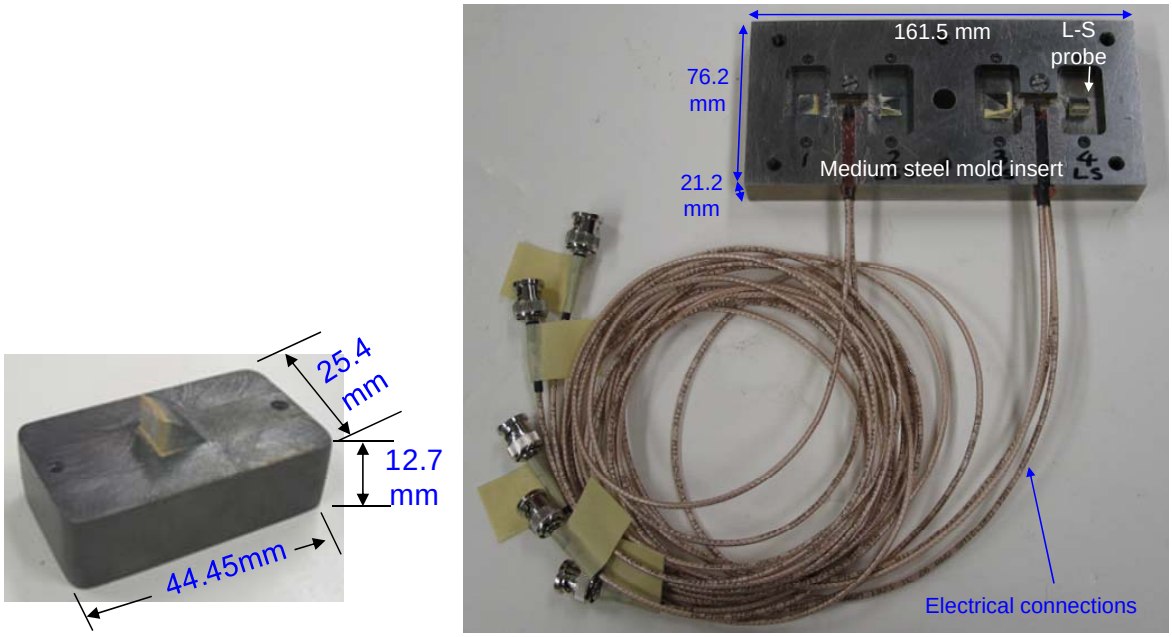

(a) (b)

Figure 3-25 (a) An L-S probe and (b) a medium steel mold insert with the L-S probe and electrical connections.

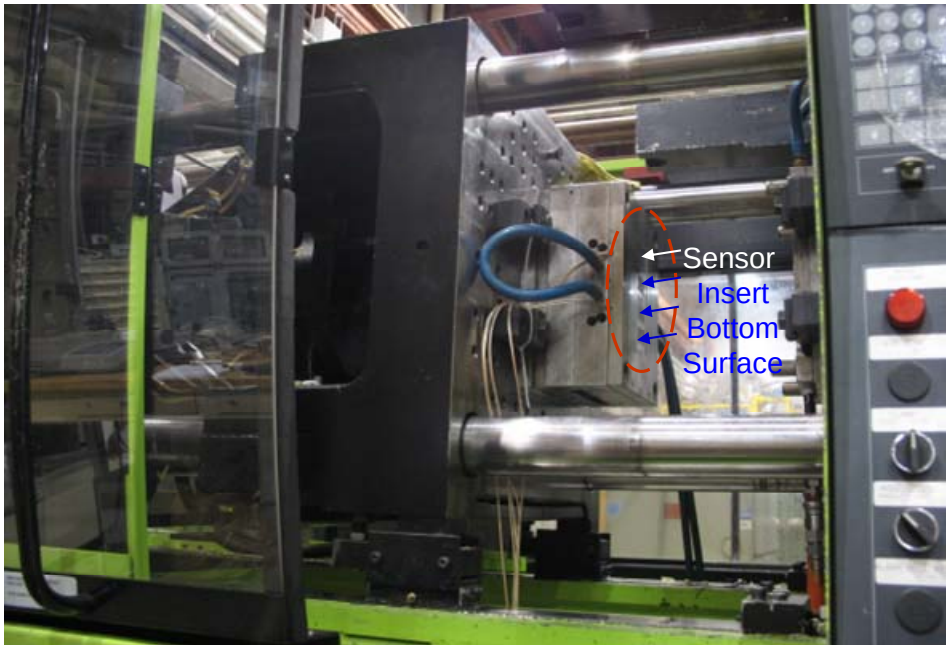

Figure 3-26 Mold insert integrated into an IM machine.

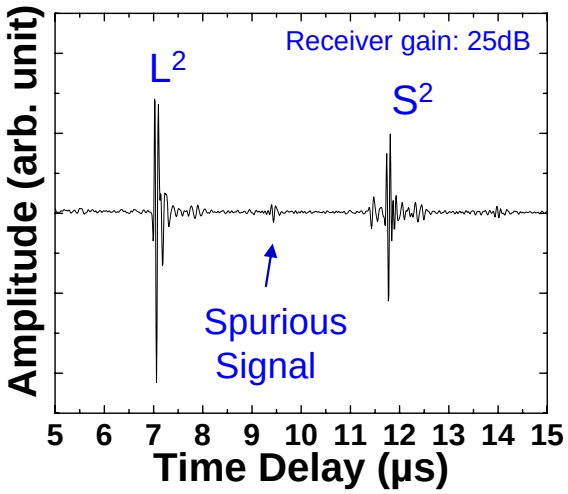

Figure 3-27 Ultrasonic signal in time domain of the L and S probe shown in Figure 3-25 (a) reflected from the bottom of the probe at room temperature.

Figure 3-28 shows the results of acquired signals with the integrated mold insert probe shown in Figure 3-25 (a) during the IM process of a high density polyethylene (HDPE) part at 210°C. However, at the IUT position the temperature is lower than 200°C, which is the maximum operation temperature of the PZT-c film IUT. It is noted that all the electrical connections shown in Figure 3-26 can bear the HT situation during IM of HDPE part at 210°C. L^2 is the echo reflected at the insert/polymer or air interface depending if the polymer melt existed at the probe location or not. This L^2 echo can be obtained regardless of the thickness of the melt. In Figure 3-28 (a) the timings T_A and T_B represent the melt flow front arrival and the molded part ejection at the probe location, respectively [113][114][115]. When the HDPE melt arrives at the probe location at T_A, the L_2 echo having propagated a round trip through the thickness of the HDPE melt within the mold cavity of 0.75 mm height starts to appear because the probe operates in a pulse/echo mode. When the polymer melt contacts the cold mold internal surface, the melt starts to solidify. Because HDPE is a semi-crystalline polymer, the attenuation will reach a peak which causes a dip in the profile of L_2 [112]. This dip is indicated at T_C in Figure 3-28 (a). During the IM, the cavity pressure changes because of the plunger movement [113]. The measured time of flights (TOFs) of the L and S waves travelled within the polymer melt are shown in Figure 3-28 (b). After the cavity pressure becomes steady near the timing T_P indicated in Figure 3-28 (b), the TOFs of both L and S waves decrease due to the solidification of the melt in the mold cavity in which the L and S

wave velocities increase. Since the attenuation of S wave is high in the melt, its TOF can be only observed when the melt solidifies into a viscous condition in which S wave probe has enough sensitivity to detect the round trip echo within the melt as indicated as T_S in Figure 3-28 (b). Assuming the density of the HDPE during the period between T_S and T_B is 0.94 g/cm^3, the *in situ* measured Young's and shear modulus are shown in Figure 3-29. It is the expectation that such probes shown in Figure 3-25 (a) may be used for the cure monitoring of the Gr/Ep composite within the autocave.

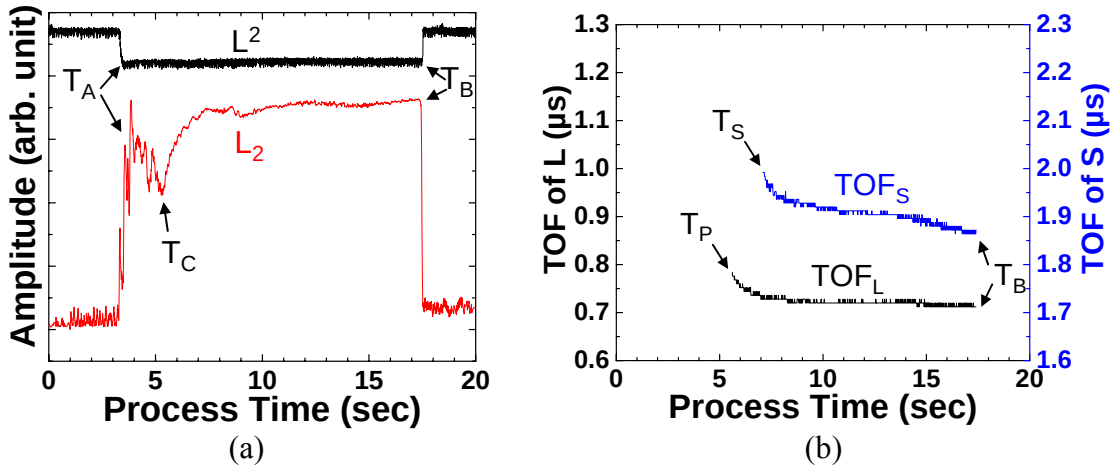

Figure 3-28 (a) Amplitude variations of L^2 and L_2 echoes measured by the mold insert probe shown in Figure 3-25. (b) TOF of the measured L and S. Arrows T_A and T_B indicate the time for flow front arrival and the molded part ejection at probe location, respectively.

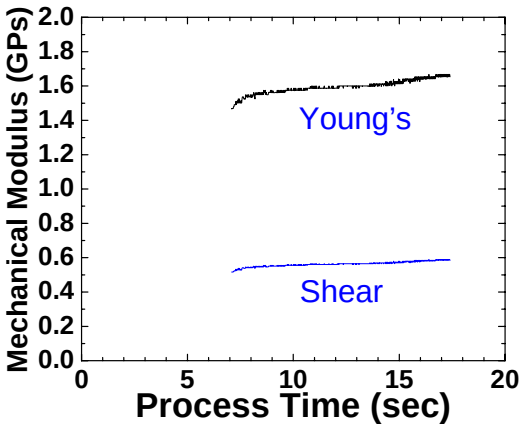

Figure 3-29 *In situ* measured Young's and shear modulus.

3.3 Ultrasonic Probes Simultaneously Producing One L and Two S Waves and Their Applications

Thickness measurement including corrosion and erosion monitoring using ultrasonic technology is routinely used in aerospace industries. Certainly high accuracy is desired. However, factors affecting the measurement accuracy using ultrasound can come from texture [15][99], stress [16][99][100][101] etc, which all alter the ultrasonic velocities in the material. In other words, if the thickness of the material is given, ultrasonic velocity variations may be applied to measure the stress and texture [15][16][99][100][101]. The combination of using L and S wave UTs was used to obtain L wave and two orthogonally polarized S wave velocities and measure the residual stress or texture in the textured steel at room temperature [15][99]. Let the particle displacement [78][10] of the L wave be along the Z direction of a Cartesian coordinate, then S_X and S_Y are designated as two orthogonal S waves whose particle displacements are along the X and Y directions, respectively. Also acoustic birefringence involving just S_X and S_Y measurements were also reported [116]. Some of experiments for the above mentioned studies were performed using EMAT [16][101]. However, EMAT cannot be used to measure the non-conducting substrates, and may be bulky and have low sensitivity for certain NDT and SHM applications.

3.3.1 Probes for two orthogonally polarized S waves

Using the L to S wave mode conversion principle shown in Figure 3-3 if one would like to generate two S waves with orthogonal polarizations (birefringence) simultaneously, θ will be made at two orthogonal edges as shown in Figure 3-10 and Figure 3-14. Because the screw is made with the same mild steel as that shown in Figure 3-4, $\theta = 61.5°$ is chosen. Figure 3-30 (a) shows a screw with IUTs made at two orthogonal edges which can generate and receive two orthogonally polarized S waves (S_X and S_Y) along the screw axis. The zoomed probe head is presented in Figure 3-30 (b). Let one S be the S_Y polarized in Y direction and the other S_X polarized in X direction as shown in Figure 3-30 (b). This probe is not designed to generate and receive L waves. Figure 3-31 (a) and Figure 3-31 (b) show the measured ultrasonic signal S_Y^n and S_X^n,

respectively reflected from the end of the probe in time domain and pulse-echo mode at room temperature where the time delay of S^n is that of the nth trip S echo through the probe length plus that of the L wave travelling through the length from L IUT to the steel/air interface. The signal S_S indicated in Figure 3-31 is a spurious signal which probably comes from the multiple reflections of L or S waves from an undetermined boundary. The measurement results shown in Figure 3-31 can be made simultaneously using a two-channel ultrasonic system. The center frequencies and 6 dB bandwidths of the S_Y^2 and S_X^2 signals shown in Figure 3-31 are 12 MHz and 11 MHz, and 13.4 MHz and 12 MHz, respectively. Their SNRs are 36.1 dB and 36.6 dB, respectively. It is noted that such a probe may be used as an ultrasonic interferometer which is sensitive to, for example, the anisotropy of the material to be measured, which induces a difference in particle displacement direction or velocity or both between two S wave propagations along the material.

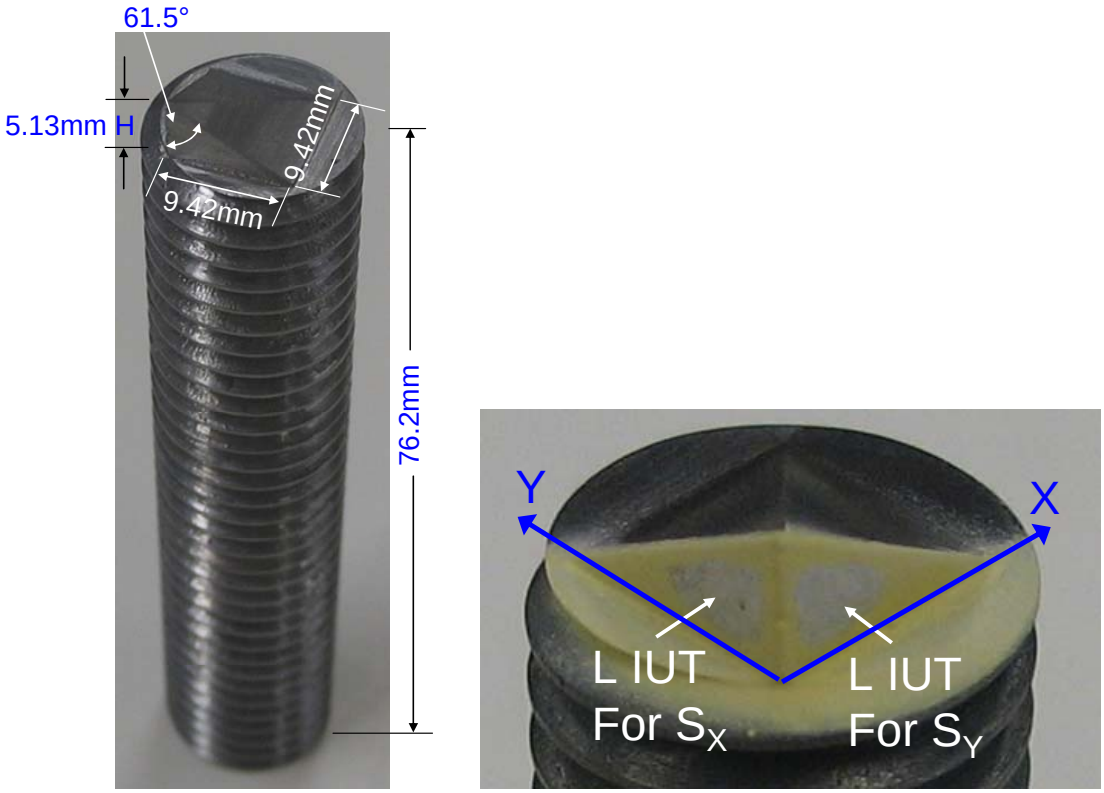

Figure 3-30 (a) An integrated S wave probe having two polarizations (S_X and S_Y) and (b) zoomed probe head having two IUTs.

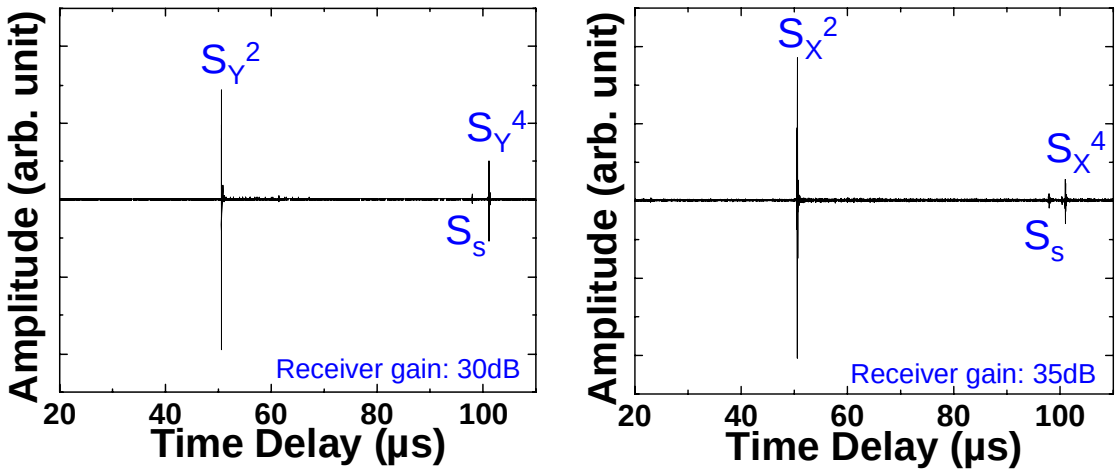

Figure 3-31 Ultrasonic signal in time domain of the (a) S_Y and (b) S_X wave generated by the L IUTs shown in Figure 3-30 reflected from the end of the probe at room temperature.

3.3.2 Three wave probes

Let a Cartesian coordinate system be XYZ with the Z direction being the through thickness direction for normal direction to a plate of the material, and X and Y being the rolling and transverse directions of a plate such as steel. The stress-free velocities for the propagation along the Z direction only depend on the texture coefficients W_{400} and W_{420} [15][16][100][101] and are given in an Voight [117] and approximation [16] by

$$\rho V_L^2 = \rho h^2 / t_{d,L}{}^2 = C_{11} - 2C\left[\frac{1}{5} - \frac{16\sqrt{2}\pi^2 W_{400}}{35}\right]$$

$$\rho V_{SX}^2 = \rho h^2 / t_{d,SX}{}^2 = C_{44} + C\left[\frac{1}{5} - \frac{16\sqrt{2}\pi^2}{35}\left[W_{400} + \sqrt{\frac{5}{2}}W_{420}\right]\right] \quad (3\text{-}5)$$

$$\rho V_{SY}^2 = \rho h^2 / t_{d,SY}{}^2 = C_{44} + C\left[\frac{1}{5} - \frac{16\sqrt{2}\pi^2}{35}\left[W_{400} - \sqrt{\frac{5}{2}}W_{420}\right]\right]$$

where V_L, V_{SX} and V_{SY} are the ultrasonic velocity and $t_{d,L}$, $t_{d,SX}$ and $t_{d,SY}$, the ultrasonic time delay of L, S_X and S_Y waves in the substrate with a thickness of h, and $C = C_{11} - C_{12} - 2C_{44}$, respectively. Let the polarization of S_X wave be along the X direction and that of S_Y be along the Y direction during the experiments. Using Eq. (3-5), if one adopts an averaging method and knows the signal crystal elastic constants C_{ij} [15][16][100][101] and the density ρ of the material in Eq. (3-5), two texture coefficients, W_{400} and W_{420}, can be calculated from the measured ultrasonic time delays, $t_{d,L}$, $t_{d,SX}$ and $t_{d,SY}$. Also an accurate measurement of the substrate (plate) thickness, h that is corrected for texture variations may be made [15].

If a probe is desired to generate and receive the above mentioned three waves with the orthogonally polarized particle displacements, namely L, S_X and S_Y signals simultaneously, then one side of the probe may be made as the one shown in Figure 3-19 and another side as the one shown in Figure 3-30. Certainly the ones shown in Figure 3-10 may be made as well. Here the former design is used. Figure 3-32 (a) shows the integrated probe having three polarizations and zoomed probe head is given in Figure 3-32 (b). Figure 3-33 (a) and Figure 3-33 (b) show the measured ultrasonic signal L^n, S_X^n and S_Y^n, respectively in time domain and pulse-echo mode at room temperature from the end of the probe. The time delay of L^n is that of the nth trip L echo through the probe length plus that of the L wave travelling through the length from L IUT to the 45° steel/air interface. The results of the measurements shown in Figure 3-33 can be carried out simultaneously using a two-channel ultrasonic system. During the top electrode fabrication for the device shown in Figure 3-32, the area of the top electrode and position can also be adjusted so that the amplitude ratio of the reflected L^2, S_X^2 and S_Y^2 can be varied. The center frequencies and 6 dB bandwidths of the L^2, S_X^2 and S_Y^2 signals are 19.1 MHz and 17 MHz, 17 MHz and 16 MHz, and 18 MHz and 17 MHz, respectively. Their SNRs are 23.2 dB, 23.3 dB and 38.4 dB, respectively. It is demonstrated here that such probes which can generate and receive three orthogonally polarized waves may be able to measure Young's modulus, shear modulus, anisotropy, axial load, etc at room or elevated temperatures off-line or on-line.

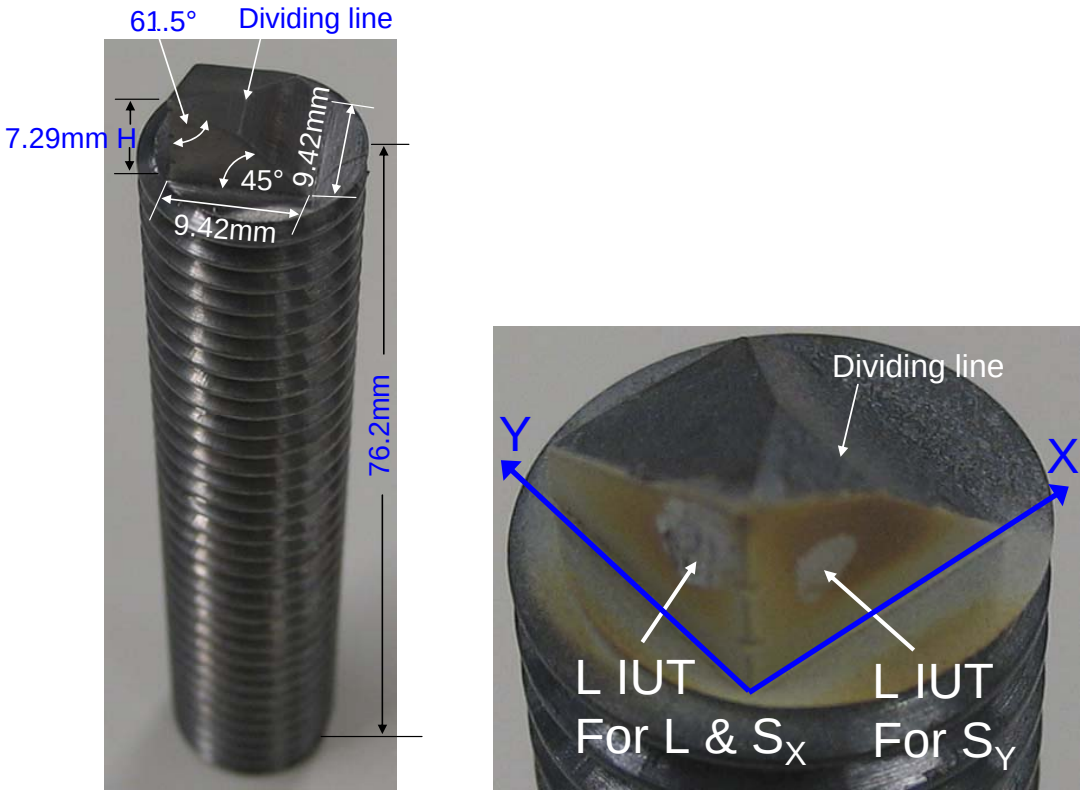

(a) (b)

Figure 3-32 (a) An integrated probe which can generate and receive L and S_X and S_Y waves simultaneous and (b) zoomed probe head having two IUTs.

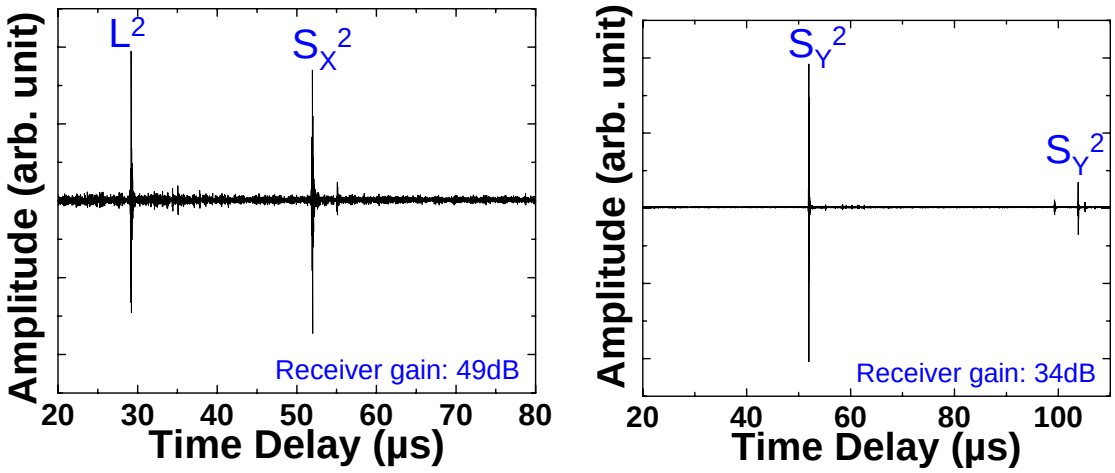

(a) (b)

Figure 3-33 Ultrasonic signal in time domain of the (a) L and S_X and (b) S_Y wave generated by the L IUTs shown in Figure 3-32 reflected from the end of the probe at room temperature.

3.4 Summary

Thick (> 75 μm) PZT-c and BIT-c films as piezoelectric IUTs were deposited on metallic substrates by the sol-gel spray technique to serve as L wave UTs. Using mode conversion technique, HTUT probes for S wave, those for one L and one S waves, and those for one L and two orthogonally polarized S waves, were presented in this chapter. Temperature measurement ranging from 24°C to 400°C and the *in situ* measurement of Young's and shear modulus of melted composite performed by these probes were also demonstrated.

In Section 3.1, integrated ultrasonic S wave and L-S wave probes were fabricated onto steel and Plexiglas substrates with the use of mode conversion from L to S waves. The L UTs were made in a plane parallel to the propagation direction of the mode converted S waves at the $\theta = 61.5°$ for steel substrates and at the $\theta = 63.2°$ for Plexiglas substrates. The reduction of energy conversion rate for steel substrates at $\theta = 61.5°$ is only 0.8% smaller than the maximum conversion rate 97.5% at $\theta = 67.2°$. A probe that can simultaneously generate and receive both L and S waves by one IUT by making a slanted surface with 45° at the intersection of the slanted plane with angle θ for mode conversion from L to S waves and the line from the center of the IUT was demonstrated. The S wave and L-S wave probes of BIT-c film IUTs have been made and operated at up to 350 °C with a center frequency of 6.7 and 7 MHz, 6 dB bandwidth of 3 and 3.8 MHz, and SNRs of more than 20 dB.

As mentioned above a 45° slanted surface was made in the L-S wave probe to generate L and S waves simultaneously by one IUT. However, the calculated energy reflection coefficient from L wave to L wave for the 45° reflection plane between steel and air was only 16.8%. An alternative approach using two UTs for L-S wave probes was presented. An L-S steel probe using two IUTs and an L-S Plexiglas probe gluing two FUTs were demonstrated at temperatures up to 150°C, and room temperature, respectively. A 2.28 mm thick flat glass plate and a 0.83 mm thick Plexiglas were used as samples for the measurements of V_L and V_S of materials. The V_L and V_S of the samples calculated from the ultrasonic signals measured by the steel probe agreed well with the

ones measured by the Plexiglas probes. Because of the improved acoustic impedance matching between the Plexiglas probe and the samples at the probe-sample interface, more acoustic energy was transmitted into the samples, and thus may enable to measure the material properties such Young's and shear modulus of relatively thin samples.

In Section 3.2, a miniature PZT-c film IUT with dimensions of 7 mm by 4 mm by 75 μm was directly deposited onto a mild steel screw head. The screw had a length of 76.2 mm and a diameter of 15.9 mm including the thread. L and S waves were able to propagate simultaneously along the axial direction of the screw using a 45° reflection and 61.5° mode conversion angles, respectively. Due to more than 12 dB SNRs for both L and S wave echoes at 150°C it is expected that the axial load of this screw may be measured on-line using the time delays of these two waves together with digital signal processing [14]. In order to use every possible screw for on-line average temperature measurements one discontinuity of a 1.72 mm step was made near the end of the above screw. The clearly separated L and S echoes reflected from this discontinuity and screw end were used for the average temperature measurements. Such a screw with a step discontinuity was used to measure the temperatures (up to 400°C) above the IUT operation temperatures (200°C maximum). The calculated S velocities from room temperature of up to 400°C using the S wave signals reflected from the 1.72 mm step and screw end were presented.

L-S probe of steel mold inserts for cure monitoring of plastics during fabrication process were presented. The dimensions of the mold insert probe are 44.45 mm by 25.4 mm by 12.7 mm, and a 6 mm by 5 mm by 81 μm PZT-c film IUT was coated to generate and receive L and S waves simultaneously. Due to the limitation of the equipment availability the cure monitoring of a polymer melt in an IM machine was carried out to simulate the cure monitoring of Gr/Ep composites commonly used as aerospace materials. The results of acquired signals with the L-S mold insert probe during the IM process of a HDPE part at 210°C were presented while at the IUT position the temperature was lower than 200°C, which is about the maximum operation temperature of the PZT-c film IUT. The *in situ* measured Young's and shear modulus were presented.

In Section 3.3, two integrated ultrasonic orthogonally polarized S_X and S_Y (shear birefringence) and three orthogonally polarized L, S_X and S_Y probes have been presented. They were fabricated onto the heads of steel rods in screw shape through the sol-gel spray technique. The typical PZT-c film thickness in this section is 75 μm. Mode conversion from L to S waves and reflection from a 45° slope for L waves have been used. All the above mentioned probes were operated at room temperature with a center frequency ranging between 12 MHz and 19 MHz, and a 6 dB bandwidth ranging between 11 MHz and 17 MHz, and a SNR of more than 23 dB. It is noted that these PZT-c film IUTs may operate at up to more than 150°C. If BIT-c film is used, the operation temperature may be up to 400°C. Such probes may be used to measure accurately the thickness of a sample with a correction of texture including texture coefficients such as W_{400} and W_{420} [15].

CHAPTER 4

PLATE ACOUSTIC WAVE AND SURFACE ACOUSTIC WAVE

NDT and SHM [5][17] is a major concern of the aerospace community when considering aging aircrafts whose growing maintenance costs can reduce their economic life extension. Also emerging new airplanes are increasingly required to be equipped with intelligence for improved diagnostics of the health condition of the critical parts and structures. Therefore, there are demands for miniaturized light weight integrated *in situ* sensors and associated techniques for local and global (long distance) damage diagnostics [3]. In this chapter, IUTs and FUTs for the generation and receiving of PAW and SAW [78][10][118][119][120] which propagated many hundreds of mms along 2 mm thick Al plates for global line defect detections will be developed. PZT-c film IUTs will be directly fabricated, or PZT-c film FUTs will be glued, at the end edges of the plates by the sol-gel spray technique described in Section 2.1. They normally operate as thickness vibration L mode UTs. Therefore mode conversion techniques [78][121][122][123] will be used in conjunction with such UTs to excite and detect symmetrical, anti-symmetrical and SH types of PAWs. The operation temperature of these PZT-c film and BIT-c film IUTs will be tested up to 150°C and 350°C, respectively. The comparisons among these mode converted PAWs will be discussed.

Wedges made of Plexiglas are commonly used to convert L or S waves in the Plexiglas into guided PAWs and SAWs along metallic plates or pipes for NDT [10][124] and SHM purposes. However, the operation temperature of the Plexiglas wedges is

limited to less than 100°C. In this chapter HT wedges made of brass will be presented for excitation and detection of guided acoustic waves.

Mechanical line-shape gratings have been used to effectively convert bulk L wave to SAW [125][126]. The main applications were aimed at high frequency SAW filters or as reflectors for touch screen panels recently [127][128][129]. In this chapter HT guided acoustic PZT-c film IUTs and FUTs using mechanical gratings for NDT or SHM will be presented at up to 150°C.

HT IUTs with IDT shape of top electrode is also developed to generate and receive PAW or SAW. The ultrasonic performance of these transducers will be demonstrated at 150°C for an Al plate and a steel cylinder using PZT-c film IUTs, and at 350°C for a SS plate using BIT-c film IUTs.

4.1 HT Piezoelectric PAW UTs Using Mode Conversion

In this chapter PZT-c film IUTs will be presented for the experiments carried out in Sections 4.1-4.4 and BIT-c film in Section 4.4 only. The experiment measurements using PZT-c film FUTs will be given in Section 4.1.3.

4.1.1 HT piezoelectric PAW IUTs fabrication

PZT-c films were coated onto an Al plate directly by the sol-gel spray technique as described in Section 2.1, and silver paste was used to fabricate top electrodes. The heat treatment for the PZT-c film IUT here was carried out at 300°C in order not to harm or change the material properties of the Al plates. For this study the top electrode size for IUT was chosen for the size and shape of the active area for PAW generation and receiving and their detail dimensions will be given later. Figure 4-1 shows a schematic of an IUT directly coated onto the end edge of an Al plate. The Cartesian coordinates are also shown.

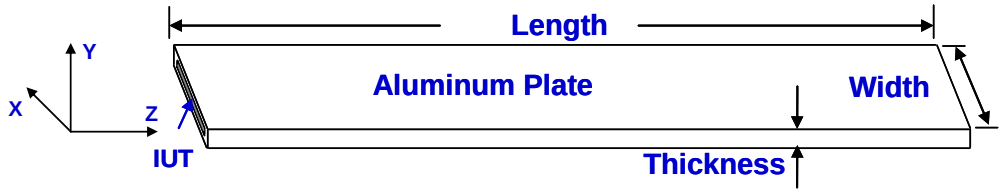

Figure 4-1 Schematic diagram of an IUT deposited onto the end edge of an Al plate to generate and receive predominantly symmetrical and anti-symmetrical PAWs.

4.1.2 Mode conversion technique

The PZT-c film IUT shown in Figure 4-1 is, in principle, an L wave thickness vibration UT. However, when IUT deposited onto the end edge of a 2 mm thick Al plate as shown in Figure 4-2 this IUT will generate and receive predominantlly symmetrical and anti-symmetrical PAWs [78][10][118] due to the finite thickness of the plate.

Mode conversion [79][122][123] presented in Chapter 3 showed that L wave can be converted into S waves for NDT applications. It was demonstrated that there existed shear vertical (S_Y: particle displacement parallel to Y axis) and SH (S_X: particle displacement parallel to X axis) in bulk materials [78][10]. Here using IUTs the analogies of mode conversion from L wave to S_Y and to SH modes have been developed for the mode conversion from L like waves to predominantly symmetrical & anti-symmetrical and SH PAWs, respectively as shown in Figure 4-2 and Figure 4-3. In Figure 4-2 the particle displacement of the L waves will be mode converted to an S_Y with the same particle displacement direction if the Al plate is thick (> 10 S wavelength) enough; however, because the Al plate is just a few wavelengths thick, it is not able to support S_Y, but rather predominantly symmetrical and anti-symmetrical PAWs. Similarly, in Figure 4-3, the particle displacement of the L waves will be mode converted predominantly to the SH PAWs with the particle displacement direction parallel to X axis. The mode conversion angles ϕ and θ shown in Figure 4-2 and Figure 4-3, respectively will be discussed in the latter sections.

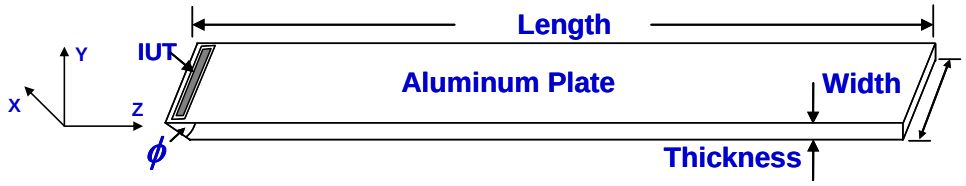

Figure 4-2 Schematic diagram of an IUT deposited onto the end edge of an Al plate to generate and receive predominantly symmetrical and anti-symmetrical PAWs.

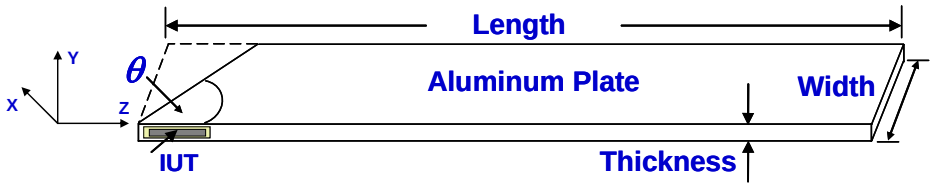

Figure 4-3 Schematic diagram of an IUT deposited onto the end edge of an Al plate to generate and receive predominantly SH PAWs.

4.1.3 Ultrasonic performance

For NDT and SHM the ability of PAWs to detect defects in long distances is essential. Therefore the focuses in this section will be to evaluate (i) the propagation distance of symmetrical, anti-symmetrical and SH PAWs excited and received by the developed PZT-c film IUTs deposited onto the end edges of 2 mm thick Al plates and (ii) the ability of these three types of PAWs to detect artificial line defects at room temperature and up to 150°C. In order to detect the defect locations, the pulse/echo mode is chosen although the transmission mode can be used. The maximum heat treatment temperature for the PZT-c film to be deposited onto the Al plate as IUTs will be limited, for example, 300°C, because the heat treatment temperature is not allowed to harm or change the material properties of the Al parts and structures, for example, of the airframes. Due to the low heat treatment temperature the piezoelectric strength of the PZT-c film will be reduced compared with the PZT-c films having the normal heat treatment of 650°C as mentioned in Chapter 2. Therefore the merits of FUTs glued at the end edges of the 2 mm thick Al plate for the generation and receiving of SH PAW will

also be presented in this section. The signal strength obtained by the FUT will be compared with that obtained by the IUT.

4.1.3.1 Symmetrical and anti-symmetrical PAWs

Figure 4-4 shows the symmetrical and anti-symmetrical PAWs ($S_{L,2}$) generated and received by the 88 μm thick PZT-c IUT shown in Figure 4-1 at 150°C in an 2 mm thick, 50.8 mm wide and 406.4 mm long Al plate. This IUT has dimensions of 1 mm high and 48 mm wide and it can generate and receive PAWs nearly entire end surface of the Al plate. The subscript 2 of the $S_{L,2}$ echo denotes the 1st round trip echo from the IUT location to the other edge of the plate. The center frequency and 6 dB bandwidth of the $S_{L,2}$ echo are 6.2 MHz and 0.5 MHz, respectively. It means that $S_{L,2}$ has traveled a total distance of 812 mm.

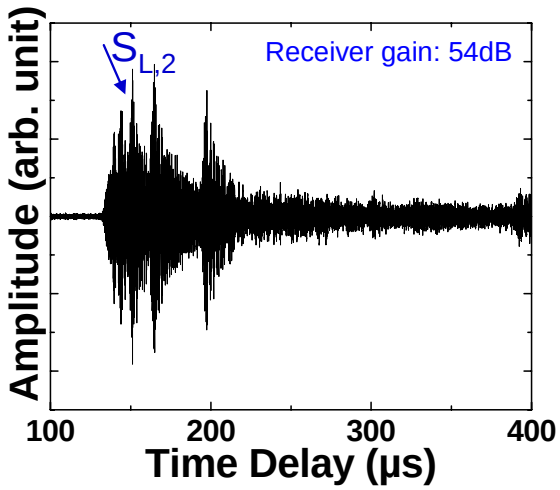

Figure 4-4 Ultrasonic PAW signals obtained in a 2 mm thick Al plate using IUT shown in Figure 4-1 at 150°C.

The group velocity of the $S_{L,2}$ echo at the leading edge was about 5462 m/s which is slower than that of the measured through Al plate thickness L wave velocity, V_L = 6364 m/s. Using the measured V_L and V_S of the Al plate at room temperature and the formulas in refs. [78] and [118], the PAW velocity dispersion curves are calculated. The calculated phase and group velocities for several low order symmetrical and anti-symmetrical modes are given in Figure 4-5. Figure 4-5 implies that $S_{L,2}$ consists of many lower order

symmetrical and anti-symmetrical modes. From the measured group velocity of 5462 m/s and the center frequency of 6.2 MHz it is believed that the main mode contribution to the $S_{L,2}$ PAW signal would be the 4th order symmetrical S_4 mode shown in Figure 4-5.

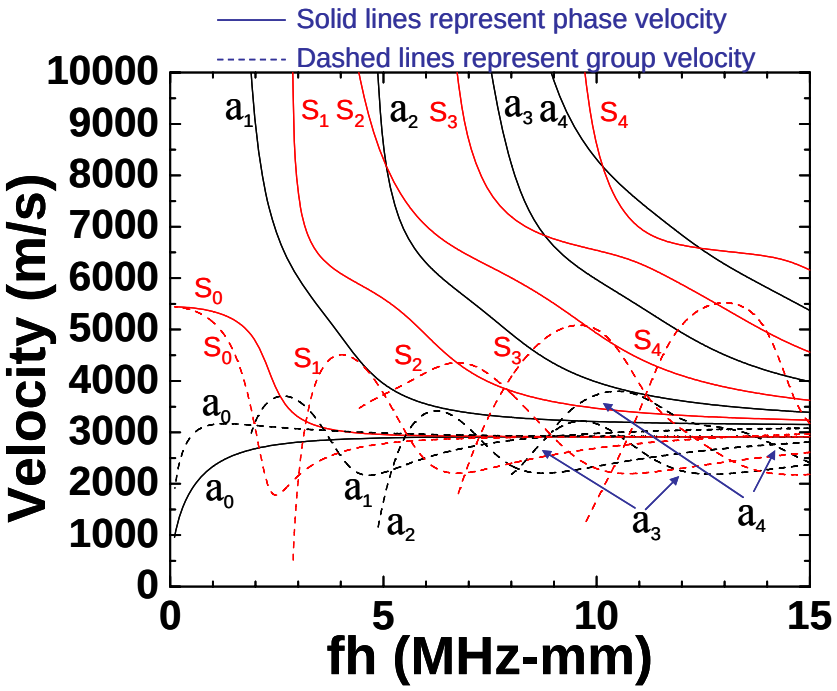

Figure 4-5 Theoretically calculated phase and group velocities versus the product of PAW frequency, *f*, and plate thickness, *h*, curves for the first few symmetrical (S) and anti-symmetrical PAW modes in the 2 mm thick Al plate.

To examine the long distance capability of SHM of the symmetrical S_4 PAWs two artificial line defects, D1 and D2 with 1 mm depth and 1 mm width were made onto the Al plate shown in Figure 4-1. D1 and D2 had length of 25.4 mm and 50.8 mm, respectively as shown in Figure 4-6. At 150°C the measured symmetrical S_4 PAWs are given in Figure 4-7. Figure 4-4 in which no line defect exists and Figure 4-7 in which two line defects are present clearly confirm that symmetrical S_4 PAWs can be used to perform SHM of defects at 150°C. In Figure 4-7, almost all the energy of the symmetrical S_4 PAWs have been reflected by the two line defects, so the $S_{L,2}$ echo reflected from the end of the plate cannot be sufficiently detected. In Figure 4-6 the two line defects were 146.3 mm and 223.5 mm away from the IUT.

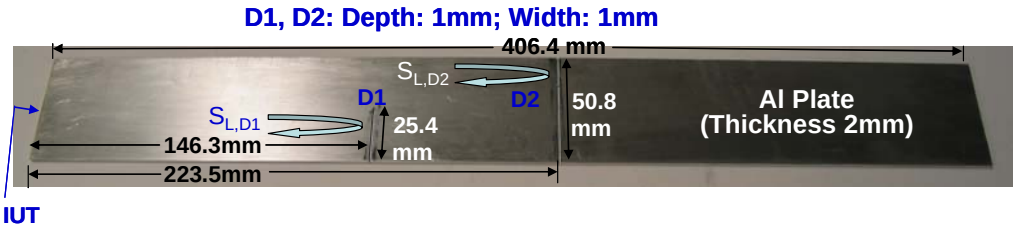

Figure 4-6 Two artificial line defects, D1 and D2 were made onto a 2 mm thick Al plate.

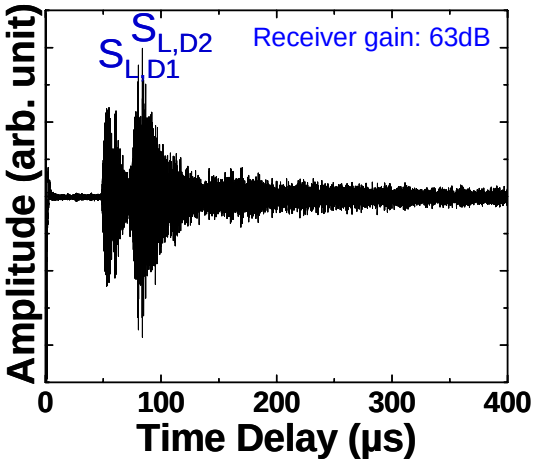

Figure 4-7 Symmetrical S_4 PAW signals detecting two artificial line defects, D1 and D2 in a 2 mm thick Al plate shown in Figure 4-6 at 150°C.

A 90 μm thick PZT-c film IUT was coated on top of an Al plate as shown Figure 4-2. This IUT has dimensions of 1.8 mm in length and 15.0 mm in width so that strong ultrasonic signals can be obtained. The chosen mode conversion angle ϕ using the analogy of bulk L wave to S_Y for this configuration was 63.7° which was obtained from the phase matching angle [123] of the measured bulk L and S wave velocities of the Al plate. In a bulk Al sample the energy conversion rate from the bulk L wave to the S wave at this angle is 83.1%, which is only 0.02% smaller than the maximum conversion rate. Due to this mode conversion configuration the S_Y becomes predominantly symmetrical and anti-symmetrical modes (A_{SV}) because of the finite thickness of the Al plate (< 10 S wavelength). The A_{SV} is excited although the angle ϕ has not been optimized, because this is a plate (finite dimensions) configuration, the analogy of the bulk (infinite dimensions) material configuration is only used for initial studies. In the future theoretical evaluation to obtain optimal conversion angle ϕ will be performed.

Figure 4-8 shows the reflected PAW $A_{SV,2}$ echoes at 150°C in the time domain. The subscript 2 of the $A_{SV,2}$ echo denotes the 1st round trip echo from the IUT location to the other edge of the plate. It indicates that $A_{SV,2}$ has traveled a total distance of ~812 mm. The center frequency and bandwidth of the $A_{SV,2}$ echo are 7 MHz and 4.9 MHz, respectively. From the measured group velocity of 3130 m/s and a center frequency of 7 MHz, it is believed that $A_{SV,2}$ may be composed of mainly the zeroth order (a_0) anti-symmetrical PAW [78][10][118][137]. Since this Al plate supports multimode anti-symmetrical PAW propagation, some of the higher order modes having traveled faster than the zeroth order anti-symmetrical mode arrived earlier as shown in Figure 4-5 in which the group velocities of a_1, a_2 a_3 and a_4 are larger than that of a_0.

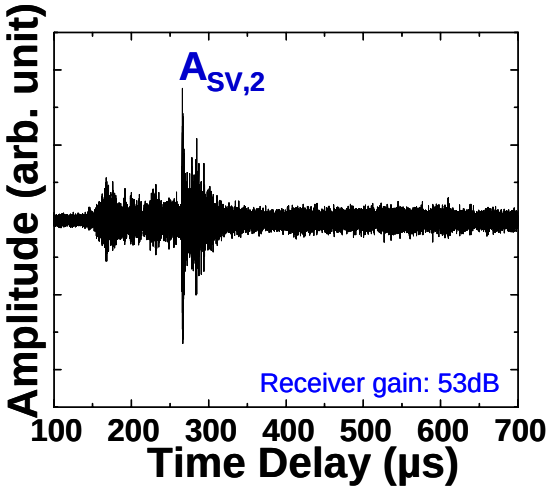

Figure 4-8 Ultrasonic PAW signals obtained using IUT shown in Figure 4-2 at 150°C with mode conversion. The Al plate length was 406.4 mm.

To evaluate the defect detection ability of the current PAW configuration two line defects with dimensions and locations away from the IUT nearly identical to those (D1 and D2) for S_4 PAWs shown in Figure 4-6 were created for the 2 mm thick Al plate as shown in Figure 4-9. Figure 4-10 shows that two line defects and the end of the plate can be detected simultaneously at 150°C. Because the pulse widths of $A_{SV,D1}$, $A_{SV,D2}$ and $A_{SV,2}$ are relatively shorter comparing to those of $S_{L,D1}$, $S_{L,D2}$ and $S_{L,2}$, it is further confirmed that mainly a_0 anti-symmetrical PAW which has a nearly constant group velocity over the excitation frequency range was generated and received.

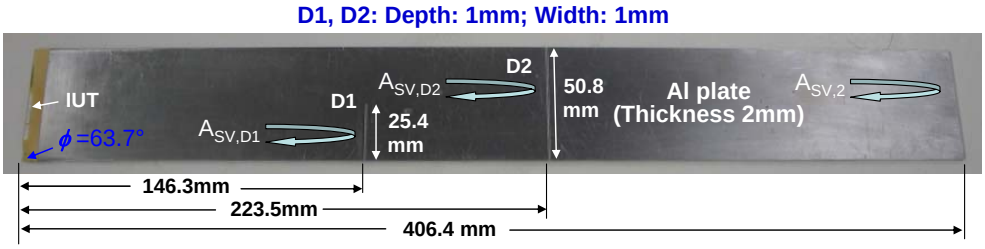

Figure 4-9 One IUT coated directly onto the end edge of a 2 mm thick Al plate shown in Figure 4-2 with an angle of 63.7° to generate and receive PAW using mode conversion. Two artificial line defects, D1 and D2 were also made onto the Al plate.

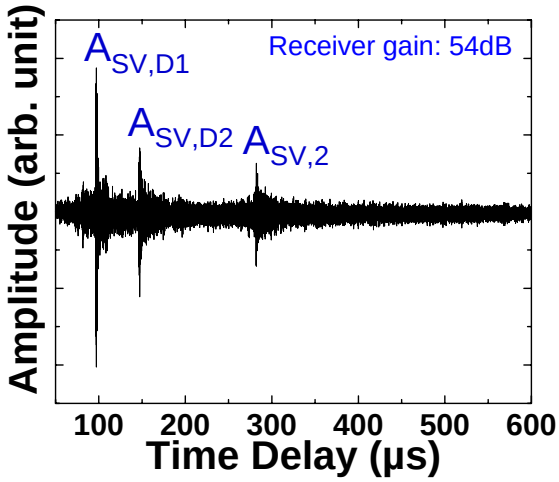

Figure 4-10 Anti-symmetrical a_0 PAW signals detecting two artificial line defects, D1 and D2, in the 2 mm thick Al plate shown in Figure 4-9 at 150°C.

4.1.3.2 SH PAWs

If the IUT or FUT is located at the edge indicated in Figure 4-3, predominantly SH PAWs [78][10], in which particle displacement is parallel to X axis (S_X), can be produced and received using mode conversion. In Figure 4-3 the thickness of the PZT-c film was 90 μm. The IUT has dimensions of 1.6 mm in height and 20.0 mm in length so that strong SH PAWs can be generated and received. For this configuration symmetrical PAW echoes traveled nearly 25.4 mm and then converted to SH PAW modes and vice versa. For this configuration the chosen mode conversion angle θ using the analogy of bulk L wave to SH was 61.7° which was calculated using the phase matching between measured PAW velocity $S_{L,2}$ and the S wave velocity of the Al plate. The purpose of the phase

matching is to achieve the generation and receiving of predominantly the lowest order SH PAW (SH_0). Similar to the mode conversion angle ϕ, θ will be optimized in the future study.

Using the IUT shown in Figure 4-3 the reflected predominantly SH PAWs echoes at 150°C without two line defects in time domain is given in Figure 4-11. After traveling nearly a distance of 813 mm the center frequency of the $S_{H,2}$ echo was 6.3 MHz. The subscripts 2 and 4 denote the 1st and 2nd round-trip echo, respectively. $S_{H,4}$ echo traveled a distance of 1.625 m. Compared with the PAW signals obtained for symmetrical and anti-symmetrical modes, SH PAW echoes show the highest SNR. Using the measured V_L and V_S of the Al plate at room temperature, and the formulas in [78] and [118], the PAW velocity dispersion curves are calculated. Theoretical calculation results as shown in Figure 4-12 also reveal that $S_{H,2}$ echo mainly comes from the zeroth order SH PAW having the bulk S wave velocity [78][10]. Also the group velocities of the higher order SH PAWs in the current configuration are slower that that of bulk S wave velocity as shown in Figure 4-12 and that is why they arrived a little bit later than $S_{H,2}$ echo.

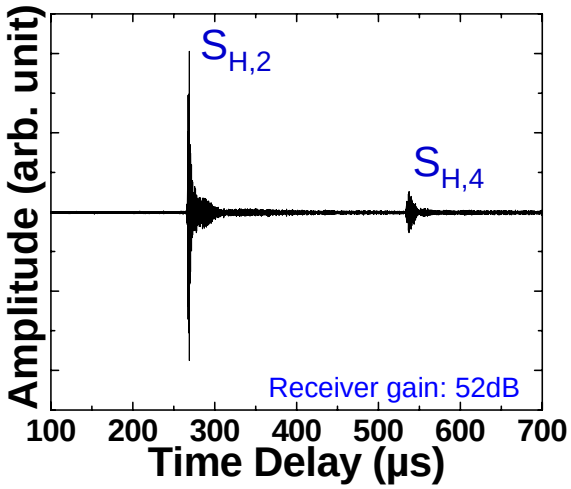

Figure 4-11 Ultrasonic SH PAW signals obtained using IUT shown in Figure 4-3 on a 2 mm Al plate at 150°C with mode conversion.

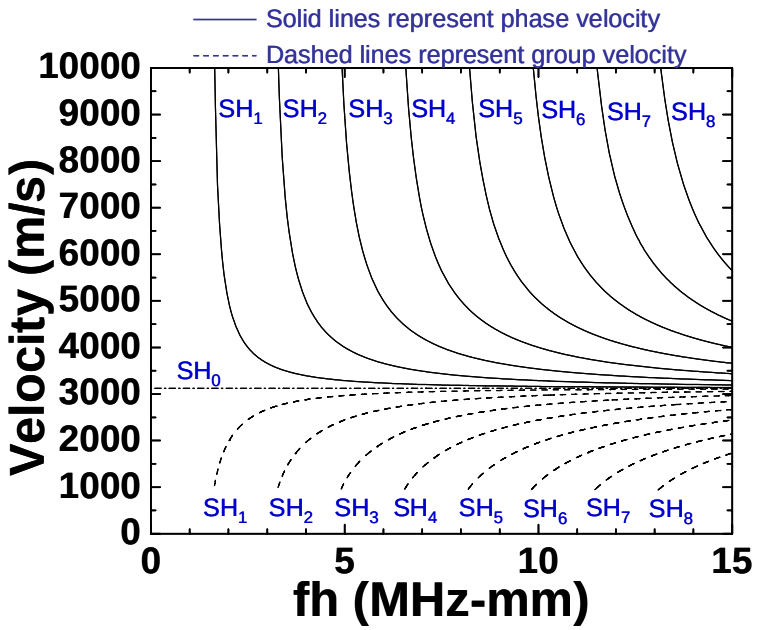

Figure 4-12 Theoretical calculated phase and group velocities versus the product of PAW frequency, *f*, and plate thickness, *h*, curves for the first few SH PAW in the 2 mm thick Al plate.

As mentioned earlier, the heat treatment temperature of the PZT-c film deposited onto Al plate will be limited, for example, to 300°C to avoid the potential damaging or changing of the material properties of the Al parts and structures of the airframes. Such low heat treatment will reduce the piezoelectric strength of the PZT-c film. As an alternative to coat IUT on the side edge of the Al plate, indicated in Figure 4-3, a PZT-c film FUT deposited onto a 75 μm thick Ti membrane was glued at that location, as shown in Figure 4-13 (a), to generate and receive SH PAWs. The FUT not only has the advantage of on-site installation capability but also of providing high piezoelectric strength because it can be fabricated off-line with mass production in mind to reduce the transducer costs. The glue used is cured at room temperature for 24 hours and can sustain thermal cycle temperature range between -80°C and 100°C which covers the common airplane operation temperature. This glue which serves as the ultrasonic couplant between the FUT and the Al plate has been successfully tested together with the PZT-c film FUT within this temperature range. The top rectangular electrode of the PZT-c film FUT has been made with a height of 2 mm and a width of 25 mm, which define this FUT active area. The measured predominant SH PAW signals at 100°C are shown in Figure

4-13 (b). The $S_{H,2'}$ and $S_{H,4'}$ are the 1st and 2nd round-trip echo from the FUT location to the other edge of the Al plate, respectively. The measurement was carried out at temperatures of up to 100°C which is limited by the glue used here. Compared with the results shown in Figure 4-11 measured by IUT on the Al plate, the ones shown in Figure 4-13 and measured by FUT of Ti membrane are about 30 dB stronger. It is also noted that the bonding of FUT is a convenient and attractive on-site installation approach for NDT and SHM applications.

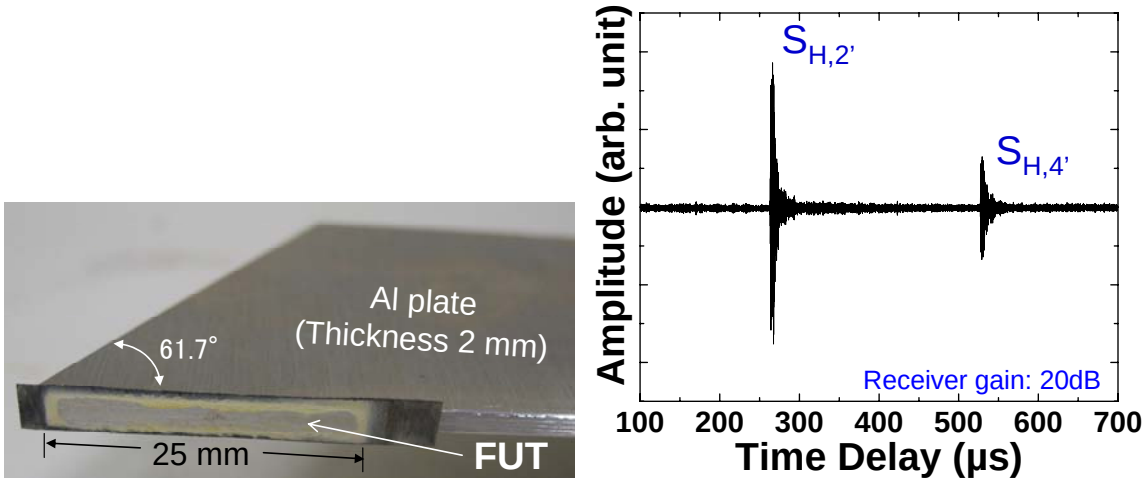

(a) (b)

Figure 4-13 (a) One FUT glued onto the side surface near the end edge of an Al plate as shown in Figure 4-3 with an angle of 61.7° to generate and receive SH PAW using mode conversion. (b) Measured predominant SH PAW signals at 100°C.

In order to demonstrate the NDT and SHM capability using guided acoustic waves two line defects with dimensions and locations away from the IUT nearly identical to those (D1 and D2) for symmetrical PAWs shown in Figure 4-6 were created in the plate as shown in Figure 4-14. At 150°C the reflected SH PAW signals are given in Figure 4-15. Figure 4-11, in which no line defects exist, and Figure 4-15, in which two line defects are present, clearly confirm that SH PAWs can be used to perform NDT and SHM of line defects at 150°C. In the case shown in Figure 4-15 not only can SH PAWs clearly detect the defects which are 146.3 mm and 223.5 mm away from the IUT, but they also travel to the end of the plate and return back to the IUT as indicated by the echo $S_{H,2}$ with

good SNR. Therefore for the 2 mm thick Al plate SH PAW showed better NDT and SHM capability than symmetrical and anti-symmetrical PAWs.

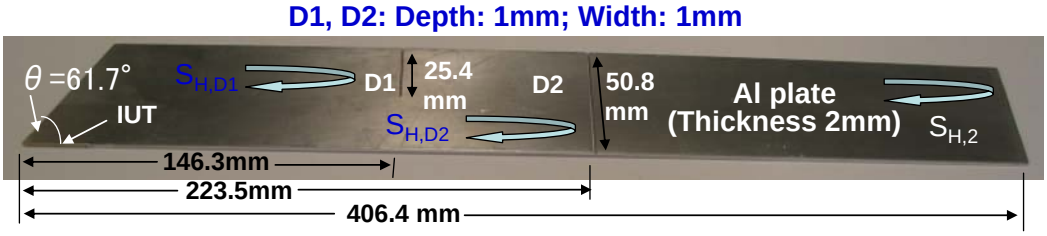

Figure 4-14 One IUT coated directly onto the side surface near the end edge of an Al plate as shown in Figure 4-3 with an angle of 61.7° to generate and receive SH PAW using mode conversion. Two artificial line defects, D1 and D2 were also made onto the 2 mm thick Al plate.

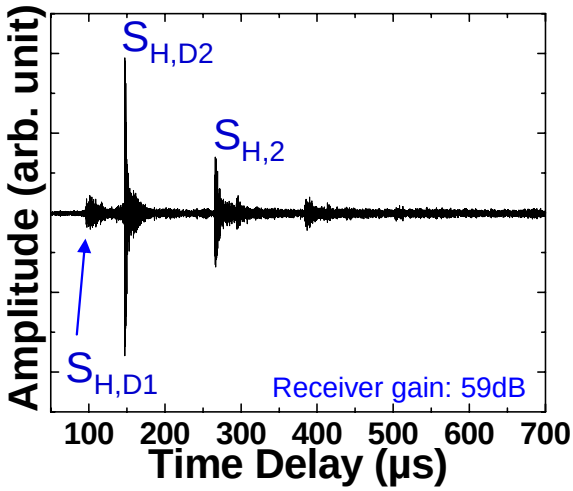

Figure 4-15 SH PAW signals detecting two artificial line defects, D1 and D2 in the 2 mm thick Al plate shown in Figure 4-14 at 150°C.

A real size Bombardier regional jet horizontal stabilizer coupon shown in Figure 4-16 is then used as a test sample. The thickness of the Al frame is not uniform and ranges from 1.1 to 1.3 mm. At one edge of the Al plate indicated in Figure 4-16 an angle of θ = 61.7° is created to generate and receive SH PAW using mode conversion. An IUT consisting of 75 μm PZT-c film and having a top silver paste electrode size of 12 mm by 1 mm was made at the location indicated in Figure 4-16. The reflected SH PAW signals at room temperature are given in Figure 4-17. $S_{H,F}$ is SH PAW reflected from the location

with a line-shape bolted joint underneath the frame, and $S_{H,2}$ is that reflected from the end of the frame. Figure 4-17 demonstrates the promising results of PZT-c film IUT to generate and detect SH PAW in a real airframe for possible NDT and SHM applications.

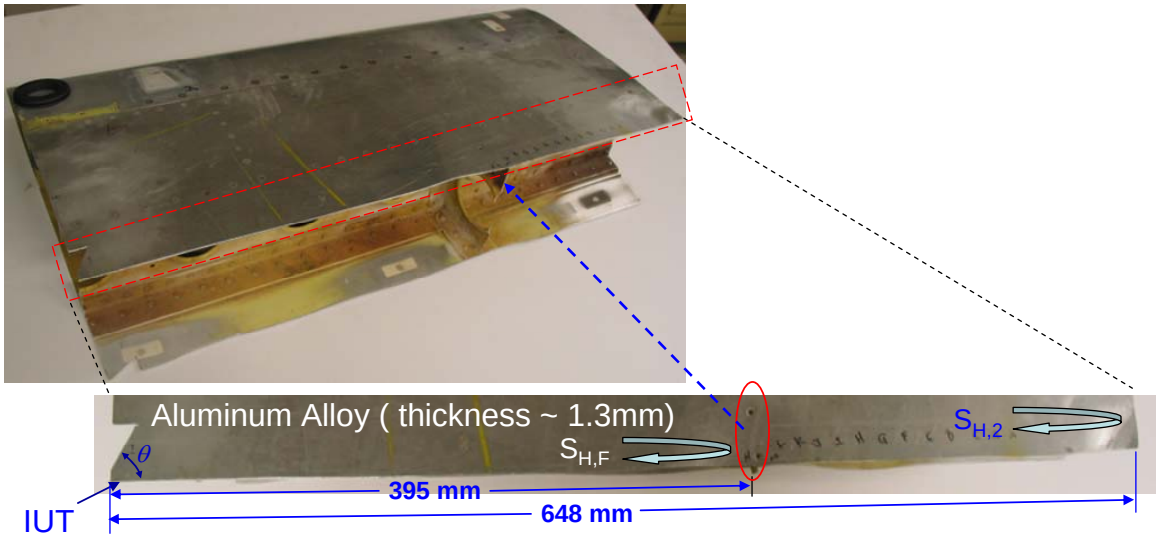

Figure 4-16 One IUT coated directly onto the side surface near the end edge of an Al horizontal stabilizer with an angle θ of 61.7° to generate and receive SH PAW using mode conversion. $S_{H,F}$ is SH PAW reflected from the location with a line-shape bolted joint underneath the frame, and $S_{H,2}$ is that reflected from the end of the frame.

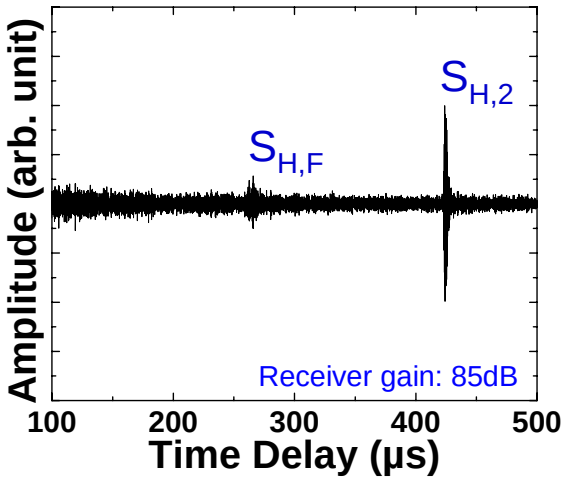

Figure 4-17 Ultrasonic SH PAW signals obtained using IUT on an Al stabilizer shown in Figure 4-16 at room temperature.

4.1.4 Comparison between theoretical calculations and experimental results

In order to reduce the number of experiments to investigate the sensitivity of defect detection, numerical simulation is valuable. Figure 4-18 (a) and Figure 4-18 (b) show the measured and numerically calculated results, respectively, in time domain at room temperature for the PAW defect detection configuration shown in Figure 4-6. The numerical simulation used a commercial available software package (Wave3000, CyberLogic Inc., New York, NY) based on a finite difference method which solves the 3D visco-elastic wave equations. Comparing Figure 4-18 (a) and Figure 4-18 (b) a good agreement between the experimentally obtained and numerically calculated signals in signal bandwidth and time delay has been achieved. The simulated results took the computation time of 21 days using a computer equipped with a 64-bit operation system and 16GB memory. Also the measured and numerically simulated results in time domain and at room temperature for the SH PAW defect monitoring configuration shown in Figure 4-14 are shown in Figure 4-19 (a) and Figure 4-19 (b), respectively. Also a good agreement between the results shown in Figure 4-19 (a) and Figure 4-19 (b) can be seen. The numerical simulation for Figure 4-19 (b) took 21 days of calculation. It is noted that because of the texture of the plates the measured time delay is slightly less than the calculated one in which the textures are not considered. The texture depending on the grain structure of the Al plate may lead to a higher PAW velocity if the grain is aligned with the propagation direction; otherwise there will be a slower velocity if the grain is perpendicular to the propagation direction. Such a simulation approach will be used in the future for the detection sensitivity evaluation of cracks using the symmetrical, anti-symmetrical and SH PAW configurations presented in this study.

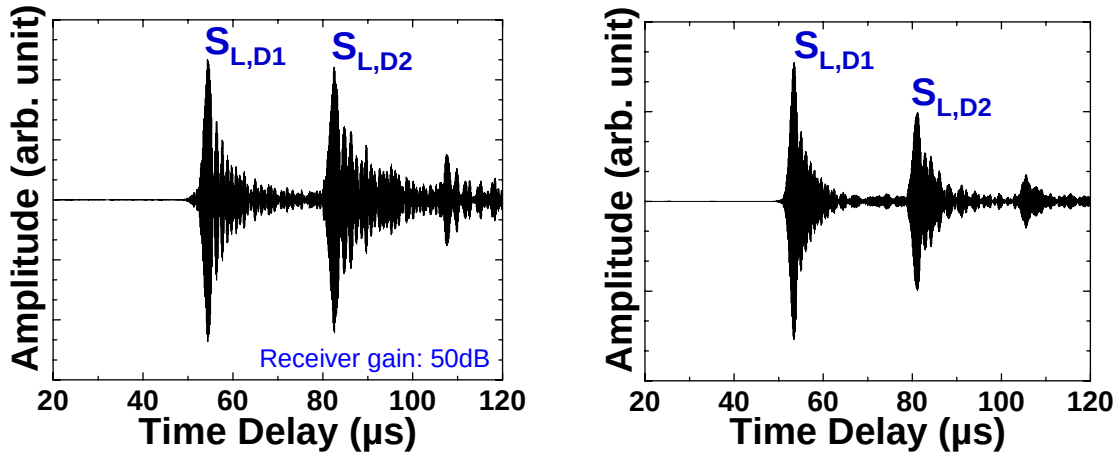

Figure 4-18 (a) Measured and (b) numerically calculated symmetrical PAW signals in time domain at room temperature in the Al plate as shown in Figure 4-6.

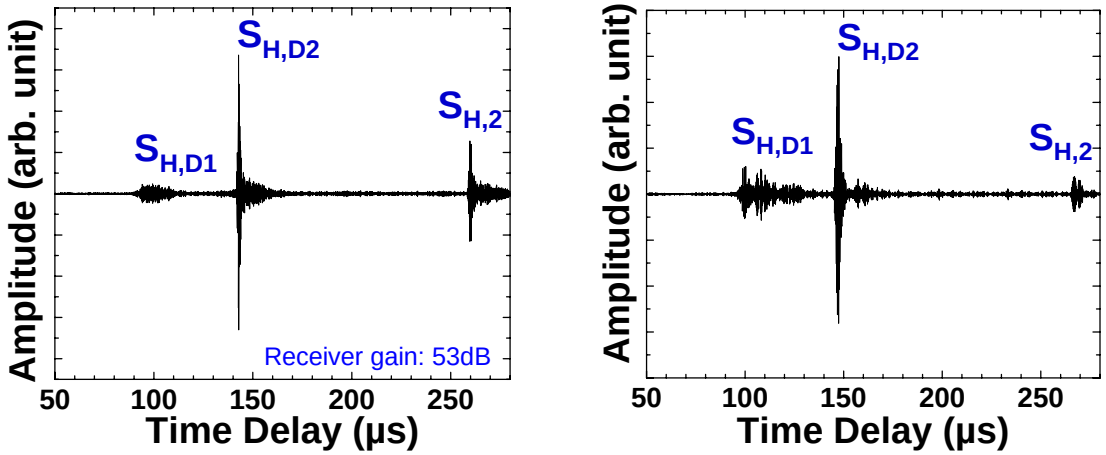

Figure 4-19 (a) Measured and (b) numerically calculated SH PAW signals in time domain at room temperature in the Al plate as shown in Figure 4-14.

4.2 Generation and Detection of PAWs for NDT Using HT Wedge

As mentioned in the Introduction, guided acoustic waves are of attraction for NDT [124][130] and SHM applications [5][131] because they may inspect parts or structures, in particular, those made of metals of a large area within a short time period using a few UTs. For aerospace industry such NDT and SHM may require that the UTs operate from -

80°C to 100°C. In other areas the operation temperatures may be required to be higher [7][8][132]. Guided waves may be PAWs or SAWs. In this investigation, SH PAWs as shown in Figure 4-12 are focused due to the fact that the fundamental SH PAW (SH_0) is non-dispersive and has the same velocity as the S wave in the substrate (e.g. plate). The non-dispersive nature means that the propagation of the SH_0 PAW mode is insensitive to the thickness variation of the plate and enables a broadband signal which provides high range resolution for defect detection. Typically EMAT [45][46][47] are used to generate and receive SH PAWs along metal structures even at elevated temperatures; however, they may suffer low signal strength and bandwidth, and be large in size, and are not considered here.

In the past SH PAWs were not commonly selected for NDT because of the unavailablility of the HT and broadband piezoelectric S wave UTs and inconvenient HT S wave couplant, in particular, for scanning purposes. In this study, HT S waves will be generated and received through mode conversion [79][122] from HT piezoelectric L wave UTs in a metal delay line. Then S waves will be coupled to a metal plate by this metal delay line serving as a wedge but with a wedge angle so as to excite and detect SH PAWs depending on the plate thickness. The HT wedge (delay line) will be permanently bonded to the plate by a HT bonding material such as glue which serves as HT S wave ultrasonic couplant. Such permanent bonding may ensure the good ultrasonic coupling at low, room and elevated temperatures.

Usually wedges are used to convert L or S waves in the wedges into guided PAWs along metallic plates or pipes for NDT [10][124] and SHM purposes. Often wedges are made of Plexiglas. The main advantages of Plexiglas are due to its low ultrasonic velocity, $V_{L,Wedge}$, or $V_{S,Wedge}$ and ease for machining, where V_L and V_S are the L and S wave velocity, respectively. The low velocity of a wedge is necessary to meet the conversion angle according to Snell's law (or acoustic phase matching condition). For example, in the case of a plate, $Sin\ \theta = V_{Wedge}/V_{PAW}$, where θ is the angle of the wedge and V_{PAW} is the phase velocity of the specific mode of PAWs of a plate. It also means that V_{Wedge} is slower than V_{PAW}. However, the operation temperature of the Plexiglas is limited

to less than 100°C. In order to operate at HT, wedges made of metal may be preferred. Since brass provides low V_L and V_S and it may function at up to more than 600°C, it is therefore chosen as the wedge material in this investigation. It also seems that there is no published work on HT SH PAWs using piezoelectric UTs.

For NDT and SHM broad bandwidth of the ultrasonic signals is also desired. Normally the broad bandwidth of an UT is ensured with a proper backing. However, it is difficult to construct a robust backing material for HT UT [7][8]. In this study the sol-gel fabricated HT integrated L wave UTs mentioned in Chapter 2 will be used together with L to S wave mode conversion technique [79][122] to produce broad bandwidth S waves in the brass wedge in order to launch SH PAWs in the metal plate for NDT and SHM purposes.

Theoretical analyses of wedges for the generation and receiving of SAW and symmetrical and anti-symmetrical PAWs [10][118] have been reported [133][134][135][136]. In [133][134][135][136] coupled wave equation formulation has been presented to predict the performance of wedge transducers. However, in [133] and [136] liquid wedges are used for the analyses, while in [133] and [134] SAWs were excited and received but [134] used solid wedges. In [136] modal analysis for symmetrical and anti-symmetrical PAWs in plates was performed using a liquid wedge. In [133][134][136] the coupling efficiency loss from the wedge to the plate due to the back scattering (radiation) of the waves into the wedge itself caused by the reciprocity has been included. Such loss was not included in [135] which presented the analysis of solid wedge transducers for generation and detection of symmetrical and anti-symmetrical PAWs in plates. In this study the normal mode formalism using a solid wedge to generate SH PAWs in plates will be presented.

4.2.1 IUT and mode conversion

It is the objective here to use IUTs to achieve L UTs. The typical PZT-c film thickness in this study is about 89 μm. Such IUTs have been operated with a center frequency ranging from 2.6 MHz to at least 40 MHz. Their ultrasonic signal strength and

bandwidth are comparable to those of the commercially available broadband UTs with backing. However, IUTs can be used at high temperatures as reported in this thesis.

The mode conversion from L to S waves due to reflection at a solid-air interface, as shown in Figure 3-9, was demonstrated in Chapter 3. The L IUT was in a plane parallel to the axial direction of the probe as shown in Figure 3-9, and $Cot\ \theta$ is equal to V_S / V_L in the probe so that the mode converted S waves will propagate in the direction parallel to the axial direction of the probe. In Figure 3-9 L_i, L_r and S_r are the incident L, reflected L and reflected S wave, respectively. In this study, a brass with the L wave velocity V_L = 4372 m/s and S wave velocity V_S = 2121 m/s was used as the probe material. Therefore one can obtain θ = 64.1°. Using Eq. (3-6) the calculated energy conversion rate versus θ is given at Figure 4-20. In Figure 4-20 at θ = 64.1° the energy conversion rate is 79.7% that is also the maximum conversion rate. Figure 4-21 shows an actual brass delay line for L and S waves. Let the Cartesian coordinates of this probe be X'Y'Z'. In Figure 3-9 and Figure 4-21 an L wave PZT-c film IUT is also made at the top flat surface of the wedge and it can generate and receive the L wave along the axial direction of the probe as well. The arrangement shown in Figure 3-9 and Figure 4-21 enables L, $S_{X'}$ and $S_{Y'}$ waves to propagate together along the axial direction of the probe which will be further explained below. $S_{X'}$ and $S_{Y'}$ waves are S waves predominately polarized along the X' and Y' directions, respectively.

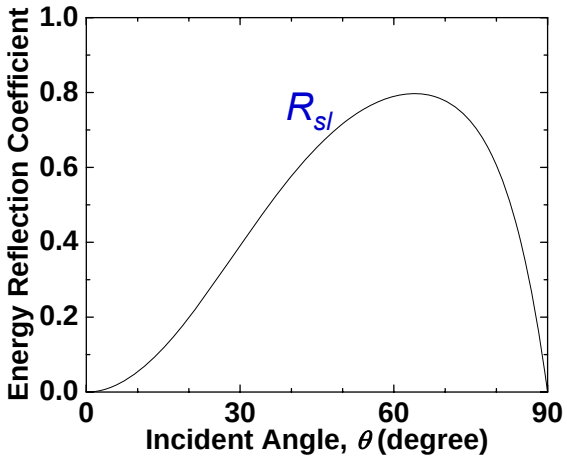

Figure 4-20 Energy reflection coefficient of the mode conversion from L to S waves with an incidence of L wave at a brass-air interface.

Figure 4-22 and Figure 4-23 show the measured ultrasonic signal L^n and $S_{X'}^n$ in time domain and pulse-echo mode from the end of the probe at 150°C. L^n is the nth trip echo through the axial direction of the probe. $S_{X'}^n$ is that of the nth trip S echo through the probe length plus that of the L wave travelling through the length from L IUT to the brass/air interface. The center frequency and 6 dB bandwidth of the L^2 signal shown in Figure 4-22 are 6 MHz and 3.7 MHz, respectively, with 43.7 dB SNR. The SNR is defined as the ratio of the signal L^2 over that of the surrounding noises. The center frequency and 6 dB bandwidth of the $S_{X'}^2$ shown in Figure 4-23 are 4.9 MHz and 2.8 MHz, respectively, and its SNR is 23.9 dB.

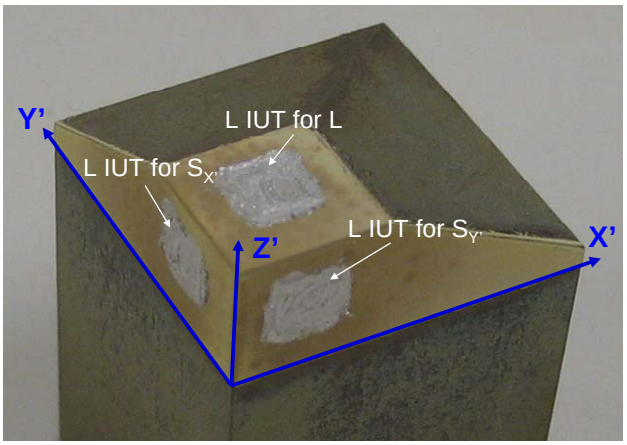

Figure 4-21 An integrated three wave brass probe having one L and two orthogonally polarized S ($S_{X'}$ and $S_{Y'}$) generated and received by three L IUTs.

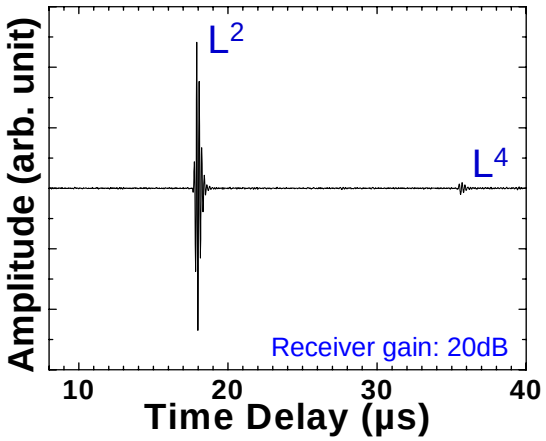

Figure 4-22 Ultrasonic signals in time domain of the L wave generated by the L IUT at the top surface shown in Figure 4-21 and reflected from the end of the probe at 150°C.

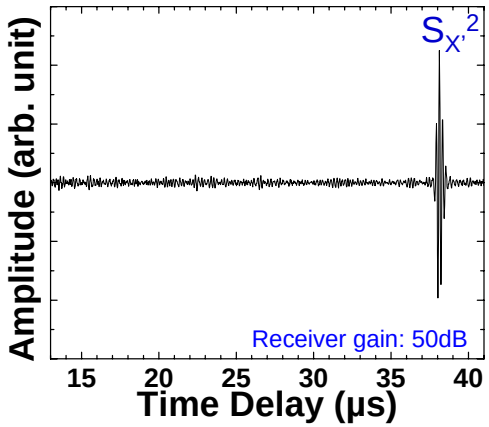

Figure 4-23 Ultrasonic signals in time domain of the S wave converted from the L wave generated by the L IUTs at one side surface shown in Figure 4-21 and reflected from the end of the probe at 150°C.

4.2.2 Conversion from S waves in brass wedge to SH PAWs in a metal plate

Figure 4-24 shows the schematic in which the $S_{X'}$ wave propagating in the brass wedge will be converted into the metal plate as SH PAWs or SAWs for intended NDT and SHM applications. The Cartesian coordinates XYZ are shown where Z axis is the SH PAWs propagation direction, X the particle displacement direction and Y the plate thickness direction. The X axis in Figure 4-24 is the same as the X' direction in Figure 4-21. In Figure 4-24 the brass delay line shown in Figure 4-21 is cut into a slanted angle ϕ_i. The first substrate used for the experiment is a SS plate which has the dimensions of 406.4 mm long, 50.8 mm wide and 1.9 mm thick. The operation can be in transmission mode which means that the one wedge shown in Figure 4-24 is used as the transmitting transducer and the other the receiver. If the wedge is operated in pulse-echo mode, each of them can be used as both the transmitting and receiving transducer.

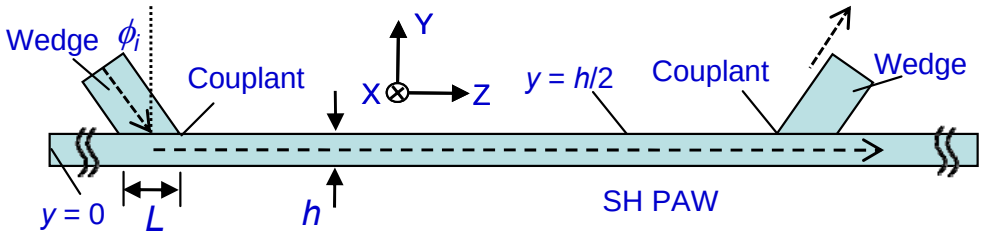

Figure 4-24 Configuration of wedges for S waves converted into SH PAWs.

4.2.2.1 Dispersion Curve Calculations

For the SS plate of 1.9 mm thick the dispersion curves of both phase (dashed lines) and group velocities (solid lines) of SH_n waves are calculated and presented in Figure 4-25, respectively, where SH_n are the SH PAWs and n denotes high order modes. The frequency of the PAW and the plate thickness are expressed as *f* and *h*, respectively.

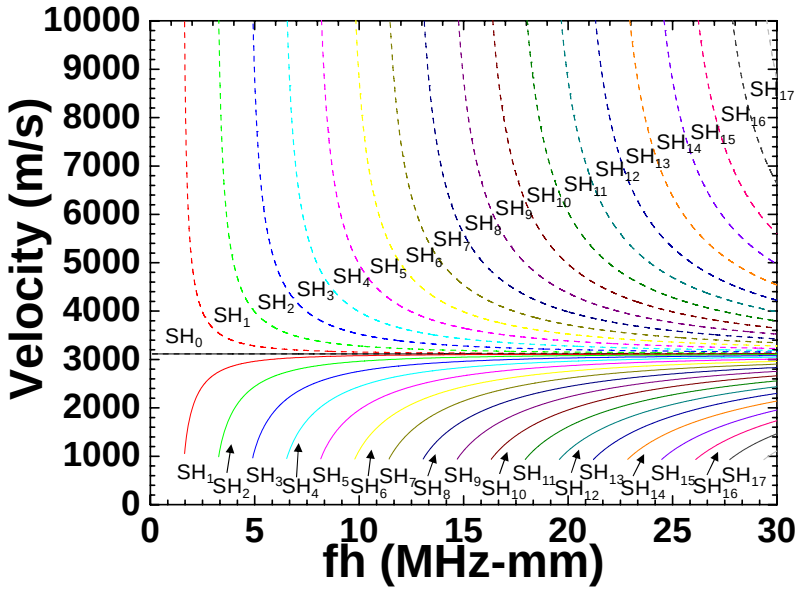

Figure 4-25 Theoretical calculated velocities versus *f* * *h*, curves for the SH_n PAWs in the 1.9 mm thick SS plate. Dashed and solid lines represent phase and group velocities, respectively.

4.2.2.2 Coupling coefficient analysis for SH PAWs

The analysis of the generation and receiving of SH PAWs is carried out using the coupled wave equation formulation [133][134][135][136] applied to the solid wedge transducer shown in Figure 4-24. The analysis takes into account the effects of acoustic wave reflection and back scattering (radiation) at the wedge-plate interface which was not included in the analysis in [135]. In such formulation the particle displacement and stress inside the plate generated by the wedge transducer are assumed to be independent of the X coordinate and can be expressed by the mode expansion,

$$\vec{U}(y,z) = \sum_n a_n(z)\overrightarrow{U_n}(y) \tag{4-1a}$$

$$T(y,z) = \sum_n a_n(z)T_n(y) \tag{4-1b}$$

where $\overrightarrow{U_n}(y)$ and $T_n(y)$ denote the particle displacement and the stress of the nth eigenvalue of a plate waveguide and $a_n(z)$ is the mode amplitude.

Taking into account the orthogonal relations between the acoustic plate modes and applying the coupled mode formulation to the solution proposed, as given by Eqs. (4-1a) and (4-1b), it can be shown that the mode amplitude of the SH PAWs in sinusoidal form ($e^{j\omega t}$) is governed by the following differential equation

$$\frac{da_n(z)}{dz} + j\beta_n a_n(z) = \frac{j\omega u_{nx} T_{xy}}{4P_n} \tag{4-2}$$

where β_n and P_n are, respectively, the propagation constant and the acoustic power of the nth SH PAW mode; T_{xy} is the stress generated by the wedge transducer at the top surface of the waveguide, i.e. y = h/2 as shown in Figure 4-24. The result given in Eq. (4-2) is quite similar to what has been reported in [134] and [136] which refer to liquid wedge transducer. However, it shows that the solid wedge transducer drives the plate mode through the T_{xy} stress component, which is a non-existent stress component in the case of the liquid wedge transducer.

Bearing in mind the boundary conditions which must be satisfied by the particle displacement and the stress at the interface between the plate and the bottom of the solid wedge transducer, one is able to rewrite Eq. (4-2) as:

$$\left(\frac{d}{dz} + j\beta_n + \alpha_n\right)a_n(z) = -\frac{d\omega^2 Z_W \cos\phi_i u_{nx}^* u_{ix}}{2P_n} \tag{4-3}$$

where d is the wedge transducer dimension along the X-axis, Z_W is the SH acoustic impedance of the wedge transducer material, ϕ_i is the acoustic wave incident angle at the wedge base, u_{ix} is the amplitude of the incident particle displacement, α_n is the attenuation coefficient which comes from acoustic energy leakage of the guided mode into the interface between the plate and the wedge transducer and is given by

$$\alpha_n = \frac{d\omega^2 Z_W |u_{nx}|^2 \cos\phi_i}{4P_n} \tag{4-4}$$

An examination of Eq. (4-3) right hand side reveals that only those SH plate modes which exhibit horizontal particle displacement u_{nx} at $y = h/2$ can be generated by the wedge transducer. Therefore, only the lowest order, SH_0, and the modes having particle displacement with even symmetry with respect to y = 0 axis (i.e. even n) can be generated. The acoustic attenuation α_n plays a major role on the efficiency of the wedge. Therefore before calculating the efficiency, one should examine α_n, as given by Eq. (4-4), which, by its turn, needs the acoustic power of the SH_n PAW mode, P_n, given by

$$P_n = \frac{1}{2}\rho\omega^2 V_{g,n}\int_{-h/2}^{h/2}|u_{nx}|^2 dy \tag{4-5}$$

where $V_{g,n}$ is the group velocity of the nth mode. After some lengthy, albeit standard mathematical manipulations, one concludes that the acoustic attenuation for the two lowest order modes (SH_0 and SH_2 PAW) can be given by

$$\alpha_0 = \frac{1}{2h}\left(\frac{Z_W}{Z_P}\right)\left[1-\left(\frac{V_{S,W}}{V_{S,P}}\right)^2\right]^{1/2} \tag{4-6a}$$

$$\alpha_2 = \frac{1}{h}\left(\frac{Z_W}{Z_P}\right)\frac{\left\{1-\left(\frac{V_{S,W}}{V_{S,P}}\right)^2\left[1-\left(\frac{\omega_{C2}}{\omega}\right)^2\right]\right\}^{1/2}}{\left[1-\left(\frac{\omega_{C2}}{\omega}\right)^2\right]^{1/2}} \tag{4-6b}$$

where Z_W and $V_{S,W}$ are, respectively, the impedance and the S wave phase velocity of the wedge; Z_P and $V_{S,P}$ are the impedance and the phase velocity of the S wave in the plate; $\omega_{C2} = 2\pi V_{S,P}/h$ is the cut off radian frequency of the second order mode SH_2. In the calculation, one should bear in mind that the incidence angle ϕ_i must obey Snell's law for each plate mode, hence for the lowest order SH_0 and second order SH_2 PAW mode, the following relationship holds

$$\sin\phi_i^{(0)} = \frac{V_{S,W}}{V_{S,P}} \tag{4-7a}$$

and

$$\sin\phi_i^{(2)} = \frac{V_{S,W}}{V_{S,P}}\sqrt{1-\left(\frac{\omega_{C2}}{\omega}\right)^2} \tag{4-7b}$$

respectively.

An examination of Eq. (4-6a) reveals that the attenuation α_0 of the SH_0 mode is dispersionless and it is inversely proportional to the plate thickness. However, according to Eq. (4-6b), SH_2 has a rather dispersive attenuation α_2, which is also inversely proportional to the plate thickness. The dependence of the attenuation characteristics on the acoustic frequency is illustrated in Figure 4-26, which refers to a plate and wedge made of stainless steel and brass, respectively. As shown in Figure 4-26, irrespective of the frequency, the attenuation of the SH_2 mode is always higher than the attenuation of the SH_0 mode. Such a feature plays a major role on the performance of the wedge. For example, the wedge can provide single SH PAW mode excitation if $\omega < \omega_{C2}$.

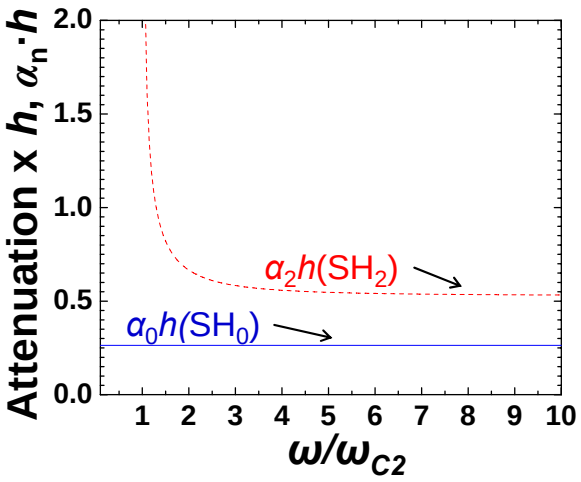

Figure 4-26 Attenuation dependence on the normalized frequency; solid line α_0h and dashed line $\alpha_2 h$, ω_{C2} is the cut-off frequency of SH_2 mode.

In [134] the performance of the wedge is determined by its efficiency, which is defined as the ratio of the excited mode power to the incident acoustic power. Based on Eq. (4-3) one obtains the following expression for the wedge efficiency

$$\eta_n = 2\left[1-\exp(-\alpha_n L)\right]^2/(\alpha_n L) \tag{4-8}$$

where L is the length of the wedge transducer along the Z axis as shown in Figure 4-24. It should be pointed out that since the wedge efficiency was calculated based on the coupled wave equation, it was expected that it should be governed by the standard mathematical expression presented in the previous publications, which is given in Eq. (4-8). However, bearing in mind some rather unique characteristics of the attenuation as shown in Figure 4-26, it is worthwhile to investigate the dependence of the transducer efficiency on the frequency for the two modes under present consideration. The dependence of wedge efficiency with respect to both the attenuation, α_0 and α_2 for the SH_0 and SH_2 PAW modes, respectively, and geometry, L, is calculated and shown in Figure 4-27.

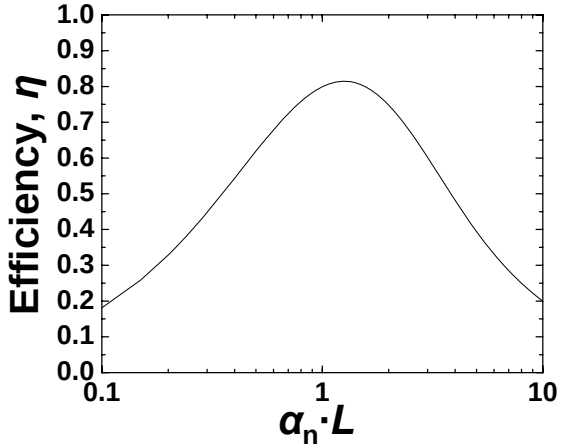

Figure 4-27 Wedge conversion efficiency, η, versus normalized length, $\alpha_n L$, for the SH_0 and SH_2 PAW modes.

Regarding SH_0 PAW, one must take into account that its attenuation, α_0, does not depend on the frequency. Therefore, the wedge efficiency for such a mode is also dispersionless. However, when considering the SH_2 PAW mode one must take into account that α_2 strongly depends on the frequency, especially near to its cut-off frequency, as shown in Figure 4-26. It can also be shown that the wedge efficiency is higher than 50% as long as

$$0.54\left(\frac{Z_P}{Z_W}\right)\left[1-\left(\frac{V_{S,W}}{V_{S,P}}\right)^2\right]^{-1/2} \le \frac{L}{h} \le 9.6\left(\frac{Z_P}{Z_W}\right)\left[1-\left(\frac{V_{S,W}}{V_{S,P}}\right)^2\right]^{-1/2} \tag{4-9}$$

Thus the tolerance on the choice of L/h is relatively large.

Furthermore, Figure 4-27 in combination with Eq. (4-7a) enables one to conclude that in order to operate the SH_0 mode at the maximum efficiency, $\alpha_0 L = 1.26$, the following relationship between the length of the wedge L along the Z axis and the plate thickness h must be

$$\frac{L}{h} = 2.52\left(\frac{Z_P}{Z_W}\right)\left[1-\left(\frac{V_{S,W}}{V_{S,P}}\right)^2\right]^{-1/2} \tag{4-10}$$

4.2.2.3 Experimental results

The experimental setup for the S wave in the wedge to excite and receive SH PAWs in a SS plate is shown in Figure 4-28. The SS plate is 1.9 mm thick and 50.8 mm wide. The angle 42.9° of ϕ_S is chosen because of Snell's law $\phi_S = Sin^{-1}(V_{S,Wedge}/V_{L,Wedge}) = Sin^{-1}$ (2121/3116) for mode conversion in the brass wedge [79][122]. The L IUT which excites S wave polarized in X' axis in Figure 4-21 (also X axis in Figure 4-24) is used here. It will generate and receive predominately the S waves which have the particle displacements along the X axis. In Figure 4-25 one can see that SH_0 PAW has almost no dispersion and thus is preferred for many NDT and SHM applications. Also the higher order modes of SH_n ($n \neq 0$) have slower group velocities than that of SH_0 and may not be excited and received efficiently. Figure 4-29 (a) and Figure 4-29 (b) show the result of the measurement in transmission mode while the SS plate is at room temperature and at 200°C, respectively. The separation distance between the centers of the two wedges on the SS plate was 150 mm. The echo P_{SH0} indicated in Figure 4-29 (a) and Figure 4-29 (b) does not go through any signal processing. The calculated group velocity for SH PAW is 2905 m/s, which corresponds to that of the lowest order SH_0 PAW mode in this SS plate. Its center frequency and 6 dB bandwidth of the P_{SH0} signal in Figure 4-29 (a) and Figure 4-29 (b) are 3.5 MHz and 3.4 MHz, and 3.5 MHz and 3.3 MHz, respectively. The P_{SH0} signal strength at 200°C is 12 dB smaller than that at room temperature and this increased loss at high temperatures comes from the piezoelectric film, propagation at the wedge, glue and propagation at the SS plate.

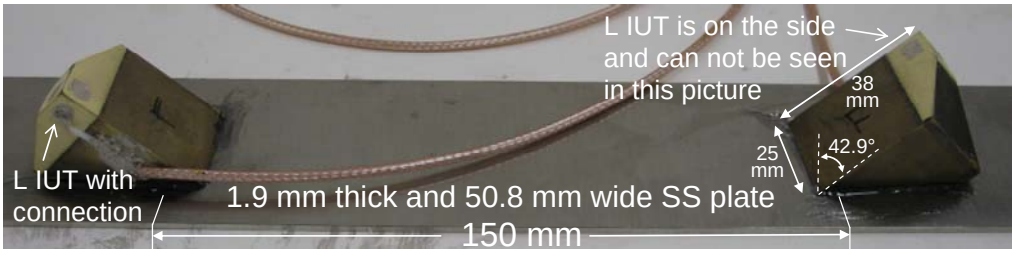

Figure 4-28 Experimental setup for the $S_{X'}$ wave in the wedge to excite and receive SH PAWs in the SS plate.

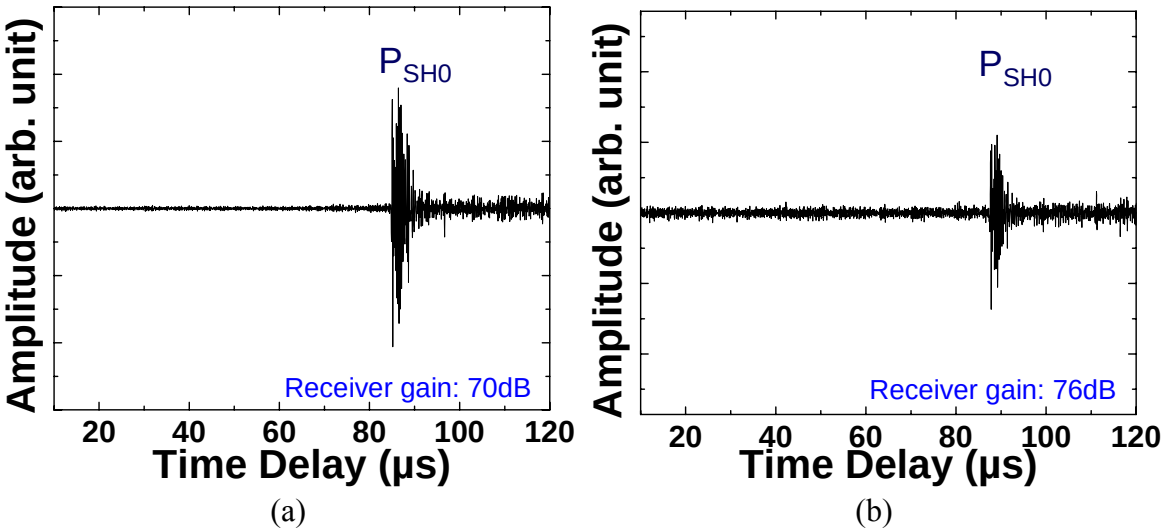

Figure 4-29 Measured ultrasonic signals of the experimental setup shown in Figure 4-28 in transmission mode while the SS plate is (a) at room temperature (b) at 200°C. The distance between the centers of the two wedges is 150 mm

4.2.3 Conversion from L and S waves in brass wedge to symmetrical and/or anti-symmetrical PAWs in a metal plate

The probe shown in Figure 4-21 is able to generate one L wave and two orthogonally polarized S waves simultaneously, so it is also our intention to see which S_n or a_n PAW can be generated and received by that wedge. Figure 4-30 (a) and Figure 4-30 (b) show the schematic in which the L and $S_{Y'}$ waves propagating in the brass wedge will be converted into the metal plate as symmetrical and/or anti-symmetrical PAW. As the same brass wedges and SS plate were used as described in the previous section, the slanted angle ϕ_L in Figure 4-30 (a) and $\phi_{SY'}$ in Figure 4-30 (b) are equal to the ϕ_i in Figure 4-24. However, the two L IUTs used here are for the generation and receiving of L and $S_{Y'}$, respectively, and are different from the one for $S_{X'}$ in Section 4.2.2. If the three L IUTs can be connected electrically, the same wedge can generate different PAWs and even simultaneously.

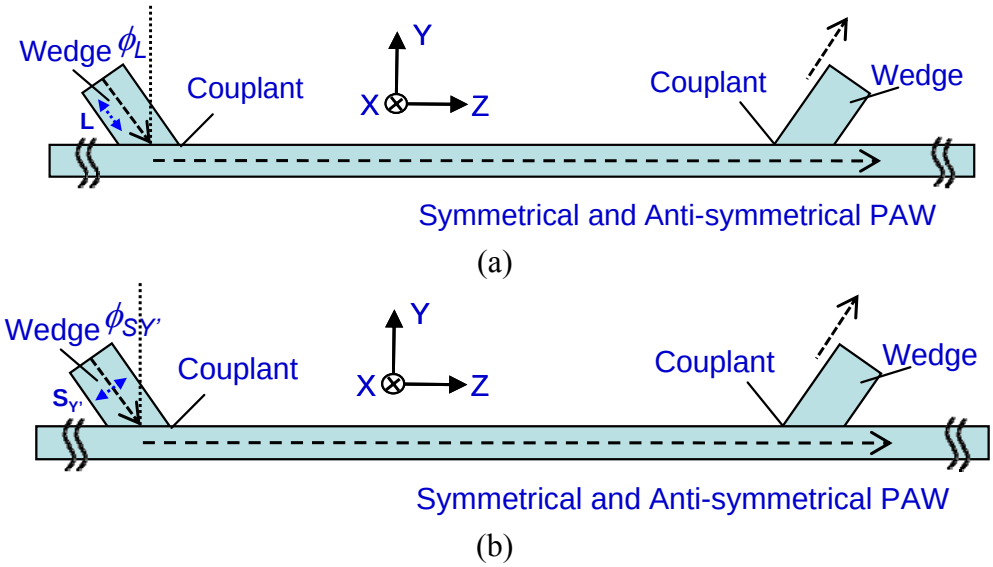

Figure 4-30 Configurations of wedges for (a) L waves to S_n and/or a_n (b) $S_{Y'}$ waves to S_n and/or a_n PAWs.

4.2.3.1 Theoretical calculations

Using the measured V_L and V_S of the SS plate at room temperature, and the formulas in [78] and [118], the PAW velocity dispersion curves for the 1.9 mm thick and 50.8 mm wide SS plate are calculated. For this SS the dispersion curves of both phase (dashed lines) and group velocities (solid lines) of S_n and a_n waves are calculated and given in Figure 4-31 and Figure 4-32, respectively, where n indicates the high order modes. The frequency of the PAW and the plate thickness are expressed as f and h, respectively. It is noted that the coupling coefficient for the symmetrical and anti-symmetrical PAWs is not presented and is not the scope of this thesis either.

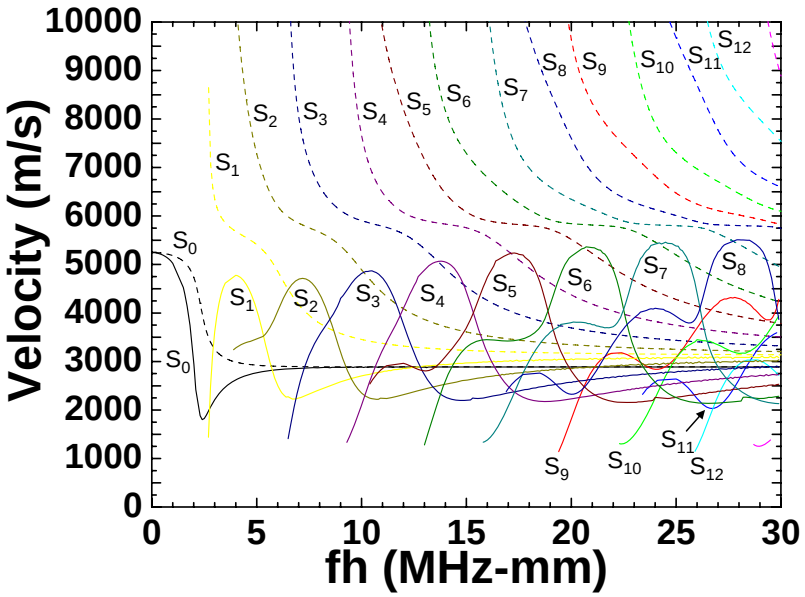

Figure 4-31 Theoretical calculated velocities versus *f* * *h*, curves for the S_n PAWs in the 1.9 mm thick SS plate. Dashed and solid lines represent phase and group velocities, respectively.

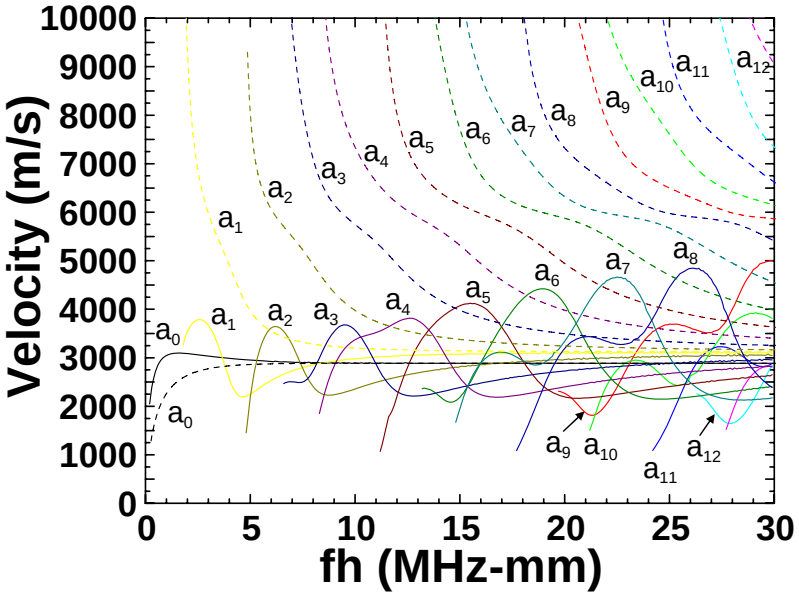

Figure 4-32 Theoretical calculated velocities versus *f* * *h*, curves for the a_n PAWs in the 1.9 mm thick SS plate. Dashed and solid lines represent phase and group velocities, respectively.

The experimental setup for the L wave in the wedge to excite and receive PAWs in the SS plate is shown in Figure 4-33. The angle of ϕ_L equal to 45.5° which is the same as

$\phi_{SY'}$ is chosen because it is the intention to see which S_n or a_n PAWs can be generated and received. From Snell's law, if ϕ_L is equal to 45.5°, the V_{PAW} should be a value of near 6022 m/s, thus according to the data shown in Figure 4-31 and Figure 4-32 S_5 and/or a_5 PAWs may be excited and received. Figure 4-34 shows the measurement result in transmission mode at room temperature. The separation distance between the centers of the two wedges is also 200 mm. The echo P_{a5} indicated in Figure 4-34 has gone through a band pass filter between 7.5 MHz and 8.5 MHz. The preliminary analysis indicates that this echo with a group velocity of 4160 m/s and a center frequency near 8.0 MHz comes mainly from the fifth order anti-symmetrical a_5 mode shown in Figure 4-32 and S_5 was not efficiently excited and received using this configuration.

Figure 4-33 Experimental setup for the L wave in the wedge to excite and receive PAWs in the SS plate

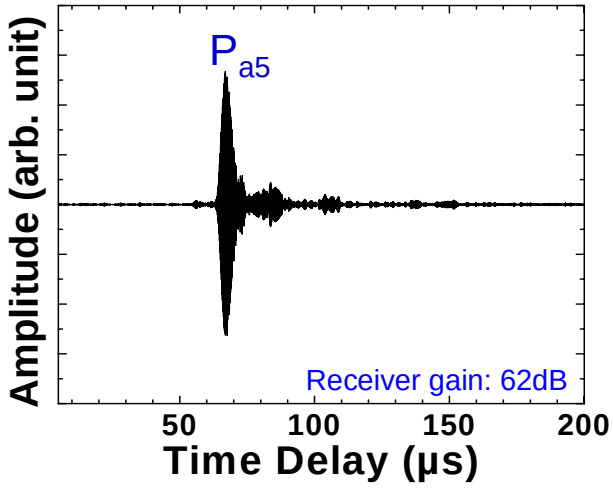

Figure 4-34 Measured ultrasonic signals of the experimental setup shown in Figure 4-33 at room temperature in transmission mode.

Figure 4-35 The experimental setup for the $S_{Y'}$ wave in the wedge to excite and receive PAWs in the SS plate.

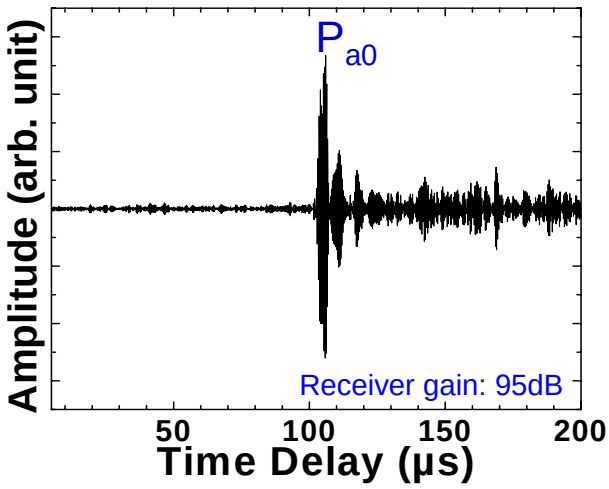

Figure 4-36 Measured ultrasonic signals of the experimental setup shown in Figure 4-37 at room temperature in transmission mode.

For the $S_{Y'}$ wave in the wedge to excite and receive S_n and/or a_n PAWs in the plate, the angle of $\phi_{SY'}$ equal to 45.5° is again chosen with an intention to see that if the same wedge used in Figure 4-33 is used, then which PAW can be excited and received. The measurement setup is shown in Figure 4-35. Figure 4-36 provides the measurement result in transmission mode at room temperature. The separation distance between the centers of the two wedges is 200 mm as well. The echo P_{a0} indicated in Figure 4-36 has gone through a band pass filter between 2 MHz and 3 MHz. The preliminary analysis indicates that the echo comes mainly from a_0 mode shown in Figure 4-32 because of the slow velocity of 2941 m/s at a center frequency near 2.5 MHz.

It is interesting to note that the wedges used in the measurement setups shown in Figure 4-33 and Figure 4-35 have the same ϕ. The reason is that in future research it is our intention to discover if for a specific plate sample, one can use wedges of same ϕ to

excite and receive three different PAWs efficiently using the L $S_{X'}$ and $S_{Y'}$ waves in the wedge. If this can be achieved, this wedge will be a promising candidate for NDT and SHM of this SS plate.

4.3 HT Guided Acoustic Wave UTs Using Mechanical Gratings

As mentioned in Section 4.2, guided acoustic waves are of attraction for metallic NDT and SHM applications because they may inspect parts or structures of a large area within a short time period at HT using a small number of UTs [130][131]. Mechanical line-shape gratings have been used to effectively convert bulk L waves to SAW [125][126]. The main applications were aimed at high frequency SAW filters. However, in the last decade such gratings have been also applied as mode converters from L to SAW or PAWs and as reflectors for the touch screen panels (or displays) made of glass substrates [127][128][129]. Such touch screen panels are widely used at many major transportation industry stations, department stores, different institutions, etc, and become a convenient tool involved in human daily living. The main motivation of this approach is to regard the touch display panel as an approach for SHM or NDT of a large metallic part. The analogy is that if any defect is initiated or propagated within this panel, the guided SAWs or PAWs propagating in the entire panel can detect the defect location and even the size. In this investigation thin and light weight guided acoustic wave IUTs and FUTs, involving the use of line-shape mechanical gratings only as mode converters, are studied for the NDT and SHM applications at temperatures of up to 150°C. The numerical simulation results will be presented as well.

4.3.1 UT fabrication

The line mechanical gratings are machined with a line width of 0.3 mm, an aperture of 10 mm and different depths and number of gratings using electrical discharge machining (EDM). The gratings will be used to convert L waves into SAWs [125][127] and PAWs depending on the substrate thicknesses. PZT-c films serving as L wave IUTs

were made by the sol-gel spray technique mentioned in Section 2.1 onto the opposite surface of the metallic substrate having mechanical gratings. The merit of this approach is that IUT can be at the internal surface of a structure and mechanical gratings at the external surface. If the substrates are 75 μm thick membranes, then it is an FUT. FUTs may be attached or bonded to metal parts even with curved surfaces and used for guided wave NDT and SHM as reported earlier.

4.3.2 Integrated guided SAW UTs on a SS plate

In order to show the capability of integrated guided SAW transducer line-shape mechanical gratings as shown in Figure 4-37 with a line interval of 0.6 mm, a width of 0.3 mm, a depth of 0.06 mm, an aperture of 10 mm and 6 gratings have been made onto the grating side of 10 mm thick SS plate. According to [125] the optimum depth of the grating is 0.6 mm, but here 0.06 mm is chosen for easy machining. The gratings may be made to have symmetrical or anti-symmetrical shape to increase the efficiency of mode conversion and directivity [125]. PZT-c films have been also made as IUTs at the direct opposite side of these gratings and their thicknesses are about 82 μm thick which corresponds to a center frequency of an L wave of 7.9 MHz with a 6 dB bandwidth of 4 MHz. The dimensions of the top electrodes are about 9 mm by 3.5 mm which covers about 6 gratings area.

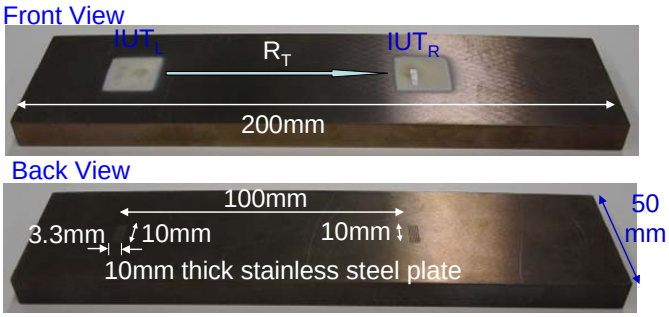

Figure 4-37 Line-shape mechanical gratings with a line interval of 0.6 mm, a width of 0.3 mm, a depth of 0.06 mm, an aperture of 10 mm and 6 gratings have been made onto a 10 mm thick SS plate. PZT-c films with 82 μm thick were deposited on the opposite side of gratings directly.

At room temperature the measured V_L and V_S of this SS substrate are 6056 m/s and 3328 m/s, respectively. Along with these data, the calculated SAW group (also phase) velocity is 3022 m/s with 5 MHz of center frequency in this design of 0.6 mm wide line interval grating. Figure 4-38 shows the measured ultrasonic signals in transmission mode in time domain of the measurement (a) at room temperature and (b) at 150°C. The data shown in Figure 4-38 (a) and Figure 4-38 (b) were filtered with a band pass filter centered at 5 MHz. R_T is the first SAW arrival signal. Because of the 10 mm thick SS plate, bulk L waves generated and received by the IUT also travel back and forth from the top and bottom surfaces of this plate. The large echoes R_T' and R_T" follow the echo R_T come from such reverberation with a time delay of about 3.3 µs. Such echoes R_T' and R_T" can be significantly reduced if the incident L waves toward the line gratings is at an inclined angle or the SS plate has a non-parallel top and bottom surfaces. At room temperature the measured SAW group (phase) velocity is 3012 m/s which agrees well with the theoretically calculated value of 3022 m/s. It is noted that for isotropic substrate the SAW phase velocity is equal to the SAW group velocity [78][118]. At 150°C, as shown in Figure 4-38 (b), the measured SAW group (phase) velocity is about 2905m/s.

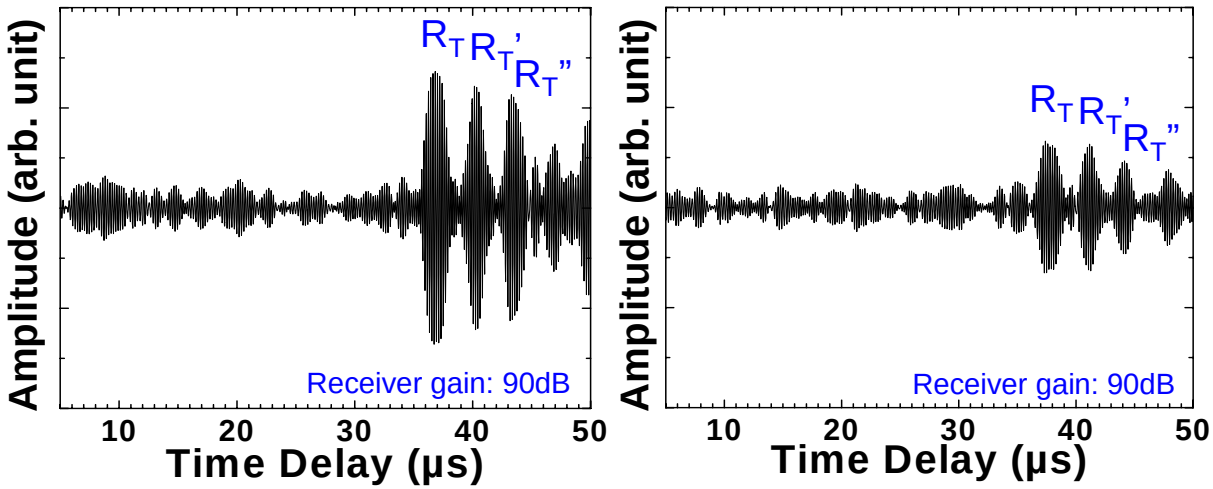

Figure 4-38 Ultrasonic performance of the IUTs shown in Figure 4-37 and operated in transmission mode (a) at room temperature (b) at 150°C.

Figure 4-39 shows the numerical simulated results of this configuration at room temperature using Wave3000 commercial available software, which agreed well with the

experimental result shown in Figure 4-38 (a). In addition the center frequency of the received signal in Figure 4-39 is also around 5 MHz. Figure 4-38 (a) and Figure 4-38 (b) provide the possibility of HT guided SAW generation and receiving for 150°C NDT and SHM.

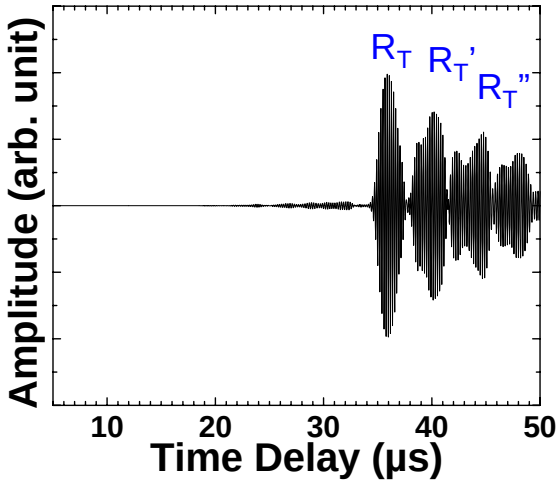

Figure 4-39 Numerically calculated SAW signals in time domain at room temperature in the SS plate as shown in Figure 4-37.

4.3.3 Flexible guided PAW UTs on 75 μm SS membranes

Since the grating has been approved to be able to generate and receive SAW at room temperature [125][126] and at 150°C as demonstrated above, it is also of interest to study whether flexible guided PAW grating transducer can be developed if the above 10 mm thick SS plate is replaced with a 75 μm SS membrane. The PZT-c film can be still deposited at the opposite site of the line grating. Using SS membranes HT high efficient bulk L wave PZT-c film FUTs were presneted in Section 2.3. For guided PAW grating FUTs line-shape mechanical gratings with a line interval of 0.6 mm, a width of 0.3 mm, a depth of ~0.03 mm, an aperture of 10 mm and 17 gratings have been made onto SS membranes of 75 μm thick by the EDM. The depth of ~0.03 mm of the grating is almost a half of the membrane thickness. Again these mechanical gratings are made in symmetrical shape because of convenience in machining. PZT-c films have been made as FUTs at the direct opposite side of these gratings and their thicknesses are about 62 μm

thick which corresponds to a center frequency of an L wave of 15 MHz. In this study such transducers are named as PAW grating FUTs.

At first, ultrasonic measurements in transmission mode were carried out. In Figure 4-40 FUT_L was used as the transmitting UT and FUT_R as the receiver. The ultrasonic signals obtained in this transmission configuration at room temperature with the FUT top electrode which covers 3, 7 and 10 line-grating areas are shown in Figure 4-41, Figure 4-42 and Figure 4-43, respectively. In theses figures, the time and frequency domain signals are given in (a) and (b), respectively. As expected [125] a higher number of line gratings provide a narrower bandwidth of the PAWs. The propagation paths of echoes P_T, P_{A+T}, P_{T+B}, and P_{A+T+B}, are indicated in Figure 4-40. Because the edges of the SS membrane serve as PAW reflectors, for example, the propagation path of echo P_{A+T} starts from the FUT_L together with the mechanical grating to the Edge A and reflected and received by FUT_R together with the mechanical grating. It also means that pulse-echo capabilities of such PAW grating FUTs have been demonstrated as well. From the time delays of P_T, P_{A+T}, P_{T+B}, and P_{A+T+B} the velocity of the PAW is 4870 m/s which indicates the zeroth order (S_0) symmetrical PAW for the SS membrane used. The SNR of the received signal P_T in Figure 4-41, Figure 4-42 and Figure 4-43 is 17 dB, 16.6 dB and 8.7 dB, respectively.

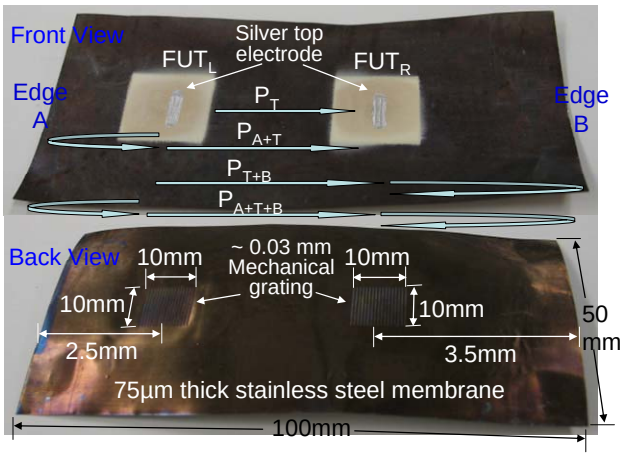

Figure 4-40 A 75 µm thick SS membrane with two 62 µm thick PZT-c films. Line-shape mechanical gratings with a line interval of 0.6 mm, a width of 0.3 mm, a depth of ~0.03 mm, an aperture of 10 mm and 17 gratings have been made onto the SS membrane.

The anti-symmetrical mode propagation, in particular, the first order (a_0) anti-symmetrical PAW was also expected to be generated and received by such PAW grating FUTs; however it was weak. Their arrival time comes much later because of the slow velocity, and interfered with by the later arriving of multiple echoes of the symmetrical mode traversing back and forth within the SS grating FUT membrane. It will be studied further in the future.

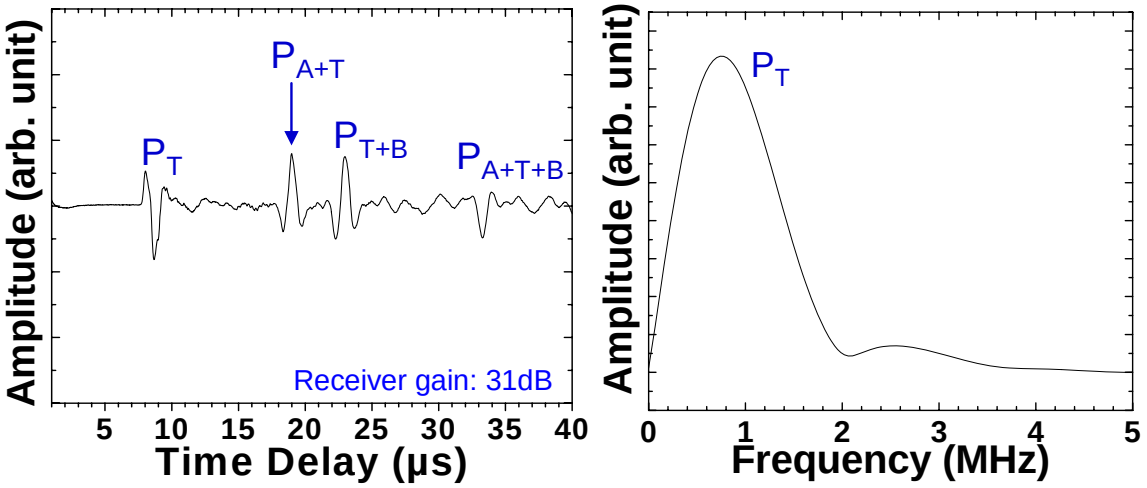

Figure 4-41 Ultrasonic performance of the FUTs shown in Figure 4-40 and operated in transmission mode. 3 line-grating area is covered by silver top electrode.

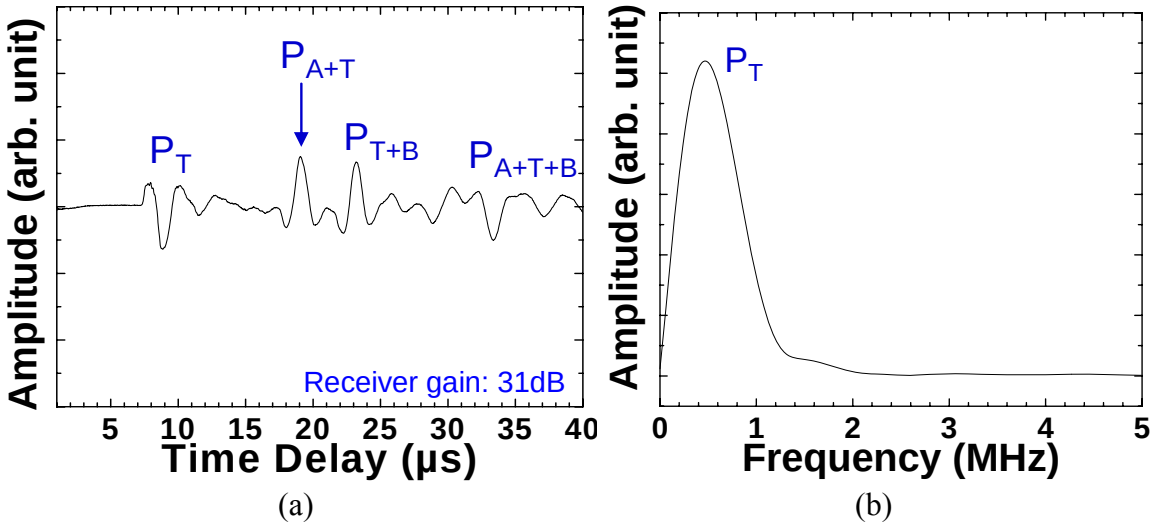

Figure 4-42 Ultrasonic performance of the FUTs shown in Figure 4-40 and operated in transmission mode. 7 line-grating area is covered by silver top electrode.

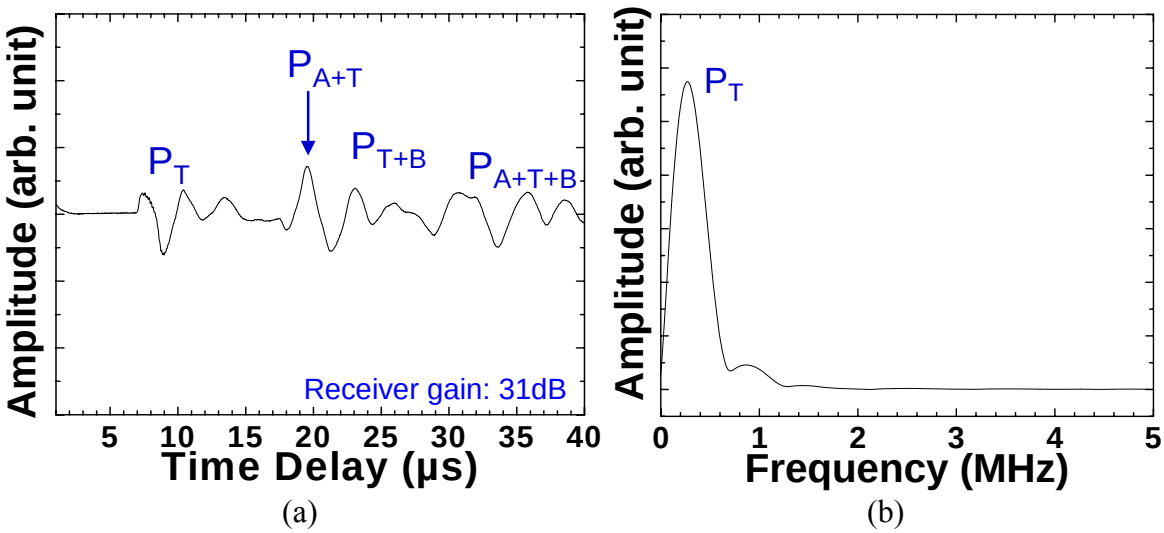

Figure 4-43 Ultrasonic performance of the FUTs shown in Figure 4-40 and operated in transmission mode. 10 line-grating area is covered by silver top electrode.

In order to demonstrate the HT operation capability the whole PAW grating FUT membrane shown in Figure 4-40 was directly put on top of a hot plate. Figure 4-44 shows the ultrasonic signals obtained in transmission mode at 150°C with PZT-c film FUTs covering only 3 line-grating areas (~9 mm by 2 mm). The SNR of the received signal P_T is 11.4 dB. The choice of 3 line-grating was because it gave the broader bandwidth of the received signal.

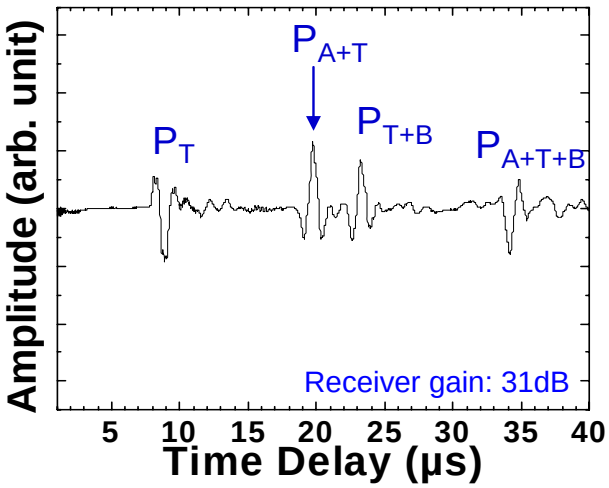

Figure 4-44 Ultrasonic performance of the FUTs shown in Figure 4-40 operated in transmission mode at 150°C. 3 line-grating area (~9 mm by 2 mm) is covered by silver top electrode.

4.3.4 Flexible guided PAW UTs to generate and receive PAW in a SS plate

In order to demonstrate the potential of using PAW grating FUTs for NDT and SHM, the grating FUTs shown in Figure 4-40 were cut into to two. Each part consisting of the gratings with the PZT-c film below serves as a guided PAW grating FUT. These two PAW grating FUTs were placed at the two ends of a 1.9 mm thick 100 mm long 50 mm wide SS plate as shown in Figure 4-45 (a), and their ultrasonic signals obtained in transmission mode are shown in Figure 4-45 (b). The SNR of the received signal is 20 dB. Then an artificial line defect with 1 mm depth and 1 mm width across the entire width 50 mm of the SS plate was made onto the middle of the SS plate, and the measured ultrasonic signal P_T was 3.4 dB weaker than the measured signal on SS plate without line defect. The line defects on plate can be detected by the amplitude change of ultrasonic signals, generated and detected by the grating FUTs, in transmission mode. The guided PAW grating FUTs may be attached or bonded onto plate structure like the bulk L wave FUTs reported in [91] for HT NDT or SHM.

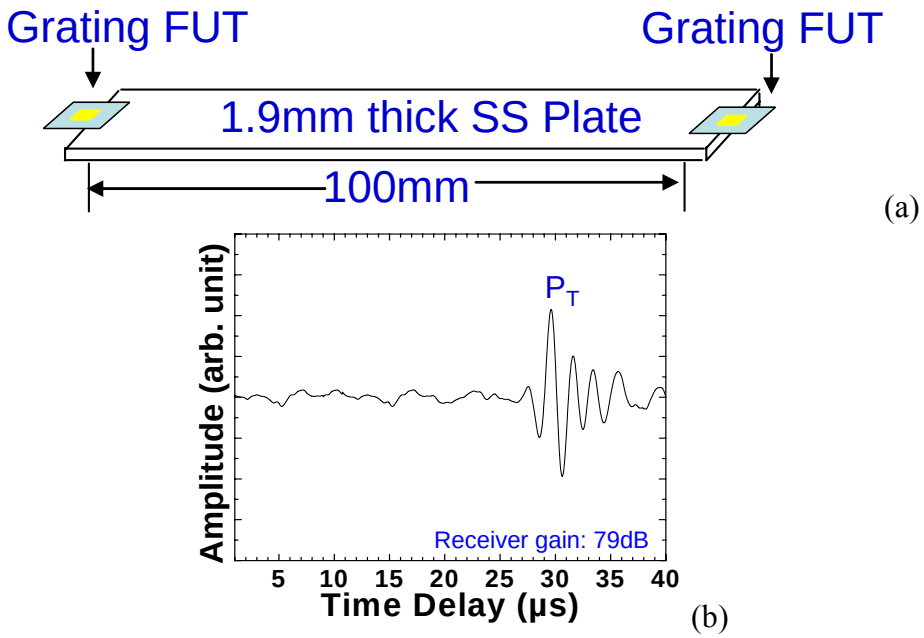

Figure 4-45 (a) Ultrasonic performance of the PAW grating FUTs shown in Figure 4-40 are placed at the two end of a 1.9 mm thick stainless steel plate. (b) Ultrasonic performance of measurement setup in (a). The two grating FUTs were operated in transmission mode.

4.4 Integrated HT SAW and PAW UTs Using IDTs

The purpose of the study of this section is to develop techniques for integrated SAW and PAW transducers directly onto desired metallic structures for SHM applications using IDTs. The selected frequencies are between 0.5 MHz and 2.0 MHz.

HT IUTs with the function of IDTs will be presented. The demonstration of integrated IDTs using PZT-c films on an Al alloy plate and the one on a steel cylinder will be carried out at 150°C. Moreover, integrated IDTs using BIT-c films on an SS plate will be demonstrated at 350°C.

4.4.1 Integrated IDT fabrication

Sol-gel sprayed PZT-c films were fabricated for the experimental demonstration at 150°C, and sol-gel sprayed BIT-c films were fabricated for the demonstration at 350°C, although the sol-gel sprayed BIT-c films could work at 400°C with good signal strength and SNR as presented in Section 2.2. Top electrodes with IDT shapes which are different from the regular shape of top electrodes used in the other chapters were used here. Colloidal silver was sprayed to form the IDT electrodes at room temperature for the application up to 150°C, and the Al IDT electrodes for the application above 300°C was formed by a vacuum deposition for this particular investigation. Certainly other top electrode fabrication methods without the usage of vacuum technology may be used. The IDT masks (negative) were made by an EDM method. The IDT shape top electrodes were sprayed or deposited through these IDT masks and forms the IDT (positive).

Since in this study the desired PAW and SAW operation frequency range is between 0.5 MHz and 2.0 MHz, one mask used in this study is designed, fabricated by the EDM and shown in Figure 4-46. The top and bottom connection electrodes parallel to the wave propagation direction are called bus-bars; the other thin electrodes perpendicular to the wave propagation direction are called fingers. The finger widths of the IDT are 0.5 mm for the IDT. The separation among the fingers is also 0.5 mm wide. The mask is made of a 0.57 mm thick SS plate. The thickness is chosen so that the mask is flat, has

negligible shadow effect during the colloidal silver spray and is reusable. Such finger width is convenient for the colloidal silver spray method. This IDT fabrication technique makes the selection of finger size and transducer size simple and convenient.

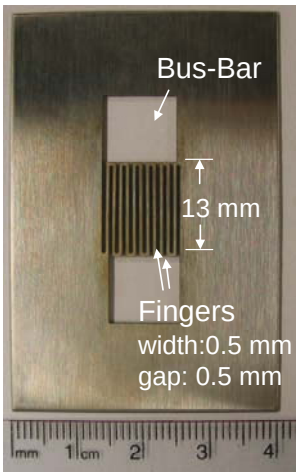

Figure 4-46 Mask used for IDT pattern.

4.4.2 Performance of integrated IDTs for SAW and PAW

Al alloy and SS plates of different thicknesses and a steel cylinder are used for the SAW and PAW experiments demonstrated below. For theoretical calculation of the velocities of SAW and PAW, the measured bulk L wave V_L and S wave V_S velocities and the densities of these metals are used. Since pulse-echo modes are of interest for NDT and SHM applications, most of our measurement data will be shown for this mode although measurement data in transmission modes will be demonstrated as well.

4.4.2.1 Integrated IDTs for SAW on an Al alloy plate

A 25 mm thick Al alloy plate is used here for the SAW experiment. Since Al alloy is an isotropic medium, SAW propagation on it can be also regarded as Rayleigh wave. Two IDTs were made on top of the 86 μm thick PZT-c film. Figure 4-47 shows the integrated PZT-c film transducer with an IDT operated in pulse-echo mode at 150°C and the measured SAW (Rayleigh) signal with a band pass filter between 0.5 MHz and 2.0 MHz in time domain is given in Figure 4-48. In Figure 4-48, R_{2A}, R_{2B} and R_{2A+2B} are the reflected echoes either from the edge A or the edge B through the corresponding Rayleigh

wave travel paths of 2A, 2B, 2(A+B), respectively. The longest travel distance in this figure was 306 mm (for R_{2A+2B}).

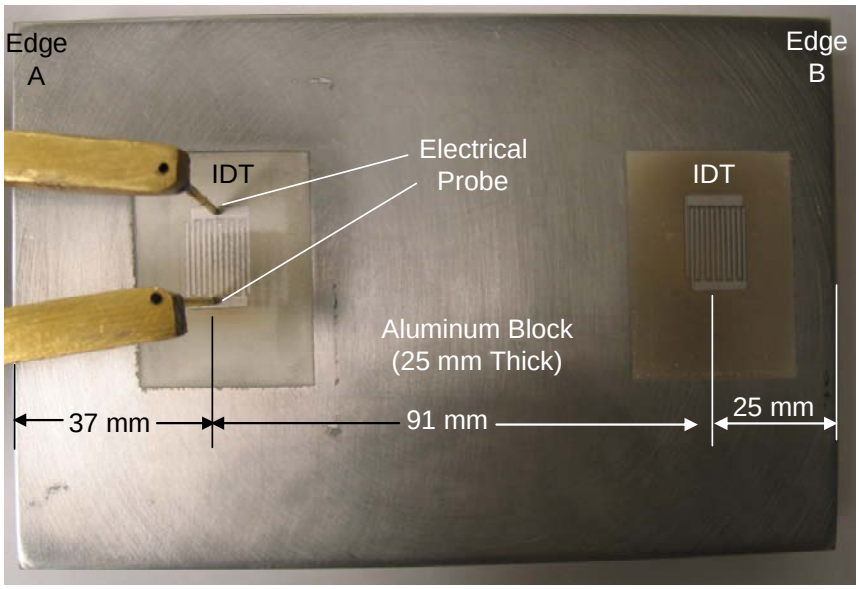

Figure 4-47 A 25 mm thick Al alloy plate with an IDT SAW transducer operated in pulse-echo mode. The 86 μm thick piezoelectric film was made of a PZT-c composite.

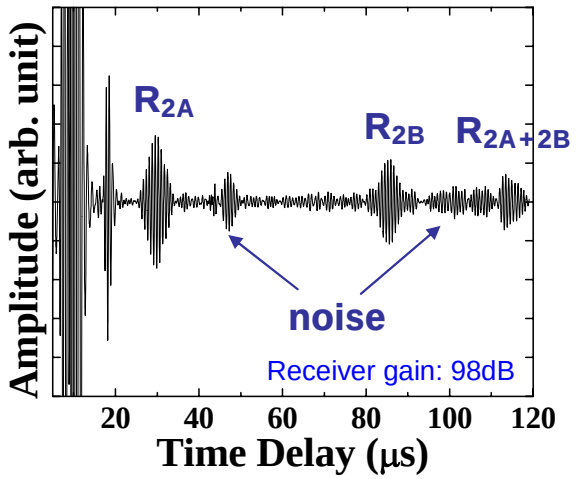

Figure 4-48 Ultrasonic performance of an IDT SAW transducer shown in Figure 4-47 and operated in pulse-echo mode at 150°C in time domain with a band pass filter between 0.5 MHz and 2.0 MHz.

At room temperature the measured density, V_L and V_S of this Al alloy substrate are 3530 kg/m^3, 6343 m/s and 3044 m/s, respectively. Using these data and the calculated

SAW (Rayleigh wave) group (phase) velocity is 2846 m/s. At room temperature the measured SAW velocity is 2840 m/s which agree well with the theoretically calculated value of 2846 m/s. At 150°C, as shown in Figure 4-48, the measured SAW velocity is 2700 m/s.

If the band pass filter used is between 0.5MHz and 10.0MHz, then the ultrasonic signals shown in Figure 4-48 become those shown in Figure 4-49. Figure 4-49 shows the existence of bulk L waves through the thickness direction of the Al alloy substrate and they are generated and detected by the same IDT transducer on top of the piezoelectric PZT-c film. These films are promising bulk wave IUTs as illustrated in Section 2.2. The strength of the bulk L wave can be adjusted by the size of the upper and lower bus-bars of the IDT. By comparing the IDT shown in Figure 4-46 with that shown in Figure 4-47 one can see that the width of the bus-bars of the IDT pattern in Figure 4-47 is narrower. The narrower the width of these bus-bars, the weaker is the bulk L wave and the stronger the strength of SAW. This indicates that NDT and SHM can be carried out not only by the SAW along the surface of the Al alloy substrate but also by the bulk L wave along the thickness direction when a proper band pass filter is used.

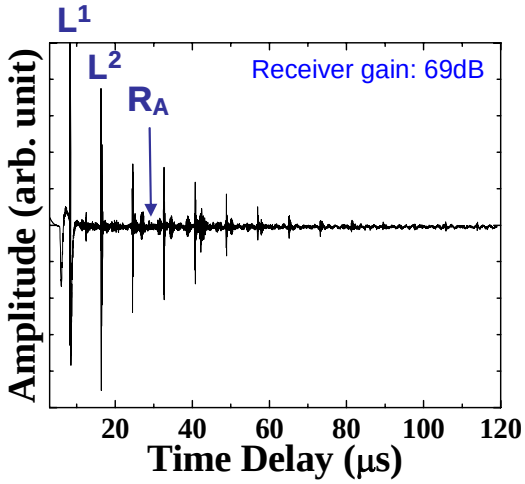

Figure 4-49 Ultrasonic performance of an IDT SAW transducer shown in Figure 4-47 and operated in pulse-echo mode at 150°C in time domain with a band pass filter between 0.5 MHz and 10 MHz.

It is noted that the band pass filtering can be carried out by software and that has real-time processing capability. Since the SAW transducer shown in Figure 4-47 is of layers structure which consists of PZT-c film and Al alloy substrate, the excitation efficiency [138] of the SAW device with respect to the PZT-c film thickness and operating frequency which affect the finger width design of IDT will be further investigated in order to strengthen the SAW signals.

4.4.2.2 Integrated IDTs for SAW on a steel cylinder

In order to demonstreate the ability of the sol-gel spray technology to fabricate SAW UTs onto curved surfaces a steel tube with 102 mm outer and 46 mm inner diameter was used as a sample as shown in Figure 4-50. An 89 μm thick PZT-c film and an IDT shape of top electrode were deposited onto the right side of this tube's cylindrical surface. The IDT together with the PZT-c film serves as a SAW generator and receiver. Figure 4-51 shows the SAW measurement at 150°C in the time and frequency domains in the pulse-echo mode, where R_n is the nth trip echo around the cylindrical surface of the tube. The center frequency, 6 dB bandwidth and SNR of R_1 were 1.5 MHz, 0.3 MHz and 24 dB, respectively. Each trip travels in a diatance of 320.4 mm. In Figure 4-51 the R6 echo has travelled a distance of 1,922 mm.

Figure 4-50 A steel tube with 102 mm external diameter and 46 mm inner diameter and IDT for SAW generation and detection in pulse-echo mode.

At room temperature the measured L wave velocity and S wave velocity of this steel tube along the axial direction are 5904 m/s and 3227 m/s, respectively. Using these data the calculated SAW (Rayleigh wave) group (phase) velocity 2986 m/s. At room

temperature the measured SAW velocity was 2980 m/s which agreed well with the theoretically calculated value. At 150°C, as shown in Figure 4-51, the measured SAW velocity was 2853 m/s and the signal strength at 150°C was 3 dB stronger than that at room temperature.

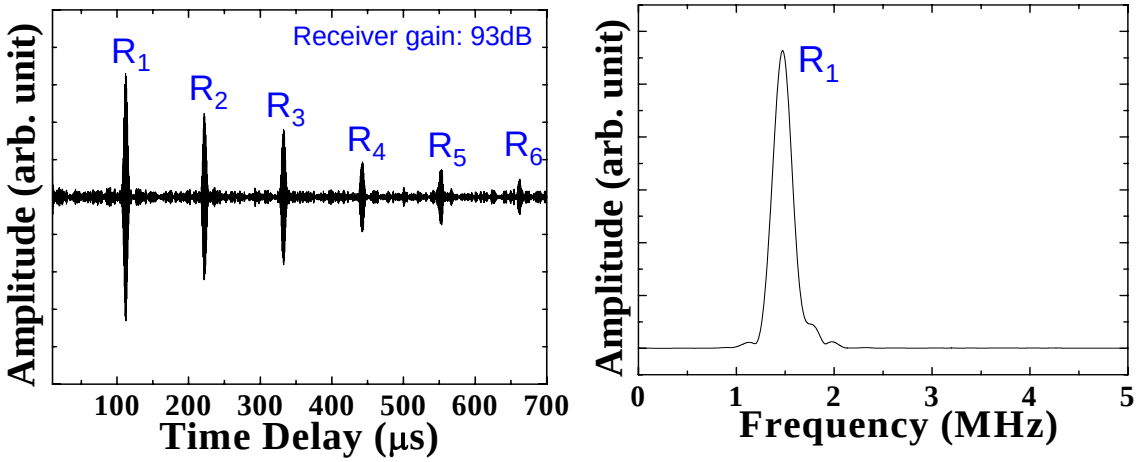

Figure 4-51 Ultrasonic performance of the IDT on the steel tube at 150°C in (a) time and (b) frequency domain, where R_n was the nth trip echo around the tube external cylindrical surface.

4.4.2.3 Integrated IDTs for PAW on a SS plate

For PAW experiments at temperatures higher than150°C a 111 μm thick BIT-c film was deposited on a 0.702 mm thick SS plate as shown in Figure 4-52. Then two IDT electrodes were made on the top of the film by the vacuum deposition technique using the IDT mask shown in Figure 4-46. Their thickness was 0.1 μm. Figure 4-53 shows the measured PAW signals in time domain using the integrated PAW transducer shown in Figure 4-52 near edge "A" operated in the pulse-echo mode at 350°C. The pass band of the band pass filter in our signal acquisition system was set between 0.5 MHz and 2.0 MHz. In Figure 4-53 P_{2A}, P_{2B} , P_{2A+2B}, P_{4A+2B} and P_{2A+4B} are the reflected echoes either from the edge "A" or the edge "B" through the corresponding PAW travel paths (distance) of 2a, 2b, 2(a+b), 2(2a+b) and 2(a+2b), respectively, as shown in Figure 4-52. The longest travel distance in this experiment was 594 mm (for P_{2A+4B}). The echoes of P_{2A} and P_{2B} are weaker than the P_{2A+2B} because they travel unidirectionally along A or B direction, respectively, but the echo P_{2A+2B} travel both along "A" and "B" direction and

are summed at the IDT near the edge "A" when received. Along the longer propagation distance echo strength will be the weaker due to the higher loss in the path. However, the echoes in Figure 4-53 show good SNRs. The two edges may be considered as large deep defects (cracks) in practical NDT and SHM applications. It means that this integrated PAW transducer may be regarded as a promising NDT and SHM tool at 350°C for sensing defects with the distance as long as 594 mm, i.e. P_{2A+4B}.

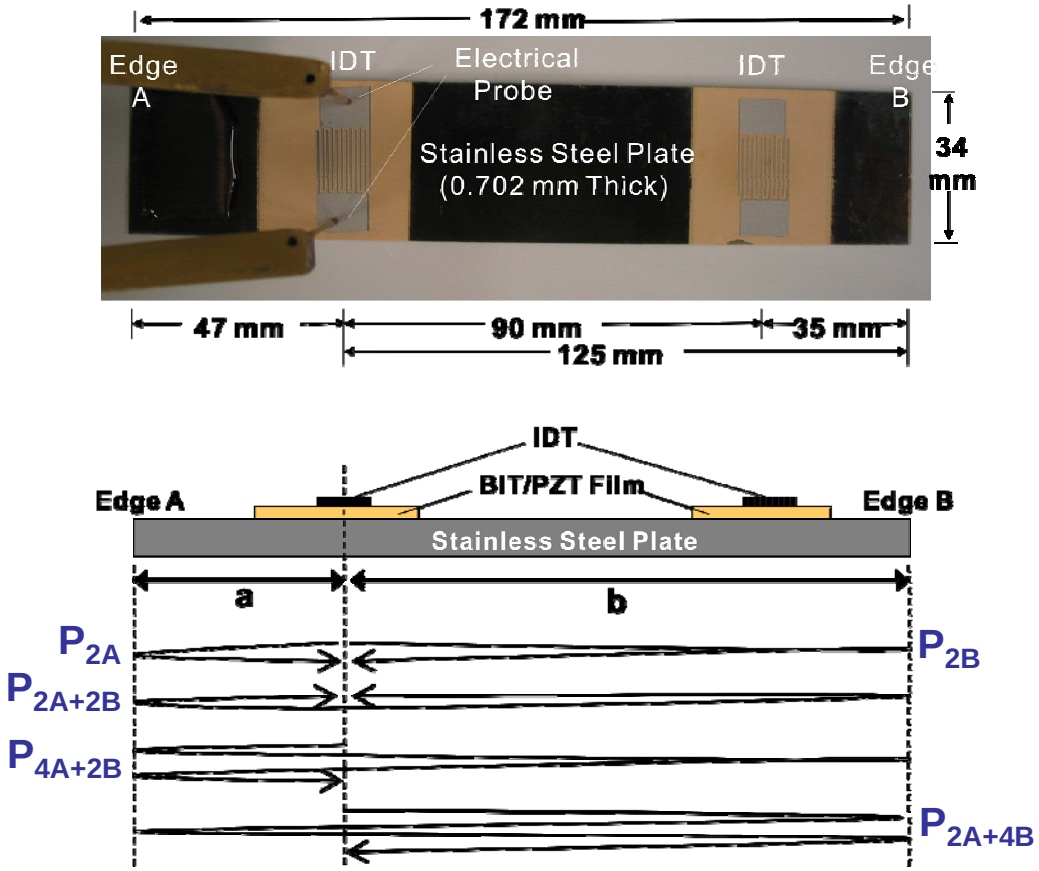

Figure 4-52 Photograph of the PAW transducers and a schematic view indicating propagation paths of PAWs in the SS plate. A 0.702 mm thick SS plate with a PAW transducer and an IDT electrode was operated in pulse-echo mode. The 111 μm thick piezoelectric films were made of a BIT composite.

At room temperature the measured PAW group velocity of the device shown in Figure 4-52 was 2936 m/s. The measured V_L and V_S of the SS plate at room temperature were 5828 m/s and 3151 m/s, respectively. Using these data and the formulas in [78] and [118], the calculated PAW phase velocity V_p (in solid lines) and group velocity V_g (in

dashed lines) are shown in Figure 4-54. V_R indicates the phase velocity of Rayleigh wave on the substrate having semi-infinite thickness. It is found that at the plate thickness h = 0.702 mm and f = 1 MHz the theoretically calculated V_g for the zeroth order anti-symmetrical mode a_0 is 3030 m/s which agrees well with the measured V_g of 2936 m/s. Note that the calculated result does not include the effect of the BIT-c film loading. Therefore the PAW shown in Figure 4-53 is the zeroth order anti-symmetrical plate wave mode a_0. Because the BIT-c film has slower L wave velocity than that of SS plate, the 111 μm thick BIT-c film will slow down the PAW velocity in the plate region coated with this film. In addition to measurement errors of time delays of the echoes in Figure 4-53 used in determining the V_g, a cause of the difference between the experimental result and theoretical calculation could be that the steel plate used in the experiments was not perfectly homogeneous or isotropic while such conditions were assumed in the calculation.

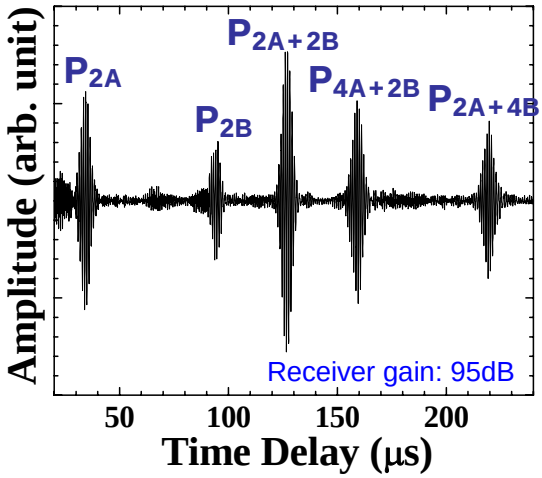

Figure 4-53 Ultrasonic performance of PAW transducer shown in Figure 4-52 with an IDT operated in pulse-echo mode at 350°C in time domain.

The geometry of the PAW transducer, such as thickness of the BIT-c film and finger widths of the IDT which affect operating frequency will be investigated in the future study in order to excite PAW waves efficiently. By comparing the measurement data shown in Figure 4-53 with those at room temperature it is found that the signal strength was 5 dB weaker at 350°C. The measured PAW (a_0) group velocity at 350°C was 2754 m/s.

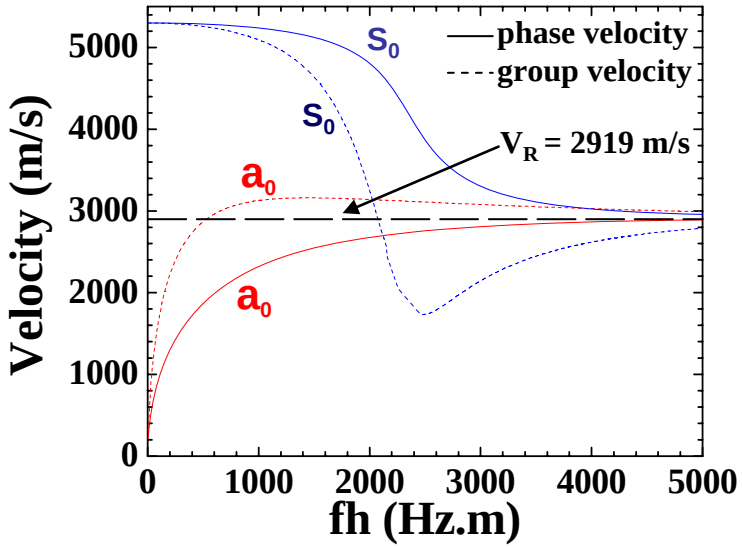

Figure 4-54 Calculated PAW dispersion curves for the 0.702 mm thick SS plate shown in Figure 4-52. V_R indicates the phase velocity of a Rayleigh wave on a substrate having semi-infinite thickness.

4.5 Summary

HT PAW and SAW UTs using sol-gel sprayed piezoelectric composite films and mode conversion techniques were presented in this chapter. The mode conversions between L waves generated and received by sol-gel sprayed UTs and PAWs or SAWs were achieved through the geometry of substrates, wedges, mechanical gratings, or IDTs.

In Section 4.1, sol-gel sprayed PZT-c thick (> 75 μm) films were directly coated onto three 2 mm thick Al plates with different configurations for the NDT and SHM capability evaluation of symmetrical, anti-symmetrical and SH PAWs. With a top line electrode these PZT-c films served as L IUTs. One IUT was fabricated at the end edge of the Al plate, and it can excite and detect predominately symmetrical PAW due to the finite thickness of the Al plate. One IUT was coated onto the top surface of a slanted edge at the end of another Al plate, and L waves were converted into S wave with out-of-plane partical displacement in the Al plate due to mode conversion at the slanted edge, and then became predominantly anti-symmetrical PAW due to finite Al thickness. One IUT was deposited onto the side surface of a slanted edge at the end of the other Al plate,

and the IUT generated the extension wave in the beginning and then converted to predominantly SH PAW in the Al plate at the slanted edge. Each guided acoustic wave mode in plates used for the experiments was identified by using the theoretical calculated dispersion curves compared with the experimentally measured group velocity. Two artificial line defects of 1 mm width and 1 mm depth on the Al plates were clearly detected at temperatures up to 150°C in pulse-echo mode for using symmetrical, anti-symmetrical and SH PAWs. Results indicated that for 2 mm thick Al plates SH PAWs were the best for the line defect detection, and have the capability to travel a distance of 1.625 meters. A real regional jet horizontal stabilizer made of Al plate of thicknesses ranging from 1.1 mm to 1.3 mm was also demonstrated for SH PAW propagation. The results indicated that SH PAWs may be used for NDT and SHM purposes. Also numerical simulations by solving the 3D visco-elastic wave equation with a finite difference based method were performed, and the simulation results agreed with the experimental results.

In Section 4.2, theoretical and experimental investigations of ultrasonic wedges which can generate and receive SH PAWs in a metal plate at temperatures up to 200°C were presented. Brass which has a slow S wave velocity was chosen as the high temperature wedge material. PZT-c film IUTs were coated on the brass wedges. The mode conversion method is used to convert L waves generated by an IUT to S waves in the brass wedge. The calculated mode energy conversion efficiency is 79.7% with a conversion angle of 64.1°. The S waves in the wedge which is glued to a SS plate with a wedge angle of 42.9° have been converted to SH PAWs in the SS plate.

The acoustic attenuation α_0 caused by the back scattering into the wedge of the SH_0 mode is dispersionless and it is inversely proportional to the plate thickness. SH_2 PAW mode has a rather dispersive attenuation α_2; however, it is also inversely proportional to the plate thickness. Regardless of the operating frequency, the acoustic attenuation of the SH_2 mode is always higher than that of the SH_0 mode. Such a feature plays a major role in the performance of the wedge. For example, the wedge can provide single SH PAW mode excitation if $\omega < \omega_{C2}$. Analysis of the coupling coefficient from the S waves in the

wedge to the SH PAWs in the plate is also presented. The dependence of wedge efficiency with respect to both the attenuation, α_0 and α_2 for the SH_0 and SH_2 PAW modes, respectively, and geometry, L, are presented as well. In order to operate the SH PAW modes at the maximum efficiency, $\alpha_n L$ must be 1.26. In the transmission mode predominantly SH_0 PAW has been obtained at a plate temperature of up to 200°C. Measurement results demonstrated that SH PAWs using such wedges may be a promising approach for NDT and SHM of metal structures because of less dispersion and high SNR.

In Section 4.3, integrated and flexible guided acoustic wave UTs have been made using line shape mechanical gratings made by EDM together with sol-gel fabricated IUTs at the opposite side. IUTs served as bulk L wave UTs and these L waves were converted to SAWs or PAWs when they interacted with the line mechanical gratings depending on the substrate thickness. Guided SAW grating IUTs have been made and for such transducers IUTs are made directly under the line gratings in a 10 mm thick SS plate. The measured SAW velocity and frequency agreed well with the theoretical and numerical calculation. When the SS substrate is 75 μm thick which is flexible, the gratings together with IUTs served as guided PAW grating FUTs. The experimental results indicated that the more the number of line gratings, the narrower is the bandwidth of the PAW. Zeroth order (S_0) symmetrical PAW was generated and received by the guided PAW grating FUTs. The detection of an artificial line defect created on a 100 mm long 50 mm wide SS plate was also demonstrated in a transmission mode using two guided PAW grating FUTs. These FUTs may be attached or bonded to parts even with curved surfaces. The preliminary results have indicated that they may be used for NDT and SHM purposes.

In Section 4.4, HT IUTs with IDT shape of top electrodes were developed to generate and receive PAWs or SAWs. The IDT mask was made by EDM. A colloidal silver spray method was used to form IDT electrodes onto sol-gel sprayed PZT-c films at room temperature through the IDT mask for the applications up to 150°C. For the applications up to 350°C, IDT shape of Al electrodes were formed by vacuum deposition onto sol-gel sprayed BIT-c films. The results of experiments show SAW propagation along a 25 mm thick Al alloy plate and along a steel cylinder with 102 mm diameter, and

PAW propagation in the zeroth order (a_0) anti-symmetrical mode along a 0.702 mm thick SS plate. The pass band of the filters for SAW or PAW is between 0.5 MHz and 2.0 MHz. The measured SAW and PAW results agreed well with the theoretically calculated values. If the edges of the substrates can be considered as large defects or cracks, the measured signals with good SNR demonstrated the NDT and SHM capability in a distance of several centimeters or tens of centimeters. If the substrate is thick, both SAW and bulk L wave may be generated and detected simultaneously for NDT and SHM applications along the surface or thickness direction, respectively of the substrate. Arrays of these transducers may be readily achieved as well.

CHAPTER 5

NON-CONTACT ULTRASONIC MEASUREMENT TECHNIQUES

To achieve SHM, fast NDT and NDT of rotation components, non-contact ultrasonic measurement approaches are desired. In this chapter, two non-contact techniques: NDT using sol-gel sprayed PZT-c film and BIT-c film IUTs as receivers for laser generated ultrasound, and induction-based ultrasonic measurement using sol-gel sprayed PZT-c film IUTs as transmitters and receivers, will be presented.

L waves, S waves, and PAWs generated by laser ultrasonics and received by sol-gel sprayed L wave HT IUTs combing mode conversion technique will be demonstrated at room temperature, 150°C and 400°C. The estimation of thickness measurement accuracy for steel substrate by this technique will be presented. One of the applications using this technique for NDT of bonded composite patches on Al plates will also be illustrated. The objective of this study is to explore the merits of combining the usage of lasers as the remote and versatile ultrasound generating UTs with that of IUTs as the receivers. When IUTs are used just as receivers, it is expected that the required electric power is low and thus battery driven or harvested energy driven approaches including wireless communication for NDT and SHM may be feasible.

Induction-based ultrasonic measurement using sol-gel sprayed IUTs will be presented for NDT of metal substrates and composite substrates in this chapter. The study will include the generation and detection of L waves, S waves, and PAWs. The result of a measurement carried out on a rotating sample will be demonstrated.

5.1 NDT Using Laser Generated Ultrasound and IUT Receivers

The generation of ultrasound using pulsed lasers has been known since 1963 [22]. The mechanisms of laser generated ultrasound were reported and certain examples presented in [19][20][21]. Using lasers to generate ultrasound is an attractive and effective non-contact method in which the laser and the object may be meters away. In order to fully take advantage of such a non-contact nature, many detection approaches using optical means such as knife edge or position-sensitive detector [139][140] and various interferometers [22][141][142] to receive laser generated ultrasound were developed. The main advantages of the non-contact laser generation and laser detection method for NDT of materials are that (a) objects can be at elevated temperatures, (b) curved surfaces are permissible, (c) L waves, S waves, PAWs and SAWs may be used (d) high inspection rate may be achieved and (e) inspected objects can be in motion. Furthermore laser beams can be considered as versatile UTs which may have adjustable transducer size, shape, and power and be arranged in array configuration and scanned at a reasonable speed using mirrors. It is known that at present the system cost of a laser generation and laser detection approach may be high.

NDT or SHM at HT becomes of increasing interest to the aerospace and power generation community when considering aging aircrafts or power plants or gas and oil pipes [3][17][19][20][139][140][141][142][143][144][145][146] whose growing maintenance costs can reduce their economic life extension. There are demands for novel NDT and SHM techniques for large area damage diagnostics. The objective of this study is to explore the merits of combining the usage of pulsed lasers as the ultrasound generating UTs together with a contacting type of UTs as the receivers to perform NDT or SHM and achieve advantages (a), (b), (c) and possibly (d) mentioned above. Such an approach may also eliminate the high cost concern of a laser detection approach. To this direction, there have been good reports in [144][145][146] in which laser pulses not only were used for the laser generation of ultrasound but also optically scanned by a mirror scanner to produce the ultrasonic images except that the UTs fixed at the receiving locations were not yet suitable for high temperatures and curved surfaces. However, in a

recent publication [147] a PZT has been bonded onto the sample or a steel fiber welded to the sample and used as an ultrasonic guided wave receiver up to 140°C together with pulsed laser generation and a mirror scanner.

As demonstrated in the previous chapters, sol-gel fabricated piezoelectric film IUTs have been demonstrated being able to be coated onto planar and curved surfaces for possible NDT and SHM applications. In previous works [28][121][132][148] such IUTs were successfully used in pulse-echo or transmission mode of up to more than 500°C. The aim of this study is to use such IUTs as the receivers to detect the ultrasound generated by pulsed lasers for NDT or SHM. The expected advantages over the conventional UTs used are that IUTs are miniature, light weight and workable at high temperatures, on curved surfaces, usable for the receiving of L waves, S waves, and PAWs that have been presented in earlier chapters. They may be also easily arranged in array configuration, are mode selective, and have high piezoelectric sensitivities. It is noted that when IUTs are used as receivers, the electric power required may be very small; thus the approaches using battery or power obtained via energy harvested devices and including wireless communication are feasible. It means that the high electrical power pulser required for the generation of ultrasound may be replaced by a remotely applicable pulsed laser.

5.1.1 IUT receiver sensitivity evaluation

PZT-c films and BIT-c films were fabricated for the experiments in this chapter for 150°C and 400°C demonstrations respectively by the sol-gel spray method. Figure 2-8 showed an IUT made of 62 μm thick PZT-c film and deposited onto a 12.7 mm thick steel plate and measured by a handheld EPOCH model LT pulser-receiver (from Olympus-Panametrics, USA) at room temperature. The measured ultrasonic data in pulse-echo mode was also presented in Figure 2-10, where L^n is the nth trip L echo through the plate thickness, and 0 dB gain (no amplification) out of the available 100 dB receiver gain was used. The same test sample shown in Figure 2-8 is used here for the experiments to be presented in the next section.

5.1.2 Low repetition pulsed laser generation and IUT receiving of ultrasound on planar surface at room temperature

First, a pulsed laser (λ = 1.064 μm, Q switched Nd:YAG) with pulses of 45 mJ energy and 5 ns duration delivered at a low repetition rate of 10 Hz is used for the generation of ultrasound. Figure 5-1 (a) and Figure 5-1 (b) show the schematic diagram and measurement setup, respectively, of the ultrasonic measurement using the IUT coated onto the steel plate shown in Figure 2-8 to receive the laser generated ultrasound in the steel plate. The laser generation location is at the opposite side of the steel plate but located at the center of the IUT (top electrode location). Figure 5-1 (b) showed the measured ultrasonic signal displayed in an oscilloscope without any amplification where L^n is the nth trip L echo through the steel plate thickness. The laser spot size was 8 mm diameter and the energy is in the thermoelastic regime [19][20]. The SNRs of the echoes L^1 and L^3 obtained by single shot laser pulse are 28.4 dB and 22.3 dB, respectively.

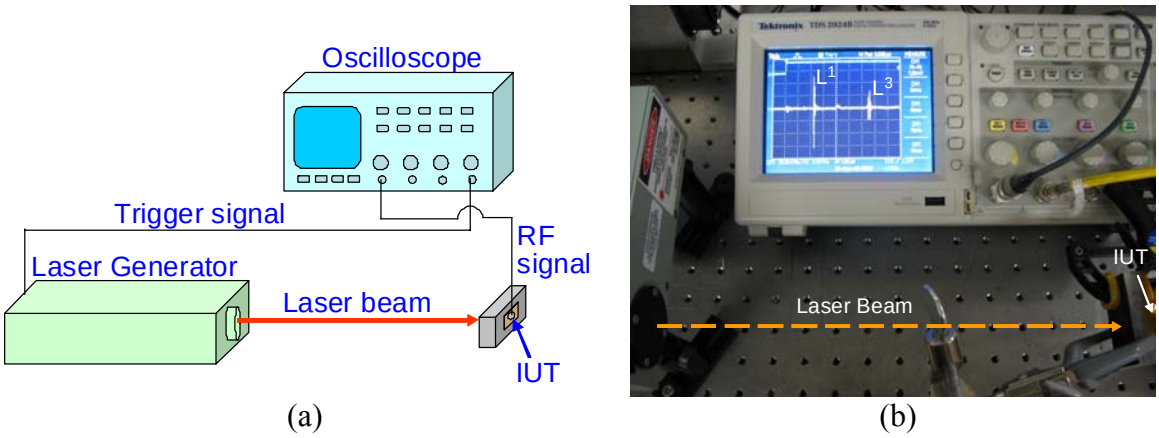

Figure 5-1 (a) Schematic diagram and (b) measurement setup of laser generation and IUT receiving in a steel plate.

Again Eq. (2-1) (Eq. 19 in [87]) is used here for the estimation of the measurement accuracy for time delay and then thickness of the steel substrate shown in Figure 5-1 (b). where f_0 is the center frequency, T is the time window length for the selection of e.g. L^1 and L^3 in Figure 5-1 (b) for the cross correlation, B is the fractional bandwidth of the signal (the ratio of the signal bandwidth over f_0), ρ is the correlation coefficient used in cross correlation, SNR_1 and SNR_2 are the SNR of the 1st echo (e.g. L^1 in Figure 5-1 (b))

and the 2nd echo (e.g. L^3 in Figure 5-1 (b)), respectively, and $\sigma(\Delta t - \Delta t')$ is the standard deviation of the measured time delay (Δt the true time delay; $\Delta t'$ the estimated time delay). Using Eq. (2-1), the calculated $\sigma(\Delta t - \Delta t')$ is 4.2 ns for the IUT in receiving mode. Since a sampling rate of 250 MS/s (Using Tektronix TDS2014B oscilloscope which has the maximum sampling rate of 2 GS/s, but it is 250 MS/s in this measurement as the time base of oscilloscope was set at 1 μs in order to display L^1 and L^3 simultaneously) is used in the experiment, with the use of the cross correlation method including interpolation [11] the time measurement error which may be additionally introduced is estimated to be 0.8 ns. The total uncertainty in time delay measurement is then 5 ns. V_L, the measured L velocity in steel substrate using pulse-echo technique at room temperature, is 5960 m/s obtained by using the thickness 12.7 mm divided by the measured time delay (cross correlation of the echoes L^1 and L^3 shown in Figure 5-1 (b)). Thus the best possible thickness measurement accuracy achievable using the above parameters given in Table 5-1 would be 14.9 μm for the IUT in receiving mode at room temperature and a laser pulse of 45 mJ energy, 5 ns duration and 8 mm spot diameter.

Table 5-1: Parameters for Eq. 2-1 and digitization resolution

Parameters	Laser Generation IUT (receiver)
f_0	11.4 MHz
T	0.4 μs
B	9/11.4
ρ	0.77
SNR_1	28.4 dB
SNR_2	22.3 dB
$\sigma(\Delta t - \Delta t')$	4.2 ns
Digitization resolution (100 MHz) together with interpolation	0.8 ns
Total time delay Uncertainty	5 ns
V_L	5960 m/s
Thickness measurement accuracy	14.9 μm

5.1.3 High repetition pulsed laser generation and IUT receiving of ultrasound on planar surface at room temperature and 150°C

In order to evaluate PZT-c film IUT as a receiver for a high repetition low power pulsed laser, a laser (λ = 0.532 μm, 2nd harmonics of a Q switched Nd:YAG) which delivers pulses of 600 ps duration, 50 μJ energy at a repetition rate up to 1 kHz was used to generate the ultrasound. The lasers with high pulse repetition rate would produce ultrasonic images with reduced frame time [144][145][146][147]. The sample was an IUT made of 51 μm thick PZT-c film and deposited onto a 12.7 mm thick steel plate. The top electrode of this IUT was 6 mm in diameter. The laser generation location was at the direct opposite side of steel substrate with the IUT. The laser spot size is 0.5 mm and the energy is in the ablation regime. Figure 5-2 (a) and Figure 5-2 (b) show the received ultrasonic signals averaged over 100 laser pulses at room temperature and 150°C, respectively. The averaging of 100 laser pulses is used to reduce the electrical noises of the current experimental setup. The center frequencies and bandwidths of the echo L^1 in Figure 5-2 (a) and Figure 5-2 (b) are 19.5 MHz, 27 MHz, 14.5 MHz and 11.4 MHz, respectively. The SNR at 150°C is lower higher than that at room temperature mainly due to the IUT receiver's better ultrasonic performance at room temperature than at 150°C. Figure 5-2 shows that IUT made of PZT-c film is capable to be an ultrasonic receiver for laser generated ultrasound using this high repetition pulsed laser up to at least 150°C.

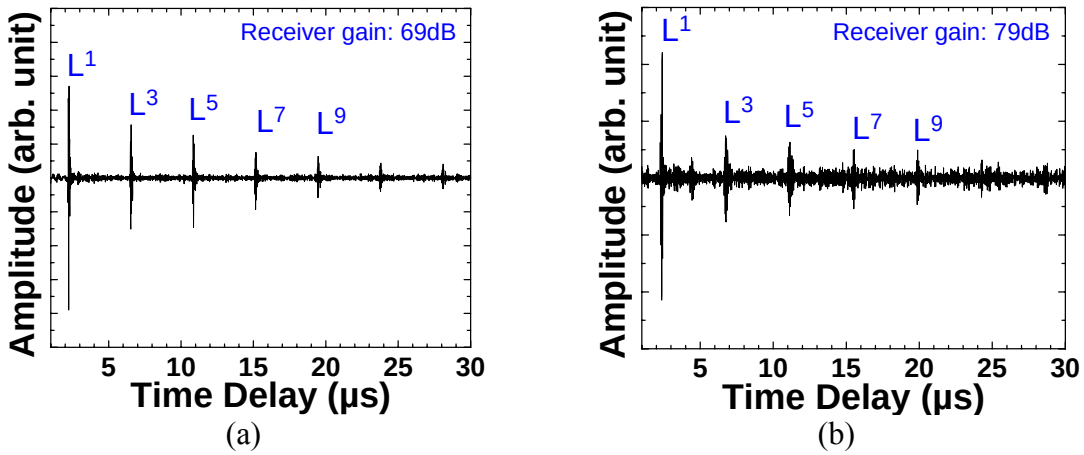

Figure 5-2 Measured ultrasonic signals using laser generated ultrasound and IUT as the receiver at (a) room temperature (b) 150°C.

5.1.4 Low repetition pulsed laser generation and IUT receiving of ultrasound at curved surface and 400°C

As shown in earlier chapters BIT-c film IUTs can be coated directly onto curved surfaces and operated at temperatures higher than 150°C as receivers. Figure 5-3 (a) shows a BIT-c film IUT made of a 60 μm thick BIT-c film and deposited onto a steel tube of a 25.4 mm outer diameter and 6.4 mm wall thickness and measured by a handheld EPOCH LT pulser-receiver at 400°C. Again, BIT-c film was chosen because as an IUT, it can operate at up to 500°C [28][149].The diameter of the top silver paste electrode of this IUT was 5 mm which was chosen to obtain the maximum signal strength at room temperature. In Figure 5-3 (a), 40.8 dB gain out of the available 100 dB receiver gain was used. The measured ultrasonic signals obtained in pulse-echo mode at 400°C is presented in Figure 5-3 (b), where L^n is the nth trip echo through the tube wall thickness. At 400°C the center frequency and the 6 dB bandwidth of the L^2 are 12.7 MHz and 5.8 MHz respectively.

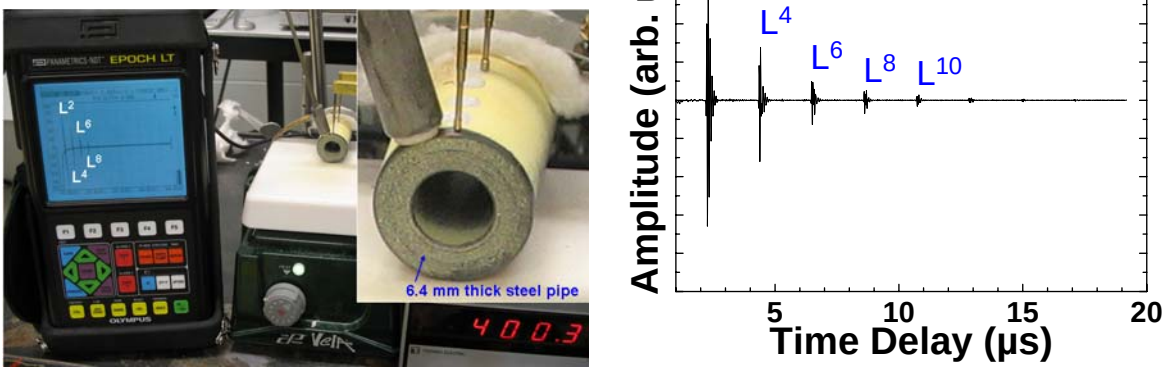

(a) (b)

Figure 5-3 (a) Measurement setup for an IUT made of BIT-c film at 400°C using an EPOCH LT and performed in pulse-echo mode; (b) Measured ultrasonic signals in pulse-echo mode at room temperature.

Since the high repetition (1kHz) and low power laser, which delivered pulses of 600 ns duration, 50 μJ energy and was used in the previous section, produced ultrasonic signals with low strength, a relative high pulse energy laser (λ = 1.064 μm, a Q switched

Nd:YAG) with a low repetition rate of 10 Hz was chosen to perform all the experiments presented below. Figure 5-4 (a) and Figure 5-4 (b) present the ultrasonic signals, which were received by the BIT-c film IUT shown in Figure 5-3 (a) and were averaged over 10 laser pulses of 2 mJ energy and 5 ns duration, at room temperature and at 400°C, respectively, where L^n is the nth trip echo through the tube wall thickness. Here the averaging of 10 laser pulses is used to reduce the electrical noises of the present experimental setup. The laser beam spot size was 0.5 mm and impinged at the center of the top silver electrode of the IUT. Since it is in the ablation regime, the silver top electrode impinged by the laser spot eventually disappeared; however, there is little change in the measured ultrasonic signal. If the center of the IUT does not have the BIT-c film and allows the 0.5 mm laser spot to impinge onto the steel tube, the received signal waveform by the BIT-c film IUT surrounding the 0.5 mm spot is expected to be somewhat different but should be sufficiently strong for thickness measurements, for example. At 400°C the center frequency and the 6 dB bandwidth of L^2 echo generated by the pulsed laser and received by the BIT-c film IUT are 13.7 MHz and 7.4 MHz respectively.

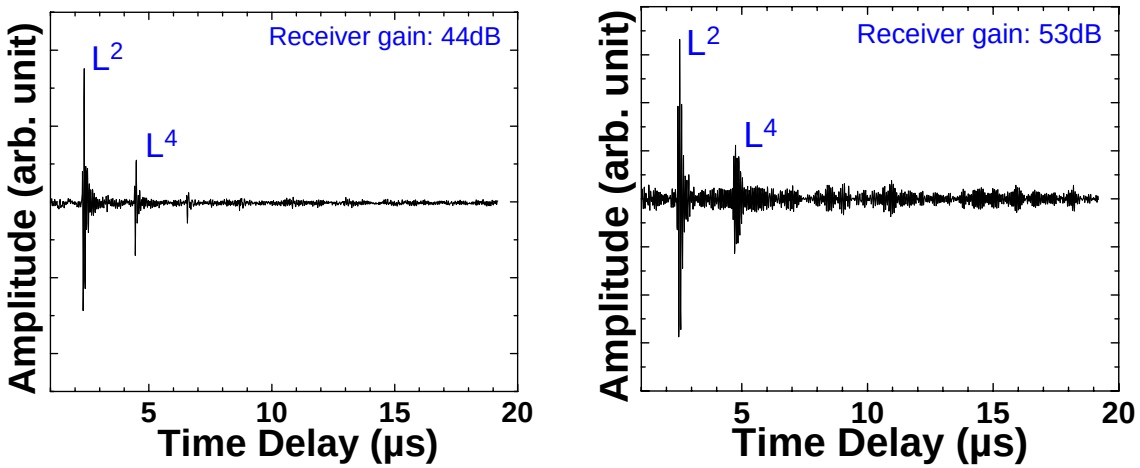

Figure 5-4 Measured ultrasonic signals using laser generated ultrasound and BIT-c film IUT shown in Figure 5-3 (a) as the receiver in pitch-catch mode (a) at room temperature (b) at 400°C.

Due to the well-separated echoes in the time domain although averaged with ten pulses, Figure 5-4 (a) and Figure 5-4 (b) also indicate the frequency bandwidth achieved

by the IUT in combination with the use of the pulsed laser generation is sufficient to inspect such a steel pipe with a 6.4 mm wall thickness. Thus IUT made of BIT-c film is capable to be a sensitive receiver at curved surface for laser generated ultrasound up to at least 400°C.

5.1.5 Low repetition pulsed laser generation and IUT receiving of both L and S waves and PAWs

In this section a pulsed laser (λ = 1.064 μm, a Q switched Nd: YAG) with pulses of 2 mJ energy and 5 ns duration delivered at a repetition rate of 10 Hz is used for the generation of ultrasound. IUTs intrinsically acting as L wave receivers will use various mode conversion approaches [122][137] and serve as L wave, S wave, symmetrical, anti-symmetrical and SH PAW receivers. Al and SS plates are used as substrates.

Figure 5-5 (a) shows an IUT made of an 80 μm thick BIT-c film and deposited onto an edge of the steel block which was the L-S probe presented in Section 3.1.2. The L wave generated by the laser beam at the laser impinging plane will propagate along the block along the path parallel to the IUT plane and be reflected by the 45° angle plane shown in Figure 5-5 (b) into the IUT L wave receiver. The S wave generated by the laser beam will propagate a similar way but be reflected with mode conversion [122] with an angle of 61.5° into the IUT L wave receiver. The reason to choose the angle of 61.5° was reported in Chapter 3. It basically confirms that the S waves propagating along the rod axis which is parallel to the plane of IUT will be mode converted to L waves and received by the L wave IUT. This angle also allows nearly 96.7% energy conversion efficiency from S to L waves [122]. The top square shape electrode was chosen to be 8 mm by 8 mm so that both L and S waves can be received. Figure 5-6 shows the ultrasonic signals in the time domain obtained with a laser spot size of 0.5 mm diameter. The laser generation was in the ablation regime and it produces both L and S waves. The sample temperature was 400°C. In Figure 5-6 the L^1 and S^1 waves were obtained simultaneously. The ratio of their amplitudes may be controlled by the adjustment of the location and the size of the BIT-c film IUT top electrode area or the laser spot size and location below or above the dividing line shown in Figure 5-5 (b). The L^1 and S^1 represent the first trip L and S wave echo,

respectively, traversing between the laser impinging plane and L wave IUT. The center frequencies of the L^1 and S^1 echoes are 8.8 MHz and 9.7 MHz and the 6 dB bandwidths are 7.4 MHz and 7 MHz, respectively. This result demonstrates that laser generated L and S waves can be detected by an IUT made of BIT-c film at 400°C.

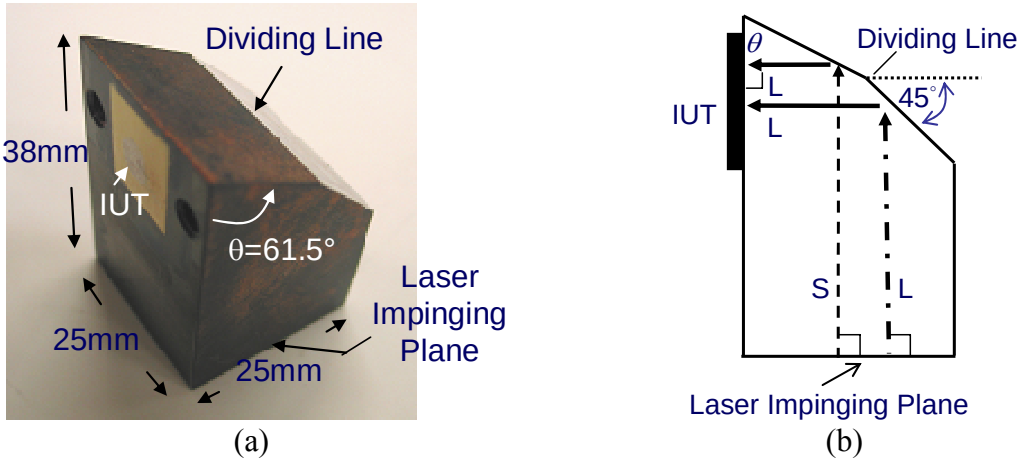

Figure 5-5 (a) Sample for measurement of both L and S waves; (b) Schematic diagram the integrated L and S wave probe. The laser impinges on the bottom surface, opposite to the tilted surface.

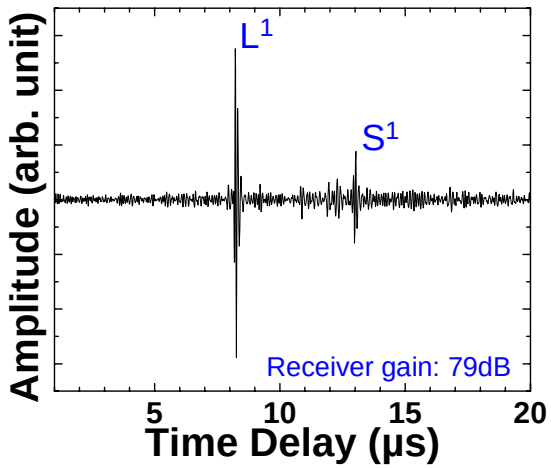

Figure 5-6 Measured ultrasonic signals using laser generated ultrasound and IUT shown in Figure 5-5 (a) as the receiver at 400°C.

When an L wave PZT-c film IUT is coated onto the edge of a thin Al plate as shown in Figure 5-7, symmetrical and anti-symmetrical PAW may be generated and received, as shown in Chapter 4. This Al plate has a length of 406.4 mm, a width of 50.8

mm and a thickness of 2 mm. One artificial line defect, D with 1 mm depth, 1 mm width and 50.8 mm length was made for the demonstration of the ability of symmetrical and/or anti-symmetrical PAW to detect such a defect. For the measurement, the PZT-c film IUT has a top electrode with a height of 1.8 mm and a width of 48 mm. Such top electrode dimensions enable PAW to receive nearly all end cross section of the Al plate. The thickness of the PZT-c film was 88 μm. The laser described in Section 5.1.4 was used. Using a line laser beam of 10 mm long and 2 mm wide to impinge onto the Al plate at the location indicated in Figure 5-7, the measured ultrasonic signals are shown in Figure 5-8. The laser generation was in the thermoelastic regime. The measurement group velocity of the arrived PAW signal indicated as L_{sym}^{1} is 4540 m/s and its center frequency is 2 MHz.

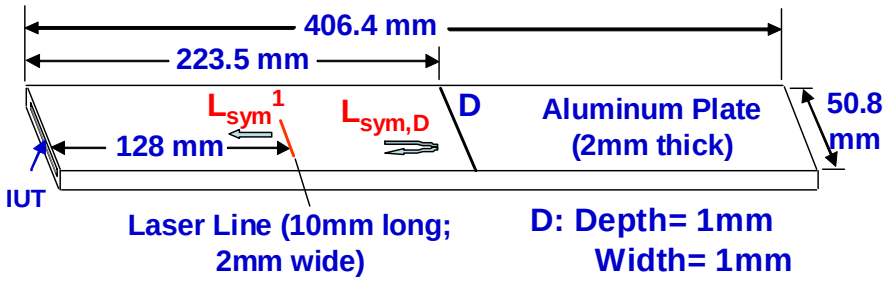

Figure 5-7 Sample and measurement setup for PAWs generated by a line laser beam and received by a PZT-c film IUT.

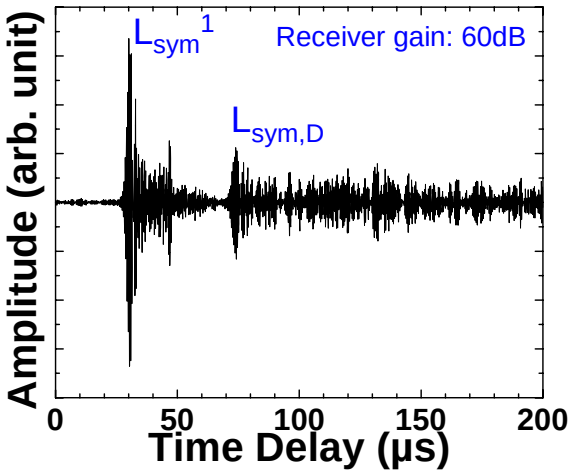

Figure 5-8 Measured ultrasonic signals of PAWs at room temperature using the measurement setup in Figure 5-7.

The theoretical calculations of phase and group velocities of the symmetrical and anti-symmetrical modes of the Al plate in Section 4.1.3.1 indicate that L_{sym}^{1} is predominantly the 1st higher order symmetrical S_1 PAW mode but existing together with many other high order modes. It means that laser beam can generate sufficient S_1 PAW mode for this IUT coated at the end of the Al plate to receive. In Figure 5-8 L_{sym}^{1} is the signal traveling a distance of 128 mm from the laser generation line to the IUT receiver at the edge. Echo $L_{sym,D}$ reflected from defect D is clearly observed and it travels a total distance of 319 mm.

A 79 μm thick PZT-c film with a top electrode area of 1 mm in width and 45 mm in length as the IUT receiver is coated onto the top of the edge of a 1.9 mm thick, 50.8 mm wide and 406.4 mm long SS plate as shown in Figure 5-9. Such top electrode dimensions were chosen so that strong PAWs can be received. Figure 5-10 presents the IUT receiving ultrasonic signals at room temperature generated by the laser described in Section 5.1.4 and a line spot of 30 mm long and 0.5 mm wide. The laser energy was in the thermoelastic regime. The generation laser line spot is about 228 mm away from the IUT of the steel plate. The measurement group velocity of the arrived PAW signal indicated as L_{asym}^{1} is 3091 m/s and its center frequency is 0.7 MHz. The theoretical calculations of phase and group velocities of the symmetrical and anti-symmetrical modes of the SS plate in Section 4.2.3.1 indicate that L_{asym}^{1} is predominately the lowest order anti-symmetrical a_0 PAW mode but existing together with many other high order modes. It means that the laser generated predominately a_0 PAW mode which is mode converted [137] into L waves and received by IUT. The mode conversion angle ϕ is 62.6°. The L_{asym}^{2} echo shown in Figure 5-10 travels from the laser line location to the end of the SS plate opposite to the IUT and is reflected by the end edge and reached IUT. The total travel distance is about 580 mm. This illustrates that the lowest order anti-symmetrical a_0 PAWs generated by the laser can be detected by the PZT-c film IUT on a SS plate in a length of 580 mm.

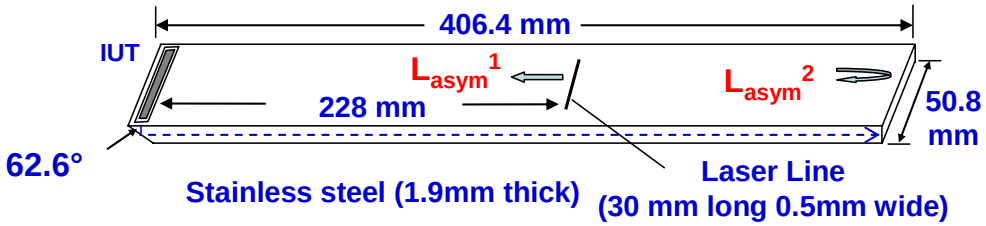

Figure 5-9 Sample and measurement setup for PAWs generated by a line laser beam and received by a PZT-c film IUT.

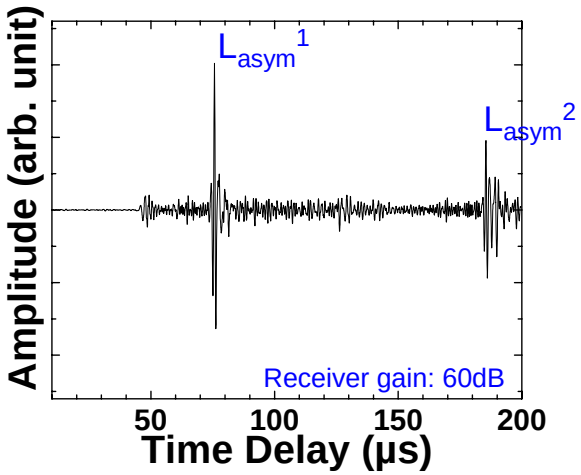

Figure 5-10 Measured ultrasonic signals of PAWs at room temperature using the measurement setup in Figure 5-9.

In Figure 5-11 an IUT made of 90 μm thick PZT-c film with a top electrode area of 1.6 mm in height and 20 mm in length as the receiver is coated onto the side near the edge of the a 2 mm thick, 50.8 mm wide and 406.4 mm long Al plate. Such top electrode dimensions were chosen so that PAWs near the center of the plate cross section can be received. A mode conversion angle θ = 61.7° is used to convert the lowest order symmetrical PAW, S_0, to the lowest order SH mode, SH_0 and vice versa presented in Chapter 4. Two artificial line defects, D1 and D2 with 1 mm depth and 1 mm width were also made for the demonstration of the ability of SH PAW to detect such defects in a long distance. D1 and D2 have a width of 25.4 mm and 50.8 mm, respectively. Figure 5-12 presents the IUT receiving ultrasonic signals at room temperature that were generated by the same laser described in Section 5.1.4, but with pulses of 4.1 mJ energy and spot size of 0.5 mm diameter. The laser generation spot is at the edge right beside the PZT-c film IUT (top electrode). The laser generated L waves are expected to be mode converted

[137] into SH PAW waves. They are reflected by the D1 and D2 defects and received by IUT. The mode conversion angle θ is 61.7° [137]. Using the reflected echoes from the defects D1 and D2, respectively, $S_{H,D1}$ and $S_{HD,2}$, the calculated velocity for SH PAW, is 2939 m/s which corresponds to that of the lowest order SH_0 PAW mode in this Al plate shown in Figure 4-14. The center frequencies of the received $S_{H,D1}$ and $S_{H,D2}$ echoes are 3.3 MHz and 3.5 MHz, respectively. Figure 5-11 and Figure 5-12 show that PZT-c film IUT can be used to receive laser generated and mode converted SH PAWs, which is predominantly the lowest order mode, for the defect detection.

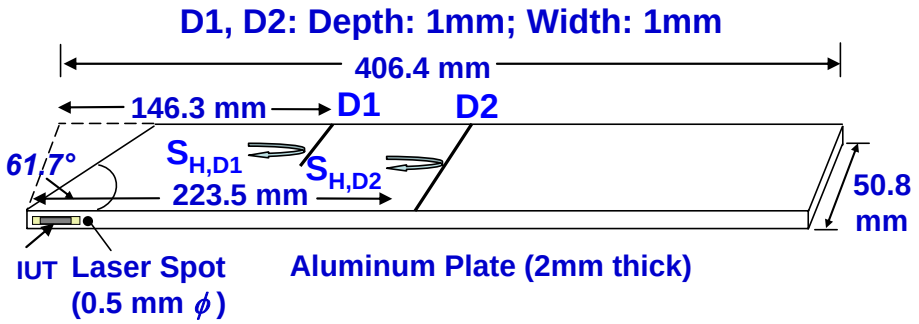

Figure 5-11 Sample and measurement setup for SH PAWs generated by a spot laser beam and received by a PZT-c film IUT.

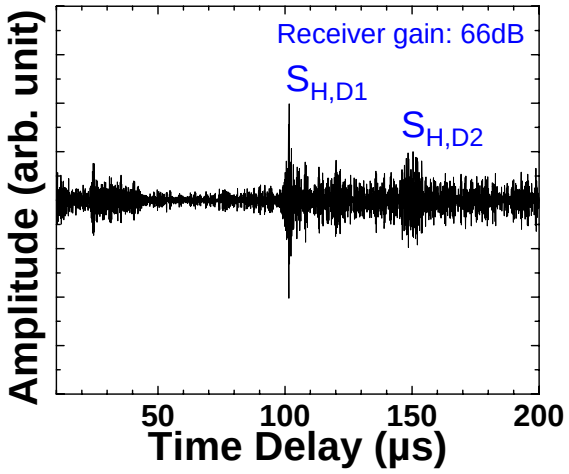

Figure 5-12 Measured ultrasonic signals of SH PAWs at room temperature using the measurement setup in Figure 5-11.

5.2 NDT of Bonded Composite Patches on Al Beams Using Laser Generated Ultrasound and IUT Receivers

In last three decades bonded repair technology [150][151][152] has become a cost-effective means of repairing cracks in metallic aircraft structures. There exist several NDT techniques to evaluate these bonded repairs while the aircraft stays in the hanger and bonded repair regions are accessible [3][5]. The objective of this study is to present an integrated NDT and potential SHM approach to detect the disbond between the Gr/Ep composite patch and Al substrate. In this study specimens, consisting of double sided six plies Gr/Ep bonded onto a 6.35 mm thick, 50.8 mm wide and 406.4 mm long Al 6061-T6 plates, will be made for the experiments. An artificial disbond using a Teflon sheet insert of 0.05 mm thickness, 25.4 mm length and 25.4 mm width, will be introduced to the interface between tapered Gr/Ep composite regions and Al plates.

In this investigation miniature and light weight PZT-c film IUTs will be directly coated at the end of the Al as receivers for ultrasonic signals. One objective is to explore the merits of combining the usage of lasers as the ultrasound generating UTs with that of IUTs as the receivers.

Another objective is to attach FUTs made on 75 μm thick Ti and 50μm thick polyimide membranes presented in Chapter 2 to the Gr/Ep composite patches, operated in pulse/echo mode and used to detect the disbonds. Such FUTs can be conformed to curved surfaces and operated at elevated temperatures as well, but they need ultrasonic couplant between the FUTs and the specimens to be tested. They may be also permanently glued or bonded onto Gr/Ep composite patches.

5.2.1 Specimen preparation and ultrasonic C-scan inspection

To meet the objectives a simple bonded repair configuration has been adopted. The schematic and an actual sample of the repair configuration are given in Figure 5-13. The host is an Al 6061-T6 plate which has a dimension of 406.4 mm by 50.8 mm by 6.35 mm.

A Teflon sheet of 0.05 mm thickness is inserted to create an artificial defect to simulate a disbond. The tapered patch is made of six plies of Gr/Ep composite which covers a total area of 50.8 mm by 101.6 mm, and the thickness of each ply is 0.25 mm.

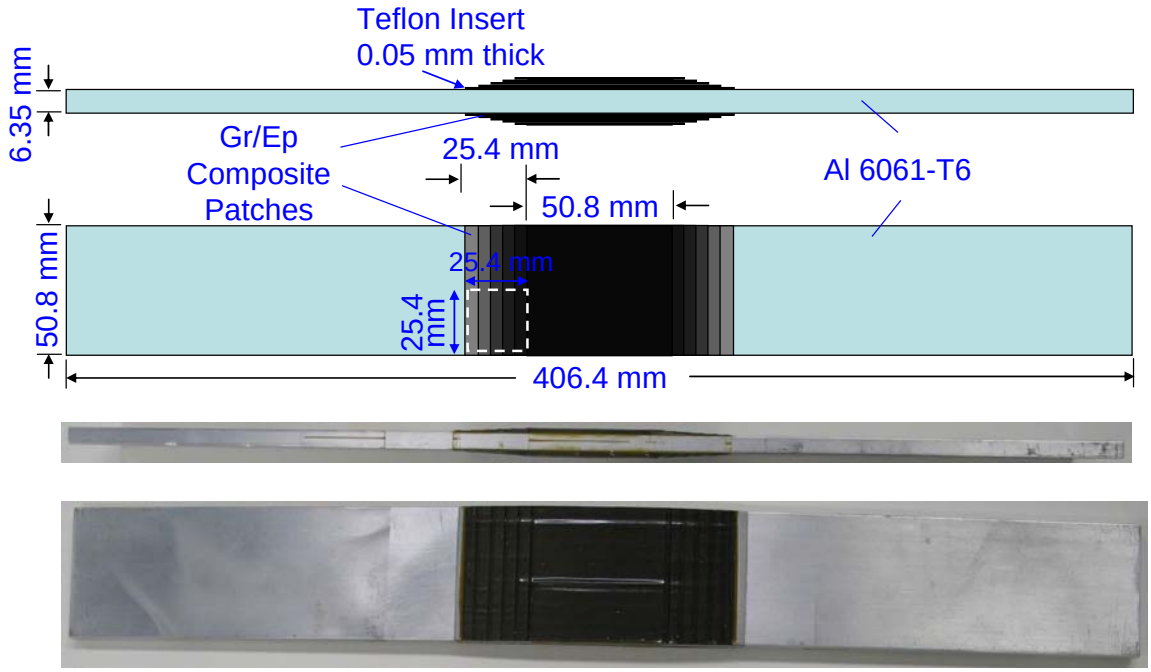

Figure 5-13 Schematic and an actual Gr/Ep composite patch specimen.

Initially, an ultrasonic C-scan of the patch sample in a water immersion tank was performed. A picture of the actual sample for Ultrasonic C-scan is shown in Figure 5-14. The imaging was carried out by a focused UT with a center frequency of 7.5 MHz, a focal length of 152.4 mm and a diameter of 19 mm. The scanning step was 0.5 mm in the lateral directions.

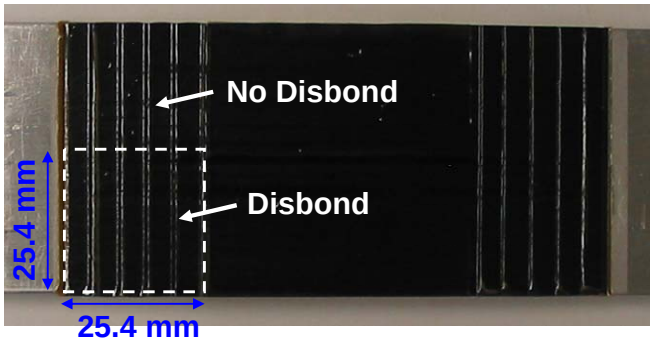

Figure 5-14 An actual patch sample for Ultrasonic C-scan.

Figure 5-15 shows the obtained C-scan image near the side with a Teflon insert indicated as the disbond region. Because the composite patch has the tapered shape, the immersion UT for C-scan image was chosen to obtain a general image and not the details of each tapered section. It is noted that Teflon was inserted only on one side of the composite patch, and the ultrasonic C-scan images obtained for the rest of this sample indicated that there were no other disbonded region.

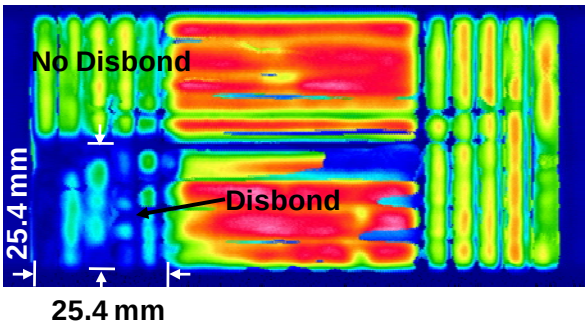

Figure 5-15 Ultrasonic C-scan images of the Gr/Ep composite patch specimen including a 25.4 mm by 25.4 mm disbonded region.

5.2.2 Performance of IUTs and FUTs

Figure 5-16 (a) shows the typical two PZT-c film IUTs fabricated at both ends of one specimen. The top electrode which determines the IUT size has an area of 20 mm by 4 mm. The typical thickness of the PZT-c film is 79 μm. It is noted that four IUTs (two at each end of the Al plate) may be used as an IUT four-transducer array for simultaneous detection of the ultrasonic signals generated by the laser. The location of the laser generation may be obtained via triangulation using the arrival times of the received signals obtained via the IUT array. Figure 5-16 (b) shows the pulse-echo measurement of one of such IUTs at the end of the Al plate of the specimen. One can see that ultrasonic waves generated by this IUT and reflected from the other end of the Al plate can be detected with good SNR. The ultrasonic wave traveled a total distance of 812.8 mm. The center frequency and 6 dB bandwidth of this first returned echo are 10 MHz and 5.5 MHz, respectively.

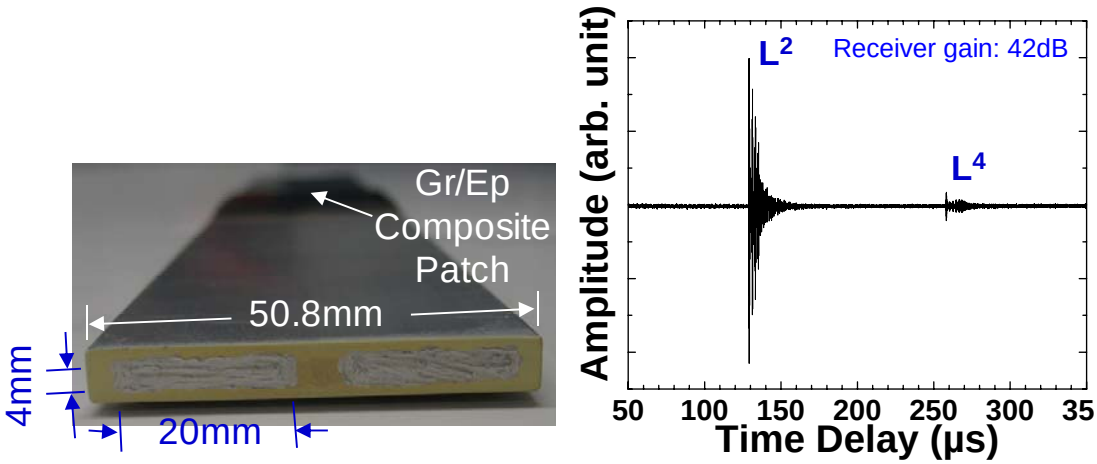

(a) (b)

Figure 5-16 (a) Two typical IUTs made at one end of the Al plate of the specimen; (b) Ultrasonic signals generated by one IUT shown in (a), reflected from the end of specimen and received by the same IUT.

When thin Ti and polyimide membranes are used as substrates for the sol-gel spray method, FUT array can be made. Figure 5-17 (a) and Figure 5-17 (b) show such FUT made on 75 μm thick Ti and 50 μm thick polyimide membranes, respectively. The typical thickness of the PZT-c film is more than 50 μm. The flexibility comes from the thinness of the membrane, PZT-c film and top silver paste electrode. Since polyimide is an insulator, a colloidal silver sprayed bottom electrode must be firstly made and then PZT-c film is fabricated on top of this silver bottom electrode as mentioned in Chapter 2. It is noted that each of the top electrodes can be used as one FUT and the spatial resolution of the inspection area is determined by the electrode size. The FUT array shown in Figure 5-17 (a) and Figure 5-17 (b) can be conveniently conformed to the surface of a pipe with an external diameter of 25.4 mm and 12.7 mm, respectively.

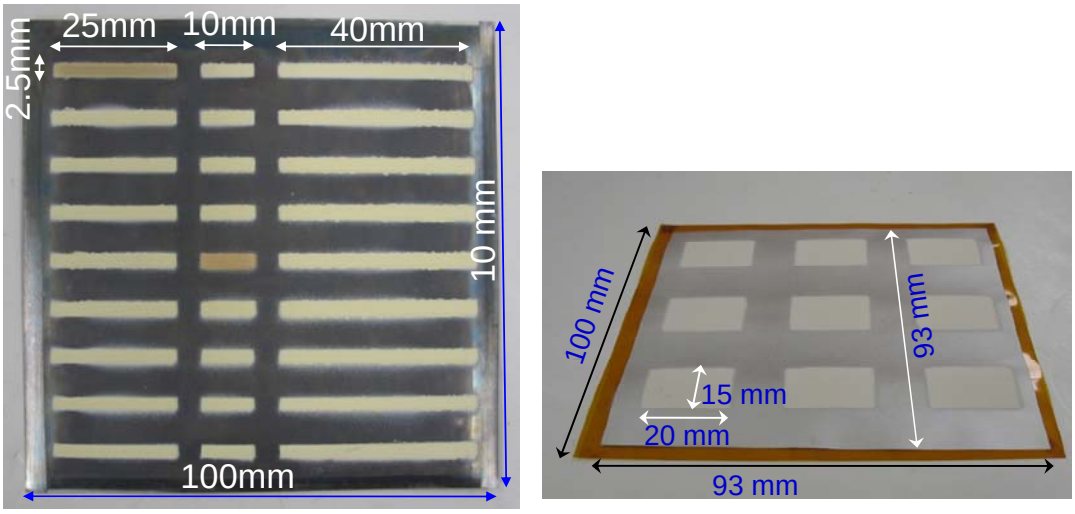

(a) (b)

Figure 5-17 FUT arrays made of (a) a 75 µm thick Ti and (b) a 50 µm thick polyimide membrane. No top electrode is present.

5.2.3 Disbond detection using FUTs

FUTs cut from the one shown in Figure 5-17 (a) were then glued onto two locations of the patch sample and the composite plate. The commercially available glue was cured at room temperature for 24 hours. Since the operation temperature of the Gr/Ep composites in aerospace industry normally ranges from -60°C to 100°C, both PZT-c thick film FUTs, together with the glue, have been tested and survived thermal cycles from -60°C to 100°C which is limited by the glue used here. It is noted that the bonding of FUT array is a convenient and attractive on-site installation approach for NDT and SHM applications.

For the Gr/Ep composite patch sample, a merit of the FUT is that it can be made into different shapes and sizes for specific applications. Because of the step shape of the patch sample, FUTs with a Ti membrane of a size of 14 mm x 4 mm, a PZT-c film size of 10 mm x 2.5 mm and a top electrode of 8 x 2 mm, were made and glued onto the patch at two different locations, without and with a disbond, as shown in Figure 5-18. The measured ultrasonic signals for these two locations are shown in Figure 5-19 (a) and Figure 5-19 (b), respectively. L_c^n is the nth trip echo through the thickness of the Gr/Ep composite patch. L_{AL}^2 is the 1st round trip echo through the thickness of the Gr/Ep

composite patch and that of the Al plate underneath. L_{AL}^4 travels one more round trip via Al plate thickness than L_{AL}^2. The echoes between the L_{AL}^2 and L_{AL}^4 come from signals travelling through the different thicknesses of the tapered Gr/Ep composite. The center frequencies and 6 dB bandwidths of the L_c^2 echo in Figure 5-19 (a) are 8.5 MHz and 7 MHz, respectively. When a disbond is present at the FUT location, L_{AL}^n disappear due to the loss of the ultrasonic coupling between the Gr/Ep composite patch and the Al plate, and there is no sufficient ultrasonic energy transmitted into the Al plate and reflected back to the same FUT.

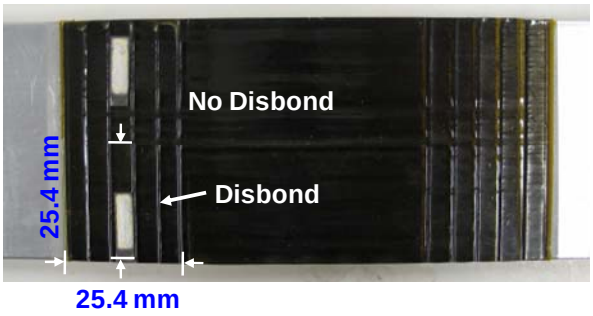

Figure 5-18 Gr/Ep composite patch with two rectangular shaped FUTs glued at two locations, without and with disbond.

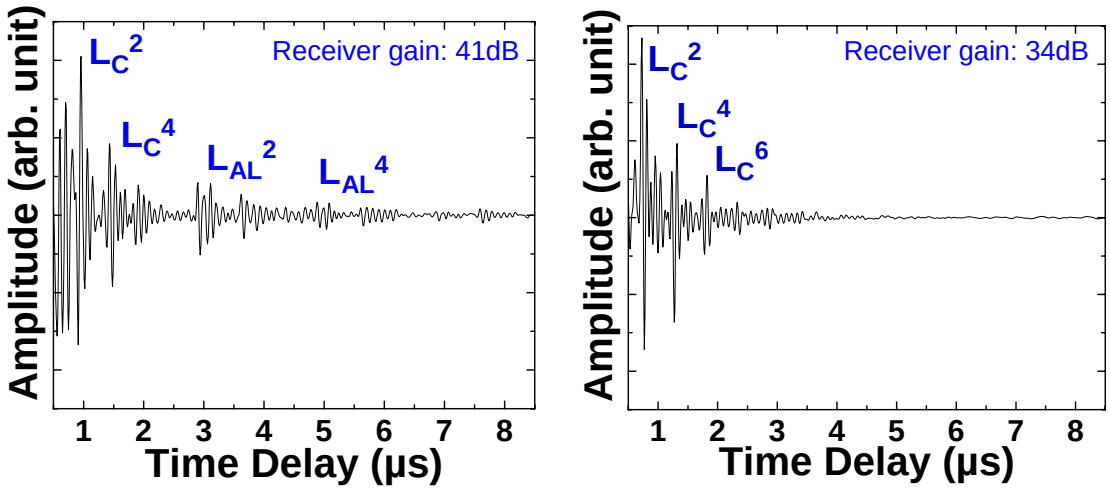

Figure 5-19 Measured ultrasonic signals in time domain at room temperature using an FUT made of 75 μm thick Ti membranes at the locations (a) without and (b) with disbond.

Figure 5-20 (a) and (b) show the ultrasonic measurement results using FUTs, based on polyimide membranes, similar to the ones shown in Figure 5-18 glued onto the regions without and with disbond, respectively. The same signal designations used in Figure 5-19 (a) and (b) are applied in Figure 5-20 (a) and (b). The center frequencies and 6 dB bandwidths of the L_c^2 echo in Figure 5-20 (a) are 8.9 MHz and 2.5 MHz, respectively. Even though the signal strengths in Figure 5-20 (a) and Figure 5-20 (b) are 23 dB weaker than those in Figure 5-19 (a) and Figure 5-19 (b), the disbond can be detected clearly.

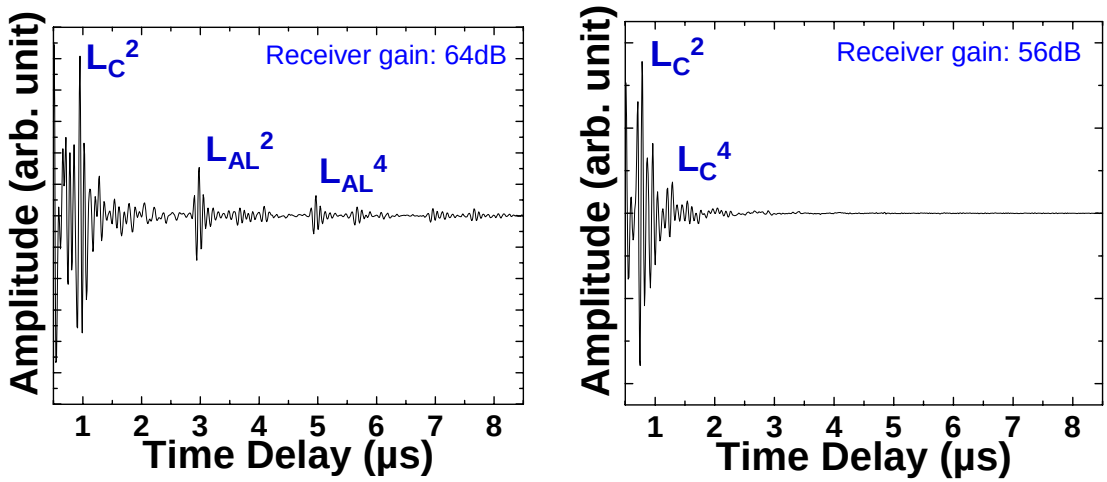

Figure 5-20 Measured ultrasonic signals in time domain at room temperature using FUTs made of 50 μm thick polyimide membranes at the locations (a) without and (b) with disbond.

5.2.4 Disbond detection using pulsed laser as generating UT and IUTs as receiving UTs

The schematic diagram of the laser generation and IUT detection is shown in Figure 5-21. In the experiments a pulsed laser (λ= 1.064 μm, a Q switched Nd:YAG) with pulses of 45 mJ energy and 5 ns duration delivered at a repetition rate of 10 Hz is used for the generation of ultrasound. The laser beam spot size is 2 mm in diameter. Ultrasonic signals averaging 10 laser pulses will be used for all the experiments described below. The laser beam impinges at the center of Gr/Ep composite patches with or without

delaminations to generate ultrasound and IUTs located at the edge of the Al plates are used as receivers. This geometry is like a transmission configuration.

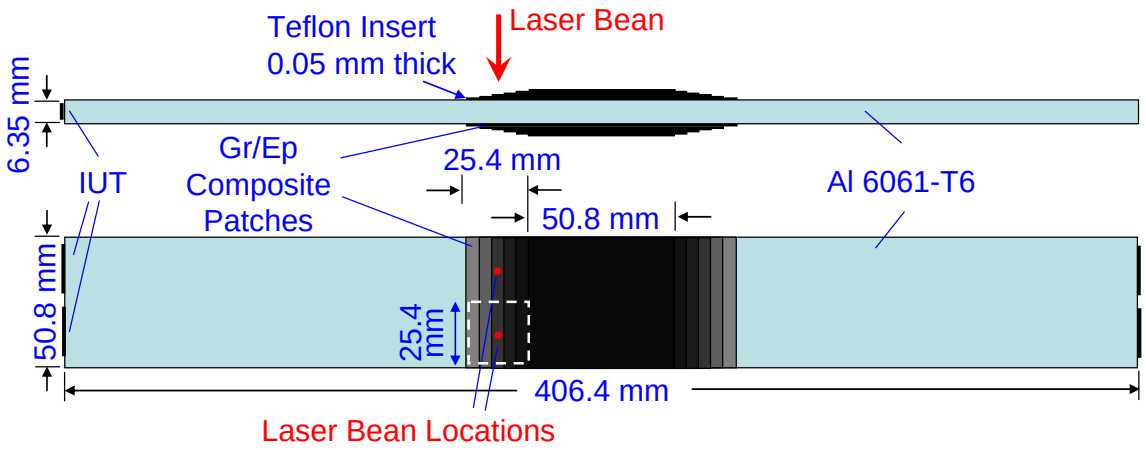

Figure 5-21 Schematic diagram of the laser generation and IUT detection configuration.

Many measurements have been performed and Figure 5-22 (a) and Figure 5-22 (b) present the typical ultrasonic signals on specimen at the locations with and without delaminations. When there is no delamination, the ultrasound generated by the pulsed laser will propagate through the Gr/Ep composite patch, the Al plate along its length, and then will reach the IUTs located at the ends of the Al plate as L_G^1, indicated in Figure 5-22 (a). When a disbond exists at the laser generation location, such an ultrasonic signal, L_G^1, will be greatly attenuated or lost completely because of the poor coupling caused by the disbond. Therefore this novel laser generation and IUT detection configuration can be used to detect the disbond in long distances (> 165 mm). The center frequencies and 6 dB bandwidths of the L_G^1 echo in Figure 5-22 are 1.5 MHz and 1 MHz respectively. When the center frequencies of IUTs are made around 1.5 MHz, it is expected that the signal strength of L_G^1 will be greatly enhanced.

It is noted that both laser generation and IUTs receiving can be applied to curved surfaces and elevated temperatures. IUTs may be also arranged in array configuration as illustrated in Figure 5-21; namely four IUTs at two ends of the Al plate. Since ultrasound generation laser beam can be scanned [144][145][146], (e.g. over the entire Gr/Ep composite patch surface, the received ultrasonic signals by an IUT or IUT array with an adjustable signal tracing mechanism), ultrasonic images of disbond may be produced.

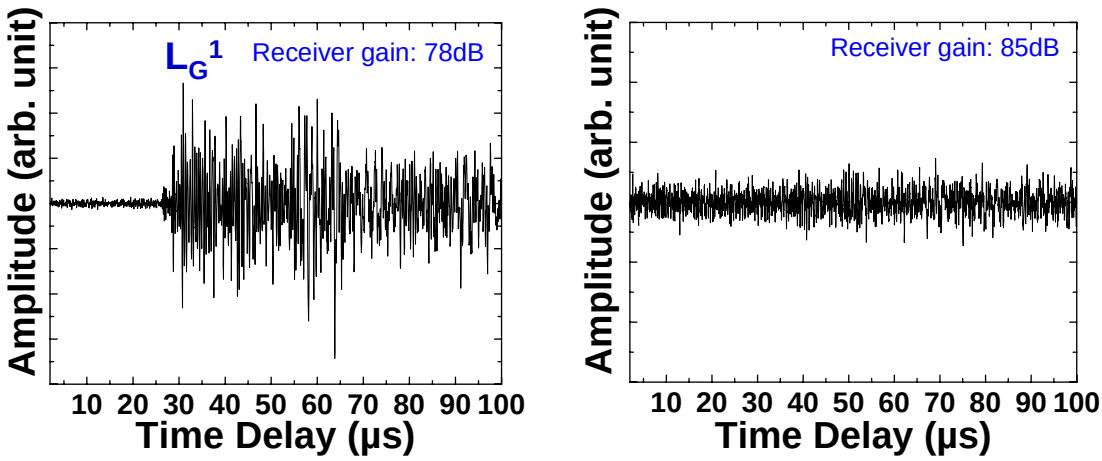

Figure 5-22 Measured ultrasonic signals on specimen in time domain at room temperature using laser to generate ultrasound at a location (a) without and (b) with disbond and IUT as the receiver.

5.3 Induction-Based Ultrasonic Measurement Technique

In order to achieve fast NDT and NDT of rotating components, a non-contact induction based method [26] is presented in addition to the one using laser generated ultrasound and IUT receivers reported in Section 5.1 and Section 5.2.

5.3.1 Induction-based non-contact ultrasonic measurement on metal

The induction based non-contact method is based on electromagnetic coupling of electrical signals between two coils with or without the aid of ferrite(s). Let us define D_{avg} to be the average diameter and n to be the number of turns of the coil as shown in Figure 5-23. The coils are made of copper wires with lacquer coating. The typical total lacquer wire diameter is ~0.16 mm. A schematic diagram of the two coils and a ferrite together with the IUT deposited onto a 12.7 mm thick steel plate is shown in Figure 5-24, where d_{gap} is the separation distance between the two coils.

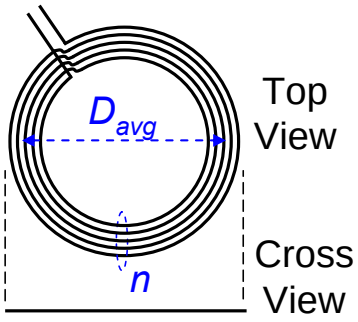

Figure 5-23 Schematic diagram of a coil. D_{avg} is the average diameter of the coil, and n is the number of turns of the coil.

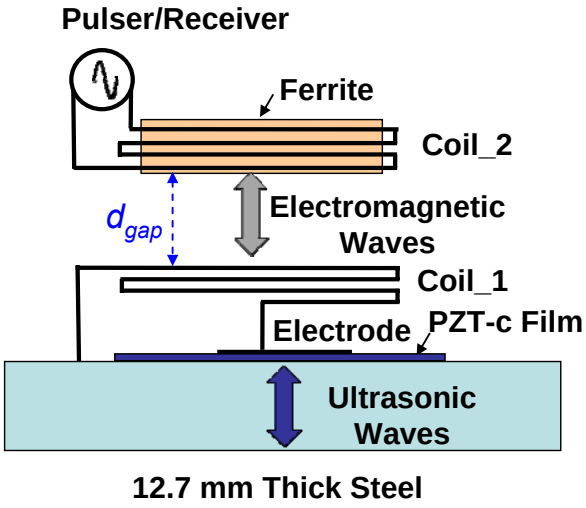

Figure 5-24 Schematic diagram of the non-contact ultrasonic measurement configuration. d_{gap} is the distance between the two coils.

5.3.1.1 L Wave

Figure 5-25 shows an actual experimental setup in which an IUT was deposited onto a 12.7 mm thick steel plate and measured by a non-contact configuration using a commercial handheld pulser/receiver. A flat coil, named Coil_1 with D_{avg} = 7 mm and n = 10 in Figure 5-25, is connected between the top electrode of the IUT and the steel substrate which serves as the bottom electrode of the IUT. It is noted that Coil_1 sits right on top of the IUT and there is no gap between Coil_1 and IUT. Directly on top of Coil_1 connected to the IUT there is the other coil, that is Coil_2 surrounding a ferrite in Figure 5-25, and its two ends are connected to the pulser/receiver. In this configuration both Coil_1 and Coil_2 have the same D_{avg} and n, and they are 7 mm and 10, respectively. Our

preliminary results indicated that compared with the direct contact configuration, the additional gains required for the non-contact configuration were 15 dB, 19 dB and 29 dB, respectively for the gap distance, d_{gap}, of 1 mm, 3 mm and 5 mm. The signal quality such as SNR, and the bandwidth change only a little between these two configurations. Figure 5-26 demonstrates the induction-based ultrasonic measurement with electrical connection between Coil_1 and the top electrode of IUT, where L^n is the nth trip echo through the steel plate thickness. Experiments using meter long wires (< 0.1 Ω) as electrical connections have been done, and have shown almost equivalent performances with the configuration in Figure 5-25. The one meter long wire connected between the IUT and Coil_1 shows the feasibility of accessing inaccessible IUTs, e.g. IUTs hidden in the structure, through their accessible coils.

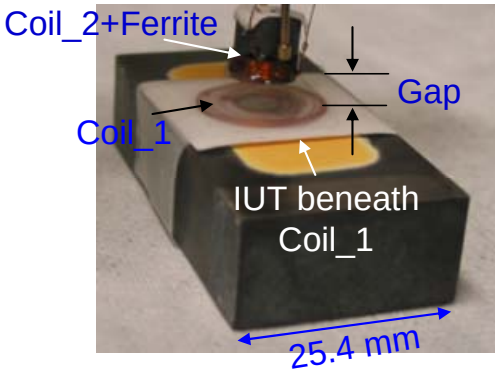

Figure 5-25 Configuration of an actual induction-based non-contact ultrasonic measurement setup. The two ends of Coil_1 are connected to the top and bottom electrodes of the IUT directly, and Coil_2 is surrounding a ferrite.

Figure 5-27 demonstrates the induction-based ultrasonic measurement without ferrites, where L^n is the nth trip echo through the steel plate thickness. Coil_1 with D_{avg} = 5 cm and n = 5 is connected to the top and bottom electrode of the IUT, and Coil_2 having the same D_{avg} and n with Coil_1 is connected to EPOCH LT. The d_{avg} in the measurement shown in Figure 5-27 is 4 cm, and 65 dB gains out of the available 100 dB receiver gain of the EPOCH LT were used. It is expected that for a large D_{ave} of coil a large dimension of ferrite should be used to enhance the signal strength. However, it is not possible to find a large diameter ferrite for our measurements. This is recommended for future study.

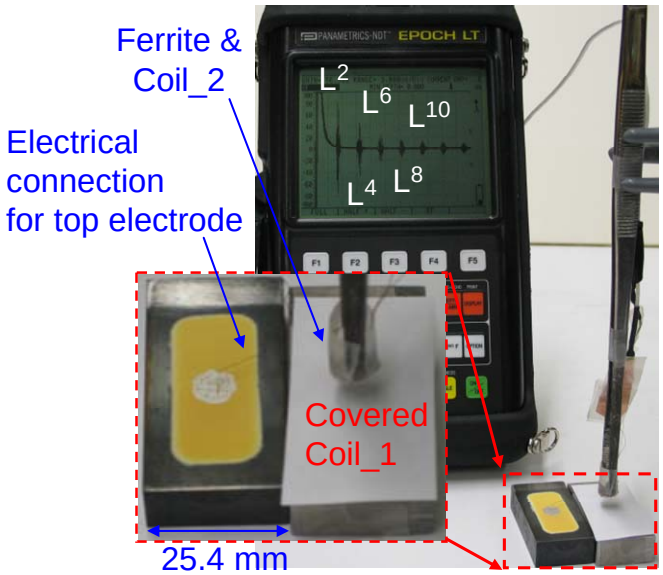

Figure 5-26 An IUT deposited onto a 12.7 mm thick steel plate measured by an induction non-contact configuration using an EPOCH LT. The two ends of Coil_1 are connected to the top and bottom electrodes of the IUT through meter long wires (< 0.1 Ω), and the two ends of Coil_2 surrounding a ferrite are connected to the EPOCH LT. In this experiment D_{avg} = 7 mm, n = 10 and d_{avg} = 5 mm.

Figure 5-27 An IUT deposited onto a 12.7 mm thick steel plate measured by a non-contact configuration using an EPOCH LT. The two ends of Coil_1 are connected to the top and bottom electrodes of the IUT directly, and there is no ferrite on Coil_2, which is different from the one shown in Figure 5-26. In this experiment D_{avg} = 5 cm, n = 5 and d_{avg} = 4 cm.

5.3.1.2 Symmetrical and anti-symmetrical PAWs

In order to demonstrate the global NDT and non-contact capability of the PAW two artificial line defects, D1 and D2 with 1 mm depth and 1 mm width, were made onto the Al plate as shown in Figure 4-6, where D1 and D2 had a width of 25.4 mm and 50.8 mm, respectively. At room temperature the measured symmetrical S_4 mode (see Figure 4-6) PAW signals in the Al plate using contact and non-contact configurations are shown in Figure 5-28 (a) and Figure 5-28 (b) respectively. The S_4 mode was confirmed by the measured group velocity and the center frequency as discussed in Section 4.1.3.1. In the non-contact configuration similar to the one shown in Figure 5-24 with a ferrite, D_{avg} = 7 mm, n = 10 and d_{gap} = 1 mm. The receiver gain used was 26 dB higher in non-contact than contact configuration. These results confirm that symmetrical PAW can be used to perform NDT of defects in long distance using the induction based non-contact method. In the present case the defects were 146.3 mm and 223.5 mm away from the IUT.

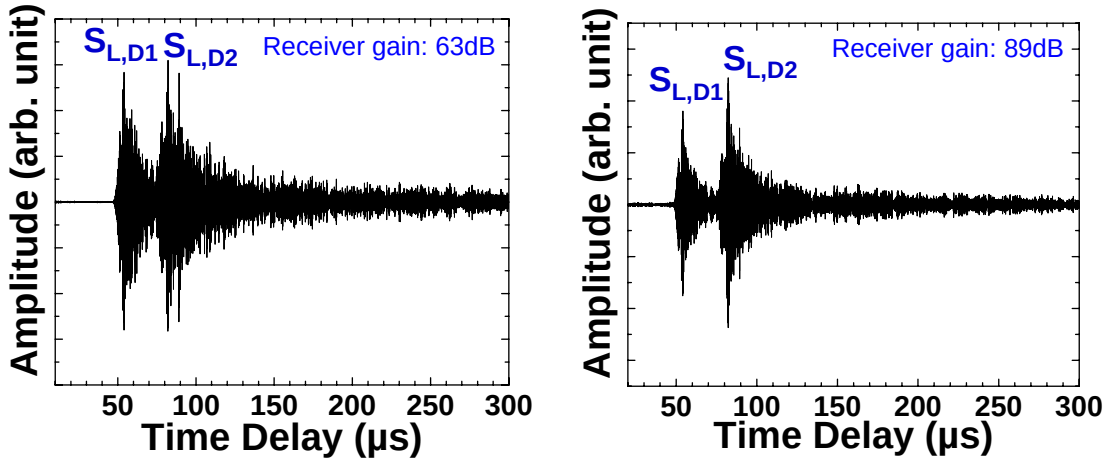

Figure 5-28 Ultrasonic symmetrical PAW signals in time domain obtained using the IUT shown in Figure 4-6 with the (a) contact and (b) non-contact configuration at room temperature.

5.3.1.3 SH PAW

Similarly the experimental setup shown in Figure 4-14 is also used for the comparison between the contact and non-contact approach. At room temperature the measured SH_0 PAW signals in the Al plate using contact and non-contact configurations

with ferrite, D_{avg} = 7 mm, n = 10 and d_{gap} = 1 mm, are shown in Figure 5-29 (a) and Figure 5-29 (b), respectively. The receiver gain used was 24 dB higher in non-contact than contact configuration. These results clearly confirm that SH_0 PAW can be used to perform NDT of defects in a distance of about 223.5 mm away from the IUT using the induction based non-contact approach.

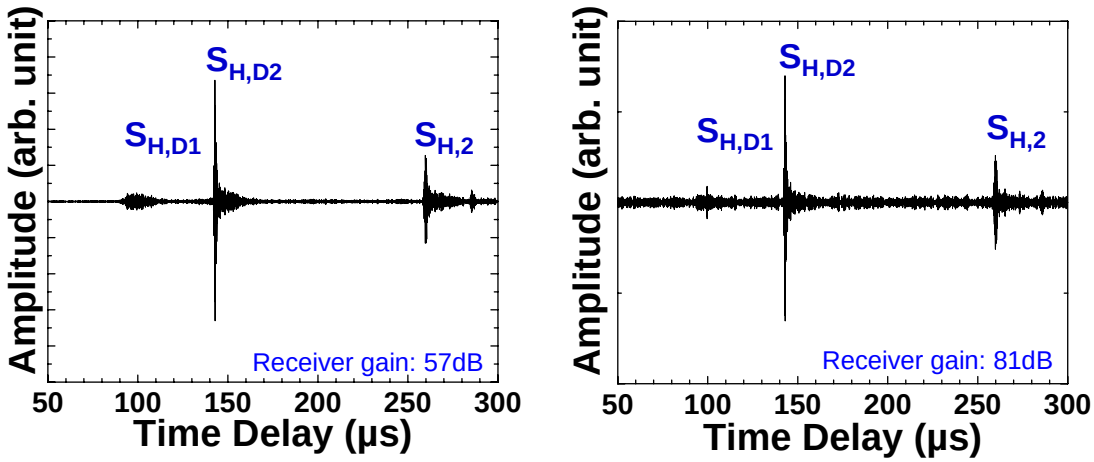

Figure 5-29 Ultrasonic SH PAW signals in time domain obtained using the IUT shown in Figure 4-14 with the (a) contact and (b) non-contact configuration at room temperature.

5.3.2 Induction-based non-contact ultrasonic measurement on composite

The induction type non-contact method for the interrogation of the Gr/Ep composites using IUTs is presented in this section. The Gr/Ep samples coated with IUT as shown in Figure 2-62 is firstly chosen for demonstration purposes. A schematic diagram of the induction based non-contact method is shown in Figure 5-30. It is similar to the configuration shown in Figure 5-24. However, in this case a 1 mm thick ferrite plate was inserted beneath Coil_1. The two ends of Coil_1 are connected to the top electrode of the IUT and the Gr/Ep substrate which serves as the bottom electrode of the IUT as shown in Figure 2-62. Beneath this coil a thin ferrite disk of 1 mm thick was inserted. It is noted that Coil_1 sits right on top of the ferrite plate which is also directly on top of the IUT and there is no gap between Coil_1 and the ferrite plate and between

the ferrite plate and the IUT. Directly on top of Coil_1 there is the other coil, Coil_2 surrounding a ferrite and the two ends of this coil are connected to the coaxial cable of the pulser/receiver. At room temperature the measured ultrasonic signals in this composite using the non-contact configuration in which D_{avg} = 7 mm, n = 10 and d_{gap} = 1 mm, are shown in Figure 5-31, where L^n is the nth trip echo through the Gr/Ep sample thickness.

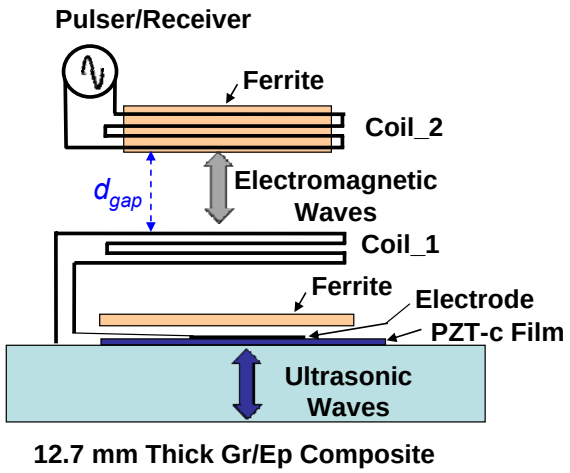

Figure 5-30 Schematic diagram of an inductive non-contact measurement performed on the IUT_P shown in Figure 2-62.

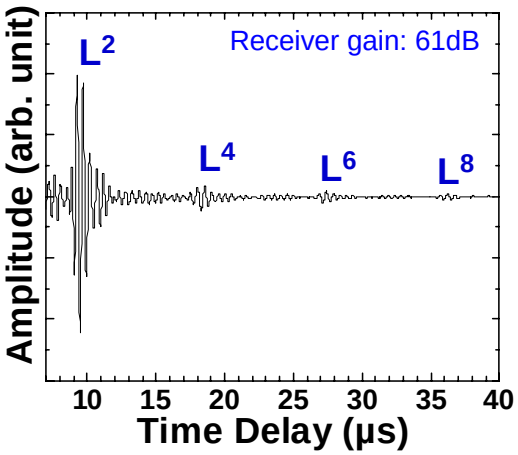

Figure 5-31 Measured ultrasonic signals in time domain using an IUT_P shown in Figure 2-62 with the non-contact configuration, as shown in Figure 5-30, at room temperature.

The ultrasonic signals shown in Figure 5-31 were 9 dB stronger in non-contact than contact configuration for which the results were given in Figure 2-64 (a). The possible

reason of this 9 dB increase could be the improved electrical impedance matching between the coil and the IUT, and the addition of an extra ferrite plate under Coil_1. The center frequency and 6 dB bandwidth of the L^2 echo are 2.2 MHz and 1.3 MHz, respectively. It means that although the signal strength in Figure 5-31 is stronger than the one in Figure 2-64 (a), the bandwidth is reduced.

Instead of IUTs, PZT-c film FUTs were used here together with the induction based non-contact method for NDT and SHM of composite plates. An 8.3 mm thick Gr/Ep composite plate with a stacking sequence of [0/45/0/-45/90/90/-45/0/45/0] x3 was made for the experiment. The same size Teflon sheet as used in Section 5.2 was introduced into the composite during fabrication to create a simulated disbond. Figure 5-32 shows the obtained ultrasonic C-scan image near the 25.4mm x 25.4 mm Teflon insert indicated as a disbonded region. Two PZT-c film FUTs using 75 μm thick Ti membranes were glued onto the Gr/Ep sample at the locations without and with the disbond for demonstration purposes as shown in Figure 5-33. Firstly, ultrasonic measurements using the conventional contact method were carried out. Then a flat coil, as Coil_1 shown in Figure 5-24, made of a ~0.16 mm diameter lacquered wire, served as a main component for induction coupling. The two ends of this coil were connected to the top electrode of the FUT and the Ti membrane which served as the bottom electrode of the FUT. Directly on top of such a coil, connected to the FUT, another flat coil, as Coil_2 shown in Figure 5-24, was connected to the coaxial cable of the pulser/receiver.

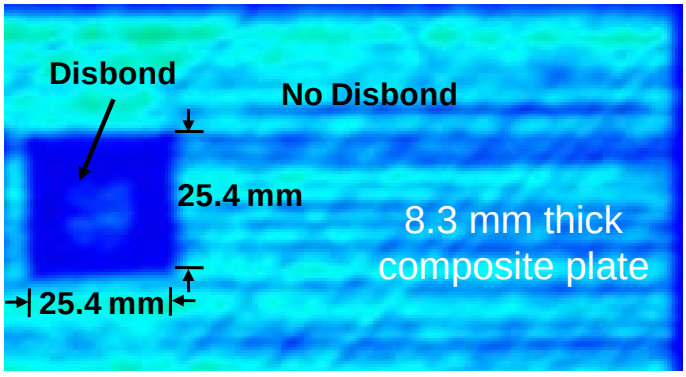

Figure 5-32 Ultrasonic C-Scan images of the Gr/Ep composite specimen near disbond region.

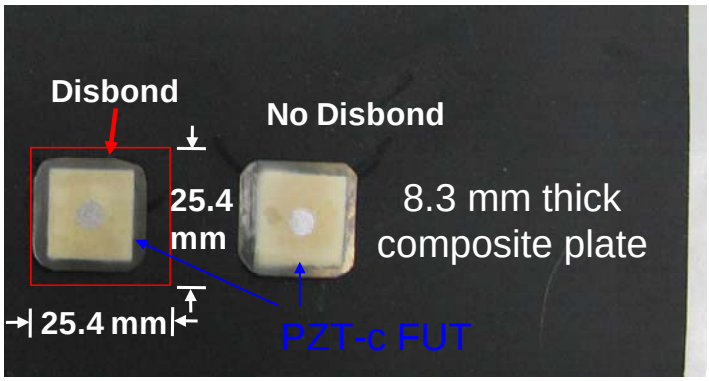

Figure 5-33 Two FUTs glued onto the Gr/Ep composite plate of Figure 5-32 above at regions with and without disbonds.

At room temperature the measured ultrasonic signals obtained by two FUTs shown in Figure 5-33 with the contact method are shown in Figure 5-34 (a) and Figure 5-34 (b). L_n is the nth trip echo through the thickness of the Gr/Ep composite and $L_{D,n}$ is the nth trip echo from the FUT to the disbond region. The center frequency and 6 dB bandwidth of the L_2 and $L_{D,2}$ echoes are 2.9 MHz and 2.1 MHz, 2.9 MHz and 1.8 MHz, respectively. The measured ultrasonic signals in this composite using the non-contact configuration in which D_{avg} = 5 cm, n = 5 and d_{gap} = 10 mm, at the location without and with the disbond, are shown in Figure 5-35 (a) and Figure 5-35 (b), respectively.

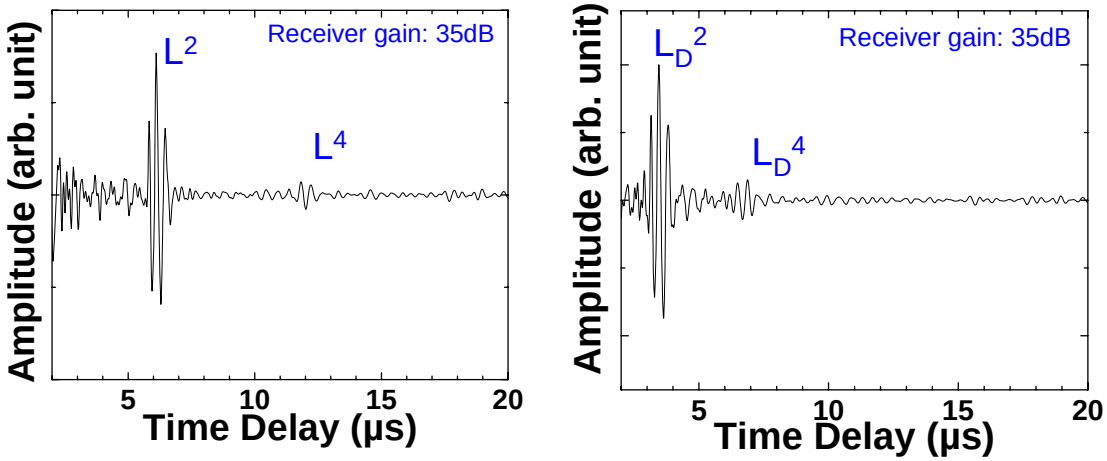

Figure 5-34 Measured ultrasonic signals in contact method at room temperature using FUTs made of 75 μm thick Ti membranes at locations (a) without and (b) with disbond. The two glued PZT-c film FUTs and the 8.3 mm thick composite plate were shown in Figure 5-33.

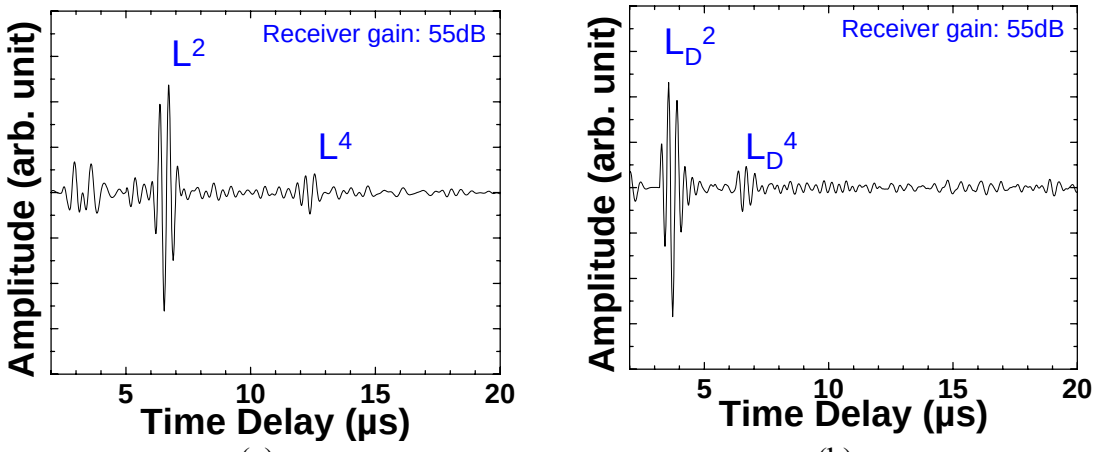

Figure 5-35 Measured ultrasonic signals in non-contact method at room temperature using FUTs made of 75 μm thick Ti membranes at locations (a) without and (b) with disbond. The two glued PZT-c film FUTs and the 8.3 mm thick composite plate were shown in Figure 5-33.

It is noted that the tuning of the electrical impedance matching between the FUTs and the size, diameter and number of turns of the coils has not been optimized. Therefore the measured ultrasonic frequency may be affected by the electrical impedance of the coil. The ultrasonic signals were 20 dB weaker in non-contact than contact configuration of which the ultrasonic signals are shown in Figure 5-34 (a) and Figure 5-34 (b), respectively.

For NDT and SHM of Gr/Ep structures, it is sometimes desirable to embed the ultrasonic sensors into the host material. Even though, at present, it is not known that the FUT shown in Figure 5-17 (b) can be embedded into the Gr/Ep composites without creating unwanted voids or defects, a simulation is carried out here. The poor conductive 1 mm thick Gr/Ep composite shown in Figure 2-65 is selected for demonstration purposes. At first, the two ends of Coil_1 are connected to the top electrode of the IUT and the nickel bottom electrode coated on the 1 mm thick Gr/Ep plate. Then an identical Gr/Ep but bare plate without IUT and nickel coating is put on top of IUT with Coil_1 without a ferrite plate as shown in Figure 5-36. It is noted that there is no gap between Coil_1 and the 1 mm thick Gr/Ep composite either below or above it. When the gap is 1 mm between Coil_2 and the top surface of the 1 mm thick Gr/Ep plate without IUT, the

measured ultrasonic signals gone through a 1 MHz high pass filter in this configuration are shown in Figure 5-37. For this case D_{avg} is 7 mm and n is 7. The ultrasonic signals shown in Figure 5-37 were 3dB weaker in non-contact than contact configuration for which the results were given in Figure 2-66. The center frequency and 6 dB bandwidth of the L^4 echo are 5 MHz and 5.2 MHz, respectively. Since the electric impedance matching between Coil_1 and Coil_2 and the pulser-receiver is not optimized yet, the L^2 echo is buried into the receiver gain recovery oscillating signals, and not shown in Figure 5-37. In the future work, electrical impedance matching should be improved so that L^2 may be observed.

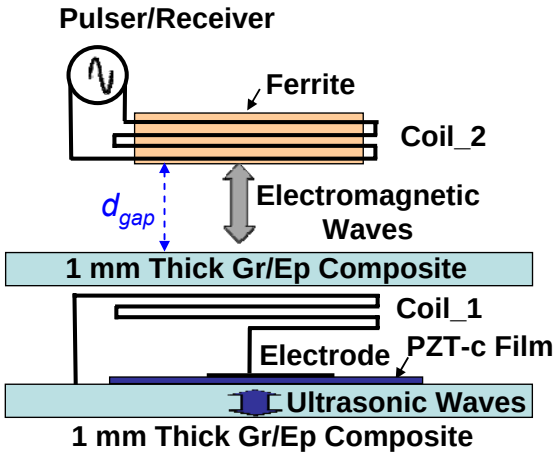

Figure 5-36 Schematic diagram of an inductive non-contact measurement performed on the IUT shown in Figure 2-65.

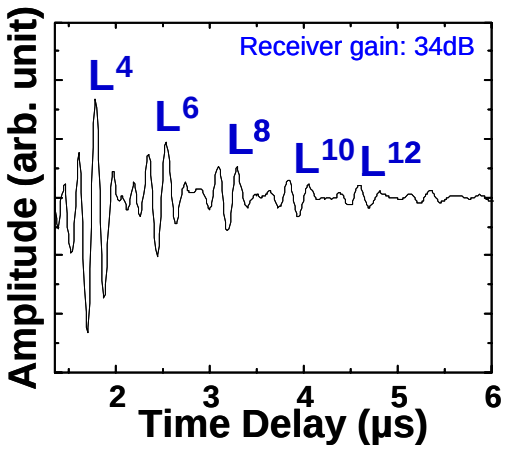

Figure 5-37 Measured ultrasonic signals in time domain using an IUT shown in Figure 2-65 with the non-contact configuration, as shown in Figure 5-36, at room temperature.

When the top 1 mm thick Gr/Ep composite which is not coated with IUT is removed from the measurement setup shown in Figure 5-36 and the d_{gap} = 1 mm is kept unchanged, the measured ultrasonic signals when the 1 mm thick Gr/Ep composite plate coated with an IUT is rotated at 1000 rpm are nearly the same as those shown in Figure 5-37. Therefore the inductive non-contact method may be a promising tool for SHM, fast NDT and NDT of rotating Gr/Ep composite parts.

5.4 Summary

Two non-contact ultrasonic measurement techniques, which use IUTs and FUTs and may be attractive for NDT and SHM of aerospace materials and structures, were presented in this chapter. One uses laser generated ultrasound and IUT receivers coated at planar or curved surfaces. When IUTs are used just as receivers, the electric power required may be little. Thus the approaches using battery, or the energy obtained via energy harvested devices, and including wireless communication, could be feasible. The other non-contact ultrasonic measurement technique presented in this chapter was induction-based ultrasonic measurement technique.

In Section 5.1, IUTs made of sol-gel sprayed thick (> 50 μm) piezoelectric PZT-c or BIT-c films have been deposited directly onto metal substrates as receivers to detect the laser generated ultrasound of up to 400°C. IUTs intrinsically acting as bulk L wave receivers used various mode conversion approaches and served as L wave, S wave, symmetrical, anti-symmetrical and SH PAW receivers. The high sensitivity of IUTs allowed the use of low energy (50 μJ) high repetition (1 kHz) pulsed lasers to produce ultrasonic signals of high SNR. Steel, SS and Al having different sizes, shapes including curved surfaces and thicknesses have been used as substrates. It was demonstrated that for a 12.7 mm steel plate, 14.9 μm of thickness measurement accuracy could be obtained using ultrasound generated by pulsed lasers and received by an IUT. Different laser generation conditions such as different spot sizes, shapes, pulse durations and energy were also applied to investigate the capabilities of IUT receivers. NDT of line defects which were nearly 223 mm away from the IUTs using PAWs were illustrated as well.

Therefore IUTs as receivers for laser generated ultrasound may be used for NDT and SHM at elevated temperatures, at curved surfaces, and using L waves, S waves, symmetrical, anti-symmetrical and SH PAWs.

In Section 5.2, PZT-c film IUTs have been directly coated onto the two end edges of an Al plate on which the top and bottom surfaces have been bonded with Gr/Ep composite patches to simulate a bonded repair aircraft specimen. An artificial disbond using a 0.05 mm thick Teflon sheet insert was introduced at the interface between the Gr/Ep composite and the Al plate. The four IUTs were made by the sol-gel spray method and have a piezoelectric film thickness near 79 μm, so the Al plate could be considered to have four IUTs array and two at each end. Disbond detection has been achieved by using laser generated ultrasound at the surface of the Gr/Ep composite patches and the IUTs deposited at the ends of Al plates as receivers. Such a laser generation IUT detection approach enables the detection of disbond in long distances. Since ultrasound generation laser beam can be scanned [144][145][146], e.g. over the entire Gr/Ep composite patch surface, using the received ultrasonic signals by an IUT or IUT array and an adjustable signal tracing mechanism, ultrasonic images of disbond may be produced.

In Section 5.3, the preliminary results of an induction type non-contact method for the interrogation of metal and Gr/Ep composites using the IUTs and FUTs have been presented. Two coils made of copper wires with lacquer coating (total diameter ~0.16 mm) were used for the induction type non-contact method. One coil was connected to the top and bottom electrodes of an IUT or an FUT, and the other coil was connected to a pulser-receiver. The distance beween the two coils in these measurements was from 1 mm to 40 mm. L waves and PAWs on metals have been generated and received by the induction type non-contact method. An 8.3 mm thick Gr/Ep composite plate was also implanted with an artificial delamination and the NDT and SHM of delamination on composite using both the contact and the non-contact method was demonstrated. Ferrite was used in some experiments to enhance the signal strength. A 1 mm thick Gr/Ep composite plate was placed between the two coils (Use the composite plate to cover one coil, IUT and composite sample) to simulate embedded UTs into the composite. Such a non-contact technique is desired for SHM and NDT using an embedded UT and NDT of

rotating composite components. Results of ultrasonic measurements of a 1 mm thick Gr/Ep composite plate rotated at 1000 rpm were obtained. Future studies on the selection and fabrication of ferrites, coils, etc to improve the ultrasonic signals in non-contact configurations will be carried out.

CHAPTER 6

CONCLUSIONS

This thesis focuses on the development of IUTs and FUTs for aerospace NDT and SHM applications. Using the sol-gel spray and acoustic mode conversion techniques, HT IUTs for L waves, S waves, SAWs, and PAWs have been developed. Sol-gel sprayed piezoelectric composite (e.g. PZT-c, BIT-c, and $LiNbO_3$-c) films have been investigated as HT IUTs, and their maximum working temperatures were demonstrated up to 150°C, 400°C, and 800°C, respectively. HT FUTs were also presented. An FUT made of BIT-c film coated onto a SS membrane was performed at up to 300°C. Metallic materials (e.g. steel, SS, Ti, Al, and brass) and composite materials (e.g. Gr/Ep and polyimide) have been used as substrates for sol-gel spray fabrication. Using the mode conversion technique, HT ultrasonic probes simultaneously exciting and detecting one L and two orthogonally polarized S waves have been developed, and some of their applications were discussed.

HT symmetrical, anti-symmetrical, and SH PAWs UTs were developed via also the mode conversion approach, and their ultrasonic measurements have been performed and compared. The results indicated that SH PAWs in plate structures may be the best candidate for NDT and SHM purposes. Three other techniques to generate and receive guided acoustic waves at elevated temperatures were also presented in this thesis, and they used metallic wedges, mechanical gratings, and IDTs. The experiments with these three techniques were demonstrated at 200°C, 150°C, and 350°C, respectively. In addition two non-contact ultrasonic measurement techniques were illustrated in this

thesis: one uses laser generated ultrasound and IUT receivers, and the other uses the induction-based ultrasonic measurement technique. The experiments using these two techniques for L waves, S waves, SAWs and PAWs, on metals and composite materials were demonstrated. In addition, NDT and SHM of bonded composite patches on Al plates have been carried out using laser generated ultrasound and IUT receivers. Furthermore NDT and SHM of delamination on composites using IUTs and FUTs through the induction-based ultrasonic measurement technique were given.

In Chapter 1, the importance of NDT and SHM in aerospace industry and six common inspection methods for NDT were briefly described. Ultrasonic testing has been widely used for NDT because of its several advantages. Six common physical mechanisms for ultrasound generation and detection were explained. However, piezoelectric UTs are commonly employed because of high electromechanical coupling efficiency and low cost. Piezoelectric sol-gel composites were chosen because they have good ultrasonic performance at elevated temperature and the capability to be fabricated at curved surfaces. The sol-gel spray technique has the advantages of low capital cost, and can fabricate piezoelectric composite films on-site; therefore it was further developed for IUTs and FUTs in this thesis.

In Chapter 2, piezoelectric thick (> than 14 μm) composite films were coated onto metallic and composite substrates as HTUTs using a sol-gel spray technique. The sol-gel spray fabrication process was briefly described. Two types of sol-gel sprayed HTUTs, e.g. IUT and FUT, were presented. The fabrication consists of six main steps: (1) powders and solution preparation, (2) mixing and ball milling, (3) spray coating, (4) heat treatment, (5) electrical poling, and (6) top electrodes fabrications. The fabrication process was firstly reported by Barrow, *et al*, and further developed by Kobayashi and Jen, but in this thesis induction heating is introduced for the heat treatment process to improve ultrasonic performance and reduce fabrication time of the sol-gel sprayed composite films. The fabrication and ultrasonic performance of sol-gel sprayed HT IUTs made of PZT-c, BIT-c and $LiNbO_3$-c films on metal substrates were presented for thickness measurement at temperatures up to 150°C, 400°C and 800°C, respectively. The results showed that the signal strength of the PZT-c IUTs and FUTs on metallic substrates

was as good as commercially available broadband UTs, and these IUTs and FUTs may have sufficiently strong signal strength for many NDT and SHM applications. Moreover, IUTs are able to be coated (FUTs are able to be glued or brazed [91]) onto curved surface and operated at HT. IUTs and FUTs with UT array configuration and connections were also demonstrated.

PZT-c films were also deposited onto the ends of 102 mm long clad steel rod ultrasonic delay lines to perform ultrasonic measurement at 150°C. The experimental results also show that the estimated rod length measurement accuracies at 150°C could reach 32 μm. This evaluation demonstrates that the presented IUTs having broad bandwidth and high SNR can be used for accurate erosion and corrosion evaluation. In certain situations parts or structures for NDT cannot be exposed to HT fabricate procedures of the IUT, and then HT FUT fabricated off-line may be used for HT NDT. An FUT made of BIT-c film coated onto a 38 μm thick SS membrane was bonded to a steel plate and ultrasonic measurement was performed at up to 303°C. Besides using metal as substrate, Gr/Ep composites of thickness ranging from 1 mm to 12.7 mm were used. For demonstration purposes PZT-c film IUTs have been deposited directly onto planar and curved Gr/Ep composites with high and low electrical conductivities and different shapes. The measured ultrasonic signals showed that IUTs could generate and receive L waves propagating in such composites for more than 300 mm. Also delaminations in the composite were detected and the ultrasonic anisotropy of 0° and 90° cross ply composite was measured. FUTs using 50 μm thick polyimide membranes as substrates were also presented. A thin electrical conductive was made, either by electroless nickel plating or by a colloidal silver spray technique, onto the insulating polyimide film to serve as the bottom electrodes of the FUTs. The flexibility of such FUTs was achieved due to the thin polyimide, porous PZT-c films and electrodes. In this thesis, FUTs have been used to evaluate Gr/Ep composites with planar and curved surfaces conveniently.

In Chapter 3, integrated ultrasonic S wave and L-S probes were fabricated onto steel and Plexiglas substrates with the use of mode conversion from L to S waves. The L UTs were made in a plane parallel to the propagation direction of the mode converted S

waves at the $\theta = 61.5°$ for steel substrates and at the $\theta = 63.2°$ for Plexiglas substrates. The reduction of energy conversion rate for steel substrates at $\theta = 61.5°$ is only 0.8% smaller than the maximum conversion rate 97.5% at $\theta = 67.2°$. By making a slanted surface with 45° at the intersection of the slanted plane with angle θ for mode conversion from L to S waves and the line from the center of the IUT, a probe that can simultaneously generate and receive both L and S waves by one IUT was demonstrated. By an alternative approach using two IUTs instead of the 45° slanted plane, another type of probe able to simultanelouly generate and receive both L and S waves was also presented. S wave and L-S wave probes of BIT-c films on steel substrates were demonstrated at temperature up to 350°C.

In addition, miniature PZT-c film IUT with dimensions of 7 mm by 4 mm by 75 μm was directly deposited onto a mild steel screw head. L and S waves were able to propagate simultaneously along the axial direction of the screw. Due to more than 12 dB SNRs for both L and S wave echoes it is expected that the axial load of this screw may be measured on-line using the time delays of these two waves together with digital signal processing [14]. In order to use every possible screw for on-line average temperature measurements, one discontinuity of a 1.72 mm step was made near the end of the above screw. The clearly separated L and S echoes reflected from this discontinuity and screw end were used for the average temperature measurements. Such a screw with a step discontinuity was used to measure the temperatures (up to 400°C) in Chapter 3.

Ultrasonic probes integrating two orthogonally polarized S_X and S_Y wave and three orthogonally polarized L, S_X and S_Y waves have been presented. PZT-c film IUTs were fabricated onto the heads of steel rods in screw shape. The typical thickness of the PZT-c films on those probes is 75 μm. Mode conversion from L to S waves and reflection from a 45° slope for L waves have been used. These probes were operated at room temperature with a center frequency ranging between 12 MHz and 19 MHz, and a 6 dB bandwidth ranging between 11 MHz and 17 MHz, and a SNR of more than 23 dB. Such probes may be used to accurately measure thickness of a sample with a correction of texture [15].

In Chapter 4, HT PAW and SAW UTs using sol-gel sprayed piezoelectric composite films and mode conversion techniques were presented. The mode conversions between L waves generated and received by sol-gel sprayed UTs and PAWs or SAWs were achieved through the geometry of substrates, wedges, mechanical gratings, or IDTs. Firstly, sol-gel sprayed PZT-c thick (> 75 μm) films were directly coated onto three 2 mm thick Al plates with different configurations for the NDT and SHM capability evaluation of symmetrical, anti-symmetrical and SH PAWs. Each guided acoustic wave mode in plates used for the experiments was identified by using the theoretically calculated dispersion curves compared with the experimentally measured group velocity. Two artifical line defects of 1 mm width and 1 mm depth on the Al plates were clearly detected at temperatures of up to 150°C in pulse-echo mode for using symmetrical, anti-symmetrical and SH PAWs. Results indicated that for 2 mm thick Al plates SH PAWs were the best for the line defect detection, and have the capability to travel a distance of 1.625 meters. A real regional jet horizontal stabilizer made of Al plate of thicknesses ranging from 1.1 mm to 1.3 mm was also demonstrated for SH PAW propagation. The results indicated that SH PAWs may be used for NDT and SHM purposes. Also numerical simulations by solving the 3D visco-elastic wave equation with a finite difference based method were performed, and the simulation results agreed with the experimental results.

Theoretical and experimental investigations of ultrasonic wedges which can generate and receive SH PAWs in a metal plate at temperatures of up to 200°C were presented. Brass which has a slow S wave velocity was chosen as the high temperature wedge material. PZT-c film IUTs were coated on the brass wedges. The mode conversion method is used to convert L waves generated by an IUT to S waves in the brass wedge. The calculated mode energy conversion efficiency is 79.7% with a conversion angle of 64.1°. The S waves in the wedge which is glued to a SS plate with a wedge angle of 42.9° have been converted to SH PAWs in the SS plate. The acoustic attenuation α_0 caused by the back scattering into the wedge of the SH_0 mode is dispersionless and is inversely proportional to the plate thickness. SH_2 PAW mode has a rather dispersive attenuation α_2. However, it is also inversely proportional to the plate thickness. Regardless of the

operating frequency, the acoustic attenuation of the SH_2 mode is always higher than that of the SH_0 mode. Such a feature plays a major role in the performance of the wedge. For example, the wedge can provide single SH PAW mode excitation if $\omega < \omega_{C2}$. Analysis of the coupling coefficient from the S waves in the wedge to the SH PAWs in the plate is also presented. In the transmission mode predominantly SH_0 PAW mode has been obtained at a plate temperature of up to 200°C. Measurement results demonstrated that SH PAWs using such wedges may be a promising approach for NDT and SHM of metal structures because of less dispersion and high SNR.

In addition, HT guided acoustic wave IUTs and FUTs have been made using line shape mechanical gratings together with sol-gel sprayed PZT-c films. The PZT-c films served as bulk L wave UTs and these L waves were converted to SAW or PAW when they interacted with the line mechanical gratings. Guided SAW grating IUTs have been made directly under the line gratings in a 10 mm thick SS plate. The measured SAW velocity and frequency agreed well with the theoretical and numerical calculation. When a 75 μm thick SS membrane was used as substrate, the gratings together with PZT-c films served as guided PAW grating FUTs. S_0 PAW was generated and received. The detection of an artificial line defect created on a 100 mm and long 50 mm wide SS plate was also demonstrated in a transmission mode using two guided PAW grating FUTs. These FUTs may be attached or bonded to parts even with curved surfaces for NDT and SHM purposes. HT IUTs made of PZT-c or BIT-c films with IDT shape of top electrodes were also developed to generate and receive PAWs or SAWs. The experimental results showed SAW propagation along a 25 mm thick Al alloy plate and along a steel cylinder with a diameter of 102 mm, and a_0 PAW propagation along a 0.702 mm thick SS plate. The measured SAW and PAW results agreed well with the theoretically calculated values. The measured signals with good SNR demonstrated the NDT capability of these integrated SAW or PAW UTs operated at temperatures up to 350°C.

In Chapter 5, two non-contact ultrasonic measurement techniques, which use IUTs and FUTs and may be attractive for NDT and SHM of aerospace materials and structures, were presented. First, IUTs made of sol-gel sprayed thick (> 50 μm) piezoelectric PZT-c or BIT-c films have been deposited directly onto metal substrates as receivers to detect

the laser generated ultrasound at up to 400°C. IUTs intrinsically acting as bulk L wave receiver used various mode conversion approaches and served as L wave, S wave, symmetrical, anti-symmetrical and SH PAW receivers. The high sensitivity of IUTs allowed the use of low energy (50 μJ) high repetition (1 kHz) pulsed lasers to produce ultrasonic signals of high SNR. Steel, SS and Al having different sizes, shapes including curved surfaces, and thicknesses have been used as substrates. It was demonstrated that 14.9 μm of thickness measurement accuracy for a 12.7 mm thick steel plate could be obtained using laser generation and an IUT as the receiver. Different laser generation conditions such as different spot sizes, shapes, pulse durations and energy were also applied to investigate the capabilities of IUT receivers. NDT of line defects which were nearly 223 mm away from the IUTs using PAWs were illustrated as well. Therefore IUTs as receivers for laser generated ultrasound may be used for NDT and SHM at elevated temperatures, at curved surfaces, and using L waves, S waves, symmetrical, anti-symmetrical and SH PAWs. The disbond detection of a simulated bonded repair aircraft specimen by using laser generated ultrasound and IUT receivers coated at the specimen was presented. Such a laser generation IUT detection approach enables the detection of disbond in long distances. Since ultrasound generation laser beam can be scanned [144][145][146], e.g. over the entire Gr/Ep composite patch surface, using the received ultrasonic signals by an IUT or IUT array and an adjustable signal tracing mechanism, ultrasonic images of disbond may be produced.

The other non-contact ultrasonic measurement technique presented in this thesis was induction-based ultrasonic measurement technique. The preliminary results of an induction type non-contact method for the interrogation of metal and Gr/Ep composites using the IUTs and FUTs have been presented. Two coils made of copper wires with lacquer coating (total diameter ~0.16 mm) together with or without ferrites were used for the induction type non-contact method. One coil was connected to the top and bottom electrodes of an IUT or an FUT, and the other coil was connected to a pulser-receiver. The distance beween the two coils in these measurements was from 1 mm to 40 mm. L waves and PAWs on metals have been generated and received by the induction type non-contact method. An 8.3 mm thick Gr/Ep composite plate was also implanted with an

artificial delamination and the NDT and SHM of delamination on composite using both contact and the non-contact method was demonstrated. Ferrite was used in some experiments to enhance the signal strength. A 1 mm thick Gr/Ep composite plate was placed between the two coils to simulate embedded UTs into composite. Such a non-contact technique is desired for SHM and NDT using an embedded UT and NDT of rotating composite components. Results of ultrasonic measurements of a 1 mm thick Gr/Ep composite plate rotated at 1000 rpm were obtained.

6.1 Claims of Originality

The original contributions of this thesis have been mentioned in different chapters. They are outlined below for the convenience of readers.

(1) Induction heating is introduced for the heat treatment of sol-gel sprayed piezoelectric composite films in the sol-gel fabrication process to improve ultrasonic performance and reduce film fabrication time.

(2) Ultrasonic probes which can simultaneously generate and receive one L and two orthogonally polarized S waves in metallic screws and Plexiglas were developed. The experiments carried out by the three-wave steel probes at 150°C were demonstrated, and their potential applications were discussed.

(3) Integrated PAW UTs using mode conversion were developed and demonstrated at 150°C. Comparisons among symmetrical, anti-symmetrical, and SH PAWs were done, and SH PAWs may be the best for *in situ* long range SHM according to the samples studied in this thesis.

(4) Ultrasonic wedges for SH PAWs were theoretically designed and experimentally investigated at HT. Regardless of the operating frequency of UTs, the acoustic attenuation of the SH_2 mode is always higher than that of the SH_0 mode. Such a feature plays a major role in the performance of the wedge.

(5) Integrated and flexible guided PAW HTUTs using mechanical grating were presented. The experiments showed that these transducers were able to operate at up to 150°C, and the preliminary results showed their potentials for NDT and SHM applications.

(6) Ultrasonic measurements using laser generated ultrasound and various IUT receivers were presented. Both metallic and Gr/Ep composite substrates were used as samples. The demonstration of IUTs coated onto curved steel surfaces was performed at 400°C. It shows the feasibility of this technique for pipe inspection at HT.

(7) Induction-based non-contact ultrasonic measurements together with IUTs and FUTs were presented. L waves and PAWs were able to be generated and received by this non-contact method for NDT and SHM. The detection of artificial defects and thickness measurements were demonstrated.

6.2 Future Works

For the development of screws simultaneously producing one L and two orthogonally polarized S waves for axial load and temperature measurement, more experiments are proposed to be carried out in the future.

The geometry of the PAW UTs with IDT shape top electrodes, such as the thickness of the composite film and finger widths of the IDT, which affects operating frequency, is suggested for future investigation in order to excite PAW waves efficiently in future studies.

The fast scanning of HT NDT using laser generated ultrasound and sol-prayed film IUT receivers should be an exciting research for the future. Ultrasonic images of defects and disbonds may be produced using the received ultrasonic signals by an IUT or IUT array and an adjustable signal tracing mechanism in a short time frame.

The selection and fabrication of ferrites, coils, etc to improve the ultrasonic signals for induction-based ultrasonic measurement techniques will be another attractive R&D direction. The tuning of the electrical impedance matching between the UT and the size, diameter and number of turns of the coil may be optimized.

References

[1] W.J. Staszewski, C. Boller and G.R. Tomlinson, Health monitoring of aerospace structures: smart sensor technologies and signal processing, Germany: John Wiley & Sons, 2004.

[2] S. Penney, "Ageing military aircraft: geriatric ward," Flight International, pp.47-48, 12-18 December 2000.

[3] A.S. Birks, R.E. Jr. Green, Jr. and P. McIntire, "Nondestructive Testing Handbook," 2nd ed., vol.7, Ultrasonic Testing, ASNT, 1991.

[4] J. Krautkrämer and H. Krautkrämer, Ultrasonic Testing of Materials, Berlin: Springer-Verlag, 1990.

[5] J.-B. Ihn and F.-K. Chang, "Ultrasonic Non-destructive Evaluation for Structure Health Monitoring: Built-in Diagnostics for Hot-spot Monitoring in Metallic and Composite Structures", Chapter 9 in Ultrasonic Nondestructive Evaluation Engineering and Biological Material Characterization, edited by T. Kundu, New York: CRC Press, 2004.

[6] A.H. Mrasek, D. Gohlke, K. Matthies and E. Neumann, "High temperature ultrasonic transducers," NDTnet, vol.1, no.9, pp. 1-10, 1996.

[7] R. Kazys, A. Voleisis, and B. Voleisiene, "High temperature ultrasonic transducers: a review," Ultragarsas, vol.63, pp.7-17, 2008.

[8] S.P. Kelly, I. Atkinson, C. Gregory and K.J. Kirk, "On-line ultrasonic inspection at elevated temperatures" Proc. IEEE Ultrasonics Symp., pp.904-908, 2007.

[9] T. Arakawa, K. Yoshikawa, S. Chiba, K. Muto and Y. Atsuta, "Applications of brazed-type ultrasonic probes for high and low temperature uses," Nondestr. Test. Eval., vol.7, pp.263-72, 1992.

[10] G.S. Kino, Acoustic Waves, Devices, Imaging & Analog Signal Processing, New Jersey: Prentice-Hall, 1987.

[11] J.-D. Aussel and J.-P. Monchalin, “Precision laser-ultrasonic velocity measurement and elastic constant determination,” Ultrasonics, vol.27, pp.165-177, 1989.

[12] G.C. Johnson, A.C. Holt and B. Cunningham, "An ultrasonic method for determining axial stress in bolts," J. Test. and Evaluation, vol.14, pp.253-259, 1986.

[13] H. Yasui and K. Kawashima, "Acoustoelastic measurement of bolt axial load with velocity ratio method," Proc. WCNDT, Rome, Italy, pp.16-21, 2000.

[14] S. Chaki, G. Corneloup, I. Lillamand and H. Walaszek, "Combination of longitudinal and transverse ultrasonic waves for in situ control of the tightening of bolts," J. Pressure Vessel Tech., vol.129, pp.383-390, 2007.

[15] A. Moreau, D. Levesque, M. Lord, M. Dubois, J.-P. Monchalin, C. Padioleau and J.F. Bussiere, “On-line measurement of texture, thickness and plastic strain ratio using laser-ultrasound resonance spectroscopy,” Ultrasonics, vol.40, pp.1047-1056, 2008.

[16] D.R. Allen and C.M. Sayers, “The measurement of residual stress in textured steel using an ultrasonic velocity combinations techniques,” Ultrasonics, vol.22, pp.179-188, 1984.

[17] M.V. Gandhi and B.S. Thompson, “Smart Materials and Structures,” London: New York, Chapman & Hall, 1992.

[18] P. Masson, R. Halkyard, “time domain localized structural intensity for damage characterization”, Smart Mater. Struct., 19, 14p., 2010.

[19] C.B. Scruby, R.J. Dewhurst, D.A Hutchins and S.B. Palmer, “Laser generation of ultrasound in metals,” Res. Techniques in Nondestructrive Testing, vol.5, R.S. Sharpe, Ed. New York: Academic Press, pp.281-327, 1982.

[20] D.A. Hutchins, “Ultrasonic generation by pulsed lasers,” Physics Acoustics, vol.18, W.P. Mason and R.N. Thurston, Ed. New York: Academic Press, pp.21-123, 1988.

[21] J.-P. Monchalin, “Laser-ultrasonics: from the laboratory to industry”, Review of Progress in QNDE, D.O. Thompson and D.E. Chimenti Eds., vol.23A, pp.3-31, 2004.

[22] R.M. White, “Generation of elastic waves by transient surface heating,” J. Appl. Phys., vol.34, pp.3559-3567, 1963.

[23] D.A. Hutchins and D.E. Wilkins, “Elastic waveforms using laser generation and electromagnetic acoustic transducer detection,” J. Appl. Phys., vol.58, no.7, pp.2469-2477, 1985.

[24] D.W. Schindel and D.A. Hutchins, “Application of micromachined capacitance transducers in air-coupled ultrasonics and non-destructive evaluation,” IEEE Trans. Ultrason. Ferroelect. Freq. Contr., vol.42, pp.51-58, 1986.

[25] W.M.D. Wright, D.A. Hutchins, G. Hayward and A. Gachagan, “Ultrasonic imaging using laser generation and piezoelectric air-coupled detection,” Ultrasonics, vol.34, pp.405-409, 1996.

[26] D.W. Greve, H. Sohn, C.P. Yue and I.J. Oppenheim “An Inductively Coupled Lamb Wave Transducer,” IEEE Sensors J., vol.7, pp.295-301, 2007.

[27] D.A. Barrow, T.E. Petroff, R.P. Tandon and M. Sayer, “Characterization of thick lead zirconate titanate films fabricated using a new sol gel based process,” J. Appl. Phys. vol.81, no.2, pp. 876-881, 1997.

[28] M. Kobayashi and C.-K. Jen, "Piezoelectric thick bismuth titanate/PZT composite film transducers for smart NDE of metals," Smart Materials and Structures, vol.13, pp.951-956, 2004.

[29] M. Kobayashi, C.-K. Jen, Y. Ono and J.-F. Moisan, “Integratable high temperature ultrasonic transducers for NDT of metals and industrial process monitoring,” CINDE Journal, vol.26, pp.5-10, 2005.

[30] M. Kobayashi, C.-K. Jen, J.-F. Moisan, N. Mrad and S.B. Nguyen, “Integrated ultrasonic transducers made by sol-gel spray technique for structural health monitoring,” Smart Materials and Structures, vol.16, pp.317-322, 2007.

[31] M. Kobayashi, K.-T. Wu, Z. Sun, C.-K. Jen, J. Bird, B. Galeote and N. Mrad, "On-line real-time engine oil condition monitoring using ultrasound," to appear in Int'l J. of Prognostics and Health Management, Aug. 2010.

[32] C.F. Dufault and G. Akhras, "Smart structure applications in aircraft," The Canadian Air Force Journal, vol.1, no.2, pp.31-39, 2008.

[33] G. Akhras, "Smart materials and smart systems for the future," Canadian Military Journal, vol.1, no.3, pp.25-32, 2000.

[34] H. Asada, T. Sotozaki, S. Endoh and T. Tomita, "Practical evaluation of crack detection capability for visual inspection in Japan," Proc. RTO AVT Workshop on "Airframe Inspection Reliability under Field/Depot Conditions", pp.15_1-15_20, Brussels, Belgium, 13-14 May 1998.

[35] G.A. Matzkanin, "Visual Inspection," Ammtiac Quarterly, vol.1, no.3, pp.7-10, 2006.

[36] N. Tracy and M. O. Patrick, Liquid Penetrant Testing in Nondestructive Testing Handbook, vol.2, Columbus: Am. Soc. NDT, Columbus, 1999.

[37] Lovejoy, David, Penetrant Testing, London: Chapman & Hall, 1991.

[38] B.J. Ingold, "Radiography," Ammtiac Quarterly, vol.2, no.2, pp.7-10, 2007.

[39] "Radiographic inspection," ASM Handbook, vol.17, NDE and Quality Control, pp.296-357, 1989.

[40] C.E. Betz, "Principles of magnetic particle testing," Am. Soc. NDT, p.234, 1985.

[41] D.J. Hagenaier, "A critical commentary on magnetic particle inspection," Materials Evaluation, vol.41, no.8, pp.1063-1068, 1983.

[42] A. Aldeen and J. Blitz, "Eddy-current investigations of oblique longitudinal cracks in metal tubes using a mercury model," NDT Int., vol.12, no.5, pp. 211-216, 1979.

[43] Ph. Beltrame and N. Burais, "Generalization of the ideal crack model in Eddy-current testing," IEEE Trans. Magnetics, vol.40, no.2, pp.1366-1369, 2004.

[44] J.R. Bowler, S.A. Jenkins, L.D. Sabbagh and H.A. Sabbagh, "Eddy-current probe impedance due to a volumetric flaw," J. Appl. Phys. vol.70, no.3, pp.1107-1114, 1991.

[45] B.W. Maxfield and C.M. Fortunko, "The design and use of electromagnetic acoustic wave transducers (EMATs)," Materials Evaluation, vol.41, pp.1399-1408, 1983.

[46] G. Alers, "A history of EMATs," in annual review of progress in quantitative NDE, D.O. Thompson and D.E. Chimenti Eds., New York, Plenum Press, vol.27, pp.801-808, 2008.

[47] H.M. Frost, "Electromagnetic-ultrasound transducers: principle, practice, and application," in Physics Acoustic, vol.14, pp.277-394, W.P. Mason and R.N. Thurston, Eds., New Your: Academic, 1979.

[48] J.-P. Monchalin, "Laser-ultrasonics: principles and industrial applications", Chapter 4 in Ultrasonic and Advanced Methods for Nondestructive Testing and Material Characterization, C.H. Chen, Ed. New Jersey: World Scientific Publ., pp.79-115, 2007.

[49] D.C. Jiles, "Theory of the magnetomechanical effect," J. Phys. D, vol.28, pp.1537-1546, 1995.

[50] H. Kwun and C.M. Teller, "Magnetostrictive generation and detection of longitudinal, torsional, and flexural waves in a rod," J. Acoust. Soc. Am., vol.96, pp.1020-1204, 1994.

[51] S.W. Han, H.C. Lee and Y.Y. Kim, "Non-contact damage detection of a rotation shaft using the Magnetostrictive effect," J. Non-Destruct. Eval., vol.22, pp.141-150, 2003.

[52] S.H. Cho, S.W. Han, C.I. Park and Y.Y.Kim, "Noncontact torsional wave transduction in a rotating shaft using oblique magnetostrictive strips," J. Appl. Phys., vol.100, pp.1049031-1049036, 2006.

[53] F.V. Hunt, Electroacoustics: The Analysis of Transduction and its Historical Background, New York: Acoustic Society of America, 1954.

[54] W. Kuhl, G.R. Schodder and F.K. Schodder, “Condenser transmitters and microphones with solid dielectric for airborne ultrasonics,” Acustica, vol.4, pp.520-532, 1954.

[55] M.I. Haller and B.T. Khuri-Yakub, “A surface micromachined electrostatic ultrasonic air transducer,” IEEE Trans. UFFC, vol.43, pp.1-6, 1996.

[56] A.S. Ergun, G.G. Yaraliogliu and B.T. Khuri-Yakub, “Capative micromachined ultrasonic transducers: theory and technology,” J. Aerospace Engineering, vol.16, no.2, pp.76-84, 2003.

[57] W.G. Cady, Piezoelectricity: An Introduction to the Theory and Application of Electromechanical Phenomena in Crystal, New York: McGraw-Hill, 1946.

[58] B. Jaffe, W.R. Cook JR, and H. Jaffe, Piezoelecric Ceramics, New York: Academic Press, 1971.

[59] R.E. Newnham, L.J. Bowen, K.A. Klicker and L.E. Cross, “ Composite piezoelectric transducers,” Materials in Engineering, vol.2, pp.93-106, 1980.

[60] R.E. Newnham, A. Safari, J. Giniewicz and B.H. Fox, “Composite piezoelectric sensors,” Ferroelectrics, vol.60, pp.15-21, 1984.

[61] H.L.W Chan and J. Unsworth, “Effect of thinning and ceramic width on properties of 1-3 PZT/Epoxy composites,” Ferroelectric Letters, vol.6, pp.133-137, 1986.

[62] L. Zou, M. Sayer and C.-K. Jen, “Sol-gel fabricated thick piezoelectric ultrasonic transducers for potential applications in industrial material processes,” Proc. IEEE Ultrason. Symp., pp.1007-1011, 1997.

[63] M. Kobayashi, C.-K. Jen and D. Lévesque, “Flexible ultrasonic transducers,” IEEE Trans. UFFC, vol.53, pp.1478-1484, 2006.

[64] T.F. McNulty, V. F. Janas, A. Safari, R. L. Loh and R. B. Cass, “Novel processing of 1-3 piezoelectric ceramic/polymer composites for transducer applications,” J. Am. Ceram. Soc., vol.78, pp.2913-2916, 1995.

[65] L.F. Brown and A.M. Fowler. “High vinylidene-fluoride content P(VDF-TrFE) films for ultrasound transducers”, Proc. IEEE Ultrason. Symp., pp.607-609, 1998.

[66] D.H. Wang and S.L. Huang, "Health monitoring and diagnosis for flexible structures with PVDF piezoelectric film sensor array," J. Intelligent Material Systems and Structures, vol.11, pp.482-491, 2000.

[67] J.-M. Park, J.-W. Kong, D.-S. Kim and D.-J. Yoon, "Nondestructive damage detection and interfacial evaluation of single-fibers/epoxy composites using PZT, PVDF and P(VDF-TrFE) copolymer sensors", Composites Science and Technology, vol.65, pp.241-256, 2005.

[68] A.C.S. Parr, R.L. O'Leary and G. Hayward, "Improving the thermal stability of 1-3 piezoelectric composite transducers," IEEE Trans. Ultrason. Ferroelect. Freq. Contr., vol.52, pp.550-563, 2005.

[69] M. Kobayashi, T.R. Olding, M. Sayer and C.-K. Jen, "Piezoelectric thick film ultrasonic transducers fabricated by a sol-gel spray technique," Ultrasonics, vol.39, pp.675-680, 2002.

[70] G. Yi, Z. Wu and M. Sayer, "Preparation of $Pb(Zr,Ti)O_3$ thin films by sol gel processing: electrical, optical and electro-optic properties," J. Appl. Phys.,vol.64, pp.2717-2724, 1988.

[71] K.D. Budd, S.K. Dey and D.A. Payne, "Sol gel processing of $PbTiO_3$-$PbZrO_3$ thin films," Br. Ceram. Proc., vol.36, pp.107-121, 1985.

[72] T. Graham, "On the properties of silicic acid and other analogous colloidal substrates," J. Chem. Soc., vol.17, pp.318-327, 1864.

[73] N. Tohge, S. Takahashi and T. Minami, "Preparation of PBZrO3-PbTiO3 ferroelectric thin films by the sol-gel process," J. Am. Ceram. Soc., vol.64, no.1, pp.67-71, 1991.

[74] S.M. Attia, J. Wang, G. Wu, J. Shen and J. Ma, "Review on sol-gel derived coatings: process, techniques and optical applications," J. Mater. Sci. Technol., vol.18, no.3, 2002.

[75] M. Syaer, M. Lukacs, T. Olding, G. Pang, L. Zou and Y. Chen, "Piezoelectric films and coating for device purposes," Mat. Res. Soc. Symp. Proc., vol.541, pp.599-610, 1999.

[76] D.A. Barrow, T.E. Petroff and M.Sayer, “Method for producting thick ceramic film by a sol gel coating process,” US Patent 5,585,136, Dec. 17, 1996 (RE 36,573, Feb. 2000).

[77] M. Kabayashi, Development and applications of high temperature piezoelectric ultrasound transducers, Ph. D thesis, McGill University, 2004.

[78] B.A. Auld, “Acoustic Fields and Waves in Solids,” vol.1 and 2, John Wiley & Sons, New York, 1973.

[79] M.O. Si-Chaib, H. Djelouah and M. Bocquet, "Applications of ultrasonic reflection mode conversion transducers in NDT," NDT&E Int’l, vol.33, pp.91-99, 2000.

[80] E.V. Abolikhina and A.G. Molyar, “Corrosion of aircraft structures made of aluminum alloys,” Materials Science, vol.39, pp.889-894, 2003.

[81] M. Mrad, Z. Liu, M. Kobayashi, M. Liao and C.-K. Jen, “Exfoliation detection using structurally integrated piezoelectric ultrasonic transducers,” Insight - NDT & Condition Monitoring, J. the British Inst. of NDT, vol.48, pp.738-742, 2006.

[82] Q. Liu, K.-T. Wu, M. Kobayashi, C.-K. Jen and N. Mrad, “In-situ ice and structure thickness monitoring using integrated ultrasonic sensors,” Smart Structures and Materials, vol.17, pp.045023_1-045023_6, 2008.

[83] L.C. Lynnworth. Ultrasonic Measurements for Process Control. New York: Academic Press, 1989.

[84] C.-K. Jen, J.-G. Legoux and L. Parent, “Experimental evaluation of clad metallic buffer rods for high temperature ultrasonic measurements” NDT & E Int., vol.33, pp.145-153, 2000.

[85] Y. Ono, J.-F. Moisan and C.-K. Jen, “Ultrasonic techniques for imaging and measurements in molten aluminum,” IEEE Trans. Ultrason. Ferroelect. Freq. Control, vol.50, pp.1711-1721, 2003.

[86] Z. Sun, C.-K. Jen, C.-K. Shih and D. Denelsbeck, "Application of ultrasound in the determination of fundamental polymer extrusion performance: residence time distribution measurement," Polymer Eng. and Science, vol.43, pp.102-111, 2003.

[87] W.F. Walker and G.E. Trahey, "A fundamental limit on delay estimation using partially correlated speckle signals," IEEE Trans. Ultrason. Ferroelect. Freq. Control, vol.42, no.2, pp.301-308, 1995.

[88] C.R. Browen, L.R. Bradley, D.P. Almond and P.D. Wilcox, "Flexible piezoelectric transducer for ultrasonic inspection of non-planar components," Ultrasonics, vol.48, no.5, pp.367-375, 2008.

[89] G. Harvey, A. Gachagan, J.W. Machersie, T. McCunnie and R. Banks, "Flexible ultrasonic transducers incorporating piezoelectric fibers," IEEE Trans. Ultrason. Ferroelectr. Freq. Control, vol.56, no.9, pp.1999-2009, 2009.

[90] X. Li and Y. Zhang "Feasibility study of wide-band low-profile ultrasonic sensor with flexible piezoelectric paint", Smart Structures and Systems, vol.4, pp.565-582, 2008.

[91] J.-L. Shih, M. Kobayashi and C.-K. Jen, "Flexible ultrasonic transducers for structure health monitoring of pipes at high temperature," Proc. IEEE Ultrasonics Symp., 2009.

[92] E. Nieto, J.F. Fernandez, C. Moure and P. Duran "Multilayer piezoelectric devices based on PZT," J. Mater. Sci: Mater. Electro., vol.7, pp.55-60, 1996.

[93] C. Galassi, E. Roncari, C. Capiani and P. Pinasco, "PZT-based suspensions for tape casting," J. Europ. Ceram. Soc., vol.17, no.2, pp.367-371, 1997.

[94] E.S. Thiele, D. Damjanovic and N. Setter, "Processing and properties of screen-printed lead zirconate titanate piezoelectric thick films on electroded silicon," J. Am. Ceram. Soc., vol.84, pp.2863-2868, 2001.

[95] K. Yao, X. He, Y. Xu and M. Chen, "Screen-printed piezoelectric ceramic thick films with sintering additives introduced through a liquid-phase approach," Sensors and Actuators A: Phys., vol.118, no.2, pp.342-348, 2005.

[96] D. Waller, T. Lqbal and A. Safari, “Poling of lead zirconate titanate ceramics and flexible piezoelectric composites by the corona discharge technique,” J. Am. Ceram. Soc., vol.72, pp.322-324, 1989.

[97] V. Giurgiutiu, A. Zagrai and J.J. Bao, “Piezoelectric Wafer Embedded Active Sensors for Aging Aircraft Structural Health Monitoring,” J. Structural Health Monitoring, vol.1, pp.41-61, 2002.

[98] D. Levesque, N. Legros and A. Ajji, “Ultrasonic determination of mechanical moduli of oriented semicrystalline polymers”, Polymer Eng. Science, vol.37, pp.1833-1844, 1997.

[99] R.H. Bergman and R.A. Shahbender, “Effect of statically applied stresses on the velocity of propagation of ultrasonic waves,” J. Appl. Phys., vol.29, pp.1736-1738, 1958.

[100] M. Hirao, K. Aoki and H. Fukuoka, “Texture of polycrystalline metals characterized by ultrasonic velocity measurements,” J. Acoust. Soc. Am., vol.81, pp.1434-1440, 1987.

[101] R.B. King and C.M. Fortuko, “Determination of in-plane residual stress states in plates using horizontally polarized shear waves,” J. Appl. Phys., vol.54, pp.3027-3035, 1983.

[102] K. Horie, M. Nishihira and K. Imano, Jpn. J. Appl. Phys., vol.44, pp.4333, 2005.

[103] H. Karasawa, M. Izumi, T. Suzuki, S. Nagai, M. Tamura and S. Fujimori, “Development of under-sodium three-dimensional visual inspection technique using matrix-arrayed ultrasonic transducer,” Journal of Nuclear Science and Technology, vol.37, pp.769-779, 2000.

[104] I. Ihara, D. Burhan and Y. Seda, “In situ monitoring of solid-liquid interface of aluminum alloy using high-temperature ultrasonic sensor,” Jpn. J. Appl. Phys., vol.44, pp.4370, 2005.

[105] J. Soejima, K. Sato and K. Nagata, Jpn. J. Appl. Phys., vol.39, pp.3083, 2000.

[106] R. Kazys, A. Voleisis, R. Sliteris, B. Voleisiene, L. Mazeika, P. H. Kupschus and H. A. Abderrahim, “Development of ultrasonic sensors for operation in a heavy liquid metal,” IEEE Sensor J., vol.6, pp.1134-1143, 2006.

[107] W.G. Mayer, “Energy partition of ultrasonic waves at flat boundaries,” Ultrasonics, vol.3, no.2, pp.62-68, 1965.

[108] D.E. Yuhas, M.J. Mutton, J.R. Remiasz and C.L. Vorres, “Ultrasonic measurements of bore temperature in large caliber guns,” Review of Quantitative Nondestructive Evaluation, vol.28, pp.1759-1766, 2009.

[109] I. Ihara and M. Takahashi, “A new method for internal temperature profile measurement by ultrasound,” Proc. IEEE Instrumentation and Measurement Technology Conference, pp.1-5, 2007.

[110] L.C. Lynnworth, E.P. Papadakis, D.R. Patch and K.A. Fowler, "Nuclear reactor applications of new ultrasonic transducers," IEEE Trans. Nucl. Sci., vol.1, pp.351-362, 1971.

[111] L.C. Lynnworth, "Temperature profiling using multizone ultrasonic waveguides," Proc. 6th Symp. on Temperature - Its Measurement and Control in Science and Industry, vol.5, pp.1181-90, 1982.

[112] L. Piche, F. Massines, G. Lessard and A. Hamel, “Ultrasonic characterization of polymers as function of temperature, pressure and frequency,” Proc. IEEE Ultrasonics Symposium, pp.1125-1130, 1987.

[113] S.-S. L. Wen, C.-K. Jen and K. T. Nguyen, “Advances in on-line monitoring of the injection molding process using ultrasonic techniques,” Int’l Polymer Processing, vol.2, pp. 175-182, June 1999.

[114] C.-C. Cheng, Y. Ono and C.-K. Jen, “Real-time diagnostics of co-injection molding using ultrasound”, Polymer Engineering and Science, vol. pp.1491-1500, Aug. 2007.

[115] M. Kobayashi, Y. Ono, C.-K, Jen and C.-C. Cheng, “High-temperature piezoelectric film ultrasonic transducers by a sol-gel spray technique and their

application to process monitoring of polymer injection molding," IEEE Sensors J., vol. 6, pp. 55-62, Feb. 2006.

[116] K. Goebbels and S. Hirsekorn, "A new ultrasonic method for stress determination in textured materials," NDT&E Int'l, vol.17, pp.337-341, 1984.

[117] W. Voigh, Lehrbuch der Kristalllphysik, Leipzig, Teubner, 1982.

[118] I.A. Viktorov, Rayleigh and Lamb Waves, New York: Plenum, 1967.

[119] R. Mohamed, P. Masson, "A time domain spectral element model for piezoelectric excitation of Lamb waves in isotropic plates", SPIE – Smart Structures/NDE, San Diego, CA, USA, 7-11 mars 2010.

[120] P. Masson, D. Langlois Demers, N. Quaegebeur, P. Micheau, "Chirplet-based imaging using compact piezoelectric array", SPIE – Smart Structures/NDE, San Diego, CA, USA, 7-11 mars 2010.

[121] C.-K. Jen and M. Kobayashi, "Integrated and flexible high temperature piezoelectric ultrasonic transducers," Chapter 2 in Ultrasonic and Advanced Methods for Nondestructive Testing and Material Characterization, C.H. Chen, Ed. New Jersey: World Scientific Publ., pp.33-55, 2007.

[122] C.-K. Jen, Y. Ono and M. Kobayashi, "High temperature integrated ultrasonic shear wave probes," Appl. Phys. Lett., vol.89, pp.183506_1-3, 2006.

[123] Y. Ono, C.-K. Jen and M. Kobayashi, "High temperature integrated ultrasonic shear and longitudinal wave probes," Review of Scientific Instruments, vol.78, pp.0249031-5, 2007.

[124] P.O. Moore, G.L. Workman and D. Kishoni, "Nondestructive Test Handbook," 3rd ed., vol.7, Ultrasonic Testing, ASNT, 2007.

[125] R.F. Humphryes and E.A. Ash, "Acoustic bulk-surface-wave transducers," Electron. Letts., vol.5, pp.175-176, 1969.

[126] A. Ronnekleiv, H.J. Shaw and J. Souquet, "Grating acoustic scanners," Appl. Phys. Letts., vol.28, pp.361-362, 1976.

[127] J. Kent and R. Adler, “Reflecting love waves by 90 degrees,” Proc. IEEE Ultrasonics Symp., pp.158-161, 2001.

[128] J. Kent, M. Takeuchi and G. Laux, “Robert Adler’s touchscreen inventions,” Proc. IEEE Ultrasonics Symp., pp.9-20, 2007.

[129] M. Takeuchi, N. Fujita, P. Gomes, J. Kent and R. Adler, “Ultrasonic attenuation in acoustic touch panels,” Proc. IEEE Symp., pp.1585-1590, 2004.

[130] R.P. Dalton, P. Cawley and M.J.S. Lowe, “The potential of guided waves for monitoring large areas of metallic aircraft structure,” J. Nondestructive Evaluation, vol.20, pp.29-46, 2001.

[131] V. Giurgiutiu, “Structural health monitoring with piezoelectric wafer active sensors,” New York, Elsevier, 2007.

[132] M. Kobayashi, C.-K. Jen, J.F. Bussiere and K.-T. Wu, “High temperature integrated and flexible ultrasonic transducers for non-destructive testing”, NDT&E Int., vol.42, no.2, pp.157-161, 2009.

[133] H.L Bertoni and T. Tamir, “Characteristics of wedge transducers for acoustic surface waves,” IEEE Trans. Sonics and Ultrason., vol.22, no.6, pp.415-420, 1975.

[134] J. Fraser, B.T. Khuri-Yakub and G.S. Kino, “The design of efficient broadband wedge transducers,” Appl. Phys. Lett., vol.32, no.11, pp.698-700, 1978.

[135] J.J. Ditri and J.L. Rose, “Excitation of guided waves in generally anisotropic layers using finite sources,” Trans. ASME, vol.61, pp.330-338, 1996.

[136] X. Jia, “Modal analysis of Lamb wave generation in elastic plates by liquid wedge transducers,” J. Acoust. Soc. Am., vol.101, no.2, pp.834-842, 1997.

[137] K.-T. Wu, M. Kobayashi and C.-K. Jen, “Integrated high temperature piezoelectric plate acoustic wave transducers,” IEEE Trans. UFFC, vol.56, no.6, pp.1218-1224, 2009.

[138] E.L. Adler, J.K. Slaboszewicz, G.W. Farnell and C.-K. Jen, “PC software for SAW propagation in anisotropic multilayers”, IEEE Trans. Ultrason. Ferroelect. Freq. Contr., vol.37, pp.215-223, 1990.

[139] R. Adler, A. Korpel and P. Desmares, “An instrument for making surface waves visible,” IEEE Trans. Sonics Ultrason., 15, pp 157-161, 1968.

[140] L.W. Kessler, P.R. Palermo and A. Korpel, “Recent developments with the scanning laser acoustic microscope,” Acoustic Holography, P.S. Green, Ed., New York: Plenum Press, pp 15-23, 1974.

[141] J.-P. Monchalin, “Optical detection of ultrasound,” IEEE Trans. Ultrason. Ferroelect. Freq. Control, vol.33, pp 485-499, 1986.

[142] J.W. Wagner, “Optical detection of ultrasound,” Physics Acoustics, 19, W.P. Mason and R.N. Thurston, Ed. New York: Academic Press, pp.201-264, 1990.

[143] R.K. Ing and J.-P Monchalin, “Broadband optical detection of ultrasound by two-wave mixing in a photorefractive crystal,” Appl. Phys. Lett., vol.59, pp.3233-5, 1991.

[144] J.-R. Lee, J. Takatsubo and N. Toyama, “Disbond monitoring at wing stringer tip based on built-in ultrasonic transducers and a pulsed laser,” Smart Materials and Structures, vol.16, no.4, pp.1025-1035, 2007.

[145] J.-R. Lee, J. Takatsubo, N. Toyama and D.-H. Kang, “Health monitoring of complex curved structures using an ultrasonic wavefield propagation imaging system,” Measurement Science and Tech., vol.18, pp. 3816-3824, 2007.

[146] S. Yashiro, J. Takatsubo, H. Miyauchi and N. Toyama. “A novel technique for visualizing ultrasonic waves in general solid media by pulsed laser scan,” NDT&E Int’l, vol.41, pp.137-144, 2008.

[147] C.-C. Chia, J.-R. Lee and H.-J. Shin, “Hot target inspection using a welded fibre acoustic wave piezoelectric sensor and a laser-ultrasonic mirror scanner,” Measurement Science and Tech., vol.20, no.12, pp.127003_1-8, 2009.

[148] K.-T. Wu, C.-K. Jen and M. Kobayashi, “High temperature integrated plate acoustic wave transducers,” Elect. Letts., vol.44, pp.776-7, 2008.

[149] M. Kobayashi, C.-K. Jen, Y. Ono, K.-T. Wu and I. Shih, "Integrated high temperature longitudinal, shear and plate acoustic wave transducers," Jpn. J. Appl. Phys., vol.46, pp.4688-4692, 2007.

[150] S.N. Atluri, S.G. Sampatch and P. Tong, "Structural integrity of aging airplanes", Springer, NY., 1991.

[151] M.P. Siener, "Stress field sensitivity of a composite patch repair as a result of varying patch thickness", Composite Materials: Testing and Design, vol.10, ASTM, STP 1120, G.C. Grimes, Ed., pp.444-464-1992.

[152] A.A. Baker and R. Jones, "Bonded repair of aircraft structures," Martinus Nijhoff Pub., 1988.